Lecture Notes in Physics 898

Fumihiko Suekane

Neutrino Oscillations

A Practical Guide to Basics and Applications

Springer

Lecture Notes in Physics

Volume 898

The Lecture Notes in Physics

The series Lecture Notes in Physics (LNP), founded in 1969, reports new developments in physics research and teaching-quickly and informally, but with a high quality and the explicit aim to summarize and communicate current knowledge in an accessible way. Books published in this series are conceived as bridging material between advanced graduate textbooks and the forefront of research and to serve three purposes:

- to be a compact and modern up-to-date source of reference on a well-defined topic
- to serve as an accessible introduction to the field to postgraduate students and nonspecialist researchers from related areas
- to be a source of advanced teaching material for specialized seminars, courses and schools

Both monographs and multi-author volumes will be considered for publication. Edited volumes should, however, consist of a very limited number of contributions only. Proceedings will not be considered for LNP.

Volumes published in LNP are disseminated both in print and in electronic formats, the electronic archive being available at springerlink.com. The series content is indexed, abstracted and referenced by many abstracting and information services, bibliographic networks, subscription agencies, library networks, and consortia.

Proposals should be sent to a member of the Editorial Board, or directly to the managing editor at Springer:

Christian Caron
Springer Heidelberg
Physics Editorial Department I
Tiergartenstrasse 17
69121 Heidelberg/Germany
christian.caron@springer.com

More information about this series at http://www.springer.com/series/5304

Fumihiko Suekane

Neutrino Oscillations

A Practical Guide to Basics and Applications

Springer

Fumihiko Suekane
Research Center for Neutrino Science
Tohoku University
Sendai
Japan

ISSN 0075-8450 ISSN 1616-6361 (electronic)
Lecture Notes in Physics
ISBN 978-4-431-55461-5 ISBN 978-4-431-55462-2 (eBook)
DOI 10.1007/978-4-431-55462-2

Library of Congress Control Number: 2015930821

Springer Tokyo Heidelberg New York Dordrecht London

Printed on acid-free paper

Springer Japan KK is part of Springer Science+Business Media (www.springer.com)

To my patient family

Preface

Neutrino oscillation is one of the most exciting subjects in elementary particle physics today. It was first confirmed in 1998 by the Super-Kamiokande group from their studies of atmospheric neutrinos. Experimental studies of neutrino oscillation have been rapidly progressing since then, and a number of positive oscillation results have been observed in atmospheric, solar, accelerator, and reactor neutrinos. The implication of the existence of neutrino oscillation is that neutrinos have finite masses and mixings, which are not accounted for in the framework of the standard model of elementary particles. Therefore, the standard model now must be extended to include the new information. Because the neutrino masses are extremely small, it is considered to be unnatural to be included in the standard model similar to the way quark and charged lepton masses are. Therefore, the neutrino oscillation is believed to provide an important new concept that will be a big step toward the unified understanding of elementary particle physics.

The author has been involved in neutrino oscillation experiments since 1996 as a member of the KamLAND and later, Double Chooz groups and has witnessed the rapid progress of neutrino oscillation studies. Along with the work for the experiments, he has given topical lectures on neutrino oscillation in summer and winter schools, as well as a number of university lectures on particle physics. While preparing these lectures, the author felt that although there were good books on neutrinos and neutrino oscillation, many of them were highly sophisticated and were not necessarily useful for experimental students and beginners in this research field.

This book is written with the intention of giving readers an intuitive image of neutrino oscillation by showing concrete examples and numerical values of calculation results. The initial conditions are specified for the general wave functions in order to see the concrete phenomena involved. The probability formulas for the various neutrino and antineutrino oscillation modes, with and without matter effects, are summarized in the Appendix to provide a useful reference.

This book begins, in Chap. 1, with a brief introduction to the motivation for neutrino oscillation study and its history. Explanation of neutrinos and their interactions in the standard model are given in Chap. 2. Neutrino spectra from various neutrino sources and reaction cross sections are also calculated in Chap. 2. The basics of the particle oscillations are introduced in Chap. 3. In Chap. 4, the ultrarelativistic three-flavor neutrino oscillations are explained in detail and a complete set of the oscillation probabilities for the three flavor neutrinos are calculated. Chapter 4 also deals with the neutrino oscillation-related subjects, such as the matter effect, a paradox from the measurement problem. Chapter 5 introduces the key experiments and their results, and the three-flavor neutrino oscillation parameters are summarized in Chap. 6. A toy model which can approximately predict the observed neutrino mixing patterns is also shown in Chap. 6. Finally, in Chap. 7, possibilities of future experiments are discussed, which include the measurement of the CP violation parameter δ, determination of the Δm^2_{31} mass hierarchy, and the absolute neutrino mass. The issues of the sterile neutrino and neutrino-less double β decay are briefly treated in Chap. 7. In the Appendix, a summary of the parameters and notations, a short review of the neutrino-related Lagrangian, Dirac equation, and a complete set of the neutrino oscillation probability formulas are given. Detailed calculations or lengthy descriptions, which are not appropriate to be in the main text, are also placed there.

While this book was being prepared, the last neutrino mixing angle, called θ_{13}, was finally measured and the door to future neutrino oscillation studies was opened dramatically. The research in this field will be very active and exciting. The author hopes ambitious students and researchers will join us and reveal the secret of the neutrinos together.

Sendai, Japan, December 2014 Fumihiko Suekane

Acknowledgments

At first, the author would like to thank Emeritus Professor H. Yuta for his careful reading of this manuscript and for a lot of comments he gave to the author. The discussions with him were very helpful to improve the contents of this book. The author would like to thank Drs. K. Hikasa, T. Schwetz-Mangold, M. Kuze, Y. Kamyshkov, I. Gil-Botella, T. Maruyama and K. Ishikawa, for their useful comments. The author would like also thank Drs. J.Y. Gruszko and T.J.C. Bezerra for checking the English. Finally, the author would like to thank Ms. H. Niko for giving the author the opportunity to write this book and the various helps she gave the author while the draft was prepared.

Contents

Chapter 1
Introduction

Abstract In the first part of this chapter, a short introduction to the study of neutrino oscillation is given. The importance of neutrino oscillation research is discussed; in contrast to other particle mixings and oscillations which have contributed much to the establishment of the standard model, the neutrino oscillation probes unprecedentedly low mass scales and has not been integrated into the standard model. The latter part of this chapter gives a brief history of neutrino oscillation studies from the prediction of the neutrino by Pauli to the discovery of the third mixing angle θ_{13}. We will see the timeline of how current knowledge of neutrino oscillation was obtained and envisage future possibilities.

Keywords Neutrino oscillation · Mixing angle · Neutrino mass · Matter effect · Mass hierarchy

1.1 Why Study Neutrino Oscillation?

Neutrino oscillation is a quantum mechanical phenomenon in which neutrino flavor changes spontaneously to another flavor. In the simple two flavor (ν_μ, ν_e) case, the probability that ν_μ changes to ν_e is expressed by[1]

$$P_{\nu_\mu \to \nu_e} = \sin^2 2\theta \sin^2 \frac{m_2^2 - m_1^2}{4E_\nu} L, \tag{1.1}$$

where E_ν is the neutrino energy, L is the distance between the neutrino source and detector, m_1 and m_2 are the neutrino masses of the mass eigenstates and θ is the mixing angle between flavor eigenstates and mass eigenstates.

The flavor eigenstates (ν_e, ν_μ) and the mass eigenstates (ν_1, ν_2) having the masses (m_1, m_2), respectively, are related as

$$\begin{pmatrix} \nu_e \\ \nu_\mu \end{pmatrix} = \begin{pmatrix} \cos\theta & -\sin\theta \\ \sin\theta & \cos\theta \end{pmatrix} \begin{pmatrix} \nu_1 \\ \nu_2 \end{pmatrix}. \tag{1.2}$$

[1] The natural unit ($c \to 1$, $\hbar \to 1$) is used throughout this book.

F. Suekane, *Neutrino Oscillations*, Lecture Notes in Physics 898,
DOI 10.1007/978-4-431-55462-2_1

Since the probability (1.1) shows the oscillatory phenomenon as a function of L, it is called the neutrino flavor oscillation, or just *neutrino oscillation*.

In fact, there are various quantum mechanical oscillations in elementary particle physics from which we have learned important physics. For instance, we learned about CP violation from $(K^0 \Leftrightarrow \overline{K^0})$ and $(B^0 \Leftrightarrow \overline{B^0})$ oscillations. The quark oscillation, $(d' \Leftrightarrow s')$ allows for the s-quark to decay, and the oscillation between the neutral gauge fields, $(B \Leftrightarrow W_3)$ defines the photon and Z^0 boson as their mass eigenstates. The quark oscillation and the gauge boson oscillation are too quick to observe so we can only see the averaged effects as the Cabbibo angle and the Weinberg angle. Studies of these oscillations contributed much to the establishment of the standard model of elementary particles. The neutrino oscillation is one such quantum mechanical oscillation.

The neutrino oscillation is unique among other oscillations because neutrinos travel with ultrarelativistic velocity and the oscillation length is very long. Using neutrino oscillations it is possible to study a very low mass scale regime which other experiments struggle to reach. The neutrino oscillation is not incorporated into the standard model. Like other oscillations and particle masses, the neutrino oscillations and masses can be understood to be generated by the transitions between the neutrino flavors. However, we do not know the origin of the very small observed transition amplitudes yet. It is expected that new physics will evolve from studies of neutrino oscillations.

Books [1–9] were widely referenced while this book was being written although they may not be cited in each part of this text.

1.2 A Brief History of Neutrino Oscillations

In 1899, nuclear β decay was discovered by E. Rutherford and in 1914, J. Chadwick found that the electron energy spectrum in β decay is continuous. This puzzled physicists because it seemed to violate the law of energy conservation. The concept of the neutrino was introduced in 1930 by W. Pauli in order to explain the energy spectrum of the β rays. A quarter century later, in 1956, the existence of the neutrino was experimentally confirmed. A team led by F. Reines and C.L. Cowan detected neutrinos from the Savanna River Nuclear Reactor[2] [10, 11]. In 1961, a Columbia Univ. and BNL group, led by L.M. Lederman, M. Schwartz and J. Steinberger, carried out an experiment striking aluminum targets with energetic neutrinos produced in $\pi \rightarrow \mu + \nu$ decay. They found that only muons were produced in the neutrino induced reactions [12]. This indicates that the neutrino produced in the pion decay is different from the one produced in the β decays in reactor. This was the discovery of the second neutrino, now called the muon neutrino (ν_μ). The neutrino produced

[2] At first they had planned to use neutrinos from a nuclear weapons test.

from nuclear β decay is now called the electron antineutrino ($\overline{\nu}_e$). Around 1969, R. Davis successfully detected solar neutrinos for the first time and found that the solar neutrino flux was significantly less than the prediction obtained from the standard solar model (SSM) [13]. After this observation, a number of experiments were carried out to measure the solar neutrinos with different energy thresholds and all of them confirmed that the solar neutrino flux is significantly less than the predicted value. The discrepancy between the measurements and the prediction was called the "solar neutrino problem" and remained unsolved until the solar neutrino oscillation was established.

In 1976, M. Perl discovered the τ lepton in the e^+e^- collider experiment at SLAC [14] and deduced the existence of the third neutrino ν_τ from the large missing energy and momentum of its decay. A quarter century later, the ν_τ was directly identified by DONUT group using a nuclear emulsion detector [15].

In 1987, M. Koshiba's Kamiokande group, together with the IMB and Baksan groups, detected neutrinos from supernova 1987A. It was the first time that neutrinos produced outside the solar system were observed.

In 1989, the total number of the standard neutrino flavors was determined to be three from the energy distribution of the Z^0 resonance in the LEP and SLAC experiments [1]. This result established that the fermion family consists of three generations and not more.

Starting in 1994, the Mainz and Troitsk groups tried to measure the $\overline{\nu}_e$ mass using β rays from tritium and set an upper limit of 2.2 eV.

The atmospheric neutrino anomaly was reported by the Kamiokande, IMB and Soudan groups in 1980s. The ratio of the fluxes of ν_μ and ν_e is expected to be close to two because two ν_μs and one ν_e are produced in the decay chain of the charged pion which is produced by cosmic ray interactions in the atmosphere. However, the observations showed that the ratio is more likely to be one.

In 1997, the first clear evidence of the neutrino oscillation was reported by the Super-Kamiokande group to account for the atmospheric neutrino anomaly [16–18]. In fact, the neutrino flavor mixing, which causes the neutrino oscillation, was suggested by Maki et al. [19] and by Pontecorvo [20][3] long before this discovery. From the atmospheric neutrino experiments, the oscillation parameters of Δm^2_{32} and $\sin^2 2\theta_{23}$ were measured. The finite Δm^2 implies that neutrinos have finite masses, which suggests new physics.

As for the solar neutrino anomaly, the SAGE, GALLEX and GNO groups found the deficit of neutrino fluxes produced from *pp* fusion in the sun using a radiochemical technique[4] [23–27]. The Kamiokande and Super-Kamiokande groups also confirmed the deficit in ^{8}B neutrinos by using the elastic scattering of neutrinos and electrons [28–36]. In these solar neutrino experiments, the deficit was found to be energy dependent. In 1978 and 1986, L. Wolfenstein, S. Mikheyev and A. Smirnov pointed out that the matter effect (MSW effect) could explain how the large solar

[3] Pontecorvo suggested $\nu \Leftrightarrow \overline{\nu}$ and $e^-\mu^+ \Leftrightarrow e^+\mu^-$ oscillations in 1957 and 1958 [21, 22].

[4] Neutrino produces long lifetime radioactive nucleus $\nu_e + {}^{71}\mathrm{Ga} \rightarrow e^- + {}^{71}\mathrm{Ge}$, then ^{71}Ge is extracted from the detector and its Auger electron is detected by a proportional counter.

neutrino deficits could result from a small mixing angle. The MSW effect was an attractive explanation because the neutrino mixing angle was thought to be small from the analogy to the small quark mixing angles.

In 2002, SNO group measured neutral current interactions of solar neutrinos using a D_2O target. They showed that the total neutrino flux was the same as that predicted by the SSM and that the observed deficits are due to the transformation of neutrino flavors [37]. Combining all the solar neutrino data, the oscillation parameters supported the Large Mixing Angle (LMA) solution [38]. In 2008, the Borexino group measured ^{7}Be solar neutrinos and detected the deficit of solar neutrinos at $\sim$1 MeV. The oscillation parameters Δm^2_{21} and $\sin^2 2\theta_{12}$ have been measured by solar neutrino experiments. From the energy dependence of the MSW effect, the mass hierarchy of $m_2 > m_1$ has also been determined.

In 2003, the KamLAND group reported the disappearance of reactor neutrinos at an average distance of 180 km from reactors [39, 40]. They also measured Δm^2_{21} and $\sin^2 2\theta_{12}$ using antineutrinos. The fact that the results of $\overline{\nu}_e$ disappearance from the KamLAND experiment agree with those of ν_e disappearance from the solar neutrino experiments confirms the CPT symmetry.

In 2004, the K2K group measured the ν_μ disappearance by sending ν_μ from KEK-PS to the Super-Kamiokande detector, located at 250 km away. The observed ν_μ disappearance is in the same parameter region as the atmospheric neutrino oscillation measurements [41]. This is the first long baseline neutrino experiment using accelerator neutrinos. In 2006, the MINOS experiment observed the ν_μ disappearance using neutrinos produced by the NuMI beam line at Fermilab [42] and measured Δm^2_{32} and $\sin^2 2\theta_{32}$. They also measured the $\overline{\nu}_\mu$ disappearance and confirmed the CPT symmetry [43].

In 2010, the OPERA group observed a $\nu_\mu \to \nu_\tau$ event at Gran Sasso Lab. using CNGS neutrino beam from CERN [44].

In 2011, T2K reported an indication of $\nu_\mu \to \nu_e$ appearance events for the first time [45] and Double Chooz showed an indication of a reactor neutrino deficit at a short baseline [46]. In 2012, Daya Bay and RENO confirmed the reactor neutrino deficit at short baselines and gave a precise measurement of θ_{13} [47, 48].

As of the summer of 2014, all of the mixing angles and Δm^2s have been measured. The CP violating parameter δ and mass hierarchy of m_3 and m_1 are the next important targets to measure.

There have been hints of oscillation to a 4th neutrino, called the sterile neutrino [49]. Several experimental projects are being planned to investigate this issue.

References

1. Particle Data Group, PRD **86**, 010001 (2012)
2. M. Fukugita, T. Yanagida, *Physics of Neutrinos* (Springer)
3. M. Fukugita, A. Suzuki (eds.), *Physics and Astrophysics of Neutrinos* (Springer)
4. F. Halzen, A.D. Martin, *Quarks and Leptons* (Wiley)
5. S. Bilenky, *Introduction to the Physics of Massive and Mixed Neutrinos* (Springer)

6. K. Zuber, *Neutrino Physics*, 2nd edn. (CRC Press)
7. J.D. Bjorken, S.D. Drell, *Relativistic Quantum Mechanics* (McGraw-Hill Book Company)
8. W. Greiner, B. Müller, *Gauge Theory of Weak Interactions*, 2nd edn. (Springer)
9. K. Hikasa, *Dirac Equation* (Saiensu-sha Co., Ltd., Publishers) (Written in Japanese)
10. C.L. Cowan Jr., F. Reines, F.B. Harrison, H.W. Kruse, A.D. McGuire, Science **124**, 103–104 (1956)
11. F. Reines, C.L. Jr Cowan, Nature **178**, 446–449 (1956)
12. G. Danby, J.M. Gaillard, K.A. Goulianos, L.M. Lederman, N.B. Misty, M. Schwartz, J. Steinberger, PRL **9**, 36–44 (1962)
13. R. Davis, Jr., Nobel Lecture (2002)
14. G.J. Feldman et al., PRL **38**, 117 (1977), Erratum-ibid. **38**, 576 (1977)
15. DONUT Collaboration, PLB **504**, 218–224 (2001)
16. Super-Kamiokande Collaboration, PRL **81**, 1562–1567 (1998)
17. Super-Kamiokande Collaboration, PRL **93**, 101801 (2004)
18. Super-Kamiokande Collaboration, PRD **81**, 092004 (2010)
19. Z. Maki, M. Nakagawa, S. Sakata, Prog. Theor. Phys. **28**, 870–880 (1962)
20. V. Gribov, B. Pontecorvo, Phys. Lett. B **28**, 493–496 (1969)
21. B. Pontecorvo, Sov. Phys. JETP **6**, 429 (1958)
22. B. Pontecorvo, Sov. Phys. JETP **7**, 172 (1958)
23. GNO Collaboration, PLB **616**, 174–190 (2005)
24. GNO Collaboration, PLB **490**, 16–26 (2000)
25. SAGE Collaboration, J. Exp. Theor. Phys. **95**, 181–193 (2002)
26. SAGE Collaboration, Zh. Eksp. Teor. Fiz. **122**, 211–226 (2002)
27. GALLEX Collaboration, PLB **447**, 127–133 (1999)
28. Super-Kamiokande Collaboration, PRL **81**, 1158–1162 (1998)
29. Super-Kamiokande Collaboration, PRL **86**, 5651–5655 (2001)
30. Super-Kamiokande Collaboration, PRL **86**, 5656–5660 (2001)
31. Super-Kamiokande Collaboration, PLB **439**, 179–187 (2002)
32. Super-Kamiokande Collaboration, PRD **73**, 112001 (2006)
33. Super-Kamiokande Collaboration, PRD **83**, 052010 (2011)
34. Kamiokande-II Collaboration, PRL **63**, 16 (1989)
35. Kamiokande-II Collaboration, PRD **44**, 2241 (1991)
36. Kamiokande-II Collaboration, Erratun-ibid. **D45**, 2170 (1992)
37. SNO Collaboration, PRL **89**, 011301 (2002)
38. SNO Collaboration, PRL **89**, 011302 (2002)
39. KamLAND Collaboration, PRL **90**, 021802 (2003)
40. KamLAND Collaboration, PRL **94**, 081801 (2005)
41. K2K Collaboration, PRL **90**, 041801 (2004)
42. MINOS Collaboration, PRL **97**, 191801 (2006)
43. MINOS Collaboration, PRL **107**, 021801 (2011)
44. OPERA Collaboration, PLB **691**, 138 (2010)
45. T2K Collaboration, PRL **107**, 041801 (2011)
46. Double Chooz Collaboration, PRL **108**, 131801 (2012)
47. Daya Bay Collaboration, PRL **108**, 171803 (2012)
48. RENO Collaboration, PRL **108**, 191802 (2012)
49. K.N. Abazajian, Light sterile neutrino: a white paper, arXive1204.5379 [hep-ph] (2012)

Chapter 2
Neutrinos and Weak Interactions in the Standard Model

Abstract Neutrinos are produced and detected by weak interactions. It is necessary to understand the weak interactions to calculate the energy spectrum of neutrinos generated in sources and the reaction cross section with detector materials. In this chapter, the weak interactions associated with the neutrinos are reviewed and neutrino reaction probabilities that will be used in the later sections are calculated. Starting from the wave function of the massless left-handed neutrinos, the neutrino-associated parts of the standard model Lagrangian are introduced. Based on the Lagrangian, the general matrix element for the four fermion interactions that include neutrino is formulated. The spectra of neutrinos produced in the pion decay, muon decay, β decay, and the neutrino detection cross section via νe elastic scatterings and inverse beta decay are quantitatively calculated.

Keywords Standard model · Weak interaction · Helicity · Neutrino source · Neutrino interaction

2.1 Introductions

In order to investigate the neutrino oscillation in experiments, we need to understand the properties and the reactions of neutrinos qualitatively within the standard model. In planning experiments and understanding their data, the production mechanism of neutrinos and its reaction cross sections with matter are particularly important. In this chapter we focus on the weak interactions that are related to the neutrino reactions based on the Lagrangian which is summarized in Sect. 8.2.

2.2 Quarks, Charged Leptons and Neutrinos

In the standard model of elementary particles, the six fermions which couple to the strong interactions are called *quarks*

$$\begin{pmatrix} u \\ d \end{pmatrix}, \quad \begin{pmatrix} c \\ s \end{pmatrix}, \quad \begin{pmatrix} t \\ b \end{pmatrix}, \tag{2.1}$$

F. Suekane, *Neutrino Oscillations*, Lecture Notes in Physics 898,
DOI 10.1007/978-4-431-55462-2_2

where u, c, t quarks have charge $+2/3$ and d, s, b quarks have charge $-1/3$ in the unit of e. The six fermions which do not couple to the strong interactions are called the *leptons*

$$\begin{pmatrix} \nu_e \\ e^- \end{pmatrix}, \quad \begin{pmatrix} \nu_\mu \\ \mu^- \end{pmatrix}, \quad \begin{pmatrix} \nu_\tau \\ \tau^- \end{pmatrix}. \tag{2.2}$$

The ν_e, ν_μ and ν_τ do not couple to the electromagnetic interactions and are called *neutrinos*. The e, μ and τ have the electric charge -1 and are called *charged leptons*. All the fermions have their antiparticles,[1]

$$\begin{pmatrix} \overline{u} \\ \overline{d} \end{pmatrix}, \quad \begin{pmatrix} \overline{c} \\ \overline{s} \end{pmatrix}, \quad \begin{pmatrix} \overline{t} \\ \overline{b} \end{pmatrix}, \quad \begin{pmatrix} \overline{\nu}_e \\ e^+ \end{pmatrix}, \quad \begin{pmatrix} \overline{\nu}_\mu \\ \mu^+ \end{pmatrix}, \quad \begin{pmatrix} \overline{\nu}_\tau \\ \tau^+ \end{pmatrix}. \tag{2.3}$$

As for the interactions, the electromagnetic interactions are mediated by the massless spin-1 photon

$$\gamma. \tag{2.4}$$

The weak interactions are mediated by the massive spin-1 charged and neutral bosons,

$$W^\pm, \quad Z^0. \tag{2.5}$$

The strong interactions are mediated by the massless spin-1 vector boson called gluon,

$$g. \tag{2.6}$$

Finally the Higgs field generates the fermion and weak boson masses.

$$H^0. \tag{2.7}$$

The three interactions have a nesting structure, illustrated as a Matryoshka doll in Fig. 2.1. The fermions that feel the EM interactions also feel the weak interactions. Fermions that feel the strong interactions also feel the EM interactions and therefore feel the weak interactions.

What makes the standard model neutrinos unique is that the neutrinos do not feel the electromagnetic, strong, nor gravitational interactions. In other words, the neutrinos are chargeless, colorless and massless particles.

$$Q_\nu = 0, \quad g_S^\nu = 0, \quad m_\nu = 0. \tag{2.8}$$

Only left-handed (LH) neutrinos and right-handed (RH) antineutrinos couple to the weak bosons. Therefore, it can be regarded that there are only LH neutrinos or RH antineutrinos in our world.

$$\nu_\mathrm{L}, \quad \overline{\nu}_\mathrm{R}. \tag{2.9}$$

The LH and RH denote helicity states which will be explained in the next subsection.

[1] Neutrinos are treated as Dirac particle in this book unless otherwise specified.

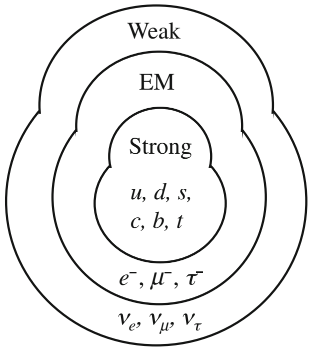

Fig. 2.1 Fermions are named based on the interactions they feel. There is a nesting structure of interactions like a Matryoshka doll

2.2.1 Wave Function of Fermions

The wave function of a spin 1/2 fermion can be obtained as the solution of the Dirac equation,

$$\left[i\gamma_\mu\partial^\mu - m\right]\psi = 0, \tag{2.10}$$

where γ_μ are 4×4 matrices called *gamma matrices* or *Dirac matrices*.

We use the Dirac representation,

$$\gamma_0 = \begin{pmatrix} I & 0 \\ 0 & -I \end{pmatrix}, \quad \gamma_k = \begin{pmatrix} 0 & \sigma_k \\ -\sigma_k & 0 \end{pmatrix}. \tag{2.11}$$

I is the identity matrix and σ_k are the Pauli matrices,

$$I = \begin{pmatrix} 1 & 0 \\ 0 & 1 \end{pmatrix}, \quad \sigma_x = \begin{pmatrix} 0 & 1 \\ 1 & 0 \end{pmatrix}, \quad \sigma_y = \begin{pmatrix} 0 & -i \\ i & 0 \end{pmatrix}, \quad \sigma_z = \begin{pmatrix} 1 & 0 \\ 0 & -1 \end{pmatrix}. \tag{2.12}$$

From Sect. 8.4, the plane wave solution of the Dirac equation with normalization $|\psi|^2 = 2E$ is

$$\psi(x) = \sqrt{E+m}\left[\begin{pmatrix} \hat{u} \\ (\eta\cdot\sigma)\hat{u} \end{pmatrix} e^{-ipx} + \begin{pmatrix} (\eta\cdot\sigma)\hat{v} \\ \hat{v} \end{pmatrix} e^{ipx}\right]; \quad \eta = \frac{\mathbf{p}}{E+m}, \tag{2.13}$$

where $p = (E,\ \mathbf{p})$ is the four momentum and $E = \sqrt{\mathbf{p}^2 + m^2}$ is the energy. $\hat{u}$ and $\hat{v}$ are two component spinors with the normalization of $|\hat{u}|^2 + |\hat{v}|^2 = 1$, which represent the spin direction. The first term of (2.13) is the positive energy state and the second term is the negative energy state that corresponds to the antiparticle.

2.2.1.1 Helicity and Spin Direction

The charged weak boson, $W^{\pm}$ couples only to the left-handed fermions. The left-handed (LH) and right-handed (RH) components of a state ψ are defined by

$$\begin{aligned} \psi_{\mathrm{L}} &\equiv \gamma_L \psi \equiv \frac{1-\gamma_5}{2}\psi = \frac{1}{2}\begin{pmatrix} I & -I \\ -I & I \end{pmatrix}\psi \\ \text{and}\quad \psi_{\mathrm{R}} &\equiv \gamma_R \psi \equiv \frac{1+\gamma_5}{2}\psi = \frac{1}{2}\begin{pmatrix} I & I \\ I & I \end{pmatrix}\psi, \end{aligned} \tag{2.14}$$

where

$$\gamma_5 \equiv i\gamma^0\gamma^1\gamma^2\gamma^3 = \begin{pmatrix} 0 & I \\ I & 0 \end{pmatrix}. \tag{2.15}$$

Any fermion wave functions are either LH or RH states, $\psi = \psi_{\mathrm{R}} + \psi_{\mathrm{L}}$.

The LH and RH components of the positive energy state at space-time $x = 0$ are,

$$\begin{aligned} \psi_L(0) &= \frac{1}{2}\begin{pmatrix} I & -I \\ -I & I \end{pmatrix}\sqrt{E+m}\begin{pmatrix} u \\ \eta\sigma u \end{pmatrix} = \frac{\sqrt{E+m}}{2}\begin{pmatrix} (1-\eta\sigma)u \\ -(1-\eta\sigma)u \end{pmatrix} \\ \text{and}\quad \psi_R(0) &= \frac{1}{2}\begin{pmatrix} I & I \\ I & I \end{pmatrix}\sqrt{E+m}\begin{pmatrix} u \\ \eta\sigma u \end{pmatrix} = \frac{\sqrt{E+m}}{2}\begin{pmatrix} (1+\eta\sigma)u \\ (1+\eta\sigma)u \end{pmatrix}. \end{aligned} \tag{2.16}$$

The probability of a fermion to be LH state is,

$$P_L = \frac{|\psi_L(0)|^2}{|\psi(0)|^2} = \frac{E+m}{2}\frac{[u^{\dagger}(1-\eta\sigma)^2 u]}{2E|u|^2} = \frac{1}{2}(1-\beta[u^{\dagger}\sigma u]). \tag{2.17}$$

In the case that the velocity vector is $\beta = \beta(\sin\theta\cos\phi,\ \ \sin\theta\sin\phi,\ \ \cos\theta)$ and the spin points to $+z$ direction $u = \begin{pmatrix} 1 \\ 0 \end{pmatrix}$, the probability becomes

$$P_L = \frac{1}{2}(1-\beta\cos\theta). \tag{2.18}$$

This means that the probability is the largest when the momentum direction is opposite to the spin direction, $\theta = \pi$, and the smallest when the momentum direction is the same as the spin one, $\theta = 0$. For ultrarelativistic case, $\beta = 1$ and $P_L = \sin^2(\theta/2)$. This means that the spin direction is opposite to the momentum direction. Similarly, for the RH state of an ultrarelativistic particle, the spin is parallel to the momentum. For a particle at rest, $\beta = 0$ and $P_L = P_R = 1/2$.

Table 2.1 summarizes the relation between the helicity and relative direction of spin and momentum.

Table 2.1 The probability of LH and RH states for relative direction between the spin and momentum

P	ψ_L	ψ_R
$\mathbf{s} \parallel -\mathbf{p}$	$(1+\beta)/2$	$(1-\beta)/2$
$\mathbf{s} \parallel \ \mathbf{p}$	$(1-\beta)/2$	$(1+\beta)/2$

This property causes the helicity suppression of the $\pi^{\pm}$ decay. "$\mathbf{s} \parallel \mathbf{p}$" means **s** and **p** are parallel

2.2.2 Wave Function of Neutrinos

Since neutrino is massless and only LH state exists in the standard model, the neutrino wave function becomes simple. By taking $m \to 0$ in Eq. (2.13), the wave function of a positive energy massless fermion becomes,

$$\psi_{m=0}(x) = \sqrt{k}\begin{pmatrix} \hat{u} \\ \hat{\mathbf{k}}\sigma\hat{u} \end{pmatrix} e^{-i(kt-\mathbf{kx})}, \tag{2.19}$$

where $p \to (k, \ \mathbf{k})$ is the four momentum with the relation $k = |\mathbf{k}|$. The pure LH state has to satisfy

$$\gamma_R\psi_{m=0}(x) = \frac{\sqrt{k}}{2}\begin{pmatrix} (1+\hat{\mathbf{k}}\sigma)\hat{u} \\ (1+\hat{\mathbf{k}}\sigma)\hat{u} \end{pmatrix} e^{-ipx} = 0, \tag{2.20}$$

at arbitrary space-time x. Since $\hat{\mathbf{k}} = (\sin\theta\cos\phi, \ \ \sin\theta\sin\phi, \ \ \cos\theta)$,

$$(1+\hat{\mathbf{k}}\sigma)\hat{u} = \begin{pmatrix} 1+\cos\theta & e^{-i\phi}\sin\theta \\ e^{i\phi}\sin\theta & 1-\cos\theta \end{pmatrix}\hat{u} = 0. \tag{2.21}$$

This relation can be satisfied if

$$\hat{u} \propto \hat{s}(-\hat{\mathbf{k}}) = \begin{pmatrix} -ie^{-i(\phi/2)}\sin(\theta/2) \\ ie^{i(\phi/2)}\cos(\theta/2) \end{pmatrix}, \tag{2.22}$$

where $\hat{s}(\hat{\mathbf{p}})$ is the spin polarization which points toward the direction of $\mathbf{p}$. Finally the wave function of the positive energy neutrino is

$$\psi_\nu^+(x) = \sqrt{k}\begin{pmatrix} \hat{s}(-\hat{\mathbf{k}}) \\ \hat{\mathbf{k}}\sigma\hat{s}(-\hat{\mathbf{k}}) \end{pmatrix} e^{-i(kt-\mathbf{kx})}, \tag{2.23}$$

where the state propagates only forward in time. Similarly the wave function of the negative energy neutrino is

$$\psi_\nu^-(x) = \sqrt{k}\begin{pmatrix} \hat{\mathbf{k}}\sigma\hat{s}(-\hat{\mathbf{k}}) \\ \hat{s}(-\hat{\mathbf{k}}) \end{pmatrix} e^{i(kt-\mathbf{kx})}, \tag{2.24}$$

where the state propagates only backward in time and we recognize it as antineutrino.

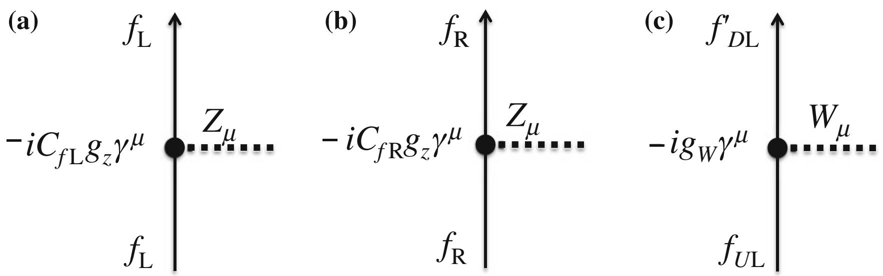

Fig. 2.2 Feynman diagram of **a** $f_L f_L Z^0$ coupling, **b** $f_R f_R Z^0$ coupling and **c** $f_U f'_D W^\pm$ coupling, where f_U is the up-type fermions and f'_D is the down-type flavor eigenstate fermions

2.3 Weak Interactions and Neutrinos

In this section, the fundamental processes of the weak interactions are described based on the standard model Lagrangian and probabilities of various neutrino interactions are calculated. The probabilities calculated here will be used later to understand neutrino oscillation experiments and their results. See also the books [2–8, Chap. 1] for details of the calculations.

2.3.1 Lagrangians for Weak Interactions

The Lagrangian of the standard model weak interaction can be obtained by setting the neutrino mixing matrix as the identical matrix in the working Lagrangian defined in Sect. 8.2. The Feynman diagrams of the weak interactions are shown in Fig. 2.2. Figure 2.2a, b shows the neutral current interactions and Fig. 2.2c shows the charged current interactions. We call ($u, c, t, \nu_e, \nu_\mu, \nu_\tau$), up-type fermions ($f_U$) and ($d,\ s,\ b,\ e,\ \mu,\ \tau$), down-type fermions ($f_D$). The weak (flavor) eigenstates ($d',\ s',\ b'$) are mixed with the mass eigenstates ($d,\ s,\ b$) by the Cabbibo-Kobayashi-Maskawa matrix as shown in Eq. (8.25) and f'_D is used instead of f_D when necessary.[2]

2.3.1.1 Neutral Current Interactions

The Lagrangian of the fermion f for the neutral current interactions is,

$$\mathscr{L}_{ffZ} = -iC_{fL}g_Z[\overline{f_L}\gamma^\mu f_L]Z_\mu - iC_{fR}g_Z[\overline{f_R}\gamma^\mu f_R]Z_\mu, \tag{2.25}$$

[2] For neutrinos, the flavor eigenstate and mass eigenstate are identical ($\nu' = \nu$) in the standard model and f'_D and f_D can be interpreted equivalently.

where g_Z is the coupling constant. $C_{f\mathrm{L}}$ and $C_{f\mathrm{R}}$ are coefficients for the couplings between Z^0 boson and the LH and RH components of the fermions. According to the standard model, $C_{f\mathrm{R}}$ and $C_{f\mathrm{L}}$ are given by

$$\begin{cases} C_{f_U\mathrm{R}} = -2Q_f \sin^2\theta_W \\ C_{f_U\mathrm{L}} = -2Q_f \sin^2\theta_W + 1, \end{cases} \qquad \begin{cases} C_{f_D\mathrm{R}} = -2Q_f \sin^2\theta_W \\ C_{f_D\mathrm{L}} = -2Q_f \sin^2\theta_W - 1, \end{cases} \tag{2.26}$$

where Q_f is the charge of the fermion f. θ_W is the parameter called the *weak mixing angle* or *Weinberg angle*, which is measured to be $\sin^2\theta_W \sim 0.23$.

The fermion currents in Eq. (2.25) can be modified as

$$\begin{aligned} \overline{f_\mathrm{L}}\gamma^\mu f_\mathrm{L} &= f^\dagger\gamma_\mathrm{L}^\dagger\gamma^0\gamma^\mu\gamma_\mathrm{L} f = \overline{f}\gamma^\mu\gamma_\mathrm{L} f = \overline{f}\gamma^\mu\frac{1}{2}(1-\gamma^5)f, \\ \overline{f_\mathrm{R}}\gamma^\mu f_\mathrm{R} &= \overline{f}\gamma^\mu\gamma_\mathrm{R} f, = \overline{f}\gamma^\mu\frac{1}{2}(1+\gamma^5)f, \end{aligned} \tag{2.27}$$

and the Lagrangian (2.25) can be rewritten as

$$\mathscr{L}_{ffZ} = -ig_Z[\overline{f}\gamma^\mu\frac{1}{2}(C_{f\mathrm{V}} - C_{f\mathrm{A}}\gamma^5)f]Z_\mu, \tag{2.28}$$

where $C_{f\mathrm{V}}$ and $C_{f\mathrm{A}}$ are called the *Vector Coupling* coefficient and *Axial-vector Coupling* coefficient which are defined by

$$\begin{cases} C_{f\mathrm{V}} \equiv C_{f\mathrm{L}} + C_{f\mathrm{R}} \\ C_{f\mathrm{A}} \equiv C_{f\mathrm{L}} - C_{f\mathrm{R}} \end{cases}. \tag{2.29}$$

Contrarily, an arbitrary mixture of vector and axial vector couplings can be expressed by a combination of LH and RH couplings

$$a + b\gamma^5 = (a+b)\gamma_\mathrm{R} + (a-b)\gamma_\mathrm{L}. \tag{2.30}$$

This means that the weak and the electromagnetic interactions can be expressed by a sum of the LH and RH couplings, as well as by a sum of the vector and axial vector couplings. These coefficients are summarized in Table 2.2.

Table 2.2 Z^0-fermion coupling coefficients. $x_W = \sin^2\theta_W \sim 0.23$

Fermions	Q	C_L	C_R	C_V	C_A	$C_\mathrm{L}^2 + C_\mathrm{R}^2$
ν_e, ν_μ, ν_τ	0	1	0	1	1	1
e, μ, τ	-1	$2x_W - 1$	$2x_W$	$4x_W - 1$	-1	$8x_W^2 - 4x_W + 1$
u, c, t	$+\frac{2}{3}$	$-\frac{4}{3}x_W + 1$	$-\frac{4}{3}x_W$	$-\frac{8}{3}x_W + 1$	1	$\frac{32}{9}x_W^2 - \frac{8}{3}x_W + 1$
d, s, b	$-\frac{1}{3}$	$\frac{2}{3}x_W - 1$	$\frac{2}{3}x_W$	$\frac{4}{3}x_W - 1$	-1	$\frac{8}{9}x_W^2 - \frac{2}{3}x_W + 1$

2.3.1.2 Charged Current Interactions

As for the quark-$W^{\pm}$ coupling, the Lagrangian is given by

$$\mathscr{L}_{ffW} = -ig_W[\overline{f'_{DL}}\gamma^{\mu} f_{UL}]W_{\mu} - ig_W[\overline{f_{UL}}\gamma^{\mu} f'_{DL}]W_{\mu}. \tag{2.31}$$

Finally, the Lagrangian for the electromagnetic interactions of the fermion f is

$$\mathscr{L}_{ffA} = -iQ_f e[\overline{f}\gamma^{\mu} f]A_{\mu}, \tag{2.32}$$

where A_{μ} represents the photon field. The Feynman diagram of the EM interactions is shown in Fig. 2.3. Since $Q_{\nu} = 0$ for neutrinos, they do not feel EM interactions.

Within the framework of the standard model, the weak interactions and electromagnetic interactions have the same origin and the three coupling constants, g_W, g_Z, and electric charge e, are related as,[3]

$$e = \sqrt{2}g_W \sin\theta_W = g_Z \sin 2\theta_W. \tag{2.33}$$

In general, reaction rates are proportional to powers of $(g^2/4\pi)$. Expressing the couplings in this form, the strength of the coupling between Z^0 boson and neutrinos is

$$\frac{g_Z^2}{4\pi} = \frac{\alpha}{\sin^2 2\theta_W} \sim 0.010, \tag{2.34}$$

where $\alpha \equiv e^2/4\pi \sim 0.0073$ is the electromagnetic fine structure constant. The strength of the coupling between $W^{\pm}$ boson and neutrino is

$$\frac{g_W^2}{4\pi} = \frac{\alpha}{2\sin^2\theta_W} \sim 0.016. \tag{2.35}$$

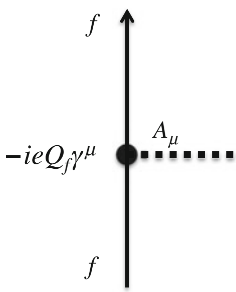

Fig. 2.3 Fermion coupling with the photon

[3] $g_W = g/\sqrt{2}$, $g_Z = g/2\cos\theta_W$, where g is the SU(2) gauge coupling constant.

Therefore, the magnitudes of the electromagnetic and weak couplings are not so different.

2.4 Neutrino Interaction Probabilities

The Lagrangians for the neutrino interactions are summarized as

$$\mathscr{L}_{\nu\nu Z} = -ig_Z \left[\overline{\nu_{lL}}\gamma^{\mu}\nu_{lL}\right] Z_{\mu}, \tag{2.36}$$

$$\mathscr{L}_{\nu l W} = -ig_W \left[\overline{l_{\mathrm{L}}}\gamma^{\mu}\nu_{lL}\right] W_{\mu} - ig_W \left[\overline{\nu_{lL}}\gamma^{\mu}l_{\mathrm{L}}\right] W_{\mu}, \tag{2.37}$$

where the wave function l stands for the charged leptons such as $e,\ \mu,\ \tau$. The Feynman diagrams which correspond to these vertexes are shown in Fig. 2.4.

The general diagram of the reaction $A + B \rightarrow A' + B'$ through intermediate gauge boson G is shown in Fig. 2.5. Its matrix element is written by

$$\begin{aligned}&\mathscr{M}_{AB\rightarrow A'B'}\\ &= -g_G^2 \frac{\left[\overline{\psi_{A'}(p_{A'})}\gamma^{\mu}\gamma_A\psi_A(p_A)\right]\left[\overline{\psi_{B'}(p_{B'})}\gamma_{\mu}\gamma_B\psi_B(p_B)\right]}{q^2 - M_G^2},\end{aligned} \tag{2.38}$$

where g_G is the coupling constant between the fermion and the intermediate boson G, p_X is the four momenta of the fermion X, and q is the four-momentum transfer, $q = p_A - p_{A'} = p_{B'} - p_B$. M_G is the intermediate boson mass. γ_X is helicity state

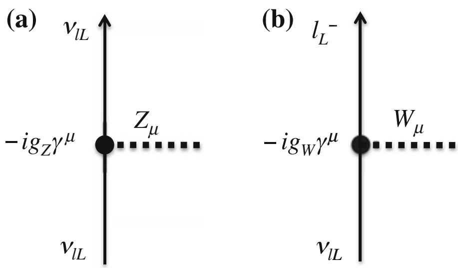

Fig. 2.4 Feynman diagram of **a** $\nu_l\nu_l Z^0$ and **b** $\nu_l l W$ couplings

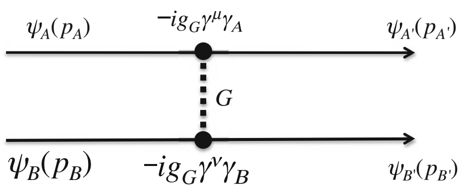

Fig. 2.5 Scattering amplitude of fermions A and B through intermediate boson G

of the coupling between fermion X and the boson G. If G is $W^{\pm}$, $\gamma_X = \gamma_{\rm L}$ and for Z^0, $\gamma_X = (C_{X\rm V} - C_{X\rm A}\gamma_5)/2$.

The wave function of each fermion is expressed as

$$\psi_X(x) = w_X e^{-ip_X x}, \tag{2.39}$$

where w_X is the four component spinor of the fermion X.

For low energy interactions, $|q^2| \ll M_G^2$, the reaction amplitude (2.38) can be expressed by the product of the spin and the exponential terms,

$$\mathscr{M}_{AB\to A'B'} = \frac{g_G^2}{M_G^2}\left[\overline{w_{A'}}\gamma_\mu\gamma_A w_A\right]\left[\overline{w_{B'}}\gamma^\mu\gamma_B w_B\right] e^{-i(p_A+p_B-p_{A'}-p_{B'})x}. \tag{2.40}$$

The exponential term becomes the delta function $\delta(p_A + p_B - p_{A'} - p_{B'})$ when integrated with respect to x, indicating the energy and momentum conservations, $p_A + p_B = p_{A'} + p_{B'}$.

The reaction probability is proportional to the absolute square of the matrix element,

$$P_{AB\to A'B'} \propto |\mathscr{M}_{AB\to A'B'}|^2 \propto G_F^2, \tag{2.41}$$

where *Fermi constant* G_F, defined by (2.42) is often used to express reaction probabilities of the weak interactions.

$$G_F = \frac{g_W^2}{2\sqrt{2}M_W^2} = \frac{g_Z^2}{\sqrt{2}M_Z^2} \sim 1.17 \times 10^{-5}[/\mathrm{GeV}^2]. \tag{2.42}$$

2.4.1 Neutrinos from Charged Pion Decay

In accelerator based neutrino experiments, the neutrinos produced in the charged pion decays are often used. The charged pion is a spin-0 pseudoscalar boson with mass $m_\pi \sim 140\,\mathrm{MeV}$. It decays with lifetime of 26 ns via the decay modes shown below,

$$\begin{aligned} \pi^{\pm} &\to \mu^{\pm} + \nu_\mu/\overline{\nu}_\mu \ \ (99.99\,\%),\\ \pi^{\pm} &\to \ e^{\pm} + \nu_e/\overline{\nu}_e \ \ (0.012\,\%), \end{aligned} \tag{2.43}$$

where the values in the parentheses are their branching fractions. There is a huge difference between the two branching fractions despite the lepton universality.

The Feynman diagram of the fundamental process of this decay is shown in Fig. 2.6a[4] and its physical process in the pion rest frame is shown in Fig. 2.6b. Since

[4] Actually the two quarks in the pion are in a bound state and the free wave functions can not be used. Nevertheless, this graphical view is useful to understand various properties of the pion decay.

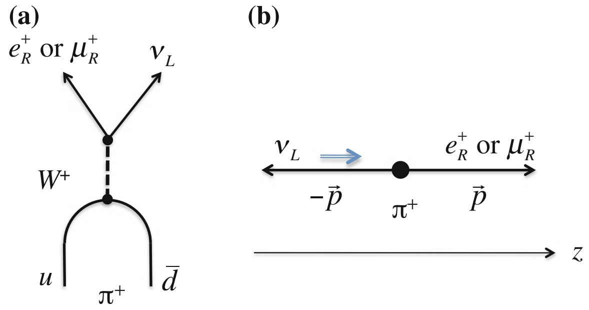

Fig. 2.6 π^+ decay. **a** A diagram. **b** Physical process in the pion rest frame. The z-axis is taken along the charged lepton's direction of motion. The neutrino moves to $-z$ and its spin points to the $+z$ direction

this is a two body decay, the final state leptons have definite energies and momentum. The energies and momentum of l and ν are[5]

$$E_\nu = \frac{m_\pi^2 - m_l^2}{2m_\pi}, \qquad E_l = \frac{m_\pi^2 + m_l^2}{2m_\pi}, \qquad p = \frac{m_\pi^2 - m_l^2}{2m_\pi}. \tag{2.44}$$

From the Feynman diagram Fig. 2.6a, the effective matrix element of this decay is,

$$\mathscr{M}_{\pi^+\to l^+\nu_l} \propto G_F[\overline{\nu_{l\mathrm{L}}}\gamma^\mu l_\mathrm{L}][\overline{d_\mathrm{L}}\gamma_\mu u_\mathrm{L}], \tag{2.45}$$

where l represents μ or e. The quark current is a bound system in the strong interaction potential and can be parametrized as

$$[\overline{d_L}\gamma_\mu u_L] \to f_\pi q_\mu, \tag{2.46}$$

where q_μ is the four momentum transfer and $f_\pi \sim m_\pi$ is the structure function of the pion, which corresponds to the overlapping density of the wave functions of the quarks in the pion. In the pion rest frame, $q_\mu = (m_\pi, \mathbf{0})$ and the matrix element (2.45) becomes

$$\mathscr{M}_{\pi\to l\nu} \propto G_F f_\pi m_\pi[\overline{\nu_{l\mathrm{L}}}\gamma^0 l_\mathrm{L}] = G_F f_\pi m_\pi[\nu_{l\mathrm{L}}^\dagger l_\mathrm{L}]. \tag{2.47}$$

By defining the z axis as the l^+ direction of motion as shown in Fig. 2.6b, the spinors of the neutrino and the charged lepton are,

$$\nu_{l\mathrm{L}} = \sqrt{E_\nu}\begin{pmatrix}\chi_1 \\ -\chi_1\end{pmatrix}, \quad l_L = \frac{\sqrt{E_l + m_l}}{2}\begin{pmatrix}-(1-\eta_l\sigma_z)\chi_l \\ (1-\eta_l\sigma_z)\chi_l\end{pmatrix}, \tag{2.48}$$

where χ_l represents the spin direction of the l^+ and $\eta_l = \frac{p}{E_l+m_l}$. Therefore, the matrix element (2.47) becomes

[5] If the neutrino has a finite mass m_ν, the energies and the momentum are $E_\nu = \frac{m_\pi^2-m_l^2+m_\nu^2}{2m_\pi}$, $E_l = \frac{m_\pi^2+m_l^2-m_\nu^2}{2m_\pi}$ and $p = \frac{\sqrt{((m_\pi-m_\nu)^2-m_l^2)((m_\pi+m_\nu)^2-m_l^2)}}{2m_\pi}$.

$$\mathscr{M}_{\pi \to l\nu} \propto G_F f_\pi m_\pi \sqrt{E_\nu (E_l + m_l)} (1 - \eta_l)[\chi_1^\dagger \chi_l]. \tag{2.49}$$

In this equation only $\chi_l = \chi_1$ (the l^+ spin points in the $-z$ direction) is allowed and the matrix element becomes

$$\mathscr{M}_{\pi \to l\nu} \propto G_F f_\pi m_\pi \sqrt{E_\nu (E_l + m_l)} (1 - \eta_l). \tag{2.50}$$

The decay rate is proportional to the absolute square of the matrix element,

$$\Gamma_l \propto |\mathscr{M}_{\pi \to l\nu}|^2 \propto G_F^2 f_\pi^2 (m_\pi^2 - m_l^2) m_l^2, \tag{2.51}$$

where Eqs. (2.44) are used to substitute the pion and charged lepton masses for the energies and momentum.

By taking into account the phase space, the decay rate of the pion can be calculated as [4, Chap. 1]

$$\Gamma_l = \frac{G_F^2}{8\pi} f_\pi^2 m_\pi m_l^2 \left(1 - \frac{m_l^2}{m_\pi^2} \right)^2. \tag{2.52}$$

The ratio of the decay rates of $e\nu$ and $\mu\nu$ modes is, therefore,

$$\frac{\Gamma_{\pi \to e\nu}}{\Gamma_{\pi \to \mu\nu}} = \left(\frac{m_e}{m_\mu} \right)^2 \left(\frac{m_\pi^2 - m_e^2}{m_\pi^2 - m_\mu^2} \right)^2 = 1.28 \times 10^{-4}. \tag{2.53}$$

This agrees with the observation (2.43). The fact that the decay to muons dominates makes it possible to obtain almost pure ν_μ or $\overline{\nu}_\mu$ beam in accelerator based neutrino experiments.

The mechanism to highly suppress $\pi \to e\nu$ decay is called the *helicity suppression*. Using the relation between helicity and spin polarization shown in Table 2.1, the helicity suppression can be described as follows. The produced massless neutrino is in the LH state and its spin points 100 % to $+z$ direction. Since the pion spin is 0, the only allowed charged lepton spin direction is $-z$ as shown in Fig. 2.7. On the other hand, the charged lepton is antifermion and therefore, it is in the RH state. The probability that e_R^+ spin points $-z$ is, from Table 2.1, given by

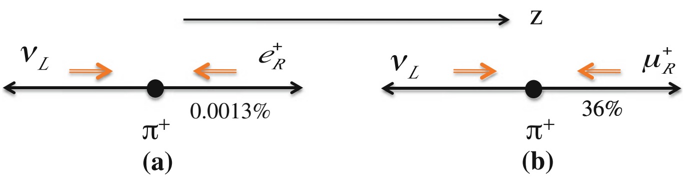

Fig. 2.7 Spin states and probabilities of **a** $\pi \to e\nu$ and **b** $\pi \to \mu\nu$ decays

$$P_{\nu e} = \frac{1-\beta_e}{2} = \frac{m_e^2}{m_\pi^2 + m_e^2} \sim 1.3 \times 10^{-5}, \tag{2.54}$$

where β_e is the velocity of the positron. Therefore, this decay channel is highly suppressed.

For $\pi \to \mu\nu$ decay, the same discussion can be applied, but the muon velocity β_μ is much smaller than β_e and the probability that μ_R^+ spin points to $-z$ is much larger,

$$P_{\nu\mu} = \frac{1-\beta_\mu}{2} = \frac{m_\mu^2}{m_\pi^2 + m_\mu^2} \sim 0.36. \tag{2.55}$$

Therefore, $\pi \to \nu\mu$ decays are not suppressed so much. Note that this suppression mechanism is not a unique property of the charged current weak interactions in which only a LH particle and a RH antiparticle can interact. It comes from the property of helicity conservation and takes place in decays of spin-0 particles with any combinations of vector and axial vector couplings.

2.4.2 Neutrinos from Muon Decay

The muons decay to

$$\begin{aligned} \mu^- &\to e^- + \nu_\mu + \bar{\nu}_e, \\ \mu^+ &\to e^+ + \bar{\nu}_\mu + \nu_e, \end{aligned} \tag{2.56}$$

with almost 100 % branching fraction. The lifetime of the muon, 2.2 μs, is much longer than the typical lifetime of other particles which decay weakly.

In some experiments, the muons are stopped in target or beam dump materials. The μ^- forms muonic atom with a nucleus in the material and quickly interact with the nucleus before it decays. On the other hand, μ^+ is repulsed from the nucleus and it decays before interacting with the nucleus. These properties can be used to obtain pure μ^+-originated neutrinos.

Since this weak decay process involves only leptons, the lifetime can be accurately calculated. From the experimental point of view, a large amount of controlled muons can be obtained and it is possible to measure its lifetime precisely. Therefore, the Fermi constant G_F has been precisely measured from the muon lifetime.

The Feynman diagram of the muon decay is shown in Fig. 2.8. The matrix element of the decay can be written from Eqs. (2.40) and (2.42) as,

$$\mathscr{M}_{\mu\to e\nu\bar{\nu}} = 2\sqrt{2}G_F[\overline{e_L}\gamma_\rho\nu_{eL}][\overline{\nu_{\mu L}}\gamma^\rho\mu_L^-]. \tag{2.57}$$

Ignoring the small m_e/m_μ terms, the calculation of the decay matrix element (2.57) shows that the energy spectrum of ν_μ is given by [2, Chap. 1] (Fig. 2.9),

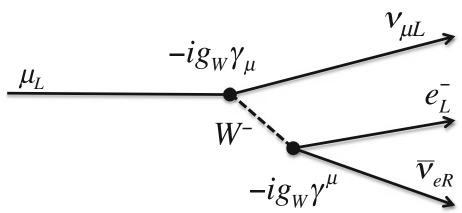

Fig. 2.8 The Feynman diagram of the muon decay

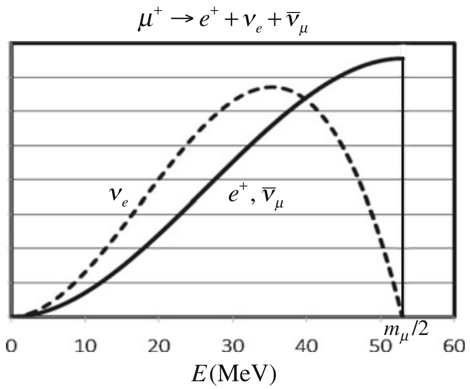

Fig. 2.9 Energy spectra of daughter particles of muon decay. m_e/m_μ terms are ignored

$$\frac{d\Gamma}{dE_{\nu_\mu}} = \frac{G_F^2 m_\mu^4}{12\pi^3}\left(\frac{E_{\nu_\mu}}{m_\mu}\right)^2\left(3-4\frac{E_{\nu_\mu}}{m_\mu}\right), \tag{2.58}$$

in the muon rest frame. For $\overline{\nu}_e$ and e, the energy spectra are

$$\frac{d\Gamma}{dE_{\overline{\nu}_e}} = \frac{G_F^2 m_\mu^4}{2\pi^3}\left(\frac{E_{\overline{\nu}_e}}{m_\mu}\right)^2\left(1-2\frac{E_{\overline{\nu}_e}}{m_\mu}\right), \tag{2.59}$$

and

$$\frac{d\Gamma}{dE_e} = \frac{G_F^2 m_\mu^4}{12\pi^3}\left(\frac{E_e}{m_\mu}\right)^2\left(3-4\frac{E_e}{m_\mu}\right). \tag{2.60}$$

The electron from the muon decay is called the *Michel electron*. Note that the Michel electron and muon neutrino have the same energy spectra. The angular distribution of ν_μ with respect to the muon spin is given by,

$$\frac{d\Gamma}{dx_{\nu_\mu}} = \frac{G_F^2 m_\mu^5}{6\pi^3}x_{\nu_\mu}^5\left(1+(1-4x_{\nu_\mu})\cos^2\frac{\theta_{\nu_\mu}}{2}\right), \tag{2.61}$$

where $x_{\nu_\mu} = E_{\nu_\mu}/m_\mu$ and θ_{ν_μ} is the ν_μ emission angle with respect to the muon spin. For $\overline{\nu}_e$, it is

$$\frac{d\Gamma}{dx_{\overline{\nu}_e}} = \frac{G_F^2 m_\mu^5}{\pi^3} x_{\overline{\nu}_e}^2 (1 - 2x_{\overline{\nu}_e}) \cos^2 \frac{\theta_{\overline{\nu}_e}}{2}, \tag{2.62}$$

where $x_{\overline{\nu}_e} = E_{\overline{\nu}_e}/m_\mu$ and $\theta_{\overline{\nu}_e}$ is the $\overline{\nu}_e$ emission angle with respect to the muon spin.

The total decay rate is calculated by integrating one of the energy distributions (2.58)–(2.60).

$$\Gamma_\mu = \int \frac{d\Gamma}{dE} dE = \frac{G_F^2 m_\mu^5}{192\pi^3}. \tag{2.63}$$

The lifetime of the muon is the inverse of the total decay rate. From the measurements of the muon lifetime and mass, G_F is precisely determined to be

$$G_F = (1.166\,378\,7 \pm 0.000\,000\,6) \times 10^{-5}\,\text{GeV}^{-2}. \tag{2.64}$$

The G_F value can be memorized by the empirical relation, $G_F \sim (1.08)^2 \times 10^{-5}$ GeV^{-2} with a precision of 20 ppm.

2.4.3 Neutrinos from Nuclear Beta Decays

Nuclear reactors produce a huge amount of low energy $\overline{\nu}_e$'s, which have been used for various neutrino studies. The reactor neutrinos are produced in the β-decays of the unstable fission products. The fundamental reaction is the β decay of a neutron,

$$n \to p + e^- + \overline{\nu}_e. \tag{2.65}$$

The Feynman diagram of this process is shown in Fig. 2.10. This diagram is similar to the muon decay diagram shown in Fig. 2.8. However, the nucleons have internal structure and the weak coupling to the $W^\pm$ boson is modified from the muon's. The effective matrix element of the neutron β-decay can be written as

$$\mathscr{M}_\beta = \sqrt{2} G_F \cos\theta_C [\overline{e_L}\gamma^\mu \nu_{eL}][\overline{p}\gamma_\mu(1 - C_A\gamma_5)n], \tag{2.66}$$

where θ_C is the Cabbibo angle and C_A is the effective axial vector coupling coefficient of the neutron which is measured to be $C_A \sim 1.3$.

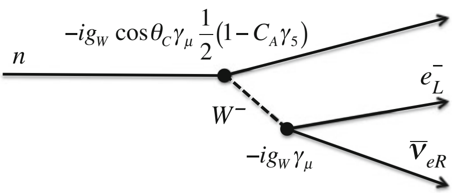

Fig. 2.10 Diagram of neutron β-decay

Using the non-relativistic reduction for the nucleon current, the squared matrix element can be expressed as

$$|\mathscr{M}_\beta|^2 = 4G_F^2 \cos^2\theta_C E_e E_\nu \left[(1+3C_A^2) + \beta_e(1-C_A^2)\cos\theta\right], \tag{2.67}$$

where θ is the angle between the electron and neutrino and $\beta_e = p_e/E_e$. The decay rate is then given by

$$\begin{aligned}\Gamma_n &= \int \frac{d^3p_e}{2E_e(2\pi)^3}\frac{d^3p_\nu}{2E_\nu(2\pi)^3} 2\pi\delta(\Delta m_{np} - E_e - E_\nu)|\mathscr{M}_\beta|^2 \\ &= \frac{G_F^2\cos^2\theta_C(1+3C_A^2)}{2\pi^3}\int_{m_e}^{\Delta m_{np}} dE_e E_e p_e E_\nu p_\nu \\ &\sim \frac{1.7m_e^5 G_F^2\cos^2\theta_C(1+3C_A^2)}{2\pi^3},\end{aligned} \tag{2.68}$$

where $\Delta m_{np} = m_n - m_p$ and the factor $1.7m_e^5$ came from the integration. The measured neutron lifetime $\tau_n = 1/\Gamma_n = 880\,\mathrm{s}$ is consistent with the expectation from the above discussions.

In nuclear β-decays, the electron in the final state is attracted by the positive charge of the final state nucleus and the decay rate is modified as follows:

$$\Gamma_A = \frac{G_F^2\cos^2\theta_C(\langle 1\rangle^2 + C_A^2\langle\sigma\rangle^2)}{2\pi^3}\int_{m_e}^{\Delta E_{if}} dE_e E_e p_e E_\nu p_\nu F(E_e, Z), \tag{2.69}$$

where $\Delta E_{if} = E_i - E_f$ and $\langle 1\rangle$ and $\langle\sigma\rangle$ terms are called the Fermi (spin non-flip) and the Gamow-Teller (spin-flip) matrix elements, respectively. $F(E_e, Z)$ corresponds to the correction factor for the final state Coulomb interactions, called the Fermi function, given by

$$F(E_e, Z) = 2(1+\xi)(2p_eR)^{2(\xi-1)}e^{\pi\zeta}\frac{|\Gamma(\xi+i\zeta)|^2}{|\Gamma(2\xi+1)|^2}, \tag{2.70}$$

where R is the radius of the nucleus, $\xi = \sqrt{1-\alpha^2Z^2}$ and $\zeta = \frac{Z\alpha E_e}{p_e}$. The Fermi function can be simplified for the nonrelativistic case as

$$F(E, Z) \sim \frac{2\pi\zeta}{1-e^{-2\pi\zeta}}. \tag{2.71}$$

The neutrino energy spectrum is, then,

$$\frac{d\Gamma_A}{dE_\nu} \propto E_\nu^2(\Delta E_{if} - E_\nu)\sqrt{(\Delta E_{if} - E_\nu)^2 - m_e^2}F(E_e, Z). \tag{2.72}$$

2.4.4 νe^- *Scatterings*

The neutrino-electron elastic scatterings are used for detection of solar neutrinos. In this section, those scattering cross sections are reviewed.

The description starts with $\nu_\mu e^-$ scattering since it involves a single reaction diagram. Then the other scattering cross sections are calculated making use of the formula developed for the $\nu_\mu e^-$ scattering. Those scattering processes include only leptons and the cross sections can be calculated precisely.

2.4.4.1 $\nu_\mu + e^- \rightarrow \nu_\mu + e^-$ Scattering

The Feynman diagram of $\nu_\mu + e^- \rightarrow \nu_\mu + e^-$ scattering process is shown in Fig. 2.11. The target electron is supposed to be at rest. The matrix element of the scattering is, from (2.40), given by

$$\begin{aligned}\mathscr{M}_{\nu_\mu e} &= 2\sqrt{2}G_F[\overline{\nu_{\mu L}(k_f)}\gamma_\rho \nu_{\mu L}(k_i)][\overline{e(p_e)}\gamma^\rho(C_{eL}\gamma_L + C_{eR}\gamma_R)e(m_e, \mathbf{0})] \\ &= 2\sqrt{2}G_F[\overline{\nu_{\mu L}}\gamma_\rho \nu_{\mu L}]\left(C_{eL}[\overline{e_L}\gamma^\rho e_L] + C_{eR}[\overline{e_R}\gamma^\rho e_R]\right),\end{aligned} \tag{2.73}$$

where the $e - Z^0$ coupling coefficients are, from Table 2.2,

$$C_{eR} = 2\sin^2\theta_W, \quad C_{eL} = -1 + 2\sin^2\theta_W, \tag{2.74}$$

respectively. The cross section is proportional to the absolute square of the scattering amplitude and is expressed by

$$\sigma_{\nu e} \propto C_{eL}^2((k_f+p_e)^2-m_e^2)^2+C_{eR}^2((k_i-p_e)^2-m_e^2)^2+C_{eL}C_{eR}m_e^2(k_f-k_i)^2. \tag{2.75}$$

From the detailed calculation, the differential cross section is given by

$$\frac{d\sigma_{\nu_\mu e}}{dy} = \sigma_{\nu e}^0(k_i)\left(C_{eL}^2 + C_{eR}^2(1-y)^2 - C_{eL}C_{eR}\varepsilon y\right), \tag{2.76}$$

where T_e is the kinetic energy of the recoiled electron, $y = T_e/k_i$ and $\varepsilon = m_e/k_i$. $\sigma_{\nu e}^0(k_i)$ is a reference νe scattering cross section expressed by

$$\sigma_{\nu e}^0(k_i) \equiv \frac{2G_F^2 m_e k_i}{\pi} \sim 1.7 \times 10^{-44}(k_i/\mathrm{MeV})\ \mathrm{cm}^2. \tag{2.77}$$

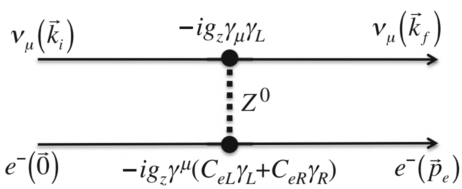

Fig. 2.11 Feynman diagram of $\nu_\mu e^-$ scattering

The total cross section can be calculated by integrating the differential cross section (2.76) and is given by

$$\sigma_{\nu_\mu e} = \int_0^{y_{\rm MAX}} \frac{d\sigma_{\nu_{\mu e}}}{dy} dy = \sigma^0_{\nu e}(k_i)\left(C_{e\rm L}^2 + \frac{1}{3}C_{e\rm R}^2 - \frac{1}{2}C_{e\rm L}C_{e\rm R}\varepsilon\right), \tag{2.78}$$

where $y_{\rm MAX} = \frac{1}{1+(m_e/2k_i)}$ corresponds to the maximum kinetic energy that the recoil electron can have. If we ignore the third term in (2.78), the total cross section is approximately given by

$$\sigma_{\nu_\mu e} = 1.55 \times 10^{-45}(k_i/\mathrm{MeV})\ \mathrm{cm}^2. \tag{2.79}$$

The cross section is proportional to the incident neutrino energy k_i.

Since the electron density in the water is $\sim 3 \times 10^{23}/\mathrm{cm}^3$, the mean free path of 10 MeV neutrinos for $\nu_\mu - e$ scattering in water is two light years.

2.4.4.2 $\overline{\nu}_\mu + e^- \rightarrow \overline{\nu}_\mu + e^-$ Scattering

Figure 2.12 shows the Feynman diagram of $\overline{\nu}_\mu e^-$ scattering. Since only $\overline{\nu}_{\mu R}$ interacts, the matrix element of the scattering is written by

$$\mathcal{M}_{\overline{\nu}_\mu e} = 2\sqrt{2}G_F[\overline{\overline{\nu}_{\mu\rm R}}\gamma_\rho\overline{\nu}_{\mu\rm R}](C_{e\rm L}[\overline{e_{\rm L}}\gamma^\rho e_{\rm L}] + C_{e\rm R}[\overline{e_{\rm R}}\gamma^\rho e_{\rm R}]). \tag{2.80}$$

The antineutrino wave function in Eq. (2.80) can be rewritten using the negative energy neutrino wave function as follows:

$$\mathcal{M}_{\overline{\nu}_\mu e} = 2\sqrt{2}G_F[\overline{\nu_{\mu\rm L}(-k_i)}\gamma_\rho\nu_{\mu\rm L}(-k'_f)]\left(C_{e\rm L}[\overline{e_{\rm L}}\gamma^\rho e_{\rm L}] + C_{e\rm R}[\overline{e_{\rm R}}\gamma^\rho e_{\rm R}]\right). \tag{2.81}$$

This amplitude is obtained by the substitution of the neutrino momentum $k_f \leftrightarrow -k_i$ in Eq. (2.73). Therefore, the cross section for the matrix element (2.80) can also be obtained from the same substitution in the $\nu_\mu e$ cross section formula of (2.75):

$$\sigma_{\overline{\nu}_\mu e} \propto C_{e\rm L}^2((p_e - k_i)^2 - m_e^2)^2 + C_{e\rm R}^2((k_f + p_e)^2 - m_e^2)^2 + C_{e\rm L}C_{e\rm R}m_e^2(k_f - k_i)^2. \tag{2.82}$$

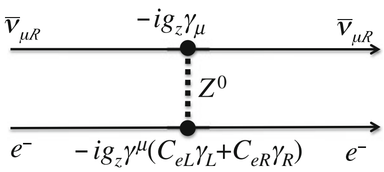

Fig. 2.12 Feynman diagram of $\overline{\nu}_\mu e^-$ scattering

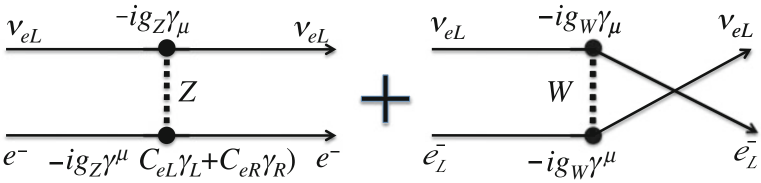

Fig. 2.13 The Feynman diagram of $\nu_e e^-$ scattering. The neutral and charged current diagrams have to be added

This is exactly the same formula obtained by substituting $C_{e\mathrm{R}} \leftrightarrow C_{e\mathrm{L}}$ in (2.75). Therefore, the form of the $\overline{\nu}_\mu e^-$ cross section is equivalent to the forms of the $\nu_\mu e^-$ cross section, (2.76) and (2.78), after substituting

$$(C_{e\mathrm{L}},\ \ C_{e\mathrm{R}}) \ \ \rightarrow \ \ (C_{e\mathrm{R}},\ \ C_{e\mathrm{L}}). \tag{2.83}$$

2.4.4.3 $\nu_e + e^- \rightarrow \nu_e + e^-$ Scattering

For the $\nu_e e^-$ scattering, the contribution from the charged current scattering has to be added to the neutral current scattering amplitude as shown in Fig. 2.13. The matrix element of this scattering is then given by

$$\mathscr{M}_{\nu_e e} = 2\sqrt{2}G_F\left([\,\overline{\nu_{e\mathrm{L}}}\gamma_\rho\nu_{e\mathrm{L}}]\big(C_{e\mathrm{L}}[\overline{e_\mathrm{L}}\gamma^\rho e_\mathrm{L}] + C_{e\mathrm{R}}[\overline{e_\mathrm{R}}\gamma^\rho e_\mathrm{R}]\big) - [\overline{e_\mathrm{L}}\gamma_\rho\nu_{e\mathrm{L}}][\overline{\nu_{e\mathrm{L}}}\gamma^\rho e_\mathrm{L}]\right), \tag{2.84}$$

where the relative minus sign in the charged current term comes from the exchange of the two leptons. Making use of the Fierz identity,[6]

$$[\overline{e_\mathrm{L}}\gamma_\rho\nu_{e\mathrm{L}}][\overline{\nu_{e\mathrm{L}}}\gamma^\rho e_\mathrm{L}] = -[\overline{\nu_{e\mathrm{L}}}\gamma_\rho\nu_{e\mathrm{L}}][\overline{e_\mathrm{L}}\gamma^\rho e_\mathrm{L}], \tag{2.85}$$

equation (2.84) can be factorized as

$$\mathscr{M}_{\nu_e e} = 2\sqrt{2}G_F[\overline{\nu_{e\mathrm{L}}}\gamma_\rho\nu_{e\mathrm{L}}]\left((C_{e\mathrm{L}}+1)[\overline{e_\mathrm{L}}\gamma^\rho e_\mathrm{L}] + C_{e\mathrm{R}}[\overline{e_\mathrm{R}}\gamma^\rho e_\mathrm{R}]\right). \tag{2.86}$$

Therefore, the cross section can be obtained by substituting

$$(C_{e\mathrm{L}},\ C_{e\mathrm{R}}) \ \ \rightarrow \ \ (C_{e\mathrm{L}}+1,\ C_{e\mathrm{R}}), \tag{2.87}$$

in Eqs. (2.76) and (2.78).

[6] See Sect. 8.1.6 and the solution of the Problem 13.9 in [4, Chap. 1].

2.4.4.4 $\overline{\nu}_e + e^- \rightarrow \overline{\nu}_e + e^-$ Scattering

The Feynman diagram for $\overline{\nu}_e e^-$ scattering is shown in Fig. 2.14. The matrix element of the scattering is given by

$$\mathscr{M}_{\overline{\nu}_e e} = 2\sqrt{2}G_F\Big([\overline{\overline{\nu}_{e\mathrm{R}}}\gamma_\rho\overline{\nu}_{e\mathrm{R}}](C_{e\mathrm{L}}[\overline{e_\mathrm{L}}\gamma^\rho e_\mathrm{L}] + C_{e\mathrm{R}}[\overline{e_\mathrm{R}}\gamma^\rho e_\mathrm{R}]) - [\overline{e_\mathrm{L}}\gamma_\rho\overline{\nu}_{e\mathrm{R}}][\overline{\overline{\nu}_{e\mathrm{R}}}\gamma^\rho e_\mathrm{L}]\Big). \tag{2.88}$$

As in the previous subsection, this amplitude can be rewritten using the negative energy neutrino wave function.

$$\mathscr{M}_{\overline{\nu}_e e} = 2\sqrt{2}G_F\left\{\begin{array}{l}[\overline{\nu_{e\mathrm{L}}(-k_i)}\gamma_\rho\nu_{e\mathrm{L}}(-k_f)]\left(C_{e\mathrm{L}}[\overline{e_\mathrm{L}}\gamma^\rho e_\mathrm{L}] + C_{e\mathrm{R}}[\overline{e_\mathrm{R}}\gamma^\rho e_\mathrm{R}]\right)\\ +[\overline{e_\mathrm{L}}\gamma_\rho\nu_{e\mathrm{L}}(-k_f)][\overline{\nu_{e\mathrm{L}}(-k_i)}\gamma^\rho e_\mathrm{L}]\end{array}\right\}. \tag{2.89}$$

Applying the Fierz identity again,

$$\mathscr{M}_{\overline{\nu}_e e} = 2\sqrt{2}G_F[\overline{\nu_{e\mathrm{L}}(-k_i)}\gamma_\rho\nu_{e\mathrm{L}}(-k_f)]\left((C_{e\mathrm{L}}+1)[\overline{e_\mathrm{L}}\gamma^\rho e_\mathrm{L}] + C_{e\mathrm{R}}[\overline{e_\mathrm{R}}\gamma^\rho e_\mathrm{R}]\right). \tag{2.90}$$

The cross section can be obtained by substituting

$$(C_{e\mathrm{L}},\ C_{e\mathrm{R}}) \quad\rightarrow\quad (C_{e\mathrm{R}},\ C_{e\mathrm{L}}+1), \tag{2.91}$$

in Eqs. (2.76) and (2.78).

2.4.4.5 Summary of νe Scattering Cross Sections

As we saw, various neutrino-electron scattering modes can be treated with the same formula. The difference is the coefficients of the electron currents. In summary, the general νe scattering cross section forms for $d\sigma_{\nu e}/dy$ and $\sigma_{\nu e}$ are

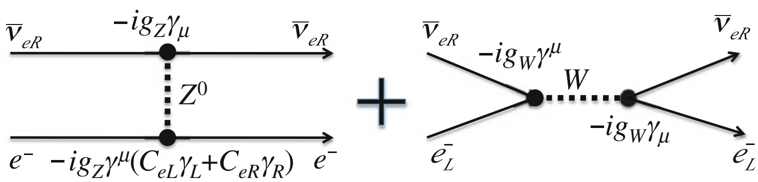

Fig. 2.14 The Feynman diagram of $\overline{\nu}_e e^-$ scattering. The neutral and charged current diagrams have to be added

$$\begin{aligned} \frac{d\sigma_{\nu e}}{dy} &= \sigma^0_{\nu e}(k_i)\left(g_L^2 + g_R^2(1-y)^2 - g_L g_R \varepsilon y\right), \\ \sigma_{\nu e} &= \sigma^0_{\nu e}(k_i)\left(g_L^2 + \frac{1}{3}g_R^2 - \frac{1}{2}g_L g_R \varepsilon\right). \end{aligned} \tag{2.92}$$

The reference νe cross section $\sigma^0_{\nu e}(k_i)$ is shown in Eq. (2.77). The effective coupling coefficients $g_{L/R}$ for various νe scattering modes are summarized in Table 2.3. The energy spectra of the νe scatterings for $k_i = 10\,\text{MeV}$ neutrinos are shown in Fig. 2.15.

The numerical total cross sections for the νe scatterings are summarized in Eq. (2.93).

$$\begin{cases} \sigma_{\nu_\mu e^-} = \sigma_{\nu_\tau e^-} \sim 1.55 \times 10^{-45}(k_i/\text{MeV})\ \text{cm}^2, \\ \sigma_{\overline{\nu}_\mu e^-} = \sigma_{\overline{\nu}_\tau e^-} \sim 1.34 \times 10^{-45}(k_i/\text{MeV})\ \text{cm}^2, \\ \qquad\qquad \sigma_{\nu_e e^-} \sim 9.52 \times 10^{-45}(k_i/\text{MeV})\ \text{cm}^2, \\ \qquad\qquad \sigma_{\overline{\nu}_e e^-} \sim 3.99 \times 10^{-45}(k_i/\text{MeV})\ \text{cm}^2. \end{cases} \tag{2.93}$$

Table 2.3 Z^0-fermion coupling coefficients $x_W = \sin^2\theta_W \sim 0.23$ is used for the numerical calculations

Mode	g_L	g_R	$g_L^2 + \frac{1}{3}g_R^2$	$\frac{1}{2}g_L g_R$
$\nu_\mu e^-$, $\nu_\tau e^-$	$-1+2x_W$	$2x_W$	0.36	0.12
$\overline{\nu}_\mu e^-$, $\overline{\nu}_\tau e^-$	$2x_W$	$-1+2x_W$	0.31	0.25
$\nu_e e^-$	$1+2x_W$	$2x_W$	2.1	0.34
$\overline{\nu}_e e^-$	$2x_W$	$1+2x_W$	0.93	0.34

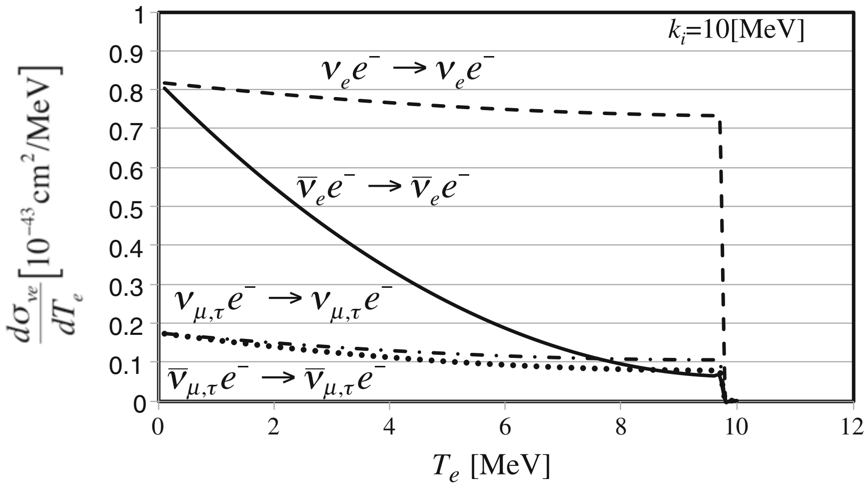

Fig. 2.15 Energy spectra of νe^- scatterings for incident neutrino energy $k_i = 10\,\text{MeV}$

Since there is the following relation between the electron scattering angle and kinetic energy,

$$T_e = m_e \frac{2\cos^2\theta}{\varepsilon(2+\varepsilon)+\sin^2\theta}, \tag{2.94}$$

the differential cross section as a function of the scattering angle is

$$\frac{d\sigma_{\nu e}}{d\cos\theta_e} = 4\sigma^0_{\nu e}\varepsilon(1+\varepsilon)^2 \\ \times \cos\theta(F(\theta))^2(g_\mathrm{L}^2 + g_\mathrm{R}^2(1-2\varepsilon\cos^2\theta F(\theta))^2 - 2g_\mathrm{L}g_\mathrm{R}\varepsilon^2\cos^2\theta F(\theta)), \tag{2.95}$$

where

$$F(\theta) = \frac{1}{\varepsilon(\varepsilon+2)+\sin^2\theta}. \tag{2.96}$$

For $k_i \gg m_e$, the electrons are scattered forward with width of $\delta\theta \sim \sqrt{\varepsilon}$. Figure 2.16 shows the $\cos\theta$ distribution of the scattered electron for $k_i = 5$ and 10 MeV.

2.4.5 *Inverse* β *Decay*

The inverse process of the β decay,

$$\overline{\nu}_e + {}^{Z}A \rightarrow e^+ + {}^{(Z-1)}A, \tag{2.97}$$

is called the *inverse* β *decay* (IBD) reaction. The IBD reaction for the proton target,

$$\overline{\nu}_e + p \rightarrow e^+ + n, \tag{2.98}$$

is often used to detect reactor neutrinos. The cross section of the low energy IBD reaction is more accurately known than those of other neutrino-nucleus interactions.

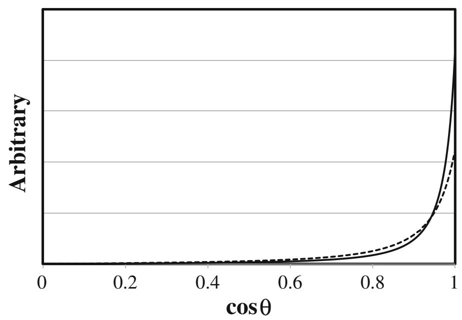

Fig. 2.16 The $\cos\theta$ distribution of electron in νe scattering. The *solid line* is for $k_i = 10$ MeV and the *dashed line* is for $k_i = 5$ MeV

Fig. 2.17 Diagram of the inverse beta decay reaction

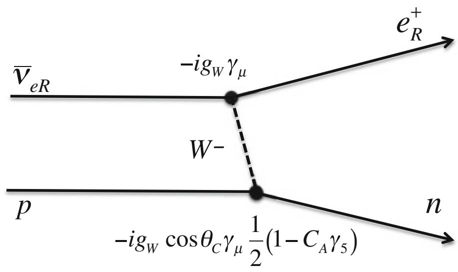

Figure 2.17 shows the diagram of the IBD reaction. The matrix element of the IBD reaction can be written as the same form as Eq. (2.66) and is given by

$$\mathcal{M}_{\text{IBD}} = \sqrt{2}G_F \cos\theta_{\text{C}}[\overline{e_{\text{L}}}\gamma^{\mu}\nu_{e\text{L}}][\overline{n}\gamma_{\mu}(1 - C_{\text{A}}\gamma_5)p]. \tag{2.99}$$

From this matrix element and the neutron decay width (2.68), the IBD cross section can be related to the neutron lifetime τ_n as

$$\begin{aligned}\sigma_{\text{IBD}}(E_\nu) &= \frac{G_F^2(1+3C_{\text{A}}^2)\cos^2\theta_{\text{C}}}{\pi}E_e p_e = \frac{2\pi^2}{1.7m_e^5\tau_n}E_e p_e \\ &\sim 1.0\times 10^{-43}(E_\nu - \Delta m_{np})\sqrt{(E_\nu - \Delta m_{np})^2 - m_e^2}\ \text{cm}^2,\end{aligned} \tag{2.100}$$

where the masses and energies are expressed in MeV and $\Delta m_{np} = m_n - m_p = 1.29$ MeV. The energy dependence of the cross section is shown in Fig. 5.32. The momentum transfer is small for reactor neutrino detection, since the typical neutrino energy is $\sim$4 MeV. Therefore, radiative and recoil corrections are small and the uncertainty is dominated by the error of the neutron lifetime measurement.

Chapter 3
Particle Oscillations

Abstract The formalism of neutrino oscillation has complicate issues. For instance, neutrinos always move ultrarelativistically in actual experimental conditions and the oscillation occurs among the three flavors. In this chapter, before going into the detail of the neutrino oscillation, we will understand the oscillations of simple cases of two flavor particles at rest. First, the Schrödinger equation of two flavor particles is understood as a differential equation that defines the time development of the basis states due to flavor-transition amplitudes. The time-dependent wave functions are derived as general solutions to the Schrödinger equation. The wave functions for mass eigenstates and flavor eigenstates are obtained by choosing initial conditions in the general wave function. The probability of the flavor oscillation is calculated from the wave function which started from a specific flavor state at time $t = 0$. The oscillation phenomena are also described as the interference between the diagrams which have the same initial flavor states and the same final flavor states but different intermediate mass eigenstates. In the course of these considerations, the relation among the mass, the mixing and the flavor oscillation becomes clear.

Keywords Mass eigenstate · Flavor eigenstate · Quantum oscillation · Transition amplitude · Mixing matrix · Neutrino interference

3.1 Introduction

Neutrino flavors such as ν_e, ν_μ or ν_τ are defined as the states which transforms to e, μ or τ, respectively via the charged current weak interactions and they are called *weak eigenstates* or *flavor eigenstates*. Since neutrinos interact only via the weak interactions, neutrinos are always produced and detected as the flavor eigenstate in experiments.

Neutrino oscillation is a phenomenon in which a certain flavor neutrino ν_α periodically changes to other flavor neutrino ν_β and vice versa. This phenomenon is caused by *transition amplitude* between ν_α and ν_β. Due to the transition amplitude, the flavor eigenstates no longer have fixed masses and become superpositions of the *mass eigenstates*.

An important purpose of the neutrino oscillation experiments is to measure the transition amplitudes via the oscillation parameters and study the origin of the

F. Suekane, *Neutrino Oscillations*, Lecture Notes in Physics 898,
DOI 10.1007/978-4-431-55462-2_3

transition. The quark transition amplitudes are understood to come from the Yukawa coupling between the quarks and the Higgs field in the standard model. However, the origin of the neutrino transition amplitudes is not understood yet.

In the following two chapters, the neutrino oscillation formulas are derived and the resulting phenomena are studied. We start with the non-relativistic two flavor oscillations in this chapter and then proceed to the ultrarelativistic three flavor neutrino oscillations in next chapter. Subjects which are related to the neutrino oscillations, such as the matter effect, CP violation in the lepton sector, a paradox of the measurement problem, etc. are also described.

3.2 Mass in Quantum Mechanics

In the standard model, the neutrino is assumed to be massless. However, from the discovery of neutrino oscillation, neutrinos are known to have non-zero masses now. In quantum mechanics, the time development of the wave function of a particle at rest with mass m is described by the equation,

$$\frac{d}{dt}\psi(t) = -im\psi(t), \tag{3.1}$$

where $\psi(t)$ is the wave function of the particle. The solution of Eq. (3.1) is given by

$$\psi(t) = \psi(0)e^{-imt}. \tag{3.2}$$

Another way to express the wave function is to use the Dirac *ket* vectors.

$$|\psi(t)\rangle = C(t)\,|\psi\rangle\,, \tag{3.3}$$

where $|\psi\rangle$ is the stationary basis state and $C(t)$ shows the time dependence of the state. The normalization condition of the wave function requires the following relation,

$$|\psi(t)|^2 = \langle\psi(t)|\psi(t)\rangle = |C(t)|^2\,\langle\psi|\psi\rangle = |C(t)|^2 = 1, \tag{3.4}$$

where $\langle\psi|$ is the Dirac *bra* vector and $\langle\psi|\psi\rangle = 1$ is used. Equation (3.1) and its solution (3.2) can be equivalently expressed by using the coefficient $C(t)$ as follows:

$$\text{Eq. (3.1)} \to \quad \dot{C}(t) = -imC(t), \tag{3.5}$$

$$\text{Eq. (3.2)} \to \quad C(t) = e^{-imt}C(0). \tag{3.6}$$

The time development of the coefficient, after infinitesimal time δt, can be expressed using Eq. (3.5) as

$$C(t+\delta t) = C(t) + \dot{C}(t)\delta t = (1 - im\delta t)C(t). \tag{3.7}$$

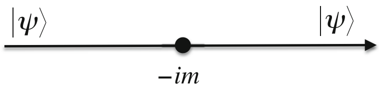

Fig. 3.1 *Transition diagram* which shows the effect of the mass. The diagram means that an imaginary state $-im|\psi(t)\rangle$ is added to the original wave function $|\psi(t)\rangle$ per unit time

This relation means that as time passes, an imaginary component $-im|\psi(t)\rangle$ is added to the original state $|\psi(t)\rangle$ per unit time due to the mass. The basis vector at time $t + \delta t$ is then,

$$|\psi(t + \delta t)\rangle \equiv C(t + \delta t)\,|\psi\rangle = (1 - im\delta t)C(t)\,|\psi\rangle = (1 - im\delta t)\,|\psi(t)\rangle. \quad (3.8)$$

In order to express this effect graphically, we will use the diagram shown in Fig. 3.1 and call it a "*transition diagram*" in this text.[1]

3.3 Two Flavor Oscillation at Rest

3.3.1 Transition Amplitudes

In order to understand various properties of oscillations, first we consider a particle of two flavor states, $|\alpha\rangle$ and $|\beta\rangle$, at rest.[2] The wave function $\psi(t)$ for this system can be written by a superposition of the two basis states,

$$|\psi(t)\rangle = C_\alpha(t)\,|\alpha\rangle + C_\beta(t)\,|\beta\rangle\,, \quad (3.9)$$

where $|\alpha\rangle$ and $|\beta\rangle$ satisfy the normalization conditions $\langle\alpha|\alpha\rangle = 1$, $\langle\beta|\beta\rangle = 1$ and the orthogonality condition $\langle\alpha|\beta\rangle = \langle\beta|\alpha\rangle^* = 0$. The absolute squares of the coefficients, $|C_\alpha(t)|^2$ and $|C_\beta(t)|^2$ correspond to the probability of finding states $|\alpha\rangle$ and $|\beta\rangle$ at time t, respectively, and the normalization condition for the coefficients is

$$|\psi(t)|^2 = \langle\psi(t)|\psi(t)\rangle = |C_\alpha(t)|^2 + |C_\beta(t)|^2 = 1. \quad (3.10)$$

The wave function (3.9) can also be expressed in the matrix form

$$\psi(t) = \begin{pmatrix} C_\alpha(t) \\ C_\beta(t) \end{pmatrix}, \quad (3.11)$$

by defining the basis states as

$$|\alpha\rangle = \begin{pmatrix} 1 \\ 0 \end{pmatrix}, \qquad |\beta\rangle = \begin{pmatrix} 0 \\ 1 \end{pmatrix}. \quad (3.12)$$

We will use the expressions in Eqs. (3.9) and (3.11) equivalently.

[1] This is not a Feynman diagram.

[2] The (α, β) can be $(K^0, \overline{K^0})$, (d', s'), (W_3, B) or (ν_μ, ν_e), etc.

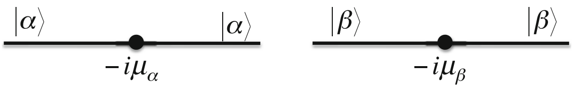

Fig. 3.2 Transition diagrams showing the two independent states $|\alpha\rangle$ and $|\beta\rangle$

In general, the Schrödinger equation with interactions is expressed by

$$\frac{d}{dt}\psi(t) = -i(H_0 + H_I)\psi(t), \tag{3.13}$$

where H_0 is the mass term and the H_I is the interaction Hamiltonian. For two component states, the mass term can be written in 2×2 matrix form as

$$H_0 = \begin{pmatrix} \mu_\alpha & 0 \\ 0 & \mu_\beta \end{pmatrix}, \tag{3.14}$$

where μ_α and μ_β are the masses of the $|\alpha\rangle$ and $|\beta\rangle$ states in the case where $H_I = 0$. In this case, the Schrödinger equation (3.13) reduces to the two separate equations

$$\begin{cases} \dot{C}_\alpha(t) = -i\mu_\alpha C_\alpha(t) \\ \dot{C}_\beta(t) = -i\mu_\beta C_\beta(t). \end{cases} \tag{3.15}$$

We can immediately solve (3.15) and obtain

$$\begin{cases} C_\alpha(t) = C_\alpha(0)e^{-i\mu_\alpha t} \\ C_\beta(t) = C_\beta(0)e^{-i\mu_\beta t}. \end{cases} \tag{3.16}$$

Therefore, the wave function is written as

$$|\psi(t)\rangle = C_\alpha(0)e^{-i\mu_\alpha t}\,|\alpha\rangle + C_\beta(0)e^{-i\mu_\beta t}\,|\beta\rangle\,. \tag{3.17}$$

This means that the two states $|\alpha\rangle$ and $|\beta\rangle$ with masses μ_α and μ_β exist independently in the system. The transition diagram for the two independent systems can be shown as in Fig. 3.2.

In some situations, there are interactions which transform $|\alpha\rangle$ to $|\beta\rangle$, and vice versa,[3]

$$|\alpha\rangle \;\Leftrightarrow\; |\beta\rangle\,. \tag{3.18}$$

The transition diagram between the different flavors is shown in Fig. 3.3, where τ represents the strength of the transition. We refer this τ as the *transition amplitude* in

[3] For example, $K^0 \Leftrightarrow \overline{K^0}$, $d' \Leftrightarrow s'$, $B \Leftrightarrow W_3$ or $\nu_\mu \Leftrightarrow \nu_e$.

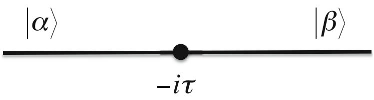

Fig. 3.3 Cross-transition amplitude between $|\alpha\rangle$ and $|\beta\rangle$

this text. Due to the transition, the coefficients of the basis states $|\alpha\rangle$ and $|\beta\rangle$ change as in Eq. (3.19) after infinitesimal time δt,

$$\begin{cases} C_\alpha(t+\delta t) = C_\alpha(t) - i\tau\delta t C_\beta(t) \\ C_\beta(t+\delta t) = C_\beta(t) - i\tau\delta t C_\alpha(t). \end{cases} \tag{3.19}$$

The wave function at $t + \delta t$ is, from (3.9),

$$\begin{aligned} |\psi(t+\delta t)\rangle &= C_\alpha(t+\delta t)\,|\alpha\rangle + C_\beta(t+\delta t)\,|\beta\rangle \\ &= C_\alpha(t)(|\alpha\rangle - i\tau\delta t\,|\beta\rangle) + C_\beta(t)(|\beta\rangle - i\tau\delta t\,|\alpha\rangle). \end{aligned} \tag{3.20}$$

This means we can interpret that the basis vector changes depending on time;

$$\begin{cases} |\alpha(t+\delta t)\rangle = |\alpha(t)\rangle - i\tau\delta t\,|\beta(t)\rangle \\ |\beta(t+\delta t)\rangle = |\beta(t)\rangle - i\tau\delta t\,|\alpha(t)\rangle\,. \end{cases} \tag{3.21}$$

Both points of view for the time development of the wave function, (3.19) and (3.21), are equivalent.

For $\delta t \to 0$, Eq. (3.19) is equivalent to the following differential equation,

$$\frac{d}{dt}\begin{pmatrix} C_\alpha(t) \\ C_\beta(t) \end{pmatrix} = -i\begin{pmatrix} 0 & \tau \\ \tau & 0 \end{pmatrix}\begin{pmatrix} C_\alpha(t) \\ C_\beta(t) \end{pmatrix}. \tag{3.22}$$

The transition matrix corresponds to the interaction Hamiltonian H_I defined in Eq. (3.13),

$$H_I = \begin{pmatrix} 0 & \tau \\ \tau & 0 \end{pmatrix}. \tag{3.23}$$

Comparing Figs. 3.2 and 3.3, the mass corresponds to the transition amplitude to the original flavor. We will call the transition in Fig. 3.2 *self transition* and that in Fig. 3.3 *cross transition* in this text.

In order to see the effect of the cross transitions, we set $H_0 = 0$ in (3.13). The Schrödinger equation becomes Eq. (3.22) and we obtain the following separate differential equations,

$$\begin{cases} \frac{d}{dt}(C_\alpha(t) + C_\beta(t)) = -i\tau(C_\alpha(t) + C_\beta(t)), \\ \frac{d}{dt}(C_\alpha(t) - C_\beta(t)) = i\tau(C_\alpha(t) - C_\beta(t)). \end{cases} \tag{3.24}$$

These equations can be solved to give

$$\begin{cases} C_\alpha(t) + C_\beta(t) = (C_\alpha(0) + C_\beta(0))e^{-i\tau t} \\ C_\alpha(t) - C_\beta(t) = (C_\alpha(0) - C_\beta(0))e^{i\tau t}. \end{cases} \tag{3.25}$$

By defining

$$\begin{pmatrix} C_- \\ C_+ \end{pmatrix} = \frac{1}{\sqrt{2}} \begin{pmatrix} 1 & -1 \\ 1 & 1 \end{pmatrix} \begin{pmatrix} C_\alpha(0) \\ C_\beta(0) \end{pmatrix}, \tag{3.26}$$

$C_\alpha(t)$ and $C_\beta(t)$ can separately be obtained as

$$\begin{cases} C_\alpha(t) = \frac{1}{\sqrt{2}}(C_+ e^{-i\tau t} + C_- e^{i\tau t}) \\ C_\beta(t) = \frac{1}{\sqrt{2}}(C_+ e^{-i\tau t} - C_- e^{i\tau t}). \end{cases} \tag{3.27}$$

Therefore, the wave function (3.9) can be written as

$$\begin{aligned} |\psi(t)\rangle &= \frac{1}{\sqrt{2}}(C_+ e^{-i\tau t} + C_- e^{i\tau t})\,|\alpha\rangle + \frac{1}{\sqrt{2}}(C_+ e^{-i\tau t} - C_- e^{i\tau t})\,|\beta\rangle \\ &= \frac{|\alpha\rangle + |\beta\rangle}{\sqrt{2}} C_+ e^{-i\tau t} + \frac{|\alpha\rangle - |\beta\rangle}{\sqrt{2}} C_- e^{i\tau t}. \end{aligned} \tag{3.28}$$

The wave function shows various physical phenomena depending on the initial values of $C_{\alpha/\beta}(0)$ or $C_\pm$.

3.3.1.1 The Mass Eigenstate

If the initial values of the coefficients $C_\pm$ are given by

$$(C_-,\ C_+) = (0,\ 1) \quad \text{or} \quad (1,\ 0), \tag{3.29}$$

the corresponding wave functions are, from Eqs. (3.28),

$$|\psi_\pm(t)\rangle = |\pm\rangle\, e^{\mp i\tau t}, \tag{3.30}$$

where the basis states $|\pm\rangle$ are defined by

$$\begin{pmatrix} |-\rangle \\ |+\rangle \end{pmatrix} = \frac{1}{\sqrt{2}} \begin{pmatrix} 1 & -1 \\ 1 & 1 \end{pmatrix} \begin{pmatrix} |\alpha\rangle \\ |\beta\rangle \end{pmatrix}. \tag{3.31}$$

Equation (3.30) means that the basis states $|\pm\rangle$ correspond to the mass eigenstates with masses of

$$m_\pm = \pm\tau, \tag{3.32}$$

respectively. Equation (3.31) shows that the mass eigenstate is a mixture of the flavor eigenstates and vice versa. The matrix in Eq. (3.31) is called the *mixing matrix*. An important remark from this example is that *the transition amplitude* τ *between different flavors becomes the mass of the particle* in the end.

3.3.1.2 Flavor Eigenstate and Oscillation

If the system is in the pure $|\alpha\rangle$ state at $t = 0$, the initial condition is

$$(C_\alpha(0),\ \ C_\beta(0)) = (1,\ 0), \quad \text{or} \quad (C_-,\ C_+) = (1/\sqrt{2},\ 1/\sqrt{2}). \tag{3.33}$$

In this case, the wave function (3.28) is determined to be,

$$|\psi(t)\rangle = \cos\tau t\,|\alpha\rangle - i\sin\tau t\,|\beta\rangle\,. \tag{3.34}$$

This shows that state $|\beta\rangle$ is spontaneously generated and the probability of finding the flavor $|\beta\rangle$ at time t is

$$P_{\alpha\to\beta}(t) = |\,\langle\beta|\psi(t)\rangle\,|^2 = \sin^2\tau t. \tag{3.35}$$

This is the simplest example of particle oscillation. Since Eq. (3.32) gives a relation $\tau = (m_+ - m_-)/2$, the oscillation probability (3.35) can also be expressed as

$$P_{\alpha\to\beta}(t) = \sin^2\frac{m_+ - m_-}{2}t. \tag{3.36}$$

The angular velocity of the oscillation corresponds to the mass difference.[4]

3.3.2 General Hamiltonian and Mass Eigenstate

We consider here the general two component Schrödinger equation with finite H_0 and H_I. From the explicit form of the Hamiltonians (3.14) and (3.23), the Schrödinger equation (3.13) is written as,

$$\frac{d}{dt}\begin{pmatrix} C_\alpha \\ C_\beta \end{pmatrix} = -i\begin{pmatrix} \mu_\alpha & \tau \\ \tau & \mu_\beta \end{pmatrix}\begin{pmatrix} C_\alpha \\ C_\beta \end{pmatrix}. \tag{3.37}$$

[4] In this particular case, $m_+ + m_- = 0$ and the oscillation probability can also be expressed as $P_{\alpha\to\beta}(t) = \sin^2 m_\pm t$. However, we will treat more general case later in which $m_+ + m_- \neq 0$. For such cases, Eq. (3.36) still holds.

Since Eq. (3.37) shows the internal state transition between $|\alpha\rangle$ and $|\beta\rangle$, we call it the *state equation* in this text. To solve the state equation, we split the Hamiltonian in Eq. (3.37) into the average mass and the transition terms,

$$\frac{d}{dt}\begin{pmatrix} C_\alpha \\ C_\beta \end{pmatrix} = -i\left[\bar{\mu}_{\alpha\beta}\begin{pmatrix} 1 & 0 \\ 0 & 1 \end{pmatrix} + \begin{pmatrix} -\Delta\mu_{\beta\alpha}/2 & \tau \\ \tau & \Delta\mu_{\beta\alpha}/2 \end{pmatrix}\right]\begin{pmatrix} C_\alpha \\ C_\beta \end{pmatrix}, \tag{3.38}$$

where $\bar{\mu}_{\alpha\beta}$ and $\Delta\mu_{\beta\alpha}$ are defined by

$$\bar{\mu}_{\alpha\beta} = \frac{\mu_\alpha + \mu_\beta}{2} \quad \text{and} \quad \Delta\mu_{\beta\alpha} = \mu_\beta - \mu_\alpha. \tag{3.39}$$

The average mass term represents the absolute mass scale and the transition term generates the oscillation. The solution for Eq. (3.38) can be factored into a plane wave component and an oscillation component, as given by

$$\begin{pmatrix} C_\alpha(t) \\ C_\beta(t) \end{pmatrix} = e^{-i\bar{\mu}_{\alpha\beta}t}\begin{pmatrix} B_\alpha(t) \\ B_\beta(t) \end{pmatrix}, \tag{3.40}$$

where $B_\alpha(t)$ and $B_\beta(t)$ are the solutions of

$$\frac{d}{dt}\begin{pmatrix} B_\alpha(t) \\ B_\beta(t) \end{pmatrix} = -i\begin{pmatrix} -\Delta\mu_{\beta\alpha}/2 & \tau \\ \tau & \Delta\mu_{\beta\alpha}/2 \end{pmatrix}\begin{pmatrix} B_\alpha(t) \\ B_\beta(t) \end{pmatrix}. \tag{3.41}$$

Normalizing the transition matrix, the equation (3.41) can be rewritten as follows:

$$\frac{d}{dt}\begin{pmatrix} B_\alpha \\ B_\beta \end{pmatrix} = -i\omega_\tau\begin{pmatrix} -\cos 2\theta & \sin 2\theta \\ \sin 2\theta & \cos 2\theta \end{pmatrix}\begin{pmatrix} B_\alpha \\ B_\beta \end{pmatrix}, \tag{3.42}$$

where ω_τ and θ are defined by

$$\omega_\tau = \sqrt{\left(\Delta\mu_{\beta\alpha}/2\right)^2 + \tau^2} \quad \text{and} \quad \tan 2\theta = \frac{2\tau}{\Delta\mu_{\beta\alpha}}. \tag{3.43}$$

As we will see later, θ and ω_τ are measurable parameters in oscillation experiments. θ is called the *mixing angle* and ω_τ corresponds to the angular velocity of the oscillation. Figure 3.4, which we call the *mixing triangle* in this text, shows the relations between these parameters and the transition amplitudes.

From Sect. 8.3, by using the unitary matrix

$$U = \begin{pmatrix} \cos\theta & \sin\theta \\ -\sin\theta & \cos\theta \end{pmatrix}, \tag{3.44}$$

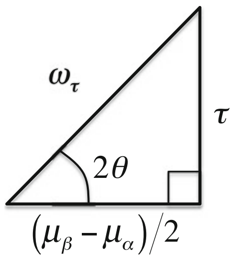

Fig. 3.4 The *mixing triangle* showing the relation between transition amplitudes (μ_α, μ_β, τ) and the oscillation parameters (θ, ω_τ)

we can show

$$U^\dagger \begin{pmatrix} -\cos 2\theta & \sin 2\theta \\ \sin 2\theta & \cos 2\theta \end{pmatrix} U = \begin{pmatrix} -1 & 0 \\ 0 & 1 \end{pmatrix}. \tag{3.45}$$

Therefore, applying $U^\dagger$ from the left, Eq. (3.42) becomes

$$\frac{d}{dt} U^\dagger \begin{pmatrix} B_\alpha \\ B_\beta \end{pmatrix} = -i\omega_\tau \begin{pmatrix} -1 & 0 \\ 0 & 1 \end{pmatrix} U^\dagger \begin{pmatrix} B_\alpha \\ B_\beta \end{pmatrix}. \tag{3.46}$$

The solution of Eq. (3.46) is

$$\begin{aligned} \begin{pmatrix} B_\alpha(t) \\ B_\beta(t) \end{pmatrix} &= U \begin{pmatrix} e^{i\omega_\tau t} & 0 \\ 0 & e^{-i\omega_\tau t} \end{pmatrix} U^\dagger \begin{pmatrix} B_\alpha(0) \\ B_\beta(0) \end{pmatrix} \\ &= \begin{pmatrix} e^{i\omega_\tau t} \cos^2\theta + e^{-i\omega_\tau t} \sin^2\theta & (e^{i\omega_\tau t} - e^{-i\omega_\tau t}) \cos\theta \sin\theta \\ (e^{i\omega_\tau t} - e^{-i\omega_\tau t}) \cos\theta \sin\theta & e^{i\omega_\tau t} \sin^2\theta + e^{-i\omega_\tau t} \cos^2\theta \end{pmatrix} \begin{pmatrix} B_\alpha(0) \\ B_\beta(0) \end{pmatrix}. \end{aligned} \tag{3.47}$$

The wave function becomes,

$$\begin{aligned} |\psi(t)\rangle &= (\cos\theta B_\beta(0) - \sin\theta B_\alpha(0))(\cos\theta\,|\beta\rangle - \sin\theta\,|\alpha\rangle) e^{-i(\bar{\mu}_{\alpha\beta}+\omega_\tau)t} \\ &\quad + (\cos\theta B_\alpha(0) + \sin\theta B_\beta(0))(\cos\theta\,|\alpha\rangle + \sin\theta\,|\beta\rangle) e^{-i(\bar{\mu}_{\alpha\beta}-\omega_\tau)t} \\ &= C_-\,|-\rangle\, e^{-im_- t} + C_+\,|+\rangle\, e^{-im_+ t}, \end{aligned} \tag{3.48}$$

where

$$\begin{pmatrix} |-\rangle \\ |+\rangle \end{pmatrix} = U \begin{pmatrix} |\alpha\rangle \\ |\beta\rangle \end{pmatrix}, \quad \begin{pmatrix} C_- \\ C_+ \end{pmatrix} = U \begin{pmatrix} B_\alpha(0) \\ B_\beta(0) \end{pmatrix}, \quad m_\pm = \bar{\mu}_{\alpha\beta} \pm \omega_\tau. \tag{3.49}$$

The basis states $|\pm\rangle$ are the mass eigenstates with masses $m_\pm$, respectively. Therefore, U corresponds to the mixing matrix because it mixes the mass eigenstates and the flavor eigenstates. It is noted that the coefficients for the mass eigenstates and the flavor eigenstates are connected with the same mixing matrix.

3.3.3 Flavor Oscillation

If we rewrite (3.48) in terms of the flavor eigenstates,

$$\begin{aligned} |\psi(t)\rangle = &(C_+ \sin\theta\, e^{-im_+t} + C_- \cos\theta\, e^{-im_-t})\, |\alpha\rangle \\ &+ (C_+ \cos\theta\, e^{-im_+t} - C_- \sin\theta\, e^{-im_-t})\, |\beta\rangle\, . \end{aligned} \tag{3.50}$$

If the system is in a pure $|\alpha\rangle$ state at time $t = 0$,

$$\begin{pmatrix} C_\alpha(0) \\ C_\beta(0) \end{pmatrix} = U \begin{pmatrix} C_- \\ C_+ \end{pmatrix} = \begin{pmatrix} 1 \\ 0 \end{pmatrix}. \tag{3.51}$$

In this case the flavor coefficients are,

$$\begin{pmatrix} C_\alpha(t) \\ C_\beta(t) \end{pmatrix} = \begin{pmatrix} \cos^2\theta\, e^{-im_-t} + \sin^2\theta\, e^{-im_+t} \\ \sin\theta\cos\theta\, (e^{-im_+t} - e^{-im_-t}) \end{pmatrix}. \tag{3.52}$$

The probability of finding the $|\beta\rangle$ state at time t is

$$P_{\alpha\to\beta}(t) = |\,\langle\beta|\psi(t)\rangle\,|^2 = |C_\beta(t)|^2 = \sin^2 2\theta \sin^2 \frac{m_+ - m_-}{2} t, \tag{3.53}$$

showing that the probability oscillates in time with the angular velocity $m_+ - m_- = 2\omega_\tau$[5] and amplitude $\sin^2 2\theta$. The mixing angle and oscillation frequency are independent of the absolute mass scale $\overline{\mu}_{\alpha\beta}$. This means that the absolute mass scale can not be measured by neutrino oscillations. From the mixing angle and oscillation frequency, a relative pattern of the transition amplitudes can be studied.

3.3.4 Oscillation as Interference

As shown in Fig. 3.5, the $|\alpha\rangle \to |\beta\rangle$ transition probability is calculated from the absolute square of the sum of the two indistinguishable diagrams in which the initial state is $|\alpha\rangle$ and the final state is $|\beta\rangle$. The diagram on the left in Fig. 3.5 shows that the mass eigenstate $|+\rangle$ propagates intermediately and the diagram on the right shows that $|-\rangle$ propagates intermediately. Those mass eigenstates acquire the phases of $e^{-im_\pm t}$ after the time t. Since the mass eigenstates and flavor eigenstates mix as

[5] $\sin^2 \frac{m_+ - m_-}{2} t = (1 - \cos(m_+ - m_-)t)/2$.

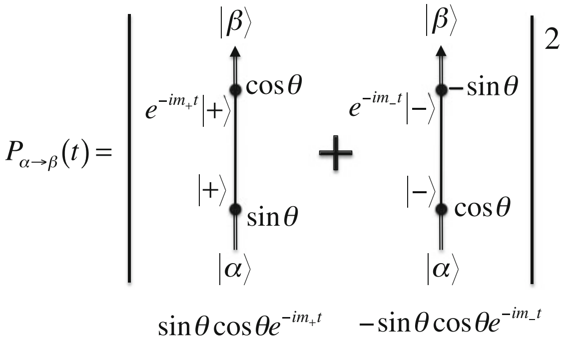

Fig. 3.5 The $|\alpha\rangle \to |\beta\rangle$ transition probability. The *left* diagram shows that $|+\rangle$ state propagates intermediately and the *right* diagram shows that $|-\rangle$ state propagates intermediately. The mass eigenstates acquire phases of $e^{-im_\pm t}$ as time passes

in Eq. (3.49), the $|+\rangle$ component of $|\alpha\rangle$ and $|\beta\rangle$ are $\sin\theta$ and $\cos\theta$, respectively. Therefore, the amplitude of the diagram on the left is

$$\mathscr{M}_+ = \sin\theta\cos\theta\, e^{-im_+t}. \tag{3.54}$$

Similarly, the amplitude of the diagram on the right is

$$\mathscr{M}_- = -\sin\theta\cos\theta\, e^{-im_-t}. \tag{3.55}$$

The oscillation probability is the absolute square of the sum of the two amplitudes,

$$P_{\alpha\to\beta}(t) = |\mathscr{M}_+(t) + \mathscr{M}_-(t)|^2 = \sin^2 2\theta \sin^2 \frac{m_+ - m_-}{2} t, \tag{3.56}$$

which agrees with the result in (3.53) as expected. From this view, it becomes apparent that the oscillation is caused by the interference between the two diagrams. They have different phases, which develop as a result of the mass difference while the particle propagates in time. The oscillation amplitude reflects the product of the mixing parameters from $|\alpha\rangle$ to $|\pm\rangle$ and from $|\pm\rangle$ to $|\beta\rangle$. The angular velocity of the oscillation corresponds to the phase difference developed per unit time.

3.3.5 Mathematical Formulation of Oscillation

The formulation of the flavor oscillation is summarized in this section. The wave function form is,

$$|\psi(t)\rangle = \sum_\alpha C_\alpha(t)\,|\alpha\rangle\,. \tag{3.57}$$

The Schrödinger equation (3.13) is written as

$$\dot{C} = -i\mathscr{T}C, \tag{3.58}$$

where C is a column matrix; $C = (C_\alpha\ C_\beta\ \ldots)^T$ and $\mathscr{T}$ is the transition matrix between the flavor eigenstates. Equation (3.58) can be explicitly written as in Eq. (3.37) for the two flavor case. From the conservation of probability, $\mathscr{T}$ is required to be Hermitian.

It is always possible to make the matrix $U^\dagger \mathscr{T} U$ real-diagonal by choosing a certain unitary matrix U,

$$M = U^\dagger \mathscr{T} U, \tag{3.59}$$

where the elements of M are $M_{ij} = m_i \delta_{ij}$. The elements of U and M are combinations of the elements of the transition matrix $\mathscr{T}$.

Using the unitary matrix U, Eq. (3.58) can be modified to,

$$U^\dagger \dot{C}(t) = -i\left[U^\dagger \mathscr{T} U\right] U^\dagger C(t) = -iMU^\dagger C(t). \tag{3.60}$$

If we define coefficients $D = (D_1\ D_2\ \ldots)^T$ as

$$D(t) = U^\dagger C(t), \tag{3.61}$$

the state equation (3.60) becomes,

$$\dot{D}(t) = -iMD(t). \tag{3.62}$$

Since M is diagonal, the solution can be obtained easily in the form

$$D(t) = W(t)D(0), \tag{3.63}$$

where $W(t)$ is also a diagonal matrix with elements $W_{ij}(t) = e^{-im_i t}\delta_{ij}$. Finally, the flavor coefficients at time t is obtained as follows:

$$C(t) = UD(t) = UW(t)D(0) = [UW(t)U^\dagger]C(0). \tag{3.64}$$

Equation (3.64) can be expressed using the elements of the matrices as follows,

$$C_\xi(t) = \sum_{ij\zeta} U_{\xi i} W_{ij}(t) U^*_{\zeta j} C_\zeta(0) = \sum_\zeta \left[\sum_i e^{-im_i t} U_{\xi i} U^*_{\zeta i}\right] C_\zeta(0). \tag{3.65}$$

If the initial state is pure $|\alpha\rangle$, $C_\alpha(0) = 1$ and other coefficients are 0. In this case,

$$C_\xi(t) = \sum_i e^{-im_i t} U_{\xi i} U^*_{\alpha i}. \tag{3.66}$$

The wave function at time t is,

$$|\psi_\alpha(t)\rangle = \sum_\xi C_\xi(t)\,|\xi\rangle = \sum_{i\xi} e^{-im_i t} U_{\xi i} U^*_{\alpha i}\,|\xi\rangle\,. \tag{3.67}$$

The probability of being $|\beta\rangle$ state at time t is,

$$P_{\alpha\to\beta}(t) = |\langle\beta|\psi_\alpha(t)\rangle|^2 = \sum_{ij} U_{\alpha i} U^*_{\beta i} U^*_{\beta j} U_{\alpha j} e^{-i(m_j - m_i)t}. \tag{3.68}$$

We can measure U and M experimentally and obtain $\mathscr{T}$ using Eq. (3.59) as

$$\mathscr{T} = UMU^\dagger, \tag{3.69}$$

and can study its origin.

For the two flavor case, from Eq. (3.69) together with Eq. (3.41), the relations between transition amplitudes and measurable parameters are

$$\tau = (m_+ - m_-)\sin\theta\cos\theta = \omega_\tau \sin 2\theta \tag{3.70}$$

$$\mu_\alpha = m_- \cos^2\theta + m_+ \sin^2\theta = \overline{m} - \omega_\tau \cos 2\theta \tag{3.71}$$

$$\mu_\beta = m_+ \cos^2\theta + m_- \sin^2\theta = \overline{m} + \omega_\tau \cos 2\theta, \tag{3.72}$$

where $\omega_\tau = \frac{m_+ - m_-}{2}$ and average mass $\overline{m} = \frac{m_+ + m_-}{2}$. Equation (3.70) indicates that oscillation experiments measure the cross-transition amplitude τ. Equations (3.71) and (3.72) show that the self-transition amplitudes μ_α and μ_β can be determined by combining the absolute masses and the oscillation parameters. There are also the following useful relations:

$$\begin{aligned} \mu_\alpha + \mu_\beta &= m_+ + m_-, \\ \mu_\beta - \mu_\alpha &= (m_+ - m_-)\cos 2\theta. \end{aligned} \tag{3.73}$$

The general wave function (3.57) can be expressed by $D(t)$ as follows:

$$|\psi(t)\rangle = \sum_\alpha C_\alpha(t)\,|\alpha\rangle = \sum_{\alpha k} U_{\alpha k} D_k(t)\,|\alpha\rangle = \sum_k D_k(0) e^{-im_k t}\left[\sum_\alpha U_{\alpha k}\,|\alpha\rangle\right]. \tag{3.74}$$

If we define a new basis vector as

$$|k\rangle \equiv \sum_\alpha U_{\alpha k}\,|\alpha\rangle, \tag{3.75}$$

The wave function (3.57) becomes,

$$|\psi(t)\rangle = \sum_k D_k(0)\,|k\rangle\, e^{-im_k t}. \tag{3.76}$$

This means that $|k\rangle$ is a mass eigenstate. The mixing matrix elements can be expressed as

$$U_{\alpha k} = \langle\alpha|k\rangle\,. \tag{3.77}$$

Chapter 4
Neutrino Oscillation

Abstract In this chapter, oscillations of the relativistic three flavor neutrinos are discussed. First, two-flavor relativistic oscillation formula is derived using the solution of the Dirac equation. It is confirmed that under realistic calculations, resulting oscillation formulas agree with the standard formula based on a simple assumption. Next, the effective state equation for relativistic neutrinos are defined and the complete set of the relativistic three flavor neutrino oscillation formulas are derived. The standard parametrization of the three flavor mixing matrix that uses θ_{12}, θ_{23}, θ_{13} and δ, is introduced. Oscillation formula for the antineutrino is derived from the CPT invariance. Correspondence between the mass number m_i and neutrino flavor ν_α is discussed and the concept of the mass hierarchy is introduced. In order to understand the solar neutrino data and plan experiments to detect CP violation and mass hierarchy, the neutrino oscillation in matter is formulated. Finally a paradox in oscillation measurements is explained.

Keywords Relativistic oscillation · Three flavor oscillation · Antineutrino oscillation · MNSP matrix · Matter effect · Measurement problem

4.1 Oscillation of Relativistic Two Flavor Fermions

So far we have studied the oscillation of two flavor particles at rest. However, the masses of neutrinos are extremely small and neutrinos always travel ultrarelativistically in actual experimental conditions. Therefore, a formulation of the oscillation for the relativistic neutrinos is necessary.

4.1.1 Oscillation of Dirac Neutrinos

The wave function of positive energy two-flavor neutrino can be generally expressed as

$$|\psi_\nu(x)\rangle = \nu_e(x)\,|\nu_e\rangle + \nu_\mu(x)\,|\nu_\mu\rangle = \nu_-\,|\nu_-\rangle\,e^{-ik_-x} + \nu_+\,|\nu_+\rangle\,e^{-ik_+x}, \qquad (4.1)$$

F. Suekane, *Neutrino Oscillations*, Lecture Notes in Physics 898,
DOI 10.1007/978-4-431-55462-2_4

where $|\nu_e\rangle$ and $|\nu_\mu\rangle$ are flavor eigenstates and $|\nu_\pm\rangle$ are mass eigenstates. We assume that there is a cross-transition amplitude τ between $|\nu_e\rangle$ and $|\nu_\mu\rangle$ just like the quark case. The Dirac equations with the transitions can be obtained by substituting α and β in Eq. (8.32) by e and μ,

$$\begin{cases} i\gamma_\rho \partial^\rho \nu_e - \mu_e \nu_e - \tau \nu_\mu = 0 \\ i\gamma_\rho \partial^\rho \nu_\mu - \mu_\mu \nu_\mu - \tau \nu_e = 0, \end{cases} \tag{4.2}$$

where the transition amplitudes are also substituted as $\mu_{\alpha\alpha} \to \mu_e$, $\mu_{\beta\beta} \to \mu_\mu$ and $\mu_{\alpha\beta} = \mu_{\beta\alpha} \to \tau$.[1] Following the same procedure in Sect. 3.3.2, we mix the ν_e and ν_μ with the mixing angle θ and obtain energy eigenstates ν_+ and ν_-,

$$\begin{pmatrix} \nu_- \\ \nu_+ \end{pmatrix} = \begin{pmatrix} \cos\theta & -\sin\theta \\ \sin\theta & \cos\theta \end{pmatrix} \begin{pmatrix} \nu_e \\ \nu_\mu \end{pmatrix}, \tag{4.3}$$

where θ is defined by

$$\tan 2\theta = \frac{2\tau}{\mu_\mu - \mu_e}. \tag{4.4}$$

Using $\nu_\pm$, the Dirac equations (4.2) can be separated into the following two independent equations.

$$\begin{cases} i\gamma_\rho \partial^\rho \nu_+ - m_+ \nu_+ = 0 \\ i\gamma_\rho \partial^\rho \nu_- - m_- \nu_- = 0 \end{cases}, \tag{4.5}$$

where

$$m_\pm = \frac{\mu_\mu + \mu_e}{2} \pm \sqrt{\left(\frac{\mu_\mu - \mu_e}{2}\right)^2 + \tau^2}. \tag{4.6}$$

The positive energy solutions for the Dirac equations (4.5) are, using Eq. (8.70),

$$\nu_\pm(x) = \sqrt{E_\pm + m_\pm} \begin{pmatrix} u_\pm \\ \eta_\pm \sigma u_\pm \end{pmatrix} e^{-ik_\pm x}, \tag{4.7}$$

where $k_\pm = (E_\pm, \mathbf{p}_\pm)$. Equation (4.7) indicates that a space-time development of the wave function is

$$\nu_\pm(x) = \nu_\pm(0) e^{-ik_\pm x}. \tag{4.8}$$

Therefore, the wave functions of the flavor eigenstates at the space-time point x are, using Eq. (4.3),

[1] For two flavor oscillation, the imaginary phase does not appear in the oscillation probability and it is omitted from the first.

$$\begin{aligned}\begin{pmatrix}\nu_e(x)\\ \nu_\mu(x)\end{pmatrix} &= \begin{pmatrix}\cos\theta & \sin\theta\\ -\sin\theta & \cos\theta\end{pmatrix}\begin{pmatrix}\nu_-(x)\\ \nu_+(x)\end{pmatrix}\\ &= \begin{pmatrix}\cos\theta & \sin\theta\\ -\sin\theta & \cos\theta\end{pmatrix}\begin{pmatrix}e^{-ik_-x} & 0\\ 0 & e^{-ik_+x}\end{pmatrix}\begin{pmatrix}\cos\theta & -\sin\theta\\ \sin\theta & \cos\theta\end{pmatrix}\begin{pmatrix}\nu_e(0)\\ \nu_\mu(0)\end{pmatrix}\\ &= \begin{pmatrix}e^{-ik_-x}\cos^2\theta + e^{-ik_+x}\sin^2\theta & (e^{-ik_+x}-e^{-ik_-x})\sin\theta\cos\theta\\ (e^{-ik_+x}-e^{-ik_-x})\sin\theta\cos\theta & e^{-ik_-x}\sin^2\theta + e^{-ik_+x}\cos^2\theta\end{pmatrix}\begin{pmatrix}\nu_e(0)\\ \nu_\mu(0)\end{pmatrix}.\end{aligned} \tag{4.9}$$

If the neutrino state is in the pure ν_μ state at space-time $x = 0$, the initial condition is

$$\nu_e(0) = 0, \tag{4.10}$$

and the coefficients of ν_e and ν_μ basis states are,

$$\begin{cases}\nu_e(x) = (e^{-ik_+x} - e^{-ik_-x})\sin\theta\cos\theta\nu_\mu(0)\\ \nu_\mu(x) = (e^{-ik_-x}\sin^2\theta + e^{-ik_+x}\cos^2\theta)\nu_\mu(0).\end{cases} \tag{4.11}$$

In this case, the wave function becomes

$$\begin{aligned}\psi_\nu(x) = &((e^{-ik_+x} - e^{-ik_-x})\sin\theta\cos\theta\,|\nu_e\rangle\\ &+ (e^{-ik_-x}\sin^2\theta + e^{-ik_+x}\cos^2\theta)\,|\nu_\mu\rangle)\nu_\mu(0).\end{aligned} \tag{4.12}$$

The probability that ν_μ state turns into ν_e at space-time x is

$$P_{\nu_\mu\to\nu_e}(x) = \frac{|\nu_e(x)|^2}{|\psi_\nu(0)|^2} = \sin^2 2\theta \sin^2\frac{(k_+ - k_-)x}{2}. \tag{4.13}$$

4.1.2 Oscillation Phase

The treatment of the oscillation phase in Eq. (4.13),

$$\Phi = \frac{(k_+ - k_-)x}{2} = \frac{(E_+ - E_-)t - (\mathbf{p}_+ - \mathbf{p}_-)\mathbf{x}}{2} \tag{4.14}$$

requires some care. Now we assume that the momenta are parallel to the $+z$ direction and $\mathbf{p}_\pm = (0, 0, p_\pm)$. If the energies happen to be the same, $E_+ = E_-(= E)$, the oscillation phase Φ becomes

$$\Phi = \frac{1}{2}\left(\sqrt{E^2 - m_-^2} - \sqrt{E^2 - m_+^2}\right)z \sim \frac{m_+^2 - m_-^2}{4E}z. \tag{4.15}$$

If instead the two momenta happen to be the same, $p_+ = p_-(= p)$, the oscillation phase becomes

$$\Phi = \frac{1}{2}\left(\sqrt{p^2 + m_+^2} - \sqrt{p^2 + m_-^2}\right) t \sim \frac{m_+^2 - m_-^2}{4p} t. \tag{4.16}$$

Since practically we can consider $t = z$ and $p = E$ for the ultrarelativistic neutrino case, Eqs. (4.15) and (4.16) can be considered as identical.[2] However, in actual processes of neutrino production, such as pion decays, both the energies and momenta of ν_- and ν_+ are different from each other. The relation of $(E_-, \mathbf{p}_-)$ and $(E_+, \mathbf{p}_+)$ can not be determined from the general solution and it is necessary to concretely consider how the neutrinos were produced to determine the initial condition. To see a more realistic situation, we consider a case that the neutrino is produced in the decay of particle X,

$$X \to \nu_\pm + Y, \tag{4.17}$$

where Y can be a single particle, like the pion decay or a multi-particle system, like the β or muon decays. In such decays, the neutrino energy and momentum in the rest frame of X are given by,

$$E_\pm \sim E_0\left(1 - \frac{m_\pm^2}{2M_X E_0}\right), \quad p_\pm \sim E_0\left(1 - \frac{1}{2}\left(1 + \frac{E_0}{M_X}\right)\frac{m_\pm^2}{E_0^2}\right), \tag{4.18}$$

where M_X is the mass of X and E_0 is the neutrino energy in case the neutrino is massless,

$$E_0 = \frac{M_X^2 - M_Y^2}{2M_X}. \tag{4.19}$$

M_Y is the invariant mass of the Y system. If the decay is three-body decay or more, M_Y differs for event by event. Substituting the $p_\pm$ and $E_\pm$ in Eq. (4.14) by Eqs. (4.18), the oscillation phase is

$$\Phi \sim \frac{\Delta m^2}{4E_0}\left(1 + \frac{E_0}{M_X}\right) z - \frac{\Delta m^2}{4M_X E_0} t \sim \frac{\Delta m^2}{4E_0} z. \tag{4.20}$$

The oscillation phase depends only on the squared neutrino mass difference and the neutrino energy. The information of the decay of X, such as a possible variation of M_Y, is included in the neutrino energy and we need not explicitly care about how the neutrino was produced when treating the neutrino oscillation.

---

[2] Rigorously speaking, if there is no ambiguity in the momentum, position becomes ambiguous due to the uncertainty principle and the position dependence of the oscillation can not be observed.

4.1.3 Wave Packet Treatment

Usually, the elementary particles we observe are localized in space and have to be treated as wave packet. The wave packet is expressed by superposition of plane waves with slightly different momenta. For simplicity, we consider a one dimensional wave packet for the neutrino with mass m_ν. The wave function of the wave packet is expressed by

$$\Psi(t, z) = \int a(k) e^{i(kz - E(k)t)} dk, \tag{4.21}$$

where $a(k)$ is a momentum distribution with narrow momentum spread and $E(k) = \sqrt{m_\nu^2 + k^2}$. Now we assume that the momentum distribution of $|a(k)|^2$ is a Gaussian with mean momentum $\hat{k}$ and the standard deviation σ_k,

$$a(k) = \frac{1}{\sqrt{\sqrt{2\pi}\sigma_z}} \exp\left[-\frac{(k - \hat{k})^2}{4\sigma_k^2}\right]. \tag{4.22}$$

The neutrino is ultrarelativistic and we assume

$$\sigma_k \ll \hat{k}. \tag{4.23}$$

The integration (4.21) can be performed,[3]

$$\Psi(t, z) \sim \frac{1}{\sqrt{\sqrt{2\pi}\sigma_z}} \exp\left[-\frac{(z - \hat{\beta}t)^2}{4\sigma_z^2}\right] \exp\left[i(\hat{k}z - \hat{E}t)\right], \tag{4.24}$$

where $\sigma_z = 1/(2\sigma_k)$, $\hat{E} = \sqrt{\hat{k}^2 + m_\nu^2}$ and mean velocity is

$$\hat{\beta} = \frac{\hat{k}}{\hat{E}} \sim 1 - \frac{m_\nu^2}{2\hat{E}^2}. \tag{4.25}$$

The probability density at space-time (t, z) is,

$$|\Psi(t, z)|^2 = \frac{1}{\sqrt{2\pi}\sigma_z} \exp\left[-\frac{(z - \hat{\beta}t)^2}{2\sigma_z^2}\right]. \tag{4.26}$$

This state exists only around $z = \hat{\beta}t$ with width of σ_z, which describes a localized particle that travels with velocity $\hat{\beta}$.

[3] See Sect. 8.4.3 for derivation.

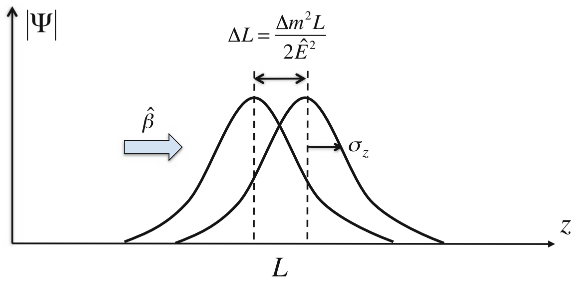

Fig. 4.1 Overlap of the two wave packets

For neutrinos, the flavor eigenstate is a superposition of the mass eigenstates, and each mass eigenstate has to be treated as a wave packet with its own mass. The wave packets of different mass eigenstates generally have different velocities and they will separate from each other after traveling some distance. The neutrino oscillation can be treated as the interference of the overlap of the wave packets. Figure 4.1 shows a sketch of the separation of the two wave packets. The distance between the two peaks of the wave packets with masses m_- and m_+ after traveling distance L is given by,

$$\Delta L = \Delta\hat{\beta}L = \frac{\Delta m^2}{2\hat{E}^2}L, \tag{4.27}$$

where $\Delta\hat{\beta}$ is the difference of the average velocities (4.25),

$$\Delta\hat{\beta} = \hat{\beta}_- - \hat{\beta}_+ = \frac{m_+^2 - m_-^2}{2\hat{E}^2} = \frac{\Delta m^2}{2\hat{E}^2}. \tag{4.28}$$

The ratio of the distance between the two peaks and the width of the wave packets is,

$$\frac{\Delta L}{\sigma_z} = \frac{\Delta m^2 L}{2\hat{E}^2\sigma_z}. \tag{4.29}$$

Usually, we set up the baseline of the experiments such a way that

$$L \sim \frac{2\pi\hat{E}}{\Delta m^2}, \tag{4.30}$$

which gives

$$\frac{\Delta L}{\sigma_z} \sim \frac{\pi}{\hat{E}\sigma_z} \sim \frac{2\pi\sigma_k}{\hat{k}} \ll 1, \tag{4.31}$$

from the assumption (4.23). Therefore, the two wave packets overlap significantly and the oscillation can be observed.

4.1.4 Oscillation of the Wave Packet

If a neutrino is produced as ν_μ, the wave function of the wave packets at the space-time x is, from the analogy to Eqs. (4.1) and (4.3) after setting $\nu_e(0) = 0$,

$$|\Psi(x)\rangle = N\left(-\sin\theta\, e^{-(\Delta\hat{z}_-)^2} e^{i\Phi_-}\,|\nu_-\rangle + \cos\theta\, e^{-(\Delta\hat{z}_+)^2} e^{i\Phi_+}\,|\nu_+\rangle\right), \qquad (4.32)$$

where $N = 1/\sqrt{\sqrt{2\pi}\sigma_z}$ is the normalization constant and

$$\Delta\hat{z}_\pm = \frac{z-\beta_\pm t}{2\sigma_z}, \quad \Phi_\pm = k_\pm z - E_\pm t. \qquad (4.33)$$

Following the same procedure used to derive Eq. (3.35), the probability of detecting ν_e at a space-time point x is,

$$\begin{aligned} |\langle\nu_e|\Psi(x)\rangle|^2 &= \left|\frac{N}{2}\sin 2\theta\left(e^{-(\Delta\hat{z}_+)^2}e^{i\Phi_+} - e^{-(\Delta\hat{z}_-)^2}e^{i\Phi_-}\right)\right|^2 \\ &= \frac{N^2\sin^2 2\theta}{4}\left(e^{-2(\Delta\hat{z}_+)^2} + e^{-2(\Delta\hat{z}_-)^2} - 2e^{-((\Delta\hat{z}_+)^2+(\Delta\hat{z}_-)^2)}\cos(\Delta kz - \Delta Et)\right), \end{aligned} \qquad (4.34)$$

where $\Delta k = k_- - k_+$ and $\Delta E = E_- - E_+$.

In actual experiments, we place a neutrino detector at a distance L from the neutrino source and measure the incoming neutrinos continuously. Therefore, the probability of finding ν_e events corresponds to the integral of (4.34) over time,[4]

$$\begin{aligned} P_{\nu_\mu\to\nu_e}(L) &\sim \int_{-\infty}^{+\infty} |\langle\nu_e|\Psi(t,L)\rangle|^2 dt \Big/ \int_{-\infty}^{+\infty} |\Psi(t,L)|^2 dt \\ &\sim \frac{\sin^2 2\theta}{2}\left(1 - \cos\left[(\Delta k - \Delta E)\,L\right]\exp\left[-\frac{1}{8}\left[\left(\frac{\Delta E}{\sigma_k}\right)^2 + \left(\frac{\Delta\beta L}{\sigma_z}\right)^2\right]\right]\right), \end{aligned} \qquad (4.35)$$

where non-leading $O((m_i/E)^2)$ terms are ignored and approximations, $\overline{\beta} = (\beta_- + \beta_+)/2 \sim 1$, $\overline{\beta^2} = (\beta_-^2 + \beta_+^2)/2 \sim 1$ are used.

Since $\Delta L = \Delta\beta L$ is the difference between the peak positions of the two wave packets, the $\exp[-(\Delta\beta)^2 L^2/8\sigma_z^2]$ term corresponds to the reduction due to the separation of the two wave packets in space. The power of this term is close to 0 as we saw in (4.31). The $\exp[-(\Delta E)^2/8\sigma_k^2]$ term represents the reduction from the difference between the neutrino energies in the two mass eigenstates. If the neutrino is produced in the decay of particle X as in Eq. (4.17) and detected at a distance $L \sim 2\pi E/\Delta m^2$,

[4] See Sect. 8.4.3.1 for derivation.

$$\frac{\Delta E}{\sigma_k} \sim \frac{\Delta m^2}{2M_X\sigma_k} \sim \frac{2\pi E}{M_X}\frac{\sigma_z}{L} \ll 1. \tag{4.36}$$

where the fact that σ_z is much smaller than the baseline L is used. Since β is close to 1, the phase of the cos term in Eq. (4.35) is, using Eqs. (4.18),

$$(\Delta k - \Delta E)L \sim \frac{\Delta m^2 L}{2E_0}. \tag{4.37}$$

Finally, the transition probability becomes,

$$P_{\nu_\mu \to \nu_e}(L) = \frac{\sin^2 2\theta}{2}\left(1 - \cos\left(\frac{\Delta m^2 L}{2E_0}\right)\right) = \sin^2 2\theta \sin^2\left(\frac{\Delta m^2 L}{4E_0}\right), \tag{4.38}$$

which agrees with the formula derived in the previous sections.

4.1.5 Effective Treatment of Relativistic State Equation

The wave function of a moving particle can be obtained from the Lorentz boost of the wave function of the particle at rest. We define the coordinate of the particle rest frame as x' and the coordinate of the laboratory frame, which is moving with velocity $-\beta$ with respect to the particle frame, as x. The plane wave of the particle at rest changes as follows by the Lorentz boost:

$$e^{-imt'} \xrightarrow{\text{L.B.}} e^{-im\gamma(t-\beta x)}, \tag{4.39}$$

where γ is the Lorentz factor ($\gamma = 1/\sqrt{1-\beta^2}$). Since the particle travels with velocity β in the lab frame, the position of the particle is $x = \beta t$. Therefore, the phase factor on the particle is,

$$e^{-im\gamma(t-\beta x)} \xrightarrow{x=\beta t} e^{-i\frac{m}{\gamma}t}. \tag{4.40}$$

This means that the mass is reduced by a factor γ if seen from the lab frame,

$$m \to \frac{m}{\gamma}. \tag{4.41}$$

If we define the neutrino wave function as

$$|\psi_\nu(t)\rangle = C_{\nu_e}(t)\,|\nu_e\rangle + C_{\nu_\mu}(t)\,|\nu_\mu\rangle\,. \tag{4.42}$$

The effective state equation for the relativistic neutrinos can be obtained by substituting the transition amplitudes, μ and τ by μ/γ and τ/γ, respectively in Eq. (3.37) as,

$$\frac{d}{dt}\begin{pmatrix} C_{\nu_e} \\ C_{\nu_\mu} \end{pmatrix} = -i\frac{1}{\gamma}\begin{pmatrix} \mu_e & \tau_\nu \\ \tau_\nu & \mu_\mu \end{pmatrix}\begin{pmatrix} C_{\nu_e} \\ C_{\mu_\mu} \end{pmatrix}. \tag{4.43}$$

Rigorously speaking, (4.43) is correct only for the case that the velocities of the two mass eigenstates are the same ($\beta = p_-/E_- = p_+/E_+$). As we saw in Sect. 4.1.2, the energy and momentum of the mass eigenstate neutrinos can vary event per event and in general, such condition may not be satisfied. However, in usual experimental conditions, the two wave packets overlaps even if the central positions are not the same. In fact, the rigorous treatment of neutrino oscillation caused by the extremely small masses is difficult and there are still some arguments (see for example [1, 2]). We will not go in detailed discussions and will use (4.43) as an effective state equation since this treatment ($m \to m/\gamma$) is easy and intuitive.

Equation (4.43) means that it is possible to obtain oscillation formula of relativistic neutrinos by substituting

$$\mu_{e/\mu} \to \frac{\mu_{e/\mu}}{\gamma} \quad \text{and} \quad \tau_\nu \to \frac{\tau_\nu}{\gamma} \tag{4.44}$$

in the oscillation formula of the particle at rest. The mixing angle is not changed by the substitutions,

$$\tan 2\theta_\nu \to \frac{2\tau_\nu/\gamma}{(\mu_\mu - \mu_e)/\gamma} = \frac{2\tau_\nu}{\mu_\mu - \mu_e} = \tan 2\theta_\nu, \tag{4.45}$$

and the relation between the mass eigenstates and the flavor eigenstates is the same as Eq. (3.49),

$$\begin{pmatrix} |\nu_-\rangle \\ |\nu_+\rangle \end{pmatrix} = \begin{pmatrix} \cos\theta_\nu & -\sin\theta_\nu \\ \sin\theta_\nu & \cos\theta_\nu \end{pmatrix}\begin{pmatrix} |\nu_e\rangle \\ |\nu_\mu\rangle \end{pmatrix}. \tag{4.46}$$

The wave functions of the mass eigenstates are,

$$|\psi_{\nu_\pm}(t)\rangle = |\nu_\pm\rangle \exp\left[-i\frac{m_{\nu_\pm}}{\gamma}t\right], \tag{4.47}$$

where,

$$m_{\nu_\pm} = \bar{\mu} \pm \sqrt{(\Delta\mu/2)^2 + \tau_\nu^2}, \tag{4.48}$$

and

$$\bar{\mu} = \frac{\mu_\mu + \mu_e}{2}, \quad \Delta\mu = \mu_\mu - \mu_e. \tag{4.49}$$

The oscillation probability of the relativistic particle is, from Eq. (3.53),

$$P_{\nu_\mu \to \nu_e}(t) = \sin^2 2\theta_\nu \sin^2 \frac{\Delta m_\pm}{2\gamma}t, \tag{4.50}$$

where $\Delta m_{\pm} = m_{\nu_+} - m_{\nu_-}$. In the lab frame, the energies of the neutrinos are given by

$$E_{\nu_\pm} = \gamma m_{\nu_\pm}. \tag{4.51}$$

Using the mean energy $\overline{E} = (E_{\nu_+} + E_{\nu_-})/2$ and the average mass $\overline{m} = (m_{\nu_+} + m_{\nu_-})/2$, the Lorentz factor can be expressed as

$$\gamma = \frac{\overline{E}}{\overline{m}}. \tag{4.52}$$

Therefore, if we use $\overline{E}$, the angular velocity of the oscillation in the lab frame becomes

$$\omega_\nu = \frac{\Delta m_\pm}{2\gamma} = \frac{m_{\nu_+}^2 - m_{\nu_-}^2}{4\overline{E}} = \frac{\Delta m_\pm^2}{4\overline{E}}. \tag{4.53}$$

Finally, the neutrino oscillation probability is

$$P_{\nu_\mu \to \nu_e}(L) = \sin^2 2\theta_\nu \sin^2 \frac{\Delta m_\pm^2 L}{4\overline{E}}, \tag{4.54}$$

where $t \sim L$ is used. Using (4.52) the transition matrix in (4.43) can be rewritten as

$$\frac{1}{\gamma}\begin{pmatrix} \mu_e & \tau_\nu \\ \tau_\nu & \mu_\mu \end{pmatrix} = \frac{\overline{m}}{\overline{E}}\left(\overline{m} + \frac{\Delta m}{2}\begin{pmatrix} -\cos 2\theta_\nu & \sin 2\theta_\nu \\ \sin 2\theta_\nu & \cos 2\theta_\nu \end{pmatrix}\right). \tag{4.55}$$

Finally, the state equation for the two flavor neutrinos is expressed by

$$\frac{d}{dt}\begin{pmatrix} C_{\nu_e} \\ C_{\nu_\mu} \end{pmatrix} = -i\left[\frac{\overline{m}^2}{\overline{E}} + \frac{\Delta m^2}{4\overline{E}}\begin{pmatrix} -\cos 2\theta_\nu & \sin 2\theta_\nu \\ \sin 2\theta_\nu & \cos 2\theta_\nu \end{pmatrix}\right]\begin{pmatrix} C_{\nu_e} \\ C_{\nu_\mu} \end{pmatrix}. \tag{4.56}$$

4.1.6 Oscillation of Antineutrinos

In experiments, we often treat antineutrinos. The reactor neutrino is an anti-electron neutrino and CP violation can be measured from the comparison of the neutrino and antineutrino oscillation probabilities. The oscillation formula of antineutrinos can be obtained from that of the neutrinos by assuming CPT invariance. The CPT transformation converts a fermion state as follows:

$$\begin{aligned} \psi(t) &= \psi_L(t) + \psi_R(t) \xrightarrow{C} \overline{\psi}_L(t) + \overline{\psi}_R(t) \\ &\xrightarrow{P} \overline{\psi}_R(t) + \overline{\psi}_L(t) \xrightarrow{T} \overline{\psi}_R(-t) + \overline{\psi}_L(-t) = \overline{\psi}(-t). \end{aligned} \tag{4.57}$$

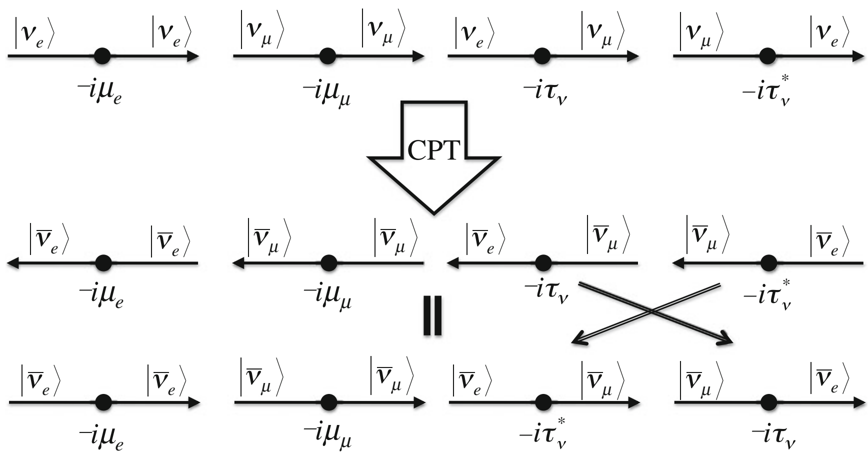

Fig. 4.2 Transition amplitudes after CPT transformations. The *second line* is CPT transformed states from the *first line*. The *arrow* of the time is arranged from *left* to *right* in the *third line*

The first line of Fig. 4.2 corresponds to the state equation of the neutrinos:

$$\frac{d}{dt}\begin{pmatrix}\nu_e\\ \nu_\mu\end{pmatrix} = -\frac{i}{\gamma}\begin{pmatrix}\mu_e & \tau_\nu^*\\ \tau_\nu & \mu_\mu\end{pmatrix}\begin{pmatrix}\nu_e\\ \nu_\mu\end{pmatrix}. \tag{4.58}$$

The hermiticity of the transition matrix requires that the self-transition amplitudes be real. The two cross-transition amplitudes can have an imaginary part and must be complex conjugates to each other.[5]

The effect of CPT transformation on the transition of the neutrino state is graphically shown in the second line of Fig. 4.2. In the third line, the arrow of time is arranged from left to right. Therefore, if the first line is correct, the third like is also correct due to CPT invariance. The state equation corresponding to the third line is

$$\frac{d}{dt}\begin{pmatrix}\bar{\nu}_e\\ \bar{\nu}_\mu\end{pmatrix} = -\frac{i}{\gamma}\begin{pmatrix}\mu_e & \tau_\nu\\ \tau_\nu^* & \mu_\mu\end{pmatrix}\begin{pmatrix}\bar{\nu}_e\\ \bar{\nu}_\mu\end{pmatrix}. \tag{4.59}$$

This is the state equation for the antineutrinos. From the comparison between Eqs. (4.58) and (4.59), we notice that the state equation for antineutrinos is the same as that for neutrinos after taking the complex conjugate of the transition matrix. If we write $\tau_\nu = |\tau_\nu|e^{i\phi}$, any antineutrino formulas that are results of Eq. (4.59) can be obtained by replacing $\phi \leftrightarrow -\phi$ in the corresponding neutrino formulas obtained

[5] The imaginary phase is not observable in the two flavor oscillations and has been ignored so far. In this section, τ_ν is treated as a complex number because the descriptions here are meant to aid in explaining the antineutrino oscillation for three flavor neutrinos. In that case, the imaginary phase plays an important role.

from Eq. (4.58). For example, the mixing matrix of the antineutrinos can be obtained from the mixing matrix of the neutrinos as follows:

$$\begin{pmatrix} |\nu_-\rangle \\ |\nu_+\rangle \end{pmatrix} = \begin{pmatrix} \cos\theta & -e^{i\phi}\sin\theta \\ e^{-i\phi}\sin\theta & \cos\theta \end{pmatrix} \begin{pmatrix} |\nu_e\rangle \\ |\nu_\mu\rangle \end{pmatrix}$$
$$\xrightarrow{\text{CPT}} \begin{pmatrix} |\bar{\nu}_-\rangle \\ |\bar{\nu}_+\rangle \end{pmatrix} = \begin{pmatrix} \cos\theta & -e^{-i\phi}\sin\theta \\ e^{i\phi}\sin\theta & \cos\theta \end{pmatrix} \begin{pmatrix} |\bar{\nu}_e\rangle \\ |\bar{\nu}_\mu\rangle \end{pmatrix}. \tag{4.60}$$

The oscillation probability formula for antineutrinos can also be obtained from the corresponding neutrino oscillation probability formula as

$$P_{\bar{\nu}_\mu \to \bar{\nu}_e} = P_{\nu_\mu \to \nu_e}(\phi \to -\phi). \tag{4.61}$$

4.1.7 Mass Hierarchy for Two Flavor Neutrinos

We have seen that the neutrino oscillation is caused by the transition amplitudes shown in Fig. 4.3. As a result of the transitions, the mixing between the mass eigenstates and the flavor eigenstates is

$$\begin{pmatrix} |\nu_e\rangle \\ |\nu_\mu\rangle \end{pmatrix} = \begin{pmatrix} \cos\theta_\nu & \sin\theta_\nu \\ -\sin\theta_\nu & \cos\theta_\nu \end{pmatrix} \begin{pmatrix} |\nu_-\rangle \\ |\nu_+\rangle \end{pmatrix}, \tag{4.62}$$

where

$$\tan 2\theta_\nu = \frac{2\tau_\nu}{\mu_\mu - \mu_e}. \tag{4.63}$$

Since τ_ν always appears in the form $|\tau_\nu|$ in the two flavor oscillation probability, we may define $\tau_\nu \geq 0$ without losing generality.

For the two flavor neutrino formulation, traditionally ν_1 and ν_2, having masses m_1 and m_2 respectively, are used as mass eigenstates instead of $\nu_\pm$. The relation between the ν_i and flavor eigenstates is defined as follows:

$$\begin{pmatrix} |\nu_e\rangle \\ |\nu_\mu\rangle \end{pmatrix} = \begin{pmatrix} \cos\theta_0 & \sin\theta_0 \\ -\sin\theta_0 & \cos\theta_0 \end{pmatrix} \begin{pmatrix} |\nu_1\rangle \\ |\nu_2\rangle \end{pmatrix}, \tag{4.64}$$

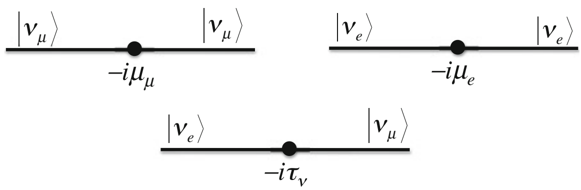

Fig. 4.3 Transition amplitudes of two flavor neutrinos

where θ_0 is the mixing angle of the standard definition. The correspondence between the flavor indexes (e, μ) and the mass indexes $(1, 2)$ is defined such a way that ν_1 is the main component of ν_e and ν_2 is the main component of ν_μ. This means that the mixing angle has, by definition, the following magnitude relation,

$$\cos^2\theta_0 \ \geq \sin^2\theta_0. \tag{4.65}$$

The case where $m_2 > m_1$ is called the *normal mass hierarchy* (NH) and the case where $m_2 < m_1$ is called the *inverted mass hierarchy* (IH). This naming comes from the analogy to the charged lepton mass hierarchy of $m_\mu > m_e$.

Since the masses $m_\pm$ are defined as (4.6), there is a relation $m_+ \geq m_-$. Hence for the NH, the correspondence between $m_\pm$ and m_i is,

$$\text{NH}: \qquad m_1 = m_- = \overline{\mu}_\nu - \omega_\nu, \quad m_2 = m_+ = \overline{\mu}_\nu + \omega_\nu, \tag{4.66}$$

where $\overline{\mu}_\nu = (\mu_\tau + \mu_e)/2$ and $\omega_\nu = \sqrt{(\mu_\mu - \mu_e)^2/4 + \tau_\nu^2}$. Substituting $|\nu_2\rangle$ and $|\nu_1\rangle$ for $|\nu_+\rangle$ and $|\nu_-\rangle$ in Eq. (4.62), we obtain

$$\text{NH}: \qquad \begin{pmatrix} |\nu_e\rangle \\ |\nu_\mu\rangle \end{pmatrix} = \begin{pmatrix} \cos\theta_\nu & \sin\theta_\nu \\ -\sin\theta_\nu & \cos\theta_\nu \end{pmatrix} \begin{pmatrix} |\nu_1\rangle \\ |\nu_2\rangle \end{pmatrix}. \tag{4.67}$$

By comparing relation (4.67) and the definition (4.64),

$$\text{NH}: \qquad \theta_0 = \theta_\nu. \tag{4.68}$$

From the domain of the definition Eq. (4.65), $\cos 2\theta_\nu = \cos 2\theta_0 > 0$ and therefore, from Eq. (4.63),

$$\text{NH}: \qquad \mu_\mu > \mu_e. \tag{4.69}$$

For the IH, $m_1 > m_2$ and hence,

$$\text{IH}: \qquad m_1 = m_+ = \overline{\mu}_\nu + \omega_\nu, \quad m_2 = m_- = \overline{\mu}_\nu - \omega_\nu. \tag{4.70}$$

Substituting $|\nu_1\rangle$ and $-|\nu_2\rangle$ for $|\nu_+\rangle$ and $|\nu_-\rangle$,[6] in Eq. (4.62), we obtain

$$\text{IH}: \qquad \begin{pmatrix} |\nu_e\rangle \\ |\nu_\mu\rangle \end{pmatrix} = \begin{pmatrix} \sin\theta_\nu & -\cos\theta_\nu \\ \cos\theta_\nu & \sin\theta_\nu \end{pmatrix} \begin{pmatrix} |\nu_1\rangle \\ |\nu_2\rangle \end{pmatrix}. \tag{4.71}$$

By comparing relation (4.71) and the definition Eq. (4.64),

$$\text{IH}: \qquad \theta_0 = \theta_\nu - \frac{\pi}{2}. \tag{4.72}$$

---

[6] The phase of the state $|\nu_2\rangle$ is chosen such the way that the mixing matrix in Eq. (4.71) becomes the identical matrix when $\tau_\nu = 0$.

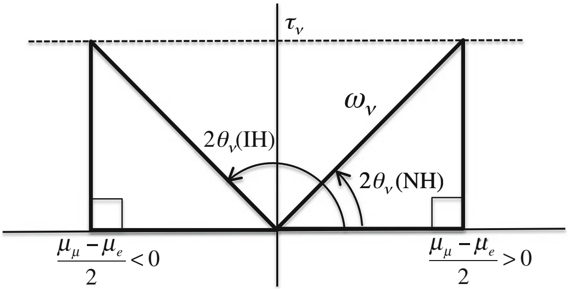

Fig. 4.4 The mixing triangles for two flavor neutrinos. For inverted mass hierarchy, $2\theta_\nu$ becomes larger than $\pi/2$

Table 4.1 Relations between neutrino oscillation parameters and transition amplitudes

Mass hierarchy	m_1	m_2	$\|\nu_1\rangle$	$\|\nu_2\rangle$	STA	θ_0	$\cos 2\theta_\nu$
NH ($m_1 < m_2$)	$\bar{\mu}_\nu - \omega_\nu$	$\bar{\mu}_\nu + \omega_\nu$	$\|\nu_-\rangle$	$\|\nu_+\rangle$	$\mu_e < \mu_\mu$	θ_ν	$+$
IH ($m_1 > m_2$)	$\bar{\mu}_\nu + \omega_\nu$	$\bar{\mu}_\nu - \omega_\nu$	$\|\nu_+\rangle$	$-\|\nu_-\rangle$	$\mu_e > \mu_\mu$	$\theta_\nu - \pi/2$	$-$

$\cos 2\theta_0$ is by definition 0 or positive, (STA = Self-Transition Amplitude)

In this case, from the definition Eq. (4.65), $\cos 2\theta_\nu = -\cos 2\theta_0 < 0$. Therefore, from (4.63),

$$\text{IH}: \quad \mu_e > \mu_\mu. \tag{4.73}$$

The above discussions show that the hierarchy of the physical masses m_1 and m_2 directly corresponds to the hierarchy of the self-transition amplitudes μ_e and μ_μ in the two flavor case.[7] The mixing angle θ_ν's for NH and IH are graphically shown in Fig. 4.4.

The relation between the oscillation parameters and the transition amplitudes depends on the mass hierarchy. It is summarized in Table 4.1.

4.2 Three Flavor Neutrino Oscillations

There are three neutrino flavors, ν_e, ν_μ and ν_τ. Accordingly there are three kinds of flavor oscillations, $\nu_e \Leftrightarrow \nu_\mu$, $\nu_e \Leftrightarrow \nu_\tau$ and $\nu_\mu \Leftrightarrow \nu_\tau$.

There are also three mass differences, which indicate that there are three oscillation frequencies. Therefore, there are generally nine combinations of oscillation terms for neutrinos.

All these facts make the neutrino oscillations much more complicated than the two-flavor non-relativistic case.

[7] For three flavor case, the hierarchies of the masses and the self-transition amplitudes are not necessarily the same.

In this section, we discuss the relativistic oscillation formula for three flavor neutrinos. To simplify the discussion, we follow the procedure described in Sect. 3.3.5 and the treatment of relativistic oscillations as in Sect. 4.1.5.

4.2.1 Transitions Between Three Neutrino Flavors

The general neutrino wave function for the three flavors ν_e, ν_μ and ν_τ is expressed by

$$|\psi_\nu(t)\rangle = C_e(t)\,|\nu_e\rangle + C_\mu(t)\,|\nu_\mu\rangle + C_\tau(t)\,|\nu_\tau\rangle\,. \tag{4.74}$$

There are nine transition amplitudes between the three neutrino states as shown in Fig. 4.5, where the hermiticity of the transition amplitude is used.

The relativistic state equation can be written as described in Eq. (4.43), giving

$$\frac{dC(t)}{dt} = -i\frac{1}{\gamma}\mathscr{T}C(t) = -i\mathscr{T}'C(t), \tag{4.75}$$

where

$$C(t) = \begin{pmatrix} C_e(t) \\ C_\mu(t) \\ C_\tau(t) \end{pmatrix}, \quad \mathscr{T}' = \frac{1}{\gamma}\begin{pmatrix} \mu_e & \tau^*_{\mu e} & \tau^*_{\tau e} \\ \tau_{\mu e} & \mu_\mu & \tau^*_{\tau\mu} \\ \tau_{\tau e} & \tau_{\tau\mu} & \mu_\tau \end{pmatrix}. \tag{4.76}$$

$\mathscr{T}'$ is the effective transition matrix for relativistic particles as described in Eq. (4.43). To solve Eq. (4.75), we diagonalize the $\mathscr{T}'$ using a unitary matrix U_ν,

$$U_\nu^\dagger \mathscr{T}' U_\nu = M' = \frac{1}{\gamma}\begin{pmatrix} m_1 & 0 & 0 \\ 0 & m_2 & 0 \\ 0 & 0 & m_3 \end{pmatrix}. \tag{4.77}$$

We write the elements of U_ν as follows:

$$U_\nu = \begin{pmatrix} U_{e1} & U_{e2} & U_{e3} \\ U_{\mu 1} & U_{\mu 2} & U_{\mu 3} \\ U_{\tau 1} & U_{\tau 2} & U_{\tau 3} \end{pmatrix}. \tag{4.78}$$

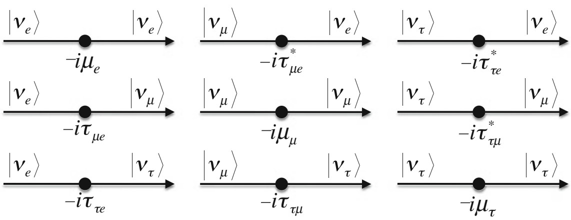

Fig. 4.5 The three flavor neutrino transition amplitudes

The matrix elements $U_{\alpha i}$ and the masses m_i are combinations of the elements of the transition amplitudes $\mathscr{T}_{\alpha\beta}$.[8]

Using the mass matrix M', the state equation (4.75) can be written as

$$\frac{dD(t)}{dt} = -iM'D(t), \tag{4.79}$$

where

$$D(t) = \begin{pmatrix} D_1(t) \\ D_2(t) \\ D_3(t) \end{pmatrix} = U_\nu^\dagger C(t). \tag{4.80}$$

This equation can be easily solved as

$$D(t) = W(t)D(0), \tag{4.81}$$

where

$$W(t) = \begin{pmatrix} e^{-i(m_1/\gamma)t} & 0 & 0 \\ 0 & e^{-i(m_2/\gamma)t} & 0 \\ 0 & 0 & e^{-i(m_3/\gamma)t} \end{pmatrix}. \tag{4.82}$$

Then, $C(t)$ can be obtained from the $D(t)$ as

$$C(t) = U_\nu D(t) = [U_\nu W(t)]D(0) = [U_\nu W(t)U_\nu^\dagger]C(0). \tag{4.83}$$

4.2.1.1 The Mass Eigenstate

The general wave function Eq. (4.74) can be written from (4.83) as the sum of the three mass eigenstates,

$$|\psi_\nu(t)\rangle = e^{-i(m_1/\gamma)t}D_1(0)\,|\nu_1\rangle + e^{-i(m_2/\gamma)t}D_2(0)\,|\nu_2\rangle + e^{-i(m_3/\gamma)t}D_3(0)\,|\nu_3\rangle\,, \tag{4.84}$$

where the mass eigenstates $|\nu_i\rangle$ are the mixtures of the three flavor eigenstates $|\nu_\alpha\rangle$ as given by

$$\begin{pmatrix} |\nu_1\rangle \\ |\nu_2\rangle \\ |\nu_3\rangle \end{pmatrix} = \begin{pmatrix} U_{e1} & U_{\mu 1} & U_{\tau 1} \\ U_{e2} & U_{\mu 2} & U_{\tau 2} \\ U_{e3} & U_{\mu 3} & U_{\tau 3} \end{pmatrix} \begin{pmatrix} |\nu_e\rangle \\ |\nu_\mu\rangle \\ |\nu_\tau\rangle \end{pmatrix} = U_\nu^{\mathrm{T}} \begin{pmatrix} |\nu_e\rangle \\ |\nu_\mu\rangle \\ |\nu_\tau\rangle \end{pmatrix}. \tag{4.85}$$

[8] The explicit formulas of $U_{\alpha i}$ and m_i consist of hundreds of terms made of the transition amplitudes $\mathscr{T}_{\alpha\beta}$ and are complicated. For the two flavor oscillation formula, θ and m_i consist of only a few terms.

We call the mixing matrix U_ν the Maki-Nakagawa-Sakata-Pontecorvo (MNSP) matrix in this book.

4.2.2 The Three Flavor Oscillation Formula

If a neutrino is produced as pure $|\nu_\alpha\rangle$ state at $t = 0$, the initial condition is given by

$$C_\alpha(0) = 1 \text{ and all other } C_x(0) = 0. \tag{4.86}$$

In this case, the coefficient of $|\nu_\beta\rangle$ at later time t is, from Eq. (4.83),

$$C_\beta(t) = U_{\beta 1}U^*_{\alpha 1}e^{-i(m_1/\gamma)t} + U_{\beta 2}U^*_{\alpha 2}e^{-i(m_2/\gamma)t} + U_{\beta 3}U^*_{\alpha 3}e^{-i(m_3/\gamma)t}. \tag{4.87}$$

The oscillation probability is,

$$P_{\nu_\alpha\to\nu_\beta} = |C_\beta(t)|^2 = \left|\sum_i U_{\beta i}U^*_{\alpha i}e^{-i(m_i/\gamma)t}\right|^2 = \sum_{i,j}\Lambda^{\alpha\beta}_{ij}\exp(i2\Phi_{ij}), \tag{4.88}$$

where

$$\Lambda^{\alpha\beta}_{ij} \equiv U_{\alpha i}U^*_{\beta i}U^*_{\alpha j}U_{\beta j}, \tag{4.89}$$

and

$$\Phi_{ij} = \frac{m_i - m_j}{2\gamma}t \to \frac{m_i^2 - m_j^2}{4E}L. \tag{4.90}$$

The oscillation probability (4.88) can also be directly obtained from the diagram in Fig. 4.6.

Sometimes it is useful to separate the probability formula into the CP-odd and CP-even terms and the oscillation probability is often expressed as[9]

$$P_{\nu_\alpha\to\nu_\beta} = \delta_{\alpha\beta} - 4\sum_{i>j}\sin^2\Phi_{ij}\Re\left[\Lambda^{\alpha\beta}_{ij}\right] - 2\sum_{i>j}\sin 2\Phi_{ij}\Im\left[\Lambda^{\alpha\beta}_{ij}\right], \tag{4.91}$$

where $\Re[\Lambda]$ and $\Im[\Lambda]$ denote the real and imaginary part of Λ, respectively. As it is seen from the third term of Eq. (4.91), the oscillation probability depends on imaginary part of $U_{\alpha i}$. This is one of the distinct differences from the two flavor oscillation. Since $\Lambda^{\beta\alpha}_{ij} = (\Lambda^{\alpha\beta}_{ij})^*$, the oscillation formula for reverse direction is,

[9] See Sect. 8.5.1 for the complete derivation.

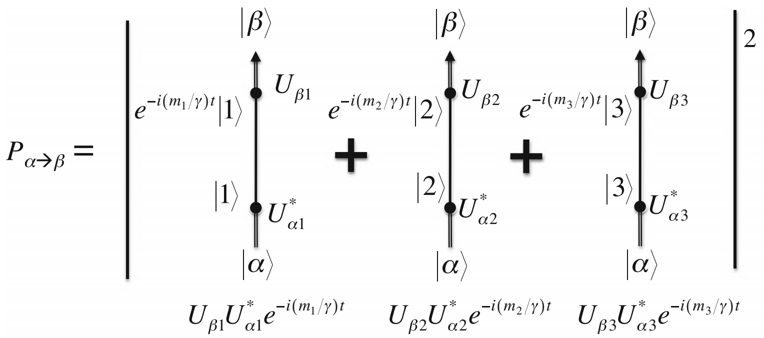

Fig. 4.6 The oscillation probability $|\alpha\rangle \to |\beta\rangle$ is the absolute square of the sum of three indistinguishable diagrams in which the initial state is $|\alpha\rangle$ and the final state is $|\beta\rangle$. See also Fig. 3.5

$$P_{\nu_\beta \to \nu_\alpha} = \delta_{\alpha\beta} - 4\sum_{i>j} \sin^2 \Phi_{ij} \Re\left[\Lambda_{ij}^{\alpha\beta}\right] + 2\sum_{i>j} \sin 2\Phi_{ij} \Im\left[\Lambda_{ij}^{\alpha\beta}\right]. \tag{4.92}$$

The oscillation probability of the antineutrino is obtained by taking the complex conjugate of the mixing matrix elements as described in Sect. 4.1.6 and is expressed by

$$P_{\overline{\nu}_\alpha \to \overline{\nu}_\beta} = \delta_{\alpha\beta} - 4\sum_{i>j} \sin^2 \Phi_{ij} \Re\left[\Lambda_{ij}^{\alpha\beta}\right] + 2\sum_{i>j} \sin 2\Phi_{ij} \Im\left[\Lambda_{ij}^{\alpha\beta}\right]. \tag{4.93}$$

The difference between the neutrino and antineutrino oscillation probability indicates CP violation, which is expressed by

$$\text{CP violation} = P_{\nu_\alpha \to \nu_\beta} - P_{\overline{\nu}_\alpha \to \overline{\nu}_\beta} = 4\sum_{i>j} \Im\left[\Lambda_{ij}^{\alpha\beta}\right] \sin 2\Phi_{ij}. \tag{4.94}$$

If CP is violated, $\Lambda_{ij}^{\alpha\beta}$ has to contain an imaginary component.

For the survival probability,

$$P_{\nu_\alpha \to \nu_\alpha} = 1 - 4\sum_{i>j} |U_{\alpha i}|^2 \left|U_{\alpha j}\right|^2 \sin^2 \Phi_{ij} = P_{\overline{\nu}_\alpha \to \overline{\nu}_\alpha}. \tag{4.95}$$

This means that CP symmetry always holds. Therefore, the CP violation effect should be searched for only in appearance measurements.

For the CPT transformation, the probabilities for CP and T transformations are given by

$$P_{\nu_{\alpha L} \to \nu_{\beta L}} \xrightarrow{\text{CP}} P_{\overline{\nu}_{\alpha R} \to \overline{\nu}_{\beta R}} \xrightarrow{\text{T}} P_{\overline{\nu}_{\beta R} \to \overline{\nu}_{\alpha R}}. \tag{4.96}$$

If there is difference between $P_{\nu_\alpha \to \nu_\beta}$ and $P_{\overline{\nu}_\beta \to \overline{\nu}_\alpha}$, CPT is violated. Experimentally it is easier to search for CPT violation by comparing the survival probabilities:

$$P_{\nu_\alpha \to \nu_\alpha} - P_{\overline{\nu}_\alpha \to \overline{\nu}_\alpha} = \text{CPT violation}. \tag{4.97}$$

Since CPT invariance was assumed when deriving the antineutrino oscillation formula (4.93), the CPT violation probability calculated using (4.91) and (4.93) is, by definition, 0.

$U_{\alpha j}$ and Δm^2_{jk} can be measured by neutrino oscillation experiments. If the absolute neutrino mass is measured by other experiments, the neutrino masses m_j can also be determined. Once $U_{\alpha j}$ and m_j are determined, the transition amplitudes can be obtained from

$$\mathscr{T} = U_\nu M U_\nu^\dagger. \tag{4.98}$$

For instance, the diagonal elements of the transition matrix are given by

$$\mu_\alpha = |U_{\alpha 1}|^2 m_1 + |U_{\alpha 2}|^2 m_2 + |U_{\alpha 3}|^2 m_3. \tag{4.99}$$

This indicates that the self-transition amplitude of flavor α is equivalent to the average mass of ν_α.[10]

4.2.3 Standard Parametrization of the Mixing Matrix

As described in Sect. 4.2.1, the transition matrix $\mathscr{T}$ defined by Eq. (4.75) is 3×3 Hermitian matrix. This form implies that there are nine free parameters. Three of them are real values and the other six are contained in three complex values. The mixing matrix U_ν is made from matrix $\mathscr{T}$ and thus also has nine free parameters.

The oscillation probability can be expressed from Eqs. (3.68) and (3.77) as

$$P_{\nu_\alpha \to \nu_\beta} = \sum_{kl} \langle \nu_\beta | \nu_k \rangle \langle \nu_k | \nu_\alpha \rangle \langle \nu_l | \nu_\beta \rangle \langle \nu_\alpha | \nu_l \rangle\, e^{-i \frac{(m_k - m_l)}{\gamma} t}. \tag{4.100}$$

This value is invariant for the following replacements,

$$|\nu_\alpha\rangle \to |\nu_\alpha\rangle\, e^{i\delta_\alpha}, \quad |\nu_i\rangle \to |\nu_i\rangle\, e^{i\delta_i}. \tag{4.101}$$

It means some of the imaginary parameters in the matrix U_ν may be removed without changing the oscillation probability. Equation (4.85) can be rewritten as

---

[10] The ν_e mass measured by tritium β decay experiments is the weighted average of the squared masses, $m_\beta^2 = |U_{e1}|^2 m_1^2 + |U_{e2}|^2 m_2^2 + |U_{e3}|^2 m_3^2$.

$$\begin{pmatrix} |\nu_1\rangle\, e^{i\delta_{e1}} \\ |\nu_2\rangle\, e^{i\delta_{e2}} \\ |\nu_3\rangle\, e^{i\delta_{e3}} \end{pmatrix} = \begin{pmatrix} |U_{e1}| & |U_{\mu 1}| & |U_{\tau 1}| \\ |U_{e2}| & |U_{\mu 2}|e^{i\delta_{12}^{e\mu}} & |U_{\tau 2}|e^{i\delta_{12}^{e\tau}} \\ |U_{e3}| & |U_{\mu 3}|e^{i\delta_{13}^{e\mu}} & |U_{\tau 3}|e^{i\delta_{13}^{e\tau}} \end{pmatrix} \begin{pmatrix} |\nu_e\rangle \\ |\nu_\mu\rangle\, e^{i(\delta_{\mu 1}-\delta_{e1})} \\ |\nu_\tau\rangle\, e^{i(\delta_{\tau 1}-\delta_{e1})} \end{pmatrix}, \tag{4.102}$$

where imaginary components are explicitly written as

$$U_{\alpha i} = |U_{\alpha i}| e^{i\delta_{\alpha i}}, \tag{4.103}$$

and

$$\delta_{ij}^{\alpha\beta} = (\delta_{\alpha i} - \delta_{\beta i}) - (\delta_{\alpha j} - \delta_{\beta j}). \tag{4.104}$$

Therefore, five phase parameters in the matrix U_ν can be moved as the phases of the wave functions. The imaginary component terms in the oscillation probability (4.91) do not change for this treatment. For example,

$$\begin{aligned} \Im[\Lambda_{23}^{\mu\tau}] &\to |U_{\mu 2}||U_{\mu 3}||U_{\tau 2}||U_{\tau 2}|\Im\left[\exp[i(\delta_{12}^{e\mu} - \delta_{13}^{e\mu} - \delta_{12}^{e\tau} + \delta_{13}^{e\tau})]\right] \\ &= |U_{\mu 2}||U_{\mu 3}||U_{\tau 2}||U_{\tau 2}|\sin[\delta_{\mu 2} - \delta_{\mu 3} - \delta_{\tau 2} + \delta_{\tau 3}] = \Im[\Lambda_{23}^{\mu\tau}]. \end{aligned} \tag{4.105}$$

In general, for n neutrinos, $2n-1$ phases can be removed from the mixing matrix in this way.

The removal of the five phase parameters from nine free parameters in the mixing matrix leaves four parameters. Since a 3×3 orthogonal matrix can have only three free parameters, U_ν can not be an orthogonal matrix and at least one parameter has to be imaginary. In general, for n neutrinos, there are n real self-transition amplitudes and $n(n-1)/2$ complex cross-transition amplitudes, resulting in n^2 parameters in the transition matrix and the mixing matrix. Of these, $2n-1$ are absorbed as phases of the wave functions, leaving $(n-1)^2$ physical parameters in the mixing matrix. Since a $n\times n$ orthogonal matrix can have $n(n-1)/2$ parameters, at least $(n-1)(n-2)/2$ parameters of the mixing matrix have to be imaginary and the rest are real.

We express the mixing matrix of the three flavor neutrinos by three real mixing angles and one imaginary parameter in the standard form, as given by

$$\begin{aligned} U_\nu &= \begin{pmatrix} 1 & 0 & 0 \\ 0 & c_{23} & s_{23} \\ 0 & -s_{23} & c_{23} \end{pmatrix} \begin{pmatrix} c_{13} & 0 & s_{13}e^{-i\delta} \\ 0 & 1 & 0 \\ -s_{13}e^{i\delta} & 0 & c_{13} \end{pmatrix} \begin{pmatrix} c_{12} & s_{12} & 0 \\ -s_{12} & c_{12} & 0 \\ 0 & 0 & 1 \end{pmatrix} \\ &= \begin{pmatrix} c_{12}c_{13} & s_{12}c_{13} & s_{13}e^{-i\delta} \\ -s_{12}c_{23} - c_{12}s_{23}s_{13}e^{i\delta} & c_{12}c_{23} - s_{12}s_{23}s_{13}e^{i\delta} & s_{23}c_{13} \\ s_{12}s_{23} - c_{12}c_{23}s_{13}e^{i\delta} & -s_{23}c_{12} - s_{12}c_{23}s_{13}e^{i\delta} & c_{23}c_{13} \end{pmatrix}, \end{aligned} \tag{4.106}$$

where $s_{ij} = \sin\theta_{ij}$ and $c_{ij} = \cos\theta_{ij}$. Although there is no one-to-one correspondence between the mixing angles and the cross-transition amplitudes, parametrization (4.106) turned out to be useful because the disappearance probabilities observed approximately correspond to the mixing angles.

If s_{ij} were small,[11] the mixing matrix would be approximated by

$$U_\nu = \begin{pmatrix} 1 & s_{12} & s_{13}e^{-i\delta} \\ -s_{12} & 1 & s_{23} \\ -s_{13}e^{i\delta} & -s_{23} & 1 \end{pmatrix} + O(s_{ij}^2). \tag{4.107}$$

Then, the transition amplitudes would be expressed as

$$\begin{aligned} \mathscr{T} = \begin{pmatrix} \mu_e & \tau_{\mu e}^* & \tau_{\tau e}^* \\ \tau_{\mu e} & \mu_\mu & \tau_{\tau\mu}^* \\ \tau_{\tau e} & \tau_{\tau\mu} & \mu_\tau \end{pmatrix} &= U_\nu \begin{pmatrix} m_1 & 0 & 0 \\ 0 & m_2 & 0 \\ 0 & 0 & m_3 \end{pmatrix} U_\nu^\dagger \\ &= \begin{pmatrix} m_1 & (m_2-m_1)s_{12} & (m_3-m_1)s_{13}e^{-i\delta} \\ (m_2-m_1)s_{12} & m_2 & (m_3-m_2)s_{23} \\ (m_3-m_1)s_{13}e^{i\delta} & (m_3-m_2)s_{23} & m_3 \end{pmatrix} + O(s_{ij}^2). \end{aligned} \tag{4.108}$$

This would give the relations,

$$m_1 \sim \mu_e, \quad m_2 \sim \mu_\mu, \quad m_3 \sim \mu_\tau, \tag{4.109}$$

and

$$s_{12} \sim \frac{\tau_{\mu e}}{\mu_\mu - \mu_e}, \quad s_{23} \sim \frac{\tau_{\tau\mu}}{\mu_\tau - \mu_\mu}, \quad s_{13}e^{i\delta} \sim \frac{\tau_{\tau e}}{\mu_\tau - \mu_e}. \tag{4.110}$$

These relations indicate that the ordering of ν_1, ν_2 and ν_3 are such that, in the limit of small mixings, $\nu_1 = \nu_e$, $\nu_2 = \nu_\mu$ and $\nu_3 = \nu_\tau$.

4.3 Matter Effects

To calculate and interpret the oscillation probabilities of neutrinos that propagate in the sun or earth, the matter effect has to be taken into account. The neutrino scattering cross section is so small that practically we can ignore the scattering effects. However, as we will see, the weak potential that causes coherent forward scattering of ultrarelativistic neutrinos becomes of the same order as $\Delta m^2/E_\nu$ and may have a sizable effect on the neutrino oscillation. It was pointed by [3–5] first and called the Mikheyev-Smirnov-Wolfenstein (MSW) effect.

[11] Experimentally it is known that s_{ij} are not small. The discussion here is just to obtain an image of the meaning of the mixing angles.

4.3.1 Weak Potentials

First we consider the neutrino-electron elastic scattering probability in the sun,

$$\nu_e + e^- \to \nu_e + e^-, \tag{4.111}$$

for which the Feynman diagram is shown in Fig. 2.13. The matrix element of the scattering is shown in Eq. (2.84) and the cross section is given in (2.93). For solar neutrinos with $E \sim 1$ MeV, the total cross section is $9.5 \times 10^{-43}\text{cm}^2$. Assuming that the neutrino passes through a 6,00,000 km thick hydrogen layer with density $\rho = 100\ \text{g/cm}^3$, the probability that the neutrino is scattered by an electron is

$$P \sim 10^{-6}. \tag{4.112}$$

Therefore, we can safely ignore the finite angle scatterings.

In order to calculate complete reactions of neutrino electron scatterings, it is necessary to take into account all possible diagrams as shown in Fig. 4.7. The reaction probability is given by

$$P \propto |\mathscr{M}_0 + \mathscr{M}_I|^2 = |\mathscr{M}_0|^2 + 2\Re(\mathscr{M}_0^* \mathscr{M}_I) + |\mathscr{M}_I|^2. \tag{4.113}$$

The first term is the probability for the two particles to just propagate in the space-time independently. The probability (4.112) is calculated from the third term of (4.113), in which the neutrino is scattered to a finite angle with respect to the original direction. This probability is proportional to G_F^2 and very small. Since $\mathscr{M}_0 = 0$ at finite momentum transfer, the second term $\Re(\mathscr{M}_0^* \mathscr{M}_I)$ is finite for only forward scattering. The probability of the second term is proportional to G_F and can be much larger than (4.112). The second term is responsible for the matter effect and we will calculate its probabilities below.

Figure 4.8 shows the Feynman diagrams for the weak potentials in matter. First we consider the ν_e-matter forward scattering. The matrix element of the ν_e-matter scattering is the sum of the charged current (a) and neutral current (c) components, given by

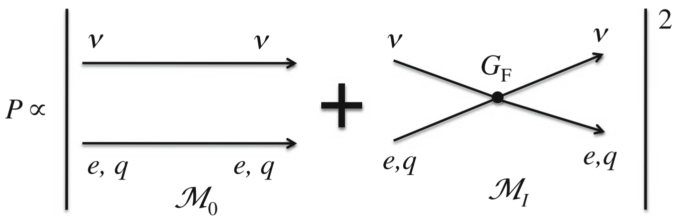

Fig. 4.7 Neutrino scattering probability. $\mathscr{M}_0$ is the diagram without scattering and $\mathscr{M}_I$ shows the diagram of the scattering

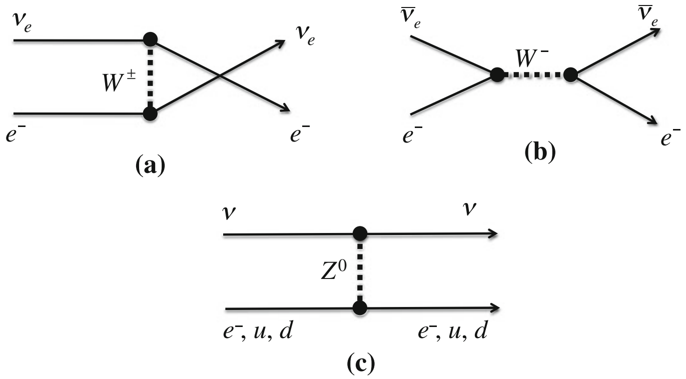

Fig. 4.8 Diagrams of the weak potentials. **a** Charged current scattering. **b** Charged current annihilation. **c** Neutral current scattering. **a** contributes for only ν_e, **b** contributes for only $\overline{\nu}_e$, **c** contributes for all the neutrinos equivalently

$$\mathscr{M}_I = \mathscr{M}_W + \mathscr{M}_Z = 2\sqrt{2}G_F[\overline{\nu_{eL}}\gamma_\rho\nu_{eL}] \times \left([\overline{e_L}\gamma^\rho e_L] + \sum_{f=e,q} [\overline{f}\gamma^\rho \frac{1}{2}(C_{fV} - C_{fA}\gamma_5)f] \right), \tag{4.114}$$

where the same factorization of the equation used in Sect. 2.4.4.3 is applied. For the neutral current potential, the ν_e is scattered by not only electron but also u and d quarks in protons and neutrons in the matter.

The Dirac equation for neutrinos in the weak potential is

$$i\gamma^\mu\partial_\mu\nu_e + (V_W + V_Z)\nu_e = 0, \tag{4.115}$$

where V_Z and V_W, respectively, are the neutral and charged current weak potentials given by

$$\begin{aligned} V_W &= 2\sqrt{2}G_F\gamma_\rho[\overline{e}_L\gamma^\rho e_L], \\ V_Z &= \sqrt{2}G_F\gamma_\rho \textstyle\sum_{f=e,q}[\overline{f}\gamma^\rho(C_{fV} - C_{fA}\gamma_5)f]. \end{aligned} \tag{4.116}$$

For V_W, the wave function of the LH electron at rest is[12]

$$e_L = \frac{1}{2}\begin{pmatrix} 1 & -1 \\ -1 & 1 \end{pmatrix}\begin{pmatrix} u \\ 0 \end{pmatrix} = \frac{1}{2}\begin{pmatrix} u \\ -u \end{pmatrix}, \tag{4.117}$$

[12] For simplicity, we omit the normalization factor $\sqrt{2m_e}$ of the wave function here. It is cancelled off later anyway.

where, u represents the spin direction. The electron spin direction is random and the $u = \chi_1$ and $u = \chi_2$ components exist with equal weight. The net contribution of the LH electron density is

$$\begin{aligned}\langle [\overline{e_{\mathrm{L}}}\gamma^{\rho} e_{\mathrm{L}}]\rangle &= \frac{1}{8}(\chi_1^{\dagger}\ \ \chi_1^{\dagger})\gamma^{\rho}\begin{pmatrix}\chi_1\\ -\chi_1\end{pmatrix} + \frac{1}{8}(\chi_2^{\dagger}\ \ \chi_2^{\dagger})\gamma^{\rho}\begin{pmatrix}\chi_2\\ -\chi_2\end{pmatrix}\\ &= \begin{cases}1/2; & \rho = 0\\ 0; & \rho = 1,\ 2,\ 3.\end{cases}\end{aligned} \tag{4.118}$$

This means that only the γ^0 term of the electron current contributes to V_W. From Eqs. (4.116), (4.118) and the electron number density in matter n_e, the charged current potential is expressed as

$$V_W = \sqrt{2} G_F n_e. \tag{4.119}$$

For neutral matter that consists of atoms whose atomic number and mass number are Z and A, the electron density is given by

$$n_e[/\mathrm{cm}^3] = (6.0 \times 10^{23}) \times \rho[\mathrm{g/cm}^3] \times \frac{Z}{A}. \tag{4.120}$$

Therefore, the charged current potential is

$$V_W[\mathrm{eV}] \sim 7.6 \times 10^{-14} \times \rho[\mathrm{g/cm}^3] \times \frac{Z}{A}. \tag{4.121}$$

Since the density of the hydrogen is $\rho \sim 100\ \mathrm{g/cm}^3$ near the center of the sun and $Z \sim A$, the magnitude of the weak potential is

$$V_W^{\odot} \sim 8 \times 10^{-12}\ \mathrm{eV}. \tag{4.122}$$

This value can be equivalent to the size of $\Delta m^2/4\overline{E}$ in (4.56), which is $\sim 10^{-11}$ eV for $\Delta m^2 \sim 10^{-4}\ \mathrm{eV}^2$ and $\overline{E} \sim 10$ MeV.

As for the neutral current potential V_Z in (4.116), a proton consists of two u-quarks and one d-quark and a neutron consists of two d-quarks and one u-quark. Therefore, the neutral current potential becomes,

$$V_Z = \sqrt{2} G_F \gamma_{\rho}\begin{pmatrix} n_e\left[\overline{e}\gamma^{\rho}(C_{eV} - C_{eA}\gamma_5)e\right] + (2n_p + n_n)\left[\overline{u}\gamma^{\rho}(C_{uV} - C_{uA}\gamma_5)u\right]\\ + (2n_n + n_p)\left[\overline{d}\gamma^{\rho}(C_{dV} - C_{dA}\gamma_5)d\right]\end{pmatrix}, \tag{4.123}$$

where n_p is the proton number density and n_n is the neutron number density. For neutral matters, the proton number density is the same as the electron number density, $n_p = n_e$. In this case, the electron potential and proton potential cancel out,

$$
\begin{aligned}
&V_Z(e) + V_Z(p) = \sqrt{2} G_F n_e \gamma_\rho \\
&\quad \times \left(\begin{array}{l} \left[\overline{e}\gamma^\rho \left((4x_w - 1) + \gamma_5\right) e\right] + 2\left[\overline{u}\gamma^\rho \left((-(8/3)x_w + 1) - \gamma_5\right) u\right] \\ + \left[\overline{d}\gamma^\rho \left(((4/3)x_w - 1) + \gamma_5\right) d\right] \end{array} \right) \\
&\quad \to 0.
\end{aligned}
\tag{4.124}
$$

The neutron potential is,

$$
\begin{aligned}
&V_Z(n) = \sqrt{2} G_F n_n \gamma_\rho \\
&\times \left(\left[\overline{u}\gamma^\rho \left((-(8/3)x_w + 1) - \gamma_5\right) u\right] + 2\left[\overline{d}\gamma^\rho \left(((4/3)x_w - 1) + \gamma_5\right) d\right] \right) \\
&\to -\sqrt{2} G_F n_n \gamma_\rho \left[\overline{f}\gamma^\rho \left(1 - \gamma_5\right) f\right] = -2\sqrt{2} G_F n_n \gamma_\rho \left[\overline{f_L}\gamma^\rho f_L\right].
\end{aligned}
\tag{4.125}
$$

Following the same procedure for V_W,

$$
V_Z = -\sqrt{2} G_F n_n. \tag{4.126}
$$

n_n is small in the sun and V_Z is also small but it can be larger than n_p or n_e in the earth.

For antineutrino scattering, $\overline{\nu}_e e^-$, the matrix element is, from Eq. (2.90),

$$
\mathscr{M}_{\overline{\nu}_e e} = 2\sqrt{2} G_F [\overline{\overline{\nu}_{eR}} \gamma_\rho \overline{\nu}_{eR}] \left([\overline{e_L}\gamma^\rho e_L] + \sum_{f=e,q} [\overline{f}\gamma^\rho \frac{1}{2}(C_{fV} - C_{fA}\gamma_5) f] \right). \tag{4.127}
$$

The electron and quark currents are the same as ν_e scattering case, (4.114). Therefore, the weak potentials for $\overline{\nu}_e$ change the sign,

$$
\overline{V}_W = -V_W \ \text{ and } \ \overline{V}_Z = -V_Z, \tag{4.128}
$$

just like the electromagnetic potential changes the sign for the anti-particles.

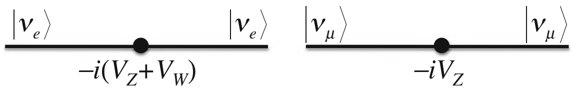

Fig. 4.9 Neutrino-matter interactions

4.3.2 Neutrino Oscillation in Matter

The weak potentials can be interpreted as the self-transitions as shown in Fig. 4.9. When calculating the probability of the neutrino oscillation in matter, these amplitudes have to be added to the state equation. The state equation of neutrinos in matter is, therefore, from (4.56),

$$\begin{aligned}\frac{d}{dt}\begin{pmatrix}C_e\\C_\mu\end{pmatrix} &= -i\left[\frac{1}{\gamma}\begin{pmatrix}\mu_e & \tau_\nu\\ \tau_\nu & \mu_\mu\end{pmatrix} + \begin{pmatrix}V_Z+V_W & 0\\ 0 & V_Z\end{pmatrix}\right]\begin{pmatrix}C_e\\C_\mu\end{pmatrix}\\ &= -i\left[\left(\frac{\overline{m}^2}{E}+V_Z+\frac{1}{2}V_W\right)I + \omega_0\begin{pmatrix}-\cos 2\theta_\nu + \upsilon_W & \sin 2\theta_\nu\\ \sin 2\theta_\nu & \cos 2\theta_\nu - \upsilon_W\end{pmatrix}\right]\begin{pmatrix}C_e\\C_\mu\end{pmatrix},\end{aligned} \tag{4.129}$$

where $\omega_0 = \Delta m_\pm^2/4E$ and θ_ν is the neutrino mixing angle in vacuum, which is defined in Eq. (4.56). The potential parameter υ_W represents the strength of the charged current weak potential,

$$\upsilon_W = \frac{2EV_W}{\Delta m_\pm^2} = \frac{2\sqrt{2}EG_F n_e}{\Delta m_\pm^2} \sim 1.5\times 10^{-7}\rho[\mathrm{g/cm^3}]\frac{Z}{A}\frac{E[\mathrm{MeV}]}{\Delta m_\pm^2[\mathrm{eV^2}]}, \tag{4.130}$$

The oscillation part of the state equation (4.129) can be rewritten in the standard form:

$$\frac{d}{dt}\begin{pmatrix}C_e\\C_\mu\end{pmatrix} = -i\tilde{\omega}\begin{pmatrix}-\cos 2\tilde{\theta} & \sin 2\tilde{\theta}\\ \sin 2\tilde{\theta} & \cos 2\tilde{\theta}\end{pmatrix}\begin{pmatrix}C_e\\C_\mu\end{pmatrix}, \tag{4.131}$$

where the tilde mark ($\tilde{}$) above the parameters represents that they are the parameters in the matter and $\tilde{\omega} = \kappa\omega_0$. The scale factor κ and the mixing angle in matter $\tilde{\theta}$ are defined as,

$$\kappa = \sqrt{(\cos 2\theta_\nu - \upsilon_W)^2 + \sin^2 2\theta_\nu}, \quad \tan 2\tilde{\theta} = \frac{\sin 2\theta_\nu}{\cos 2\theta_\nu - \upsilon_W}. \tag{4.132}$$

The relation between θ_ν and $\tilde{\theta}$ is shown graphically in Fig. 4.10a. It can also be expressed by Fig. 4.10b. These relations show that V_Z does not contribute to the mixing nor oscillation phenomena. Since this state equation in matter has exactly the same form as (3.42), we can borrow the relations derived in Sect. 3.3.2.

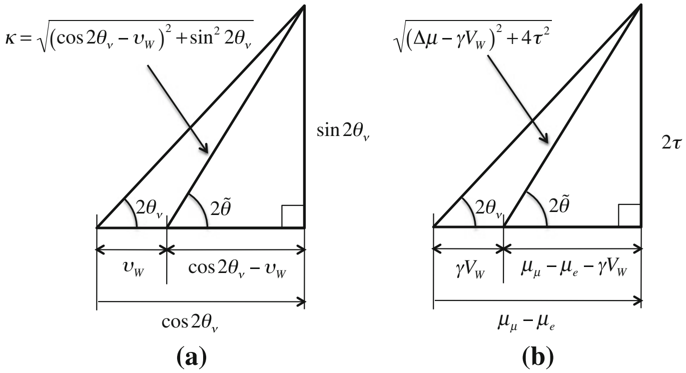

Fig. 4.10 Mixing triangles in matter. **a** Based on the relation of the mixing angles in vacuum and matter. **b** Same as **a** but based on the transition amplitudes and the weak potential

The mass eigenstates in matter are

$$\begin{pmatrix} |\tilde{\nu}_-\rangle \\ |\tilde{\nu}_+\rangle \end{pmatrix} = \begin{pmatrix} \cos\tilde{\theta} & -\sin\tilde{\theta} \\ \sin\tilde{\theta} & \cos\tilde{\theta} \end{pmatrix} \begin{pmatrix} |\nu_e\rangle \\ |\nu_\mu\rangle \end{pmatrix}, \tag{4.133}$$

with the new masses of

$$\tilde{m}_\pm = \left(\overline{m} + \frac{E}{\overline{m}}\left(V_Z + \frac{V_W}{2}\right)\right) \pm \kappa\omega_0. \tag{4.134}$$

The general wave function in matter is

$$\tilde{\psi}_\nu(t) = \tilde{C}_+ e^{-i(\tilde{m}_+/\gamma)t} |\tilde{\nu}_+\rangle + \tilde{C}_- e^{-i(\tilde{m}_-/\gamma)t} |\tilde{\nu}_-\rangle . \tag{4.135}$$

The oscillation probabilities for neutrinos passing through matter of length L are given by

$$\begin{aligned} \tilde{P}_{\nu_e\to\nu_e}(L) &= \tilde{P}_{\nu_\mu\to\nu_\mu}(L) = 1 - \sin^2 2\tilde{\theta}\sin^2\tilde{\omega}L, \\ \tilde{P}_{\nu_\mu\to\nu_e}(L) &= \tilde{P}_{\nu_e\to\nu_\mu}(L) = \sin^2 2\tilde{\theta}\sin^2\tilde{\omega}L. \end{aligned} \tag{4.136}$$

The oscillation amplitude is

$$\sin^2 2\tilde{\theta} = \frac{\sin^2 2\theta_\nu}{(\cos 2\theta_\nu - \upsilon_W)^2 + \sin^2 2\theta_\nu}. \tag{4.137}$$

This indicates that at $\upsilon_W = \cos 2\theta_\nu$, $\sin^2 2\tilde{\theta}$ can be unity no matter how small the vacuum oscillation amplitude, $\sin^2 2\theta_\nu$, is. This mechanism was used to describe the large solar neutrino deficit by small mixing angle in vacuum in the early days of solar neutrino studies. $\upsilon_W = \cos 2\theta_\nu$ is called the *resonance condition*.

The heavy neutrino component of the electron neutrino is

$$\sin^2\tilde{\theta} = \frac{1}{2}\left(1 - \frac{\cos 2\theta_\nu - \upsilon_W}{\kappa}\right). \tag{4.138}$$

Even if the mass hierarchy is normal in vacuum ($\cos 2\theta_\nu > 0$), it can be inverted in matter ($\cos 2\tilde{\theta} < 0$), if $\upsilon_W > \cos 2\theta_\nu$.

For solar neutrino oscillation,

$$\Delta m_\pm^2 \sim 8 \times 10^{-5}\left[\mathrm{eV}^2\right], \quad \rho_\odot \sim 100\left[\mathrm{g/cm}^3\right], \quad A \sim Z, \tag{4.139}$$

and the potential parameter for $\upsilon_\odot$ in the sun is

$$\upsilon_\odot \sim 0.2E_\nu[/\mathrm{MeV}]. \tag{4.140}$$

Since the solar neutrino energy is $E_\nu < 20$ MeV, some neutrinos experience the resonance condition.

For atmospheric and accelerator neutrino oscillation on earth,

$$\Delta m_\pm^2 \sim 2.4 \times 10^{-3}\left[\mathrm{eV}^2\right], \quad \rho_\oplus \sim 5\left[\mathrm{g/cm}^3\right], \quad A \sim 2Z, \tag{4.141}$$

and the potential parameter $\upsilon_\oplus$ is,

$$\upsilon_\oplus \sim 0.1\eta_C E_\nu[/\mathrm{GeV}], \tag{4.142}$$

where $\eta_C = +1$ for neutrinos and $\eta_C = -1$ for antineutrinos. Energies of atmospheric and accelerator neutrinos (~GeV) are in the ranges where matter effects can be significant.

Note that $\cos 2\theta_\nu$ changes its sign depending on the mass hierarchy of the neutrinos (Table 4.1). This dependence can be used to determine the mass hierarchy, which can not be determined by the vacuum oscillation.

Similarly for antineutrinos, the potential parameter υ_W changes sign. This dependence can introduce a spurious CP violation effect. Therefore, the matter effect has to be understood properly when measuring CP violation.

For long baseline reactor neutrino experiments,

$$\Delta m_\pm^2 \sim 8 \times 10^{-5}\left[\mathrm{eV}^2\right], \quad \rho_\oplus \sim 5\left[\mathrm{g/cm}^3\right], \quad A \sim 2Z, \quad E_\nu \sim 4\mathrm{MeV}. \tag{4.143}$$

The potential parameter is

$$\upsilon_\oplus \sim -0.02 \tag{4.144}$$

and small.

The matter effect produces effective mass, and it may seem that standard model massless neutrinos could oscillate in matter, acquiring mass from the matter effect.

However, for massless neutrinos, the potential parameter (4.130) becomes infinitely large and the mixing angle in matter (4.137) becomes 0. This indicates that massless neutrinos can not oscillate even in matter.

4.4 A Paradox in Neutrino Oscillation

The interpretation of neutrino oscillation includes a famous paradox which can be explained by the uncertainty principle.

Suppose we measure the time dependence of the probability of oscillation, $\nu_\mu \to \nu_e$. The ν_μ is assumed to be produced in a charged pion decay at rest, $\pi^+ \to \mu^+ + \nu_\mu$. Due to helicity suppression, the pion decays to ν_μ with almost 100 % probability.

From the neutrino oscillation, the probability of finding ν_e at time t is,

$$P_{\pi\to\nu_e}(t) = \sin^2 2\theta \sin^2 \frac{\Delta m^2}{4E_\nu} t, \tag{4.145}$$

where t is the time between the pion decay and the detection of the neutrino. We assume that the time of the pion decay is measured by detecting the muon. The neutrino in the $\pi \to \mu\nu$ decay is a superposition of mass eigenstates $|\nu_1\rangle$ and $|\nu_2\rangle$.

$$\psi_\nu(0) = |\nu_\mu\rangle = \sin\theta\,|\nu_1\rangle + \cos\theta\,|\nu_2\rangle\,. \tag{4.146}$$

Since the muon energy in the decay depends on the neutrino mass, we can determine which neutrino mass eigenstate is produced in the decay from the energy of the muon as shown in Fig. 4.11. If we determine which neutrino mass eigenstate is produced from the muon energy, we will observe ν_1 with a probability $\sin^2\theta$ and ν_2 with a probability $\cos^2\theta$ in the neutrino detector.

Now, we assume that we know ν_2 is generated in this measurement. In this case, at later time t, the neutrino wave function becomes,

$$\psi_\nu(t) = |\nu_2\rangle\, e^{-im_2 t} = \cos\theta\,|\nu_\mu\rangle\, e^{-im_2 t} - \sin\theta\,|\nu_e\rangle\, e^{-im_2 t}. \tag{4.147}$$

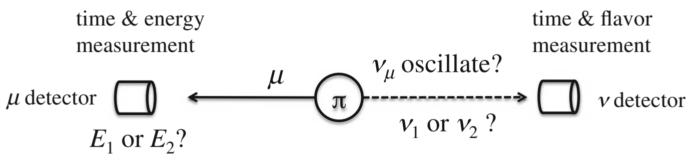

Fig. 4.11 If we measure the energy of the muon precisely, we can know which mass eigenstate neutrino, ν_1 or ν_2, is produced

Therefore, the probability of finding ν_e in the ν_2 event sample is

$$P_{\pi\to\nu_2\to\nu_e}(t) = \cos^2\theta \times |-\sin\theta\, e^{-im_2 t}|^2 = \sin^2\theta\cos^2\theta. \tag{4.148}$$

Similarly, the probability of finding ν_e in the ν_1 event sample is

$$P_{\pi\to\nu_1\to\nu_e}(t) = \sin^2\theta \times |\cos\theta\, e^{-im_1 t}|^2 = \sin^2\theta\cos^2\theta. \tag{4.149}$$

The probability of observing ν_e is the sum of Eqs. (4.148) and (4.149),

$$P_{\pi\to\nu_e}(t) = P_{\pi\to\nu_2\to\nu_e}(t) + P_{\pi\to\nu_1\to\nu_e}(t) = \frac{1}{2}\sin^2 2\theta. \tag{4.150}$$

This probability is independent of time and contradicts the oscillation probability (4.145). It seems that whether the neutrino oscillates or not depends on whether the muon energy is measured or not, even if the measured information is not used. This is an example of the *measurement problem*.

This paradox can be explained qualitatively by taking into account the uncertainty principle. The relation of neutrino mass and muon energy is, from Eq. (4.18),

$$E_\mu = E_0 - \frac{m_\nu^2}{2m_\pi}, \tag{4.151}$$

where E_0 is the muon energy in the case $m_\nu = 0$. In order to distinguish ν_1 and ν_2, the energy resolution for the muon δE_μ has to be smaller than the difference of muon energies corresponding to the decays in which ν_1 or ν_2 is produced,

$$\delta E_\mu < \frac{m_{\nu_2}^2}{2m_\pi} - \frac{m_{\nu_1}^2}{2m_\pi} = \frac{\Delta m^2}{2m_\pi}. \tag{4.152}$$

Due to the uncertainty principle, in the system in which we can measure the energy with such precision, we can not determine the time when the muon is detected with precision better than,

$$\delta t > \frac{1}{2\delta E_\mu} > \frac{m_\pi}{2\Delta m^2}. \tag{4.153}$$

Since there is an ambiguity δt in the detection time of the muon, we can not know the pion decay time with precision better than δt. Therefore, it is impossible to know the time between the production and the detection of the neutrino with precision better than δt. Since the angular velocity of the oscillation is $\omega = \frac{\Delta m^2}{2E_\nu}$, the uncertainty of the oscillation phase $\delta\Phi$ introduced by the uncertainty of the time δt is,

$$\delta\Phi = \omega\delta t = \frac{m_\pi}{2E_\mu} > 1, \tag{4.154}$$

where the relation $E_\mu = \frac{m_\pi}{2}(1-(m_\mu/m_\pi)^2) < \frac{m_\pi}{2}$ is used. This indicates that when we try to measure the oscillation in this system, the time dependence of the oscillation is averaged out and what will be observed is,

$$P_{\nu_\mu \to \nu_e} = \sin^2 2\theta \left\langle \sin^2 \frac{\Delta m^2}{4E} t \right\rangle = \frac{1}{2} \sin^2 2\theta, \tag{4.155}$$

where $\langle\ \rangle$ shows the average over time. This probability agrees with Eq. (4.150).

Contrary, it is possible to show that in a system in which neutrino oscillation can be measured (this is our system), it is impossible to measure the muon energy precise enough to distinguish ν_1 and ν_2.

The reason we thought the paradox exited is that we wrongly assumed that we could measure both the time and energy precise enough to observe the oscillation and to distinguish between two neutrino masses simultaneously.

References

1. E.K. Akhmedov, A.Y. Smirnov, Paradoxed of neutrino oscillations. Phys. At. Nucl. **72**(8), 1363–1381 (2000)
2. E.K. Akhmedov, A.Y. Smirnov, Neutrino oscillations: entanglement, energy-momentum conservation and QFT. Found. Phys. **41**, 1279–1306 (2011)
3. S.P. Mikheyev, A.Y. Smirnov, Nuovo Cimento **9C**, 17 (1986)
4. L. Wolfenstein, PRD **17**, 2369 (1978)
5. H.A. Bethe, PRL **56**, 1305 (1986)

Chapter 5
Experiments

Abstract In this chapter, the neutrino oscillation experiments that observed widely accepted positive oscillation signals are reviewed. The experiments are categorized as atmospheric, accelerator, solar, or reactor neutrino experiments. The principle and technique of each experiment, such as how neutrinos are generated, what are properties of the neutrinos, what is the structure of the neutrino detector and how the neutrinos are detected, are explained briefly. In most of the papers, the experimental data are analyzed assuming the two flavor oscillation formula and the oscillation parameters, θ and Δm^2 are derived. Significant plots and measured parameters are shown at the end of the explanation of each experiment.

Keywords Atmospheric neutrino · Accelerator neutrino · Solar neutrino · Reactor neutrino · Appearance measurement · Disappearance measurement

5.1 Introduction

In neutrino oscillation experiments, there are two types of measurements. One is the appearance measurement, which detects the generation of a different flavor neutrino from the original flavor produced. In the two flavor oscillation, the appearance probability is expressed by

$$P_{\nu_\alpha \to \nu_\beta} = \sin^2 2\theta \sin^2 \frac{\Delta m^2}{4E} L, \tag{5.1}$$

where the flavor indices are different, $\beta \neq \alpha$.

The other is the disappearance measurement, which detects the same flavor neutrinos as the original flavor produced and measures the deficit of the neutrino flux caused by the change of the flavor due to oscillation. The probability that the neutrino remains in the original flavor is given by

$$P_{\nu_\alpha \to \nu_\alpha} = 1 - \sin^2 2\theta \sin^2 \frac{\Delta m^2}{4E} L. \tag{5.2}$$

F. Suekane, *Neutrino Oscillations*, Lecture Notes in Physics 898,
DOI 10.1007/978-4-431-55462-2_5

The parameters to be measured by neutrino oscillation experiments are the mixing angle θ and the mass squared difference between the two mass eigenstates Δm^2. If the baseline L is measured in [km], the neutrino energy E is measured in [GeV] and the squared mass difference Δm^2 is measured in [eV^2], the oscillation phase can be numerically expressed as follows:

$$\Phi[\text{rad}] = \frac{\Delta m^2}{4E}L = 1.27\frac{\Delta m^2[\text{eV}^2]}{E[\text{GeV}]}L[\text{km}]. \tag{5.3}$$

A number of neutrino oscillation experiments have been carried out at various baselines with various neutrino energies. Figure 5.1 summarizes the relation between baselines and typical energies of such experiments. The solid lines in Fig. 5.1 show the relation $E = \Delta m^2 L/2\pi$, which is called *the first oscillation maximum*, and the dashed lines show the relation $E = \Delta m^2 L/6\pi$, which is called *the second oscillation maximum*.

Currently oscillations at two mass square differences, $|\Delta m^2_{\odot}| \sim 8.0 \times 10^{-5}$ eV^2 and $|\Delta m^2_{\oplus}| \sim 2.5 \times 10^{-3}$ eV^2, are confirmed by various experiments, where $\Delta m^2_{\odot}$ indicates that this Δm^2 was suggested by the solar neutrinos first and $\Delta m^2_{\oplus}$, by the atmospheric neutrinos on earth. Some experiments suggest there are other oscillations at $|\Delta m^2| \sim 1$ eV^2, but this contradicts the three flavor neutrino scheme and is not

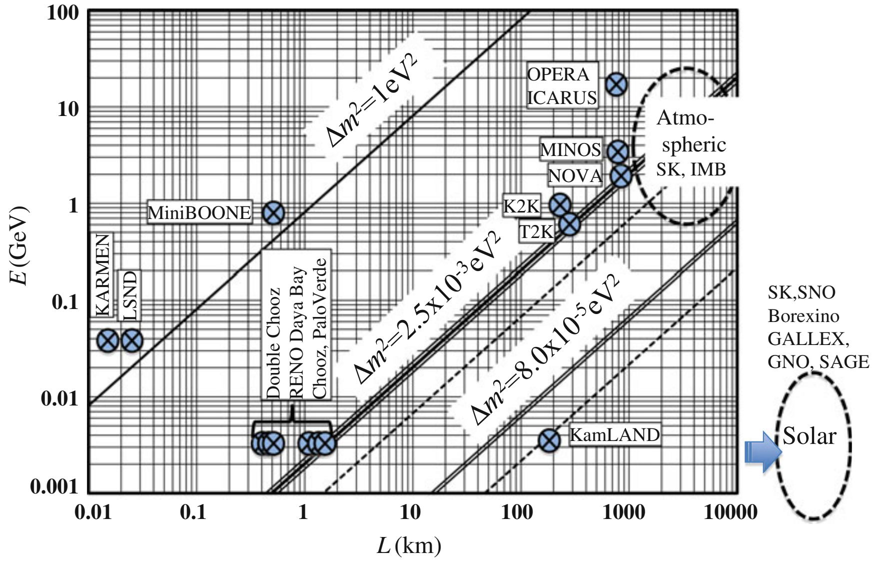

Fig. 5.1 Relation between baselines and typical energies of various neutrino oscillation experiments. The *solid lines* (single, double and triple lines) show the first oscillation maximum and the *dashed lines* show the second oscillation maximum for Δm^2 =1, 8.0×10^{-5} and 2.5×10^{-3} [eV^2], respectively

accepted yet by the community. Atmospheric, accelerator and reactor experiments measure neutrino oscillation at $|\Delta m^2_{\oplus}|$ and solar and reactor experiments measure at $|\Delta m^2_{\odot}|$. In the following subsections the major neutrino oscillation experiments are reviewed and the experimental methods and measured results are described.

5.2 Atmospheric Neutrino Oscillation

The first definite evidence of neutrino oscillation was found in atmospheric neutrinos by the Super-Kamiokande group in 1998. A large number of high energy (>GeV) cosmic-rays (mostly protons) are constantly hitting the earth. From the cosmic-ray interactions with oxygen or nitrogen nuclei in the atmosphere, charged pions are produced, which decay as $\pi^{\pm} \rightarrow \mu^{\pm} + \nu_\mu/\bar{\nu}_\mu$ with the intrinsic lifetime of $c\tau \sim 8\,\text{m}$. Then the muon decays as $\mu^{\pm} \rightarrow e^{\pm} + \nu_e/\bar{\nu}_e + \bar{\nu}_\mu/\nu_\mu$ with $c\tau \sim 700\,\text{m}$. The neutrinos produced from these reactions are called the atmospheric neutrinos. The produced neutrinos can penetrate the earth and be detected at the opposite side of the earth. Since the thickness of the atmospheric layer is much less than the radius of the earth, the neutrino production point is regarded as the surface of the earth and the distance between the neutrino generation point and detector can be determined by

$$L = 2R_{\otimes} \cos\theta, \tag{5.4}$$

as shown in Fig. 5.2, where $R_{\otimes}$ is the radius of the earth. From the process of atmospheric neutrino production, the ratio of the number of the muon-type neutrinos to electron-type neutrinos is expected to be

$$\frac{N(\nu_\mu) + N(\bar{\nu}_\mu)}{N(\nu_e) + N(\bar{\nu}_e)} \sim 2. \tag{5.5}$$

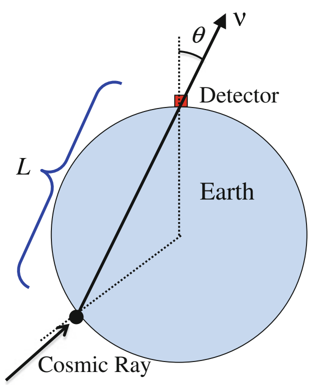

Fig. 5.2 Atmospheric neutrinos are generated within the thin layer of atmosphere and can be detected on the opposite side of the earth. The relation between the angle and the neutrino travel distance is $L = 2R_{\otimes} \cos\theta$, where $R_{\otimes}$ is the radius of the earth

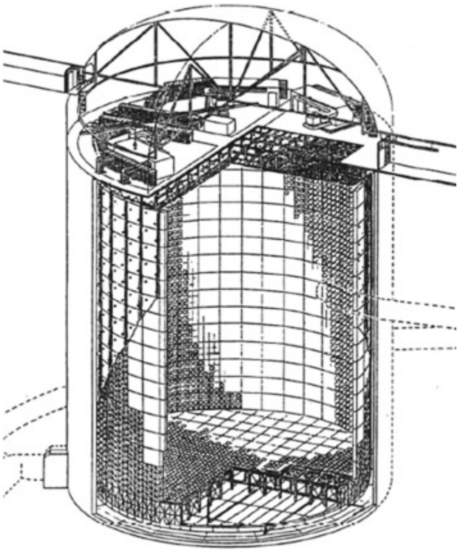

Fig. 5.3 The Super-Kamiokande detector. From [1]

However, early observations by the IMB and Kamiokande experiments showed that the ratio is roughly one. This was called the *atmospheric neutrino anomaly*. The Super-Kamiokande (SK) detector, which has 50 times more target volume than Kamiokande detector, started the operation in 1996 and concluded that the anomaly is due to neutrino oscillation. Figure 5.3 shows the structure of the SK detector. The SK detector is located 1,000 m below Ikenoyama mountain in the Gifu prefecture, Japan. It uses 50,000 tons of ultra-pure water as the neutrino target. Charged particles with velocity $\beta > 0.75$ in water emit Čerenkov light. 11,200 20-inch photomultipliers (PMT) are mounted at the inner wall of the detector to detect the Čerenkov light.

From the charged current interactions in the water, ν_μ produces muon and ν_e produces electron as shown in Eq. (5.6).

$$\begin{aligned} \nu_\mu + A &\to \mu + X, \\ \nu_e + A &\to e + X. \end{aligned} \tag{5.6}$$

The produced high energy charged leptons go forward with respect to the direction of the incoming neutrinos. If the charged lepton is a muon, it produces a clear Čerenkov ring as shown in Fig. 5.4a. The direction of the muon can be measured from the direction of the Čerenkov ring. Therefore, the baseline of the neutrino's detection can be measured from the relation (5.4). If the muon is produced and stops within the detector, which is called the fully contained event, the muon energy can be measured

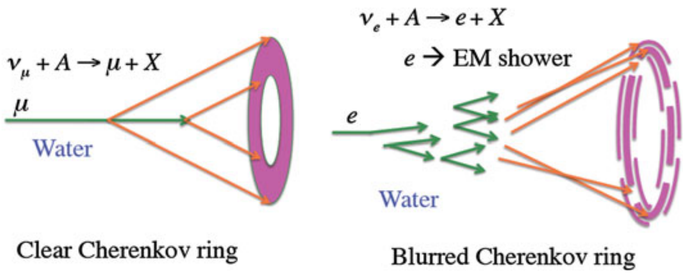

Fig. 5.4 Particle identification in a water Čerenkov detector. Muons produce clear Čerenkov rings while electrons produce blurred Čerenkov rings

from the total Čerenkov light yield and the original neutrino energy can be deduced from it.

For the ν_e interactions, the produced electrons generate an electromagnetic shower in the water, and electrons and positrons in the shower generate blurred Čerenkov ring as indicated in Fig. 5.4b. Most of the electrons and positrons are contained in the detector volume since they produce the shower, and the electron energy can be measured. The ν_μ and ν_e can be distinguished by the difference of the Čerenkov light patterns. Figure 5.5 is the plot that reported the first evidence of neutrino oscillation. Figure 5.5a shows a L/E dependence of the atmospheric neutrino events. A clear neutrino deficit is observed in the ν_μ flux while distribution of ν_e is flat which is

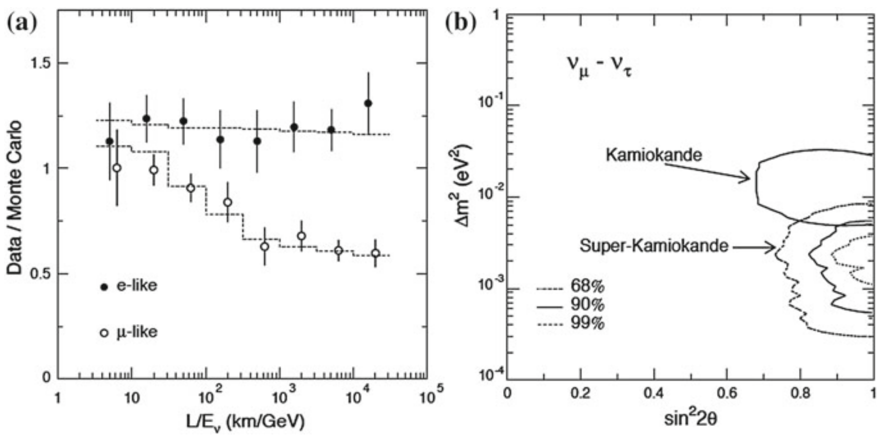

Fig. 5.5 The historical data that show the first evidence of neutrino oscillations. **a** The ratio of the fully contained Data to Monte Carlo prediction as a function of L/E. The *dashed line* shows the expected shape for $\nu_\mu \leftrightarrow \nu_\tau$ oscillation at $\Delta m^2 = 2.2 \times 10^{-3}\text{eV}^2$ and $\sin^2 2\theta = 1$. A clear deficit pattern is observed in ν_μ flux while ν_e flux stays constant. **b** Confidence intervals for $\sin^2 2\theta$ and Δm^2 for $\nu_\mu \leftrightarrow \nu_\tau$ two-neutrino oscillations. The result of the Kamiokande experiment is also shown. From [2]

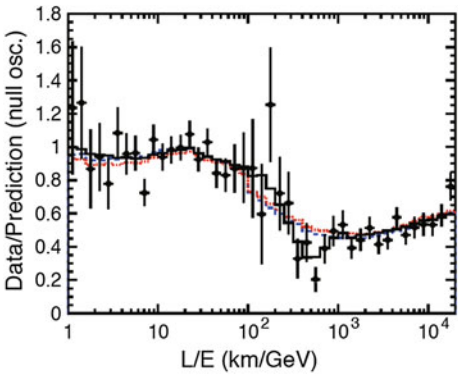

Fig. 5.6 Result of the L/E analysis of atmospheric neutrino data of Super-Kamiokande. The horizontal axis is the reconstructed L/E. The points show the ratio of the data to the Monte Carlo prediction without oscillations. The error bars are statistical only. The *solid line* shows the best fit with 2-flavor $\nu_\mu \to \nu_\tau$ oscillation. The *dashed* and *dotted lines* show the best fit expectations for neutrino decay and neutrino decoherence hypotheses, respectively. From [4]

consistent with the expectation. If the oscillation was of $\nu_\mu \to \nu_e$ type, the ν_e flux would have been increased by the rate of ν_μ disappearance. Therefore, this plot also indicates that the oscillation is mainly due to $\nu_\mu \to \nu_\tau$ oscillation. Figure 5.5b shows the contour plots of the allowed parameter region, which shows $\sin^2 2\theta \sim 1$ and $\Delta m^2 \sim 2 \times 10^{-3}$ eV^2. Now, 17 years later, the precision of the measurement is much improved. Figure 5.6 shows the recent results of L/E dependence of the ν_μ events. There is a dip at around $L/E \sim 6 \times 10^2$ km/GeV indicating the oscillation with $|\Delta m^2| \sim 2 \times 10^{-3}$ eV^2. An increase of the event rate, which is a unique characteristic of oscillation, can be seen at $L/E > 1 \times 10^3$ km/GeV. The up-to-date oscillation parameters measured by the Super-Kamiokande group are

$$0.407 < \sin^2\theta < 0.583, \quad 1.7 \times 10^{-3} < \Delta m^2 < 2.7 \times 10^{-3}\text{eV}^2, \tag{5.7}$$

at 90 % confidence level (CL) if the mass hierarchy is not specified [3].

5.3 Long Baseline Accelerator Experiments

In long baseline accelerator experiments, the neutrinos are produced mainly from charged pion decays via the reaction,

$$\begin{aligned} p + A &\to \pi^\pm + X \\ &\hookrightarrow \pi^\pm \to \mu^\pm + \nu_\mu/\bar{\nu}_\mu. \end{aligned} \tag{5.8}$$

Fig. 5.7 Locations of accelerators and detectors for K2K, T2K, MINOS, OPERA and ICARUS experiments. (The scale of the maps are different.) [Google map]

Because of the almost 100 % branching fraction of the $\pi \rightarrow \mu + \nu$ decay, the neutrino beam consists of mostly ν_μ or $\bar{\nu}_\mu$. Therefore, the accelerator neutrino beam is suitable for studying the oscillation of the muon-type neutrinos. The typical energy of accelerator neutrinos is of the order of GeV. Thus, a baseline of several hundred kilometers is necessary to study at the Δm^2 measured by atmospheric neutrino oscillation. The accelerator experiments K2K (KEK To Kamioka), T2K (Tokai to Kamioka), MINOS (Main Injector Neutrino Oscillation Search) and OPERA (Oscillation Project with Emulsion Tracking Apparatus) have measured positive neutrino oscillation signals. Figure 5.7 shows the locations and baselines of those experiments. The K2K, MINOS and T2K experiments have measured $\nu_\mu \rightarrow \nu_\mu$ disappearance. MINOS and T2K also measured $\bar{\nu}_\mu \rightarrow \bar{\nu}_\mu$ disappearance and $\nu_\mu \rightarrow \nu_e$ appearance. The OPERA experiment detected $\nu_\mu \rightarrow \nu_\tau$ appearance events.

5.3.1 The K2K Experiment

K2K is the first long baseline accelerator experiment that measured a clear neutrino oscillation signal. The neutrino beam was produced by the newly constructed neutrino beam line at the KEK proton synchrotron as shown in Fig. 5.8. A 12 GeV proton

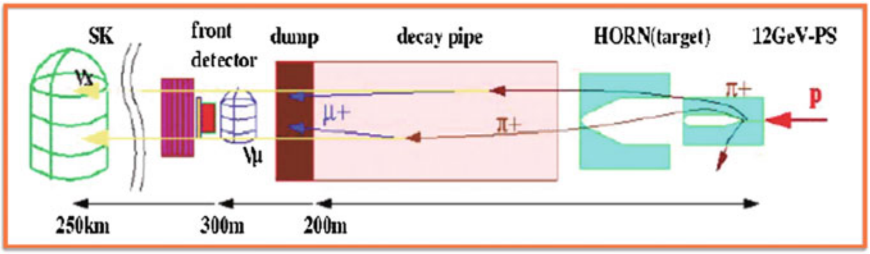

Fig. 5.8 K2K neutrino beam production and detection. From [5]

beam was fired into the target to produce secondary particles. A pair of toroidal horn magnets downstream focused π^+'s to direct the beam at the SK detector, located 250 km away. The ν_μ beam was produced from the pion decays in the decay pipe. Downstream of the decay pipe and the beam dump, the front detector measured the neutrino spectra to normalize the events measured by the far detector. The SK detector measured the ν_μ induced events by identifying the muons with the Čerenkov light, so that $\nu_\mu \to \nu_\mu$ disappearance could be measured. Figure 5.9a shows the energy distribution of the detected ν_μ. There is a dip at $E \sim 0.7$ GeV indicating $\Delta m^2 \sim 3 \times 10^{-3}$ eV^2. Figure 5.9b shows the fitting results for Δm^2 and $\sin^2 2\theta$. The measured oscillation parameters were

$$\sin^2 2\theta \sim 1, \quad \Delta m^2 = (2.8^{+0.7}_{-0.9}) \times 10^{-3}\mathrm{eV}^2, \tag{5.9}$$

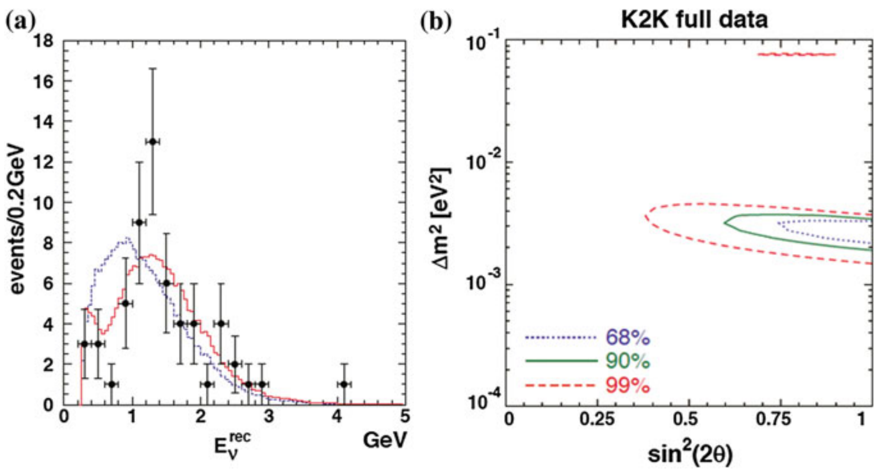

Fig. 5.9 The K2K $\nu_\mu \to \nu_\mu$ final disappearance results. **a** Reconstructed energy distribution for μ-like samples. The *solid line* is the best fit spectrum with neutrino oscillation and the *dashed line* is expectation without oscillation. **b** Allowed region of the oscillation parameters. From [6]

at 90 % CL. These results agree with the atmospheric neutrino measurements, indicating that both of the experiments are observing the same oscillation.

5.3.2 The MINOS Experiment

Using the Tevatron accelerator at Fermilab, MINOS measured the $\nu_\mu \to \nu_\mu$ disappearance with higher energy and longer baseline than the K2K experiment. The neutrinos are produced at the Fermilab Main injector and sent to the MINOS detector in the Soudan mine, 735 km away. The detector is composed of an iron and scintillator calorimeter with tracking capability, along with a toroidal magnetic field to separate the μ^+ and μ^- produced in the neutrino interactions. Figures 5.10 show the final results of the MINOS experiment. Figure 5.10a shows the energy distribution of the data sample for the fully contained ν_μ events compared to the predictions with and without oscillations. A clear deficit is observed at a few GeV. MINOS measured the oscillation parameters of $\nu_\mu \to \nu_\mu$ and $\overline{\nu}_\mu \to \overline{\nu}_\mu$ separately using both the π^+ and π^- beams, which are produced by changing the polarity of the magnets of the neutrino beam line. As the $\overline{\nu}_\mu \to \overline{\nu}_\mu$ process is the CPT inverted process of $\nu_\mu \to \nu_\mu$, CPT invariance can be tested by comparing these two oscillation modes. Figure 5.10b shows allowed oscillation parameter regions obtained from both modes. These results agree well, ensuring CPT invariance. Combining both the ν_μ and $\overline{\nu}_\mu$ data under CPT invariance, the oscillation parameters obtained were

$$\sin^2 2\theta = 0.950^{+0.035}_{-0.036}, \quad |\Delta m^2| = (2.41^{+0.09}_{-0.10}) \times 10^{-3}\,\text{eV}^2. \tag{5.10}$$

The results are consistent with the atmospheric neutrino and K2K results.

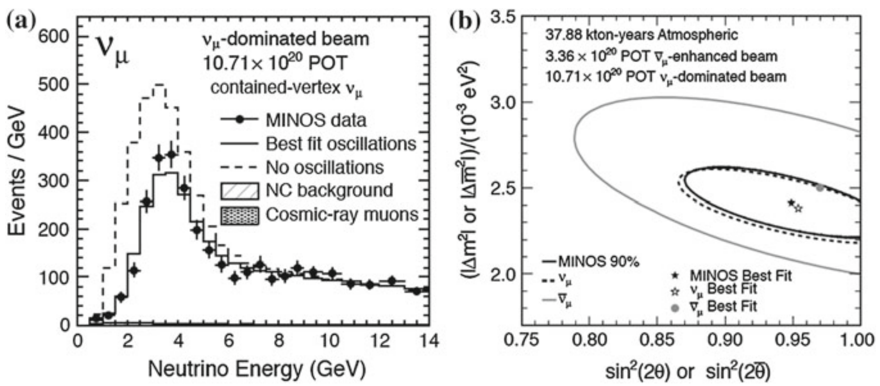

Fig. 5.10 The MINOS final results. **a** Energy distribution of the fully contained ν_μ event data sample compared to predictions with and without oscillations. **b** Allowed region of $|\Delta m^2|$ and $\sin^2 2\theta$ for ν_μ and $\overline{\nu}_\mu$ disappearances and the combined results of ν_μ, $\overline{\nu}_\mu$. From [7]

5.3.3 The T2K Experiment

The T2K experiment is the successor to the K2K experiment. Muon neutrinos are produced by the decay of pions, which are produced by a 30 GeV proton beam from the J-PARC proton synchrotron.

The neutrinos are sent to the Super-Kamiokande detector, located 295 km away. A unique feature of the T2K neutrino beam is that it uses a so-called off-axis beam, which provides the neutrinos with a narrow energy distribution. The direction of the SK detector is 2.5° from the direction of the pion beam. The energy of a neutrino that has small but finite deflection angle θ with respect to the direction of the pion is

$$E_\nu = \frac{m_\pi^2 - m_\mu^2}{2(E_\pi - p_\pi \cos\theta)} \xrightarrow{\theta\to\text{small}} \frac{dE_\nu}{dE_\pi} \propto \frac{1-(\theta\gamma_\pi)^2}{(1+(\theta\gamma_\pi)^2)^2}, \tag{5.11}$$

where γ_π is the Lorentz factor of the parent pion.

This equation means that the neutrino energy is insensitive to E_π at $\theta\gamma_\pi \sim 1$ and the neutrino energy distribution becomes narrow with the peak energy $E_\nu \sim 0.2m_\pi/\theta$. Figure 5.11 shows the neutrino flux for various deflection angles (bottom panel) and the energy distributions for the expected oscillation probabilities (top panel). The T2K experiment has measured $\nu_\mu \to \nu_\mu$ disappearance and confirmed the large deficit with significantly higher statistics than K2K as shown in Fig. 5.12. The allowed oscillation parameter region in this experiment is compared with other measurements in Fig. 5.13. The oscillation parameters used here are identified as Δm_{32}^2 and θ_{23}, based on the framework with three neutrino flavors and all measurements agree well. The best fit oscillation parameters from T2K are given by

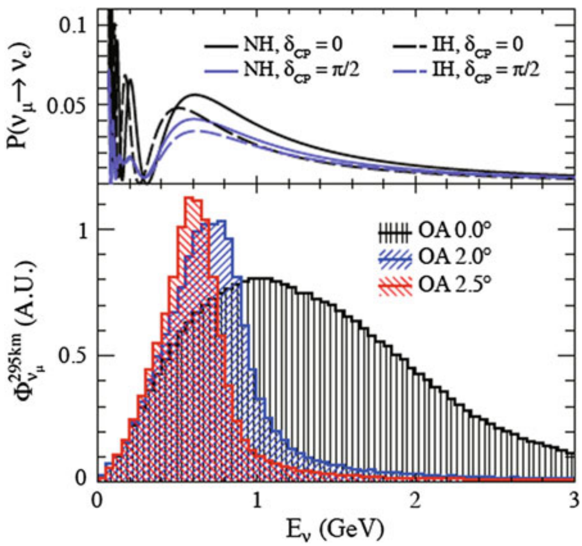

Fig. 5.11 *Top panel* expected ν_e appearance probabilities. *Bottom panel* neutrino energy spectra for various beam deflection angles. "OA" stands for "Off Axis". From [8]

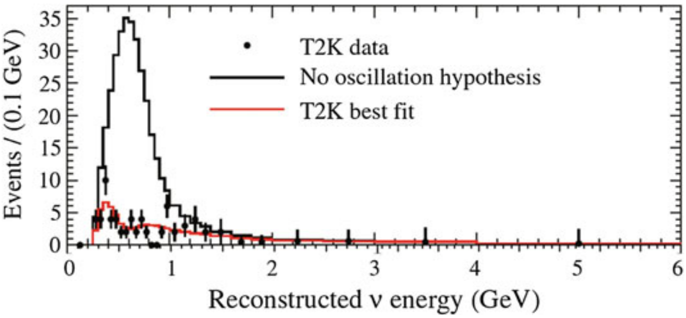

Fig. 5.12 Energy spectrum of μ-like events. The two *predicted curves* are for the no oscillation hypothesis and for the best fit parameters. The large deficit of ν_μ is observed. From [9]

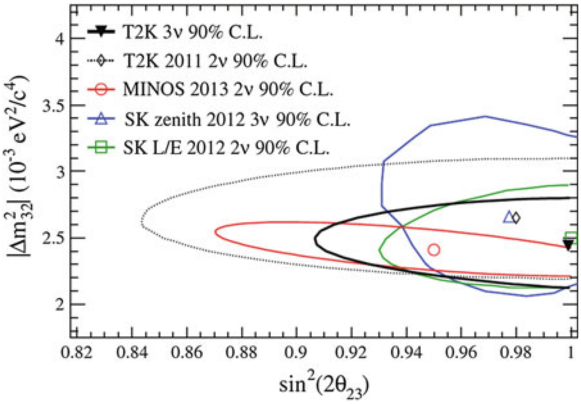

Fig. 5.13 The 90 % C.L. contour region for $\sin^2 2\theta_{32}$ and $|\Delta m^2_{32}|$. The T2K result is compared with results from other and previous measurements. From [9]

$$\sin^2\theta_{32} = 0.514 \pm 0.082, \quad |\Delta m^2_{32}| = 2.44^{+0.17}_{-0.15} \times 10^{-3}\,\text{eV}^2. \tag{5.12}$$

From the atmospheric neutrino oscillation, it was known that the $\nu_\mu \to \nu_e$ oscillation probability is small, if finite. The high ν_μ statistics allows T2K to observe $\nu_\mu \to \nu_e$ appearance signals. The measurement of the $\nu_\mu \to \nu_e$ oscillation is very important since CP violation of the neutrino oscillation can be observed only through appearance measurements (see Chap. 4). This mode is the most promising channel for the near future.

As of the year 2013, the T2K group has identified 28 $\nu_\mu \to \nu_e$ candidate events while the expected background is 4.9 events. The energy distribution of these candidate neutrinos is shown in Fig. 5.14. The energy distribution of the ν_e candidates agrees well with the expected oscillation. In the three neutrino flavor oscillation scheme, the $\nu_\mu \to \nu_e$ oscillation probability is approximated as

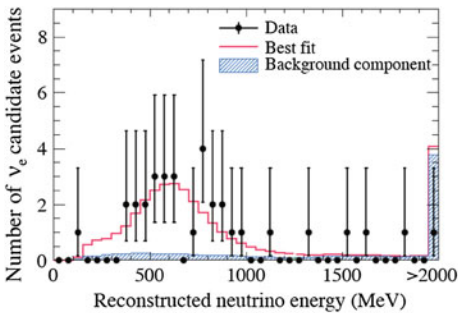

Fig. 5.14 The reconstructed energy distribution for ν_e candidates. The events with energy below 1,250 MeV (28 events) are used to calculate the oscillation probability. The *solid line* is the MC prediction at the best fit with the assumption of normal hierarchy. The hatched area is the expected background. From [10]

$$P_{\nu_\mu \to \nu_e} \sim \sin^2\theta_{23}\sin^2 2\theta_{13}\sin^2\frac{\Delta m^2_{32}L}{4E_\nu}. \tag{5.13}$$

Since $\sin^2\theta_{23}$ is measured from $\nu_\mu \to \nu_\mu$ disappearance to be close to 0.5, the smallness of $P_{\nu_\mu \to \nu_e}$ is attributed mainly to the smallness of $\sin^2 2\theta_{13}$. Assuming $\delta_{CP} = 0$, $\sin^2 2\theta_{23} = 1$ and the normal hierarchy,

$$\sin^2 2\theta_{13} = 0.140^{+0.038}_{-0.032}, \tag{5.14}$$

is obtained.

5.3.4 The OPERA Experiment

The CNGS (CERN Neutrino to Gran Sasso) project sends neutrinos from CERN in Geneva, Switzerland to the Gran Sasso laboratory in Italy located 732 km away. A ν_μ beam is produced by the charged pion decays from the Super Proton Synchrotron at CERN.

In the Gran Sasso underground lab, the OPERA and ICARUS (Imaging Cosmic And Rare Underground Signals) detectors are installed and perform the neutrino oscillation studies. OPERA is a hybrid detector of 1,300 tons of nuclear emulsion bricks with large tracking detectors behind them. The charged particle track can be measured with sub-micron level accuracy using the nuclear emulsion, which makes it possible to detect the tau-lepton decay topology directly.

The purpose of the OPERA experiment is to detect the $\nu_\mu \to \nu_\tau$ appearance oscillation signals. When a ν_τ interacts with a target material, it produces a τ lepton through the charged current interactions,

$$\nu_\tau + A \to \tau^- + X. \tag{5.15}$$

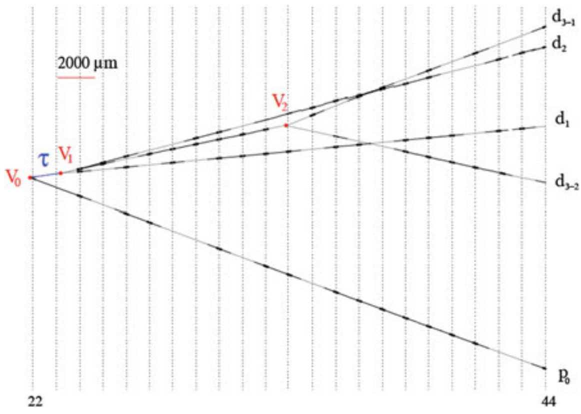

Fig. 5.15 A ν_τ appearance candidate event from the OPERA experiment. The *black segments* represent the reconstructed base-track in the emulsion while the *straight lines* are the result of track fitting. This event is consistent with $\nu_\tau + A \to \tau^- + X$, then $\tau^- \to 3h + \nu_\tau$. From [11]

Then, the τ^- decays after traveling typically 1 mm, which is measured in the emulsion. Since the τ lepton is heavy ($m_\tau \sim 1.7$ GeV), the energy of the neutrino has to be larger than 3.5 GeV so that the E/L is not optimized for the oscillation maximum. The OPERA group has identified three ν_τ candidate events as of the year 2013. The event topology of the second ν_τ candidate is shown in Fig. 5.15. This event topology is consistent with the reactions,

$$\nu_\tau + A \to \tau^- + X \ (V_0) \tag{5.16}$$

followed by

$$\tau^- \to 3h + \nu_\tau \ (V_1), \tag{5.17}$$

where V_0 and V_1 are the corresponding vertexes shown in the figure and h represents a charged hadron. One of the three hadrons interacted with the target materials at V_2 and produced another charged particle. The τ candidate is between the vertexes V_0 and V_1 with flight length 1.5 mm. Since the total energy of the three hadrons is $\sim$13 GeV, the average decay length of the τ lepton is longer than $\gamma c\tau > 0.64$ mm which is consistent with the observation.

5.4 Solar Neutrino Oscillations

The sun is made up mainly of hydrogen. The temperature at the center is 1.5×10^7 K, corresponding to hydrogen kinetic energy of 1.5 keV and density of 150 g/cm^3. The pressure at the center is 2.5×10^{11} atm. Although the temperature is below the Coulomb barrier energy, the fusion reaction is possible via the tunneling effect. The fusion reactions take place through various processes, but the net reaction is

$$4p + 2e^- \to {}^4\text{He} + 2\nu_e + 26.73\,\text{MeV} - E_\nu, \tag{5.18}$$

where the average neutrino energy $\langle E_\nu \rangle$ is, $\sim 0.6\,\text{MeV}$. This means that one ν_e is generated for every 13 MeV of energy released. Since the solar constant (solar energy flux at the surface of the earth) is $0.136\,\text{W/cm}^2$, the solar neutrino flux at the earth's surface is estimated to be

$$0.136[\text{W/cm}^2]/13 \times [\text{MeV}/\nu_e] = 6.5 \times 10^{10}\nu_e[/\text{cm}^2/\text{s}]. \tag{5.19}$$

The actual fusion reaction in the sun is more complicated, as shown in Fig. 5.16. The neutrinos are produced from pp, pep, ^{7}Be, hep and ^{8}B processes. The neutrino energy differs depending on the generation processes as shown in Fig. 5.17. The main ν_e production process is the pp process,

$$p + p \to d + e^+ + \nu_e(< 0.42\,\text{MeV}). \tag{5.20}$$

This neutrino is called the pp neutrino. More than 98 % of fusion in the sun goes through this process, with little ambiguity for the flux calculation. Since the final state has 3 bodies, the energy spectrum of the pp neutrino is continuous. The end point energy of the pp neutrino is 0.42 MeV. The next abundant neutrino flux is of ^{7}Be neutrinos, which are produced in the process

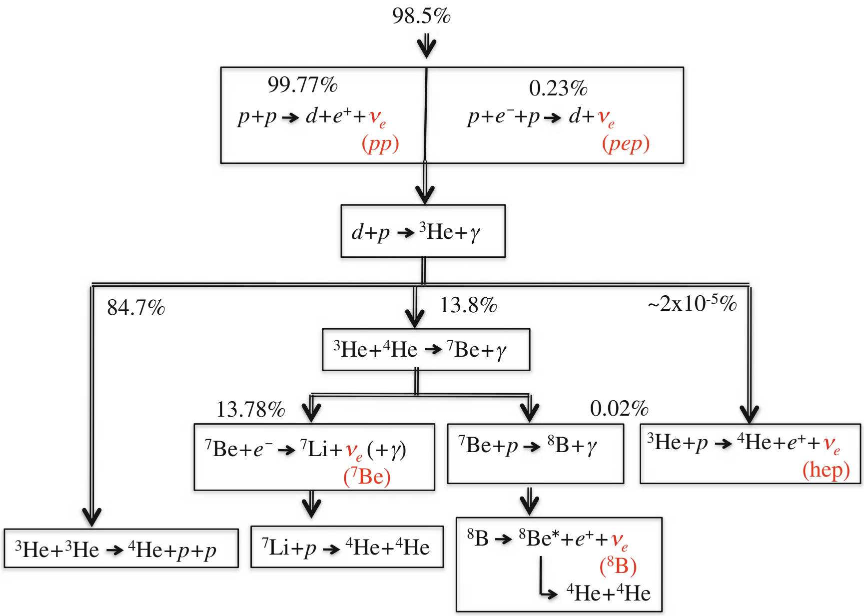

Fig. 5.16 The proton-proton chain of the fusion process in the sun. Neutrinos are produced in the *pp*, *pep*, ^{7}Be, *hep* and ^{8}B processes. 1.5 % of fusion takes place through the Carbon-Nitrogen-Oxygen catalytic cycle (CNO cycle), which is not shown here

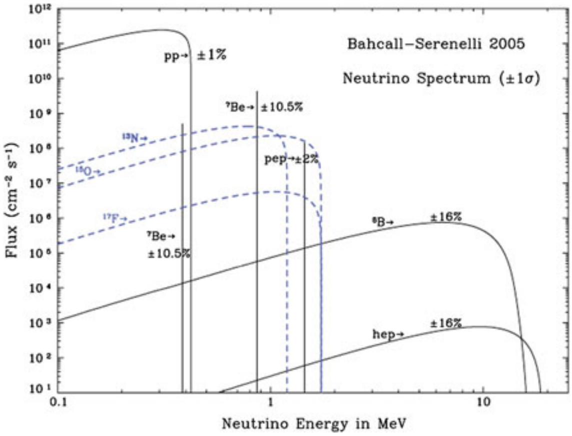

Fig. 5.17 The solar neutrino spectrum predicted by the BS05(OP) standard solar model. The neutrino fluxes are given in units of [/cm^2/s/MeV] for continuous spectra and [/cm^2/s] for line spectra. The numbers associated with the neutrino sources show theoretical errors of the fluxes. This figure is taken from the late John Bahcall's web site, http://www.sns.ias.edu/~jnb/. From [1, Chap. 1]

$$\begin{aligned} {}^7\mathrm{Be} + e^- &\to {}^7\mathrm{Li} \ + \nu_e(0.86\,\mathrm{MeV}) \quad \text{or} \\ &\to {}^7\mathrm{Li}^* + \nu_e(0.38\,\mathrm{MeV}). \end{aligned} \tag{5.21}$$

For the 2-body final state, these neutrinos have fixed energies of 0.86 MeV (90 %) and 0.38 MeV(10 %).

The most energetic solar neutrino is the *hep* neutrino. However, the flux is small and since the energy spectrum is similar to that of the ^{8}B neutrinos, it is difficult to detect. The energy of ^{8}B neutrino extends to 18.8 MeV and the flux is thousand times larger than that of the *hep* neutrinos, so it is relatively easier to detect. The ^{8}B neutrino is produced from the following β^+ decay process:

$$^8\mathrm{B} \to {}^8\mathrm{Be}^* + e^+ + \nu_e(< 18.8\,\mathrm{MeV}), \tag{5.22}$$

and its energy spectrum is continuous.

5.4.1 The Homestake Experiment

R. Davis observed the solar neutrinos for the fist time at the Homestake mine. He used ^{37}Cl as a neutrino target. His group made a 380 m^3 tank at 1,500 m underground and filled it with perchloroethylene ($Cl_2C{=}CCl_2$). Figure 5.18 shows a layout of the Homestake neutrino detector.

If a solar neutrino with energy higher than 0.82 MeV interacts with ^{37}Cl, the following reaction takes place:

$$\nu_e + {}^{37}\mathrm{Cl} \rightarrow e^- + {}^{37}\mathrm{Ar}. \quad (E_{\mathrm{th}} = 814\,\mathrm{keV}), \tag{5.23}$$

where the unstable ^{37}Ar captures the orbital electron, emitting Auger electron with a half life of $\sim$35 days through the following process:

$$^{37}\mathrm{Ar} \rightarrow {}^{37}\mathrm{Cl} + \nu_e + \text{Auger electron}. \tag{5.24}$$

The perchloroethylene was flushed with He gas once per a few weeks. The extracted gas was cooled to separate Ar from He. The decay rate of ^{37}Ar was measured with a small low-background proportional counter. Figure 5.19 shows a summary of the observed production rate of ^{37}Ar, where the background has been subtracted. The Solar Neutrino Unit (SNU) is defined as 10^{-36} neutrino captures per atom per second.

Over a period of 25 years, 2,200 atoms of ^{37}Ar were detected. As seen in the figure, the production rate is only few atoms per day, which made this experiment extremely difficult.

The results indicate that the measured neutrino flux is only 30 % of the expected value calculated from the standard solar model (SSM). Whether this deficit of the

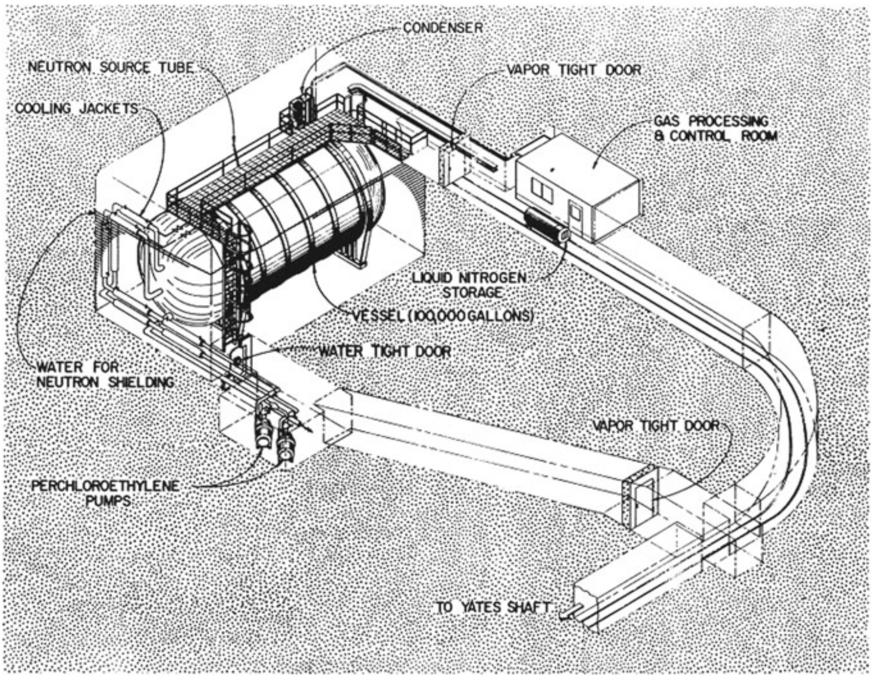

Fig. 5.18 A layout of the Homestake neutrino detector. From [12]

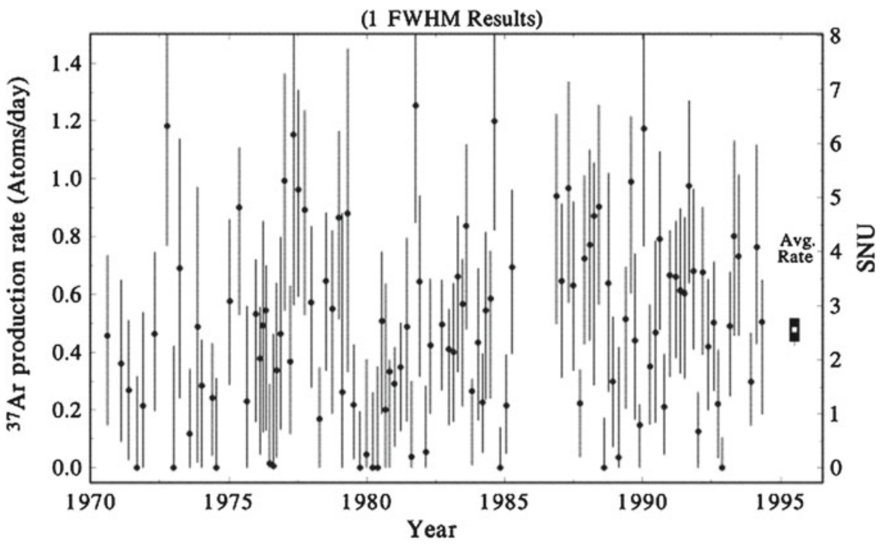

Fig. 5.19 A summary of all the runs made at Homestake after implementation of rise-time counting. Background has been subtracted. The unit of the *vertical axis* on the *right* is Solar Neutrino Unit (SNU). From [12]

solar neutrino flux was due to error in the experiment or in the SSM prediction was much debated. This problem remained unsolved for many years as the "solar neutrino anomaly" until the discovery of neutrino oscillation.

5.4.2 The GNO, GALLEX and SAGE Experiments

A weak point of the ^{37}Cl experiment is that the energy threshold of the reaction is higher than the energy of the *pp* neutrinos. The expected ^{8}B neutrino flux depends on details of the solar model. On the other hand, the *pp* neutrino process gives virtually no ambiguity in the neutrino flux prediction since most of the solar neutrinos are generated by this fusion process (5.20). The ^{71}Ga experiment was a very promising way to solve the solar neutrino flux anomaly since it can detect the *pp* neutrinos. When ν_e interacts with ^{71}Ga, the following reaction, similar to (5.23) but with much lower energy threshold, takes place,.

$$\nu_e + {}^{71}\mathrm{Ga} \rightarrow e^- + {}^{71}\mathrm{Ge}, \quad (E_{\mathrm{th}} = 233\,\mathrm{keV}), \tag{5.25}$$

where ^{71}Ge decays as,

$$^{71}\mathrm{Ge} \rightarrow {}^{71}\mathrm{Ga} + \nu_e + \text{Auger electron}, \tag{5.26}$$

with a half life of $\sim$11 days.

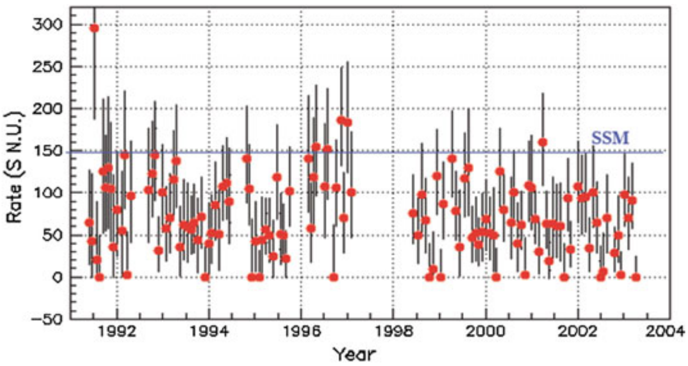

Fig. 5.20 GALLEX and GNO data. GALLEX data were taken before 1998 and GNO data where taken after 1998. The prediction of the SSM is shown as a *solid horizontal line*. The result shows that the detected neutrino flux is 51 ±4 % of the SSM prediction. From [13]

There were three ^{71}Ga experiments. GALLEX (GALLium EXperiment) used 30 tons of target and its successor GNO (Gallium Neutrino Observatory) used 100 tons at the Gran Sasso Laboratory. SAGE (Soviet American Gallium Experiment) used 50 tons of Ga target at the Baksan underground laboratory. Figure 5.20 shows the results from GALLEX and GNO and Fig. 5.21 shows the results from SAGE. Both experiments observed about half of the solar neutrino flux predicted by the SSM.

From these results, it turned out to be clear that the solar neutrino problem is originated in some aspect of particle physics we did not understand.

5.4.3 The Super-Kamiokande Experiment

In the Super-Kamiokande (SK), the solar neutrinos were detected by the νe elastic scattering,

$$\nu + e^- \to \nu + e^-. \tag{5.27}$$

The SK detector, filled with 50 kilotons of ultra-pure water, can measure the solar neutrino in real time by detecting the Čerenkov light produced by the scattered electron.

As described in Sect. 2.4.4, the cross section of $\nu_e e^-$ scattering, $\sigma_{\nu_e e}$, is significantly larger than that of $\nu_{\mu/\tau} e^-$ scattering, $\sigma_{\nu_{\mu/\tau} e}$, due to the charged current diagram. Since $\sigma_{\nu_\mu e^-} = \sigma_{\nu_\tau e^-} \sim \sigma_{\nu_e e^-}/6.1$, the elastic scattering rate observed at SK is

$$\phi_{\text{obs}} \sim \phi_{\nu_e} + \frac{1}{6.1}(\phi_{\nu_\mu} + \phi_{\nu_\tau}). \tag{5.28}$$

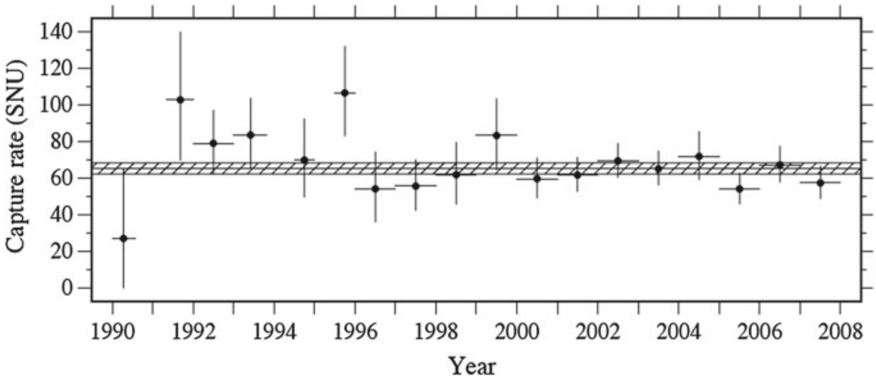

Fig. 5.21 Yearly capture rate from the SAGE experiment. The *shaded band* is the combined best fit for all years and its error. The error is statistical with 68 % confidence. The prediction of the SSM is 130 SNU and the result shows that the detected neutrino flux is about half of the SSM prediction. From [14]

If neutrino oscillation changes the ν_e to a ν_μ or ν_τ, the observable neutrino flux decreases. For νe scattering at a few MeV, the electron is scattered forward, as indicated by Fig. 2.16, emitting Čerenkov light that keeps the directionality information. Figure 5.22a shows the angular distribution for the solar neutrino candidates with respect to the direction of the sun. The clear directionality of the sun is used to distinguish the solar neutrino events from the isotropic backgrounds. Figure 5.22b shows the energy spectrum of the solar neutrinos normalized by the SSM prediction, resulting in the average ratio of 0.4. The apparent deficit of the solar neutrino flux is observed here again.

5.4.4 The SNO Experiment

Neutrino oscillation was one of several possible reasons for the deficit of solar neutrinos observed by experiments. One approach to testing the oscillation hypothesis is to measure the total neutrino flux of

$$\phi_\nu = \phi_{\nu_e} + \phi_{\nu_\mu} + \phi_{\nu_\tau}, \tag{5.29}$$

using neutral current interactions.

The cross section of neutral current interactions does not depend on the neutrino flavor. Therefore, even if the neutrino flavor changes by neutrino oscillation, the total neutrino flux can be measured using the neutral current interactions. The SNO (Sudbury Neutrino Observatory) experiment used 1,000 tons of heavy water (D_2O) as a neutrino target to measure the neutral current interactions of the solar neutrinos. The heavy water was contained in an acrylic sphere 12 m in diameter, which is located 2,070 m undergrounds at Vale Inco's Creighton Mine in Sudbury, Canada. Figure 5.23

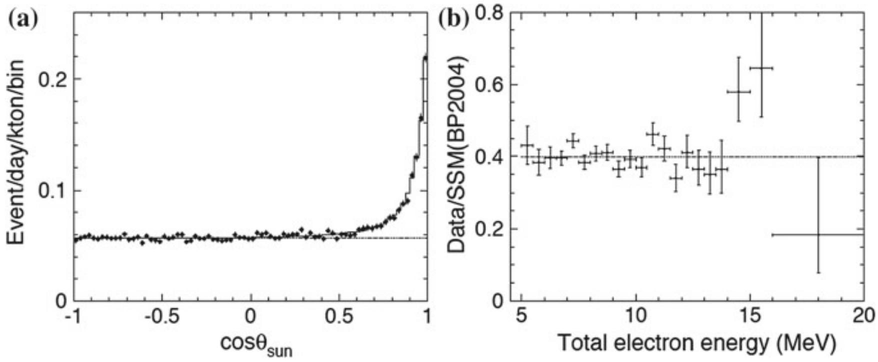

Fig. 5.22 **a** The angular distribution of the solar neutrino candidate events with respect to the direction of the sun. The *dotted line* seen under the peak in the solar direction represents background contributions. **b** Ratio of observed and expected energy spectra. The *dotted line* is the average for all data. From [15]

shows a schematic view of the SNO detector. The Čerenkov light is detected by 9,456 8-inch photomultipliers which measure γ-rays and electrons. When a neutrino interacts with a deuteron, the deuteron is broken into a proton and a neutron through the neutral current interaction as shown in Fig. 5.24a,

$$\nu_x + D \rightarrow \nu_x + p + n. \tag{5.30}$$

The energy threshold of the reaction is 2.2 MeV and ^{8}B solar neutrinos can be detected. The neutron is thermalized by scattering with deuterium or oxygen nuclei and is captured by a deuteron, forming tritium and emitting a 6.25 MeV γ,

$$n(\text{thermal}) + D \rightarrow T + \gamma(6.25\,\text{MeV}). \tag{5.31}$$

By measuring the 6.25 MeV γ events, the total neutrino flux regardless of its flavors can be measured. At the same time, electron neutrinos can interact with deuterium through the charged current reaction as shown in Fig. 5.24b,

$$\nu_e + D \rightarrow e^- + p + p. \tag{5.32}$$

This event can be identified by the Čerenkov light from the electron. The neutrino-electron elastic scattering ($\nu_x + e^- \rightarrow \nu_x + e^-$) also occurs as in the Super-Kamiokande detector, but with lower statistics. Reaction (5.32) and $\nu - e$ elastic scattering (5.27) can be statistically distinguished by using the angular distribution of the Čerenkov signals with respect to the direction of the sun.

The results obtained in the year 2002 showed that the neutrino flux measured with NC interactions is consistent with the prediction of the standard solar model.

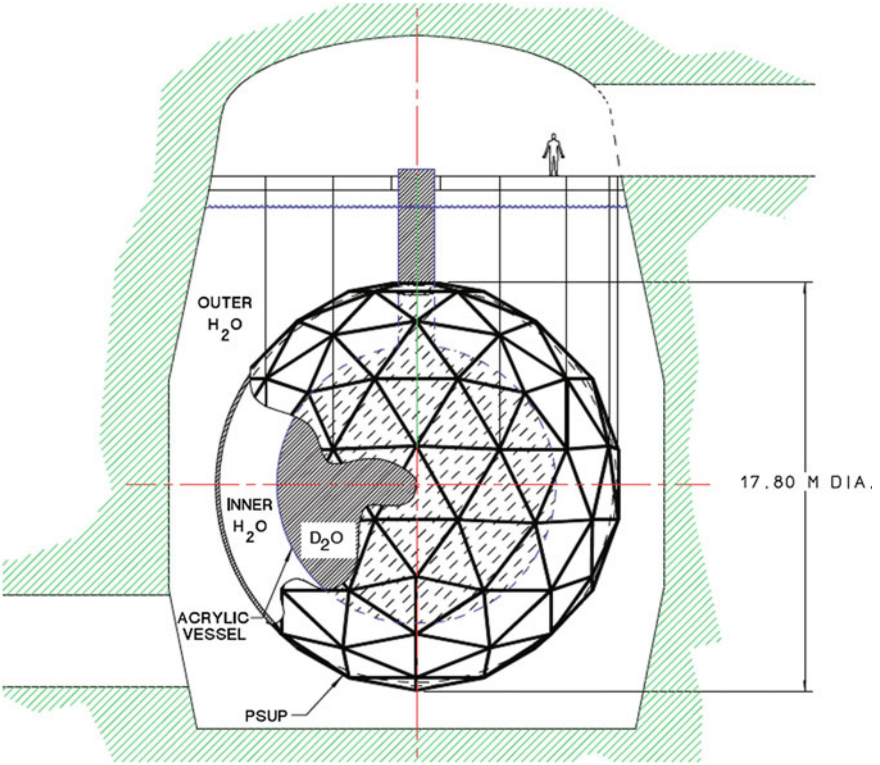

Fig. 5.23 A schematic view of the SNO detector. 1 kton of D_2O is contained in an acrylic sphere with radius 6.5 m. The acrylic sphere is submerged in the water shield. 9,456 PMTs capture the Čerenkov light. The laboratory is 2,070 m underground in the Sudbury mine, Canada. From [16]

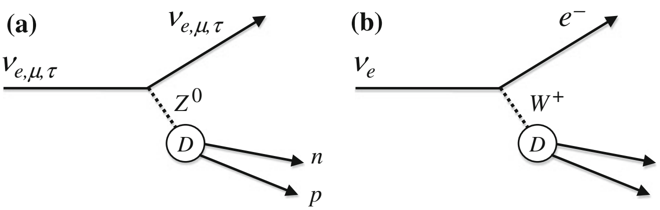

Fig. 5.24 **a** Neutral current interactions of neutrinos with deuteron. The cross section for neutral current interactions is the same for all neutrinos. Therefore, the total neutrino flux can be measured independent of flavor. **b** Only ν_e transforms to the charged lepton e^- through the charged current interaction because the solar neutrino energy is smaller than the muon mass

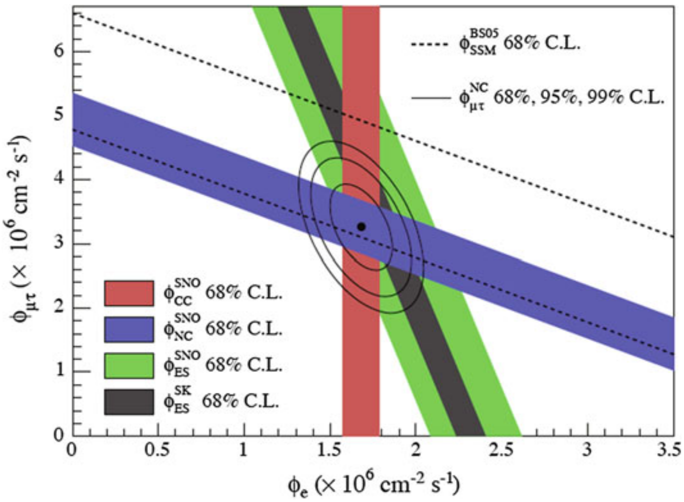

Fig. 5.25 Fluxes of ^{8}B solar neutrinos, $\phi(\nu_e)$, and $\phi(\nu_\mu$ or $\nu_\tau)$, deduced from SNO's CC, ES, and NC results of the salt phase measurement. The bands represent the 1σ error. The contours show the 68, 95, and 99 % joint probability for $\phi(\nu_e)$ and $\phi(\nu_e$ or $\tau)$. From [17]

The ratio of CC flux and NC flux is 0.3,

$$\frac{\phi_{NC}}{\phi_{SSM}} = 1.0^{+0.20}_{-0.23}, \quad \frac{\phi_{CC}}{\phi_{NC}} = 0.306 \pm 0.026 \pm 0.024. \tag{5.33}$$

The results are summarized in Fig. 5.25. These results indicate that the electron neutrino is transformed to other types of neutrinos.

Later, 2,000 kg of NaCl were dissolved in the heavy water. ^{35}Cl has large neutron absorption cross section and it emits γ's with total energy 8.6 MeV after absorbing a neutron. The NaCl increased the detection efficiency and improved the accuracy of the measurement. The group also installed ^{3}He proportional counters in the detector and measured the neutron by detecting the proton from the reaction $^3\mathrm{He} + n \to {}^3\mathrm{H} + p$.

Finally, the group obtained a total ^{8}Be neutrino flux of

$$\Phi_\mathrm{B} = \left(5.25 \pm 0.16(\mathrm{stat.})^{+0.11}_{-0.13}(\mathrm{syst.})\right) \times 10^6\ /\mathrm{cm}^2/\mathrm{s}. \tag{5.34}$$

The measured ν_e flux is about 32 % of the expectation from the standard solar model.

Figure 5.26 shows the allowed oscillation parameter region measured by SNO. There are two regions which satisfy the measurements, corresponding to the *Large Mixing Angle* (LMA) solution at $\Delta m^2 \sim 10^{-4}\,\mathrm{eV}^2$ and the *Low* solution at

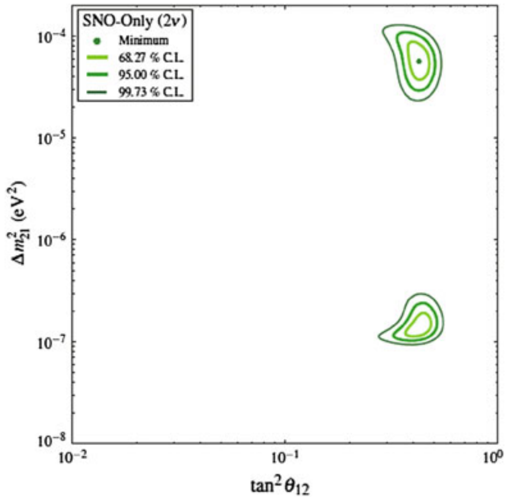

Fig. 5.26 Two flavor neutrino oscillation analysis contours. The matter effect described in the next chapter is included. From [18]

$\Delta m^2 \sim 10^{-7}$ eV^2. The Low solution has been excluded by combining other solar neutrino and reactor experiments. The measured oscillation parameters of LMA solution are

$$\tan^2\theta_{12} = 0.427^{+0.033}_{-0.029}, \quad \Delta m^2_{21} = 5.62^{+1.92}_{-1.36} \times 10^{-5}\,\text{eV}^2. \tag{5.35}$$

5.4.5 The Borexino Experiment

Borexino is an experiment that uses liquid scintillator to detect neutrinos. The liquid scintillator produces by a factor of several tens more light than Čerenkov light and the energy resolution is much better than that of Čerenkov detectors. While Čerenkov radiation has an energy threshold, the scintillator does not have such threshold and lower energy neutrinos can be detected than in water Čerenkov detectors. On the other hand, the scintillation light is emitted isotropically and the neutrino directionality information is lost. Figure 5.27 shows a schematic of the Borexino detector. The Borexino detector is composed of 300 tons of ultra low-background liquid scintillator contained in a 8.5 m diameter Nylon balloon. The balloon floats in non-scintillating buffer oil contained in an outer Nylon vessel and a stainless steel spheric tank with a diameter of 13.7 m. 2,200 8-inch PMTs with the Winston cone mounted on the inside wall of the stainless steel tank view the scintillation light. The stainless steel tank sits inside a water tank. The detector is located in the Gran Sasso laboratory in Italy, 1,400 m underground.

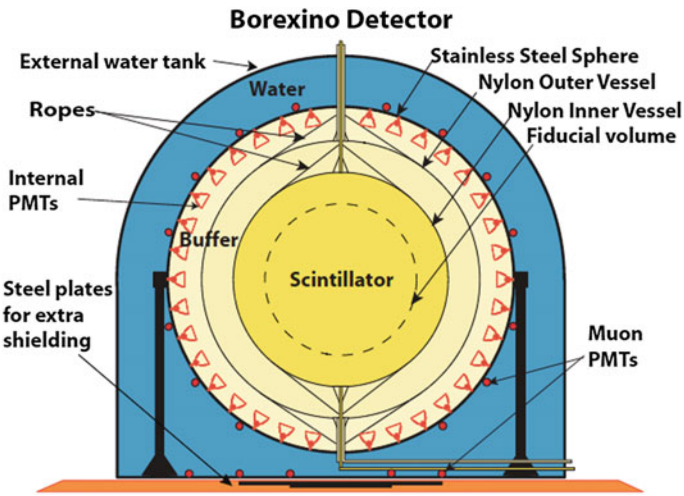

Fig. 5.27 A schematic view of the Borexino detector. From [19]

Borexino group identified ^{7}Be and pep solar neutrinos for the first time by using neutrino-electron elastic scattering, as shown in Eq. (5.27). ^{7}Be and pep solar neutrinos have energies of 862 keV and 1.4 MeV, respectively. Measuring the solar neutrino deficit in these energy regions is important because the oscillation probability of solar neutrinos is supposed to change due to the matter effect.

An experimental difficulty is to cope with the backgrounds. The energy of ^{7}Be and pep neutrinos is similar to that from natural radioactivities that come from the decay chains of ^{235}U and ^{232}Th, and the decay of ^{40}K. These naturally-occurring radioactive elements emit γ-rays with energies below 2.7 MeV, so ^{7}Be and pep neutrino signals could easily be swamped by the background signals. The Borexino group reduced backgrounds significantly by limiting the contamination of such radioactive elements in the detector and succeeded in measuring ^{7}Be and pep solar neutrinos. Figure 5.28 shows the energy spectrum of the solar neutrino candidates and various backgrounds. Although ^{7}Be neutrinos have a fixed energy, the scattered electron has a Compton scattering-like energy dependence with a sharp maximum energy edge at $E_e \sim$ 660 keV, which makes a "shoulder" in the energy spectrum. The survival probability for $\nu_e \rightarrow \nu_e$ was measured to be 51 ± 7 % of the expected value.

5.4.6 *Summary of Solar Neutrino Observations*

The deficits of the solar neutrino flux observed in all the experiments with various methods seem to depend on the neutrino energy as summarized in Fig. 5.29. As will

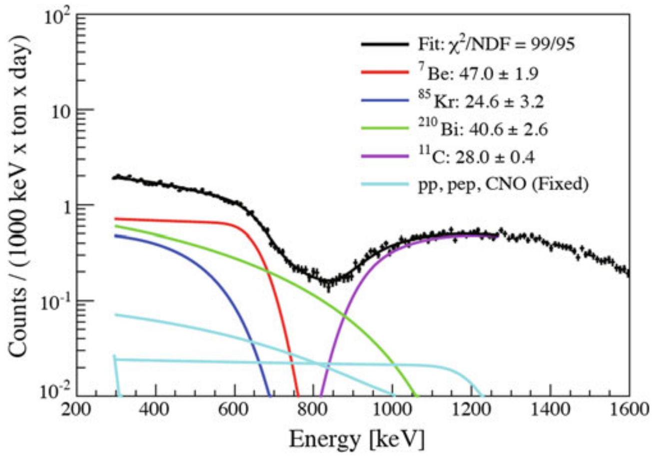

Fig. 5.28 Energy spectrum after statistical subtraction of α signal. An analytical fit to various components was done between 290 and 1,270 KeV. From [19]

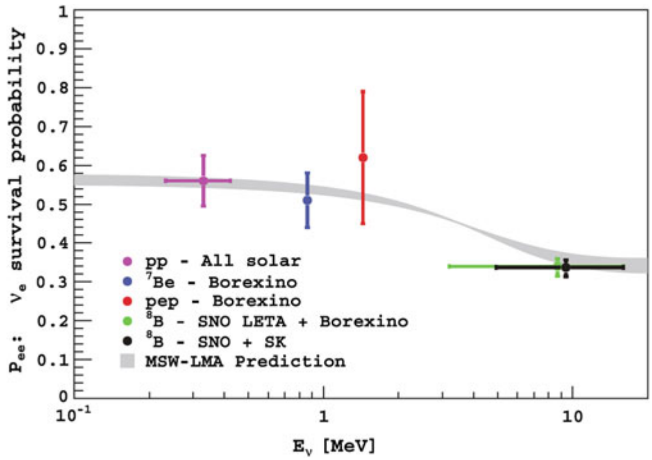

Fig. 5.29 Energy dependence of solar neutrino deficit. From [20]

be discussed in the next chapter, this energy dependence can be described by the matter effect of varying densities in the sun. Figure 5.30 summarizes all the solar neutrino experiments. Only the LMA solution remains. The measured oscillation parameters including θ_{13} in the analysis were

$$\tan^2\theta_{12} = 0.468^{+0.031}_{-0.044}, \quad \Delta m^2_{21} = 5.4^{+1.7}_{-1.1} \times 10^{-5}\,\mathrm{eV}^2, \quad \sin^2\theta_{13} < 0.030. \tag{5.36}$$

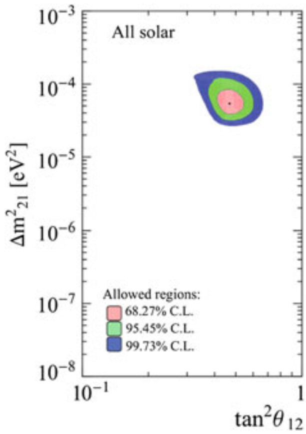

Fig. 5.30 Allowed regions of the oscillation parameters at 68 % C.L. (*inner*), 95 % (*middle*) C.L. and 99.7 % (*outer region*) C.L., respectively, for combination of all the solar neutrino results. From [19]

5.5 Reactor Neutrino Oscillations

In nuclear reactors, uranium and plutonium release energy through fission reactions. Figure 5.31 shows an example of a fission reaction process. In this example, ^{235}U absorbs a thermal neutron and breaks up into ^{140}Te and ^{94}Rb, emitting two neutrons. These fission products are neutron rich nuclei that produce the electron antineutrinos ($\overline{\nu}_e$) via β-decay. In general, these fission products become stable after six β-decays, so that every fission produces six $\overline{\nu}_e$'s, releasing 200 MeV of energy. Therefore, a reactor operating with 3 GW of thermal power produces $6 \times 10^{20}\overline{\nu}_e$'s per second. The energy of the reactor neutrinos is a few MeV, corresponding to the typical energy of nuclear β decays. The main fissile elements are ^{235}U, ^{239}Pu, ^{241}Pu and ^{238}U, for which the emitted neutrino spectra are known with a precision ∼2 %.

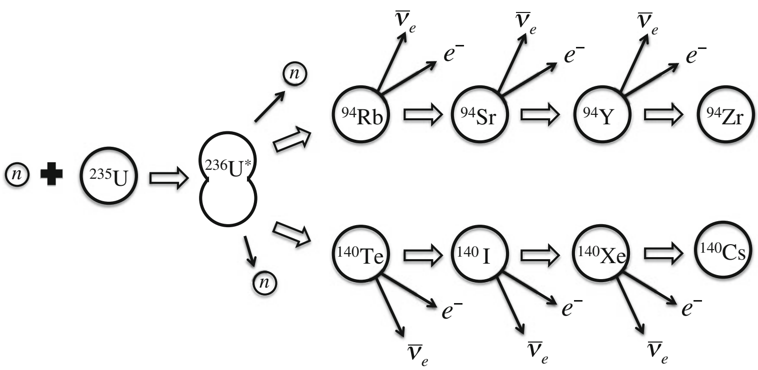

Fig. 5.31 An example of the fission reaction. $\overline{\nu}_e$'s are generated in β decays of fission products. On average about six $\overline{\nu}_e$'s are generated per fission. $\sim 6 \times 10^{20}$ $\overline{\nu}_e$'s/sec are generated in a reactor operating at 3 GW$_{\rm th}$ of power. The energy of the neutrinos is a typical β decay energy of a few MeV

Usually, the reactor neutrinos are detected by using liquid scintillator (LS), which is made of organic oil and is rich in free protons. The reactor neutrino is detected by using the inverse beta decay (IBD) reaction with a proton,

$$\overline{\nu}_e + p \to e^+ + n. \tag{5.37}$$

The threshold energy of this reaction is $m_n - m_p + m_e = 1.8\,\text{MeV}$ and the cross section is given by Eq. (2.100)

$$\sigma_{\text{IBD}} \sim 1.0 \times 10^{-43} E_{e^+} p_{e^+} [\text{cm}^2], \tag{5.38}$$

where E_{e^+} and p_{e^+} are measured in MeV and a neutron lifetime of 880 s is assumed.

The positron and its annihilation γ's deposit energy in the LS, emitting scintillation light with lowest energy of 1.02 MeV. Since the energy of the recoiled neutron is typically 0.1 MeV or less, the neutrino energy can be measured from the visible energy to be

$$E_{\overline{\nu}_e} \sim E_{\text{visible}} + m_n - m_p - m_e = E_{\text{visible}} + 0.8\,\text{MeV}. \tag{5.39}$$

Figure 5.32 shows the reactor neutrino spectrum, IBD cross section and observable reactor neutrino spectrum.

The neutron produced in the IBD reaction is instantly thermalized in the LS by recoiling and it is absorbed by a proton, forming deuteron and emitting a 2.2 MeV γ.

$$n + p \to d + \gamma \quad : \quad E_\gamma = 2.2\,\text{MeV}. \tag{5.40}$$

This absorption process takes place about 200 μs after the IBD reaction. Therefore, for one neutrino interaction, the positron signal and the neutron absorption signal are observed at a separated time. By requiring this "delayed coincidence", natural backgrounds can be substantially reduced. The positron signal is called the "prompt signal" and the neutron signal is called the "delayed signal". In some experiments,

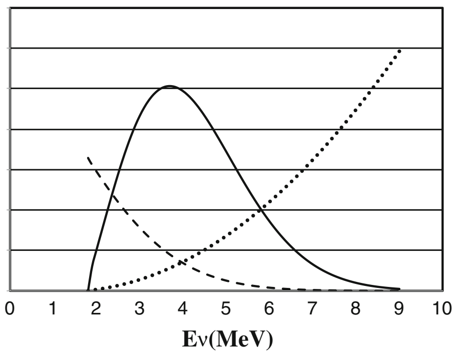

Fig. 5.32 Reactor neutrino spectrum (*dashed line*), IBD cross section (*dotted line*), and the product of them showing the visible energy spectrum of the reactor neutrino signal (*solid line*). The *horizontal axis* is the neutrino energy (E_ν). The *vertical axis* is in arbitrary units

the scintillator is doped with Gadolinium (Gd) to absorb the neutron. Gd has the largest thermal neutron absorption cross section among the natural elements, so that it is possible to shrink the coincidence timing width below 200 μs, which helps to reduce the accidental backgrounds. The excited Gd after the neutron absorption, emits cascade γ's with total energy of 8 MeV,

$$n + \mathrm{Gd} \rightarrow \mathrm{Gd}' + \gamma' \mathrm{s} \quad : \quad \sum E_\gamma \sim 8\,\mathrm{MeV}. \tag{5.41}$$

Since the energies of backgrounds from natural radioactivity are less than 5 MeV, the Gd helps to reduce backgrounds drastically.

In the presence of neutrino oscillation, the energy spectrum of the reactor neutrinos changes as follows:

$$N_\nu(E) = N_{\nu 0}(E) \left(1 - \sin^2 2\theta \sin^2 \frac{\Delta m^2}{4E} L\right), \tag{5.42}$$

where $N_{\nu 0}(E)$ is the energy spectrum of neutrinos without neutrino oscillation. Since the energy of reactor neutrinos is much smaller (typically 1/100 or less) than that of accelerator neutrinos, reactor neutrino experiments can provide sensitivity to either significantly smaller Δm^2 at the same baseline or oscillation with the same Δm^2 at a significantly shorter baseline. The low neutrino energy makes appearance experiments impossible; only disappearance measurements are possible for reactor neutrinos.

Four reactor neutrino experiments are currently in operation and all of them have observed positive oscillation signals. The KamLAND (Kamioka Liquid scintillator AntiNeutrino Detector) experiment has observed a large neutrino oscillation at $\Delta m^2 \sim 8 \times 10^{-5}\,\mathrm{eV}^2$ and Double Chooz, Daya Bay and RENO (Reactor Neutrino Oscillation) experiments have observed small neutrino oscillation at $\Delta m^2 \sim 2.5 \times 10^{-3}\,\mathrm{eV}^2$.

5.5.1 The KamLAND Experiment

The KamLAND experiment uses 1,000 tons of liquid scintillator to detect reactor neutrinos coming from reactors hundreds of kilometers away. Although 70 reactors are spread throughout Japan and Korea, most of the neutrinos detected by KamLAND come from a narrow circular band of 150–200 km from the detector. The result is that it looks as if one gigantic reactor is located at an average baseline of 180 km. Figure 5.33 shows a schematic drawing of the KamLAND detector. The 1 kton of ultra low-background liquid scintillator is contained in a 13 m-diameter transparent plastic balloon. The balloon is floating in 2 ktons of non-scintillating buffer oil. 1,879 17 or 20 in. diameters photomultipliers (PMT) in the buffer oil detect the scintillation light. The PMTs are mounted on the inner wall of a 18 m diameter stainless steel spherical

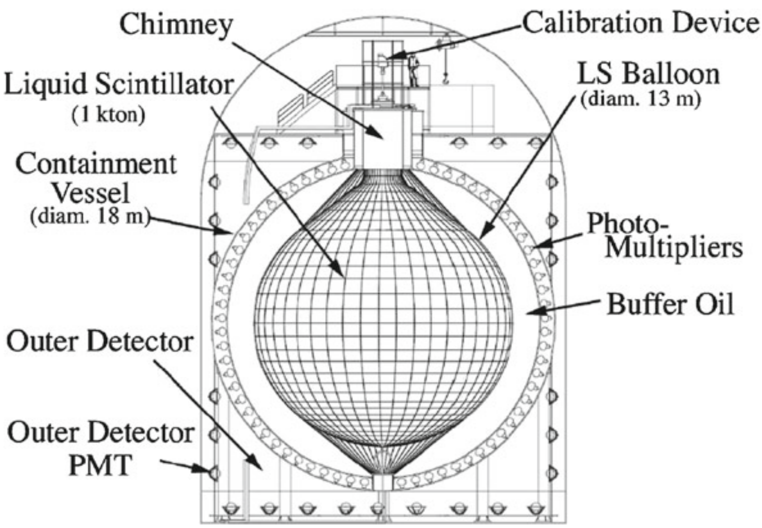

Fig. 5.33 Schematic diagram of the KamLAND detector. From [21]

tank. The stainless steel tank is submerged in 3 ktons of pure water, which works as a cosmic ray veto counter. The detector is housed in the cavern where the Kamiokande detector used to be. This location is 1,000 m below the top of the Ikenoyama mountain where the cosmic-ray rate is reduced by a factor of 10^{-5} compared with the surface. KamLAND observed a large deficit of the reactor neutrinos and a clear distortion of its energy spectrum. Figure 5.34 shows the L_0/E_ν dependence of the survival probability of $\overline{\nu}_e$, where $L_0 = 180$ km is the flux-weighted average baseline. From the oscillation pattern in the L_0/E_ν spectrum, it turned out that KamLAND is located

Fig. 5.34 Ratio of the observed $\overline{\nu}_e$ spectrum to the expectation for no-oscillation versus L_0/E. $L_0 = 180$ km is the flux-weighted average reactor baseline. A clear oscillation pattern is visible. From [22]

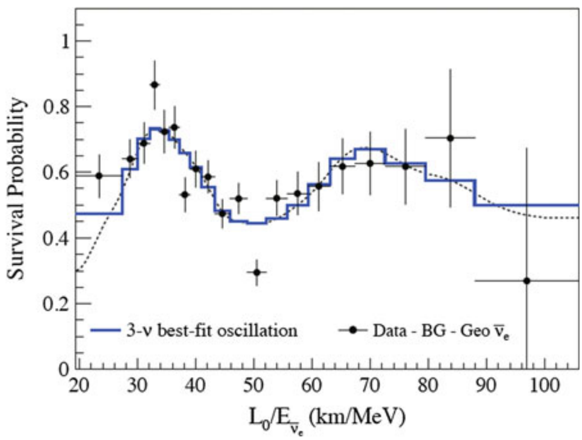

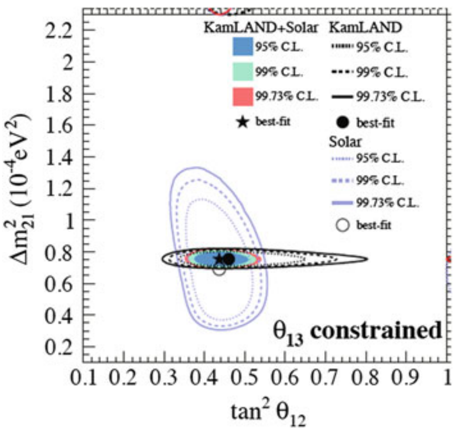

Fig. 5.35 Allowed ($\tan^2\theta - \Delta m^2$) regions from the KamLAND experiment together with the summary result of solar neutrino experiments. The *shaded regions* are from combined analysis of the solar and KamLAND data. From [22]

at around the second oscillation maximum. The increase of the $\overline{\nu}_e$ flux at $L_0/E_\nu \sim 30$ and 60 km/MeV indicates that the disappearance is caused by oscillation since the decay of the neutrino or decoherence can only decrease the $\overline{\nu}_e$ flux. The best fit of the three flavor analysis of only the KamLAND data indicates

$$\tan^2\theta_{12} = 0.481^{+0.092}_{-0.080}, \quad \Delta m^2_{21} = 7.54^{+0.19}_{-0.18} \times 10^{-5}\mathrm{eV}^2. \tag{5.43}$$

Figure 5.35 shows the allowed oscillation parameter region from KamLAND together with the result of solar neutrino experiments. The KamLAND and solar neutrino results are consistent with each other. Since KamLAND observes $\overline{\nu}_e$ disappearance and solar neutrino experiments observe ν_e disappearance, the agreement shows that CPT invariance holds. Finally, the best fit oscillation parameters combining KamLAND, solar neutrinos and the θ_{13} experiments described in the next section are,

$$\tan^2\theta_{12} = 0.436^{+0.029}_{-0.025}, \ \ \Delta m^2_{21} = 7.5 \pm 0.18 \times 10^{-5}\mathrm{eV}^2. \tag{5.44}$$

5.5.2 The Double Chooz, Daya Bay and RENO Experiments

The Double Chooz (DC), Daya Bay (DB) and RENO experiments are new generation reactor neutrino experiments, which measure the reactor $\overline{\nu}_e$ oscillation at baselines of $1 \sim 2$ km. They are sensitive to the region $\Delta m^2 \sim 2 \times 10^{-3}$ eV^2, which corresponds to the parameter observed in ν_μ disappearance by the accelerator and atmospheric neutrino experiments. When the DC, DB and RENO experiments were designed, the

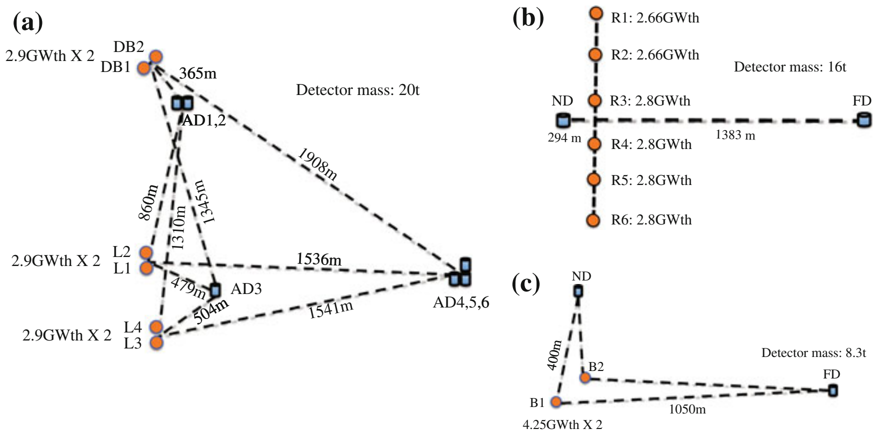

Fig. 5.36 Detector and reactor locations, baselines and detector masses of the Double Chooz, Daya Bay and RENO experiments. The *circles* show the reactor cores and the *cylinders* show the neutrino detectors (The scales are not the same.)

mixing angle, called the θ_{13}, was known to be small because the Chooz and Palo Verde experiments could not find a reactor neutrino deficit at $\sim$1 km and showed that $\sin^2 2\theta_{13} < 0.15$. This means that the disappearance probability is small and high precision measurement is necessary to detect it. Therefore, the three experiments use the near and far detectors with identical structure to significantly improve the accuracy of the neutrino deficit measurement. The baselines of the far detectors are close to the oscillation maximum ($L \sim 1.5$ km) and the baselines of the near detectors are where the oscillation is still small ($L \leq 400$ m). Since both detector sets have an identical structure, most of the systematic uncertainties are canceled out by comparing the data from the far and near detectors, and precise measurement of the $\overline{\nu}_e$ disappearance is possible.

Figure 5.36 shows the locations of detectors and reactors for the three experiments. Daya Bay uses multiple detectors and reactors to cross-check the systematic uncertainties and to obtain higher statistics. The detectors of these three experiments have very similar multi-layer structures. Figure 5.37 shows a schematic view of the Double Chooz detector as an example. The neutrino target is 8.3 tons of Gd-loaded liquid scintillator and the delayed coincidence is used to identify the reactor neutrinos. The target scintillator is contained in a cylindrical acrylic vessel, which is immersed in liquid scintillator without Gd called the γ-catcher. The γ-catcher scintillator is contained in the second acrylic vessel. The γ-catcher scintillator detects γ-rays that leak from the neutrino target region to reconstruct the original energies of the positron and Gd signals. The second acrylic vessel is immersed in non-scintillating buffer oil, which shields the scintillators from γ-rays and neutrons coming from out of the detector. 390 10 inch photomultipliers are submerged in the buffer oil and detect scintillation lights. All these layers are placed in a stainless steel tank and the tank is placed in additional scintillator layer which works as a cosmic ray veto counter.

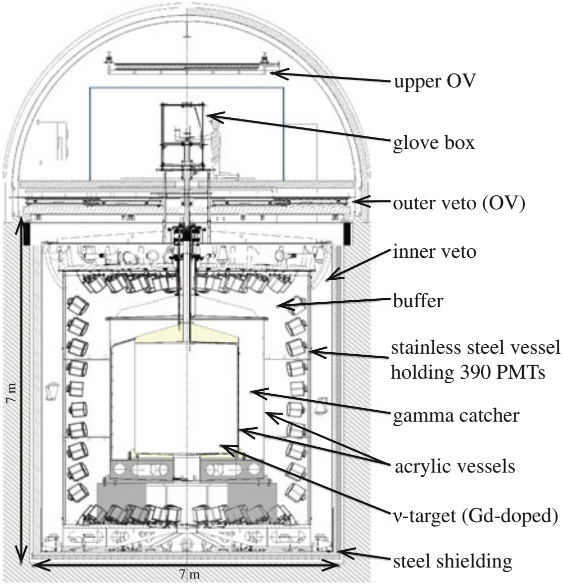

Fig. 5.37 Schematic view of the Double Chooz detector. From [23]

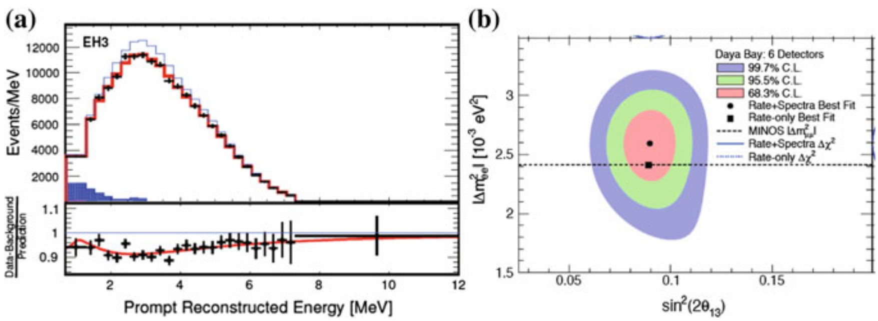

Fig. 5.38 Daya Bay data. **a** The *upper panel* shows the prompt positron spectrum (data points) of the far detectors. The *thin solid line* shows the no-oscillation prediction based on the measurements of the near detectors. The *thick solid line* is the best-fit spectrum with oscillation. The *shaded area* shows the expected background contribution. The *lower panel* shows the background-subtracted data divided by the predicted no-oscillation spectrum. **b** Allowed region for Δm^2 and $\sin^2 2\theta$, obtained from a comparison of the rates and prompt energy spectra. The *black dot* is the best fit parameters with rate + spectra analysis and the *black square* is the best fit parameters with rate-only analysis. From [24]

All three experiments observed a positive signal for the reactor neutrino deficit. $\sin^2 2\theta_{13}$ can be obtained from the deficit and Δm^2_{31} can be obtained from the spectral analysis. Figure 5.38a compares the energy spectra observed by the near and far detectors of the Daya Bay experiment. The measured oscillation parameters for the

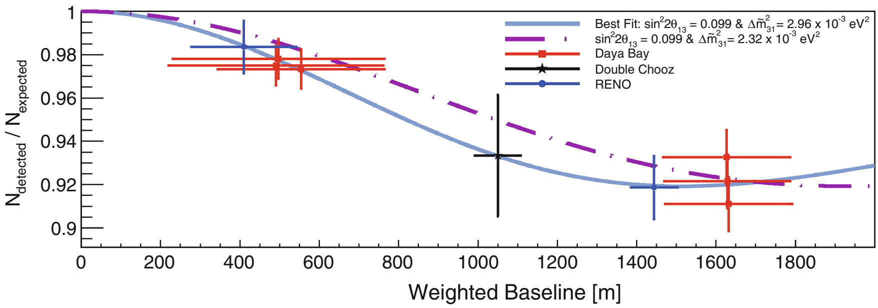

Fig. 5.39 Baseline dependence of reactor $\bar{\nu}_e$ survival probability. The *solid line* is the best fit oscillation pattern. The *dot-dashed line* uses MINOS Δm^2_{32}. Each detector sees several reactors. The *horizontal axis* is a weighted baseline and the *horizontal bar* in each data point shows the standard deviation of the distribution of the baselines. From [25]

three experiments are,

$$\begin{aligned} \text{DC}: &\quad \sin^2 2\theta = 0.109 \pm 0.039, \\ \text{DB}: &\quad \sin^2 2\theta = 0.090^{+0.008}_{-0.009}, \quad \Delta m^2 = 2.59^{+0.19}_{-0.20} \times 10^{-3}\text{eV}^2, \\ \text{RENO}: &\quad \sin^2 2\theta = 0.113 \pm 0.023. \end{aligned} \tag{5.45}$$

At this point, only Daya Bay has given a Δm^2 result.

Since these three experiments use different baselines, the baseline dependence of the neutrino deficits is observed as shown in Fig. 5.39. This baseline dependence of the neutrino deficits shows

$$\Delta m^2_{31} = 2.95^{+0.42}_{-0.61} \times 10^{-3}\,\text{eV}^2, \quad \sin^2 2\theta_{13} = 0.099^{+0.013}_{-0.012}. \tag{5.46}$$

Table 5.1 Summary of the widely accepted positive results of oscillation measurements

	Experiment	Mode	Δm^2 [eV^2]	P_{OSC}	Neutrino source
(1)	IMB, Kamiokande, SK, K2K, MINOS, T2K	$\nu_\mu \to \nu_\mu$ $\bar{\nu}_\mu \to \bar{\nu}_\mu$	$\sim \pm 2.5 \times 10^{-3}$	~ 1	Atmospheric/ Accelerator
(2)	T2K, MINOS	$\nu_\mu \to \nu_e$	$\sim \pm 2.5 \times 10^{-3}$	~ 0.05	Accelerator
(3)	Double Chooz Daya Bay, RENO	$\bar{\nu}_e \to \bar{\nu}_e$	$\sim \pm 2.5 \times 10^{-3}$	~ 0.1	Reactor
(4)	Homestake, GNO, GALLEX, SAGE, SK, SNO, Borexino	$\nu_e \to \nu_e$	$\sim +8 \times 10^{-5}$	~ 0.4	Solar
(5)	KamLAND	$\bar{\nu}_e \to \bar{\nu}_e$	$\sim \pm 8 \times 10^{-5}$	~ 0.8	Reactor
(6)	OPERA	$\nu_\mu \to \nu_\tau$	$\sim 10^{-3}$	–	Accelerator

P_{OSC} is the approximate disappearance or appearance probability at the corresponding oscillation maximum. The sign of Δm^2 shows the possibility of the mass hierarchy

5.6 Summary of the Experiments

The Table 5.1 summarizes the positive results for all the neutrino oscillation experiments. Two distinct Δm^2 values have been observed, one being much smaller than the other. These observations are consistent within the framework of three flavor neutrino oscillations, as will be described in the next chapter.

References

1. SK detector, http://www-sk.icrr.u-tokyo.ac.jp/sk/ykphd/chap3-3.html
2. Super-Kamiokande Collaboration, PRL **81**, 1562–1567 (1998)
3. Super-Kamiokande Collaboration, PRD **81**, 092004 (2010)
4. Super-Kamiokande Collaboration, PRL **93**, 101801 (2004)
5. K2K beam line, http://neutrino.kek.jp/Images/Figures/nubeam.gif
6. K2K Collaboration, PRD **74**, 072003 (2006)
7. MINOS Collaboration, PRL **110**, 251801 (2013)
8. T2K Collaboration, arXiv:1304.0842v2 [hep-ex]
9. T2K Collaboration, PRL **111**, 211803 (2013)
10. T2K Collaboration, arXiv:1311.4570v1 [hep-ex]
11. OPERA Collaboration, arXiv:1308.2553v1 [hep-ex]
12. B.T. Cleveland et al., Astrophys. J. **496**, 505 (1998)
13. GNO Collaboration, PLB **616**, 174–190 (2005)
14. SAGE Collaboration, arXiv:0901.2200v3 [nucl-ex] (2009)
15. Super-Kamiokande Collaboration, PRD **83**, 052010 (2011)
16. SNO Collaboration, arXiv:nucl-ex/0205006v1 (2002)
17. SNO Collaboration, PRC **72**, 055502 (2005)
18. SNO Collaboration, arXiv:1109.0763v1 [hep-ex] (2011)
19. Borexino Collaboration, arXive:1308.0443v1 (2013)
20. Borexino Collaboration, PRL **108**, 051302 (2012)
21. KamLAND Collaboration, PRL **90**, 021802 (2003)
22. KamLAND Collaboration, arXiv:1303.4667v2 [hep-ex] (2013)
23. Double Chooz Collaboration, PRL **108**, 131801 (2012)
24. Daya Bay Collaboration, arXiv:1310.6732v1 [hep-ex] (2013)
25. T.J.C. Bezerra, H. Furuta, F. Suekane, T. Matsubara, PLB **725**, 271–276 (2013)

Chapter 6
Present Status

Abstract In this chapter, the results from the experiments described in Chap. 5 are unified to obtain the three flavor neutrino oscillation parameters. All the mixing angles, θ_{12}, θ_{23} and θ_{13}, all the mass squared differences Δm^2_{21}, Δm^2_{32} and Δm^2_{31} have been obtained and Δm^2_{21} mass hierarchy has been determined. Using the measured oscillation parameters, the transition amplitudes are calculated assuming the lightest neutrino mass to be 0 for IH, NH and ν_e effective mass is used as a parameter for the degenerate hierarchy case. In order to obtain an insight to an possible mechanism that may determine a gross pattern of the transition amplitude, $\nu_\mu - \nu_\tau$ symmetry and tri-bimaximal mixing are introduced as an example.

Keywords Oscillation parameter · Transition amplitude · Origin of transitions · $\nu_\mu - \nu_\tau$ symmetry · Tri-bimaximal mixing

6.1 Determination of the Three Flavor Oscillation Parameters

In the formulation of the standard three flavor neutrino oscillation, the parameters to measure are three mixing angles θ_{12}, θ_{23}, θ_{13}, one CP violating phase δ and three mass square differences, Δm^2_{21}, Δm^2_{32} and Δm^2_{31}.

Table 5.1 summarized widely accepted positive experimental results for the neutrino oscillations. All the experiments except for Table 5.1(2) and (6) are disappearance measurements. Usually disappearance data are analyzed using the two flavor oscillation formula and the correspondence between the measured parameters and the three flavor neutrino oscillation parameters is not direct. In the following sections, the measured oscillations probabilities are related to the three flavor neutrino oscillation parameters and our current knowledge are summarized as the three flavor neutrino oscillation scheme.

F. Suekane, *Neutrino Oscillations*, Lecture Notes in Physics 898,
DOI 10.1007/978-4-431-55462-2_6

6.1.1 Assignment of Measured Δm^2's to Δm^2_{21} and Δm^2_{31}

As we see in Table 5.1, the Δm^2's are categorized into two distinct values. One is $\Delta m^2_{\odot} \sim 8 \times 10^{-5}\,\mathrm{eV}^2$ and the other is $\Delta m^2_{\oplus} \sim 2.5 \times 10^{-3}\mathrm{eV}^2$, where $\Delta m^2_{\odot}$ was recognized by the solar neutrino observations first and $\Delta m^2_{\oplus}$ was recognized by the atmospheric neutrino observations first.

For three flavor neutrinos, there are three masses, m_1, m_2 and m_3, which make three combinations of squared mass differences,

$$\Delta m^2_{21} \equiv m^2_2 - m^2_1, \quad \Delta m^2_{32} \equiv m^2_3 - m^2_2, \quad \Delta m^2_{31} \equiv m^2_3 - m^2_1. \tag{6.1}$$

The three squared mass differences are not independent,

$$\Delta m^2_{12} + \Delta m^2_{23} + \Delta m^2_{31} = 0. \tag{6.2}$$

We define that $\nu_{1/2/3}$ are the main components of $\nu_{e/\mu/\tau}$, respectively and from the analogy to the relation $m^2_\mu - m^2_e \ll m^2_\tau - m^2_e$, we assign

$$|\Delta m^2_{21}| = \Delta m^2_{\odot}, \quad |\Delta m^2_{31}| = \Delta m^2_{\oplus}. \tag{6.3}$$

Another squared mass difference is

$$|\Delta m^2_{32}| = |\Delta m^2_{31} + \Delta m^2_{12}| \sim |\Delta m^2_{31}| = \Delta m^2_{\oplus}. \tag{6.4}$$

The difference between $|\Delta m^2_{31}|$ and $|\Delta m^2_{32}|$ is only 3 % and it is difficult to distinguish them experimentally. This fact can explain the reason why only the two squared mass differences have been experimentally observed.

6.1.2 Oscillations at Oscillation Maximums

As shown in the three flavor oscillation formula (4.91), the oscillation probability is the sum of the $\sin^2 \Phi_{ij}$ and $\sin 2\Phi_{ij}$ terms. If an experiment is performed at $\Phi_{31} \sim \pi/2$,

$$\sin^2 \Phi_{31} \sim 1, \quad \sin^2 \Phi_{32} \sim 1. \tag{6.5}$$

On the other hand, $\Phi_{21} = \Delta m^2_{21}/\Delta m^2_{31} \times \Phi_{31} \sim 0.05$ and therefore,

$$\sin^2 \Phi_{21} \sim 0. \tag{6.6}$$

Similarly, at $\Phi_{21} \sim \pi/2$,

$$\sin^2 \Phi_{21} \sim 1. \tag{6.7}$$

On the other hand, since $\Phi_{31} = |\Delta m^2_{31}|/|\Delta m^2_{21}| \times \Phi_{21} \sim 50$, the oscillation in the energy spectrum is rapid and $\sin^2\Phi_{31}$ and $\sin^2\Phi_{32}$ are averaged to

$$\sin^2\Phi_{31} \sim \sin^2\Phi_{32} \to 1/2. \tag{6.8}$$

These approximations are used to calculate the oscillation probabilities at each baseline later.

6.1.3 Determination of θ_{12}, θ_{23} *and* θ_{13}

The three mixing angles θ_{12}, θ_{23} and θ_{13} have been determined by comparing the observed oscillation probabilities and the three neutrino oscillation formula.

(i) The Double Chooz, Daya Bay and RENO experiments (Table 5.1(3)) measure the reactor $\overline{\nu}_e$ disappearance probability to be ∼10 % at Φ_{31} oscillation maximum. In this case the oscillation probability is, from Eq. (4.95),

$$P_{\overline{\nu}_e\to\overline{\nu}_e}(@\Phi_{31}) = 1 - 4\sum_{i>j}\sin^2\Phi_{ij}|U_{ei}|^2|U_{ej}|^2, \tag{6.9}$$

where "$(@\Phi_{ij})$" means "at $\Phi_{ij} \sim \pi/2$". Since, $\sin^2\Phi_{21} \sim 0$ and $\sin^2\Phi_{31} \sim \sin^2\Phi_{32} \sim 1$ at $\Phi_{31} \sim \pi/2$, the oscillation probability (6.9) is simplified to,

$$P_{\overline{\nu}_e\to\overline{\nu}_e}(@\Phi_{31}) \sim 1 - 4|U_{e3}|^2(|U_{e1}|^2 + |U_{e2}|^2) \sim 1 - \sin^2 2\theta_{13}, \tag{6.10}$$

where the standard mixing parameters in Eq. (4.106) is used. The observed $\overline{\nu}_e$ disappearance of 10 % leads a small $\sin^2 2\theta_{13}$,

$$\sin^2 2\theta_{13} \sim 0.1. \tag{6.11}$$

(ii) The atmospheric and accelerator experiments (Table 5.1(1)) measure almost 100 % $\nu_\mu \to \nu_\mu$ disappearance at $\Phi_{31} = O(1)$. With the same discussion made in the case (i), the oscillation probability here is,

$$\begin{aligned} P_{\nu_\mu\to\nu_\mu}(@\Phi_{31}) &\sim 1 - 4|U_{\mu3}|^2\left(|U_{\mu1}|^2 + |U_{\mu2}|^2\right) \\ &= 1 - 4c^2_{13}s^2_{23}(c^2_{23} + s^2_{13}s^2_{23}) \sim 1 - \sin^2 2\theta_{23} \sim 0, \end{aligned} \tag{6.12}$$

where $s^2_{13} \sim 0.03$ (from Eq. (6.11)) is ignored. The large ν_μ disappearance observed leads a large $\sin^2 2\theta_{23}$,

$$\sin^2 2\theta_{23} \sim 1. \tag{6.13}$$

(iii) The KamLAND experiments (Table 5.1(5)) measured large reactor $\overline{\nu}_e$ disappearance around the second oscillation maximum of Φ_{21}. The disappearance probability converted to the first oscillation maximum, $\Phi_{21} = \pi/2$ is $\sim$80 %. Using the approximated $\sin^2 \Phi_{ij}$ of (6.7) and (6.8), the oscillation probability is expressed as,

$$\begin{aligned} P_{\overline{\nu}_e \to \overline{\nu}_e}(@\Phi_{21}) &\sim 1 - 4|U_{e1}|^2|U_{e2}|^2 - 2|U_{e3}|^2 \left(|U_{e1}|^2 + |U_{e2}|^2\right) \\ &\sim 1 - \sin^2 2\theta_{12} \sim 0.2, \end{aligned} \tag{6.14}$$

where the small s_{13}^2 term is ignored and we obtain

$$\sin^2 2\theta_{12} \sim 0.8. \tag{6.15}$$

(iv) The solar neutrino experiments measure averaged ν_e disappearances to be $\sim$40 % where the matter effect is small (Table 5.1(4)) . The measured Δm^2 is around 10^{-4} eV^2. The oscillation probability is the same as the reactor neutrino case,

$$P_{\nu_e \to \nu_e}(@\text{sun}) \sim 1 - 4 \sum_{i>j} \sin^2 \Phi_{ij} |U_{ei}|^2 |U_{ej}|^2. \tag{6.16}$$

Since its oscillation length ($O(10^2$ km)) is much shorter than the solar size, the $\sin^2 \Phi_{21}$ term is averaged to 1/2. Therefore, the oscillation probability becomes,

$$\begin{aligned} P_{\nu_e \to \nu_e}(@\text{sun}) &\sim 1 - 2(|U_{e2}|^2|U_{e1}|^2 + |U_{e3}|^2|U_{e1}|^2 + |U_{e3}|^2|U_{e2}|^2) \\ &= 1 - \frac{1}{2}\sin^2 2\theta_{12} \sim 0.6, \end{aligned} \tag{6.17}$$

where the small s_{13}^2 is ignored. The observed disappearance corresponds to $\sin^2 2\theta_{12}/2$ and

$$\sin^2 2\theta_{12} \sim 0.8. \tag{6.18}$$

This is consistent with the KamLAND result of (6.15).

(v) The T2K and MINOS experiments have measured $\nu_\mu \to \nu_e$ appearance probability to be $\sim$5 % @Φ_{31} (Table 5.1(2)). Since this is an appearance measurement, the $\Im[\Lambda_{ij}^{\mu e}]$ term in Eqs. (4.91) and (4.93) can be finite. However, as it is shown in Eq. (8.110), this term is suppressed by a factor $\Delta m_{21}^2/\Delta m_{31}^2$ and can be ignored here. Only $\sin^2 \Phi_{31}$ and $\sin^2 \Phi_{32}$ are non zero at the oscillation maximum of Δm_{31}^2. Therefore, the oscillation probability is,

$$P_{\nu_\mu \to \nu_e}(@\Phi_{31}) \sim -4\Re\left[\Lambda_{31}^{\mu e} + \Lambda_{32}^{\mu e}\right] = s_{23}^2 \sin^2 2\theta_{13} \sim 0.05. \tag{6.19}$$

Using the results, (6.11) and (6.13), $P_{\nu_\mu \to \nu_e}(@\Phi_{31})$ is expected to be $\sim$5 %, which is consistent with the observation.

In summary, all the experimental results shown in Table 5.1 are consistent with,

$$\sin^2 2\theta_{12} \sim 0.8, \quad \sin^2 2\theta_{23} \sim 1 \text{ and } \sin^2 2\theta_{13} \sim 0.1. \tag{6.20}$$

6.1.4 Determination of Δm^2_{31} and Δm^2_{32}

The experimentally measured $\Delta m^2_{\oplus}$ was assigned to Δm^2_{31} as in Eq. (6.3). In fact, the $\Delta m^2_{\oplus}$ does not correspond directly to Δm^2_{31}, but corresponds to a weighted average of Δm^2_{31} and Δm^2_{32}. For the short baseline reactor neutrino experiments, if we do not employ the approximation of $\Delta m^2_{31} \sim \Delta m^2_{32}$, the oscillation probability (6.9) becomes,

$$P_{\bar{\nu}_e \to \bar{\nu}_e}(@\Phi_{31}) = 1 - \sin^2 2\theta_{13} \left(c^2_{12} \sin^2 \frac{\Delta m^2_{31} L}{4E} + s^2_{12} \sin^2 \frac{\Delta m^2_{32} L}{4E} \right). \tag{6.21}$$

If this energy spectrum is analyzed to measure Δm^2 assuming two flavor oscillation formula, the two bumps closely separated in energy distribution are treated as a single bump and fitted as,

$$\sin^2 \frac{\Delta \hat{m}^2_{31} L}{4E} \sim c^2_{12} \sin^2 \frac{\Delta m^2_{31} L}{4E} + s^2_{12} \sin^2 \frac{\Delta m^2_{32} L}{4E}, \tag{6.22}$$

where $\Delta \hat{m}^2_{31}$ is measured as a weighted average of Δm^2_{31} and Δm^2_{32} given by,

$$\Delta \hat{m}^2_{31} \sim c^2_{12} |\Delta m^2_{31}| + s^2_{12} |\Delta m^2_{32}|. \tag{6.23}$$

This $\Delta \hat{m}^2$ is called the *effective* Δm^2 [1].

For the $\nu_\mu \to \nu_\mu$ disappearance observations of the accelerator and atmospheric neutrinos, the oscillation probability (6.12) can be expanded to,

$$\begin{aligned} P_{\nu_\mu \to \nu_\mu}(@\Phi_{31}) &= 1 - \sin^2 2\theta_{23} \\ &\times \left((s^2_{12} + c_\delta s_{13} t_{23} \sin 2\theta_{12}) \sin^2 \frac{\Delta m^2_{31} L}{4E} + (c^2_{12} - c_\delta s_{13} t_{23} \sin 2\theta_{12}) \sin^2 \frac{\Delta m^2_{32} L}{4E} \right), \end{aligned} \tag{6.24}$$

where $t_{23} = \tan\theta_{23}$ and $c_\delta = \cos\delta$. The effective squared mass difference, $\Delta \hat{m}^2_{32}$ is, similarly to Eq. (6.23), given by,

$$\Delta \hat{m}^2_{32} \sim (s^2_{12} + c_\delta s_{13} t_{23} \sin 2\theta_{12}) \left| \Delta m^2_{31} \right| + (c^2_{12} - c_\delta s_{13} t_{23} \sin 2\theta_{12}) \left| \Delta m^2_{32} \right|. \tag{6.25}$$

At first sight, Eq. (6.25) seems to be more complicate than Eq. (6.23). However, it is due to the definition of the mixing parameters and there is not essential difference.

In principle, $|\Delta m^2_{31}|$ and $|\Delta m^2_{32}|$ can be determined from $\Delta\hat{m}^2_{13}$ and $\Delta\hat{m}^2_{32}$ by solving the simultaneous equations (6.23) and (6.25) as

$$\begin{pmatrix}|\Delta m^2_{32}|\\|\Delta m^2_{31}|\end{pmatrix} = \frac{1}{\cos 2\theta_{12} - c_\delta s_{13} t_{23} \sin 2\theta_{12}} \times \begin{pmatrix} c^2_{12} & -(s^2_{12} + c_\delta s_{13} t_{23} \sin 2\theta_{12}) \\ -s^2_{12} & c^2_{12} - c_\delta s_{13} t_{23} \sin 2\theta_{12} \end{pmatrix} \begin{pmatrix}\Delta\hat{m}^2_{32}\\ \Delta\hat{m}^2_{31}\end{pmatrix}. \tag{6.26}$$

However, the errors of the $\Delta\hat{m}^2$ measurements are still large and it is not practical to separately determine Δm^2_{31} and Δm^2_{32} now.

For Δm^2_{21} case, the measured $\Delta m^2_\odot$ by the KamLAND and the solar neutrino experiments directly corresponds to Δm^2_{21}.

$$\Delta m^2_{21} = \Delta m^2_\odot. \tag{6.27}$$

6.2 Determination of Δm^2_{21} Mass Hierarchy

The mass hierarchy of m_1 and m_2 has been determined to be $m_1 < m_2$ by making use of the matter effect of the solar neutrinos. As shown in Fig. 5.29, the solar neutrino deficit is $\sim$50 % at $E_\nu < 2$ MeV and it increases to $\sim$70 % at $E_\nu > 5$ MeV. The energy dependence is caused by the matter effect that depends on the mass hierarchy.

The matter density of the sun, $\rho_\odot$ at a radius r can be approximated as [1, Chap. 1]

$$\rho_\odot(r) \sim \rho_\odot(0) \exp\left[-10\frac{r}{R_\odot}\right], \tag{6.28}$$

where $R_\odot \sim 7.0 \times 10^8$ m is the radius of the sun and the matter density at the center of the sun is $\rho_\odot(0) \sim 150\,\mathrm{g/cm^3}$.

In principle, it is necessary to deal with the matter effect for the three flavor neutrinos. The oscillation part of the three flavor state equation with the charged current weak potential is, from Eq. (4.129),

$$\frac{d}{dt}\begin{pmatrix}C_e\\C_\mu\\C_\tau\end{pmatrix} = -\frac{i}{\gamma}\begin{pmatrix}\mu_e + \gamma V_W & \tau^*_{\mu e} & \tau^*_{\tau e}\\ \tau_{\mu e} & \mu_\mu & \tau^*_{\tau\mu}\\ \tau_{\tau e} & \tau_{\tau\mu} & \mu_\tau\end{pmatrix}\begin{pmatrix}C_e\\C_\mu\\C_\tau\end{pmatrix}. \tag{6.29}$$

In general, it is difficult to solve Eq. (6.29) and we adopt the following approximation. In the limit of $\theta_{13} \to 0$, the mixing matrix (4.106) becomes

$$U_\nu = \begin{pmatrix} c_{12} & s_{12} & 0 \\ -s_{12}c_{23} & c_{12}c_{23} & s_{23} \\ s_{12}s_{23} & -s_{23}c_{12} & c_{23} \end{pmatrix}. \tag{6.30}$$

The mixing matrix for the basis state shown in (4.85) is,

$$\begin{pmatrix} |\nu_1\rangle \\ |\nu_2\rangle \\ |\nu_3\rangle \end{pmatrix} = \begin{pmatrix} c_{12} & -s_{12}c_{23} & s_{12}s_{23} \\ s_{12} & c_{12}c_{23} & -c_{12}s_{23} \\ 0 & s_{23} & c_{23} \end{pmatrix} \begin{pmatrix} |\nu_e\rangle \\ |\nu_\mu\rangle \\ |\nu_\tau\rangle \end{pmatrix}. \tag{6.31}$$

This equation can be rearranged as

$$\begin{pmatrix} |\nu_1\rangle \\ |\nu_2\rangle \\ |\nu_3\rangle \end{pmatrix} = \begin{pmatrix} c_{12} & -s_{12} & 0 \\ s_{12} & c_{12} & 0 \\ 0 & 0 & 1 \end{pmatrix} \begin{pmatrix} |\nu_e\rangle \\ c_{23}\,|\nu_\mu\rangle - s_{23}\,|\nu_\tau\rangle \\ s_{23}\,|\nu_\mu\rangle + c_{23}\,|\nu_\tau\rangle \end{pmatrix}, \tag{6.32}$$

which shows that $|\nu_e\rangle$ and $|\nu_3\rangle$ are decoupled. If we define the new neutrino states as follows:

$$\begin{cases} |\nu_\xi\rangle \equiv c_{23}\,|\nu_\mu\rangle - s_{23}\,|\nu_\tau\rangle \\ |\nu_\zeta\rangle \equiv s_{23}\,|\nu_\mu\rangle + c_{23}\,|\nu_\tau\rangle \end{cases}, \tag{6.33}$$

ν_ζ is a mass eigenstate,

$$|\nu_\zeta\rangle = |\nu_3\rangle\,. \tag{6.34}$$

The other mass eigenstates are mixings of ν_e and ν_ξ,

$$\begin{pmatrix} |\nu_1\rangle \\ |\nu_2\rangle \end{pmatrix} = \begin{pmatrix} c_{12} & -s_{12} \\ s_{12} & c_{12} \end{pmatrix} \begin{pmatrix} |\nu_e\rangle \\ |\nu_\xi\rangle \end{pmatrix}. \tag{6.35}$$

Therefore, the oscillation occurs between ν_e and ν_ξ through the mass eigenstates ν_1 and ν_2 just like the oscillation between ν_e and ν_μ for the two flavor case. The solar neutrinos are generated as ν_e and oscillate to ν_ξ. Equation (6.33) shows that the ratio of the oscillation probabilities, $P_{\nu_e\to\nu_\tau}$ to $P_{\nu_e\to\nu_\mu}$ is $\tan^2\theta_{23}$. Since both ν_μ and ν_τ are not affected by the charged current weak potential, ν_ξ is not affected either and the matter effect of the $\nu_e \Leftrightarrow \nu_\xi$ oscillation is the same as that for the $\nu_e \Leftrightarrow \nu_\mu$ oscillation. Therefore, by substituting $\nu_\mu \to \nu_\xi$, it is possible to borrow the results of the matter effect discussed in Sect. 4.3.

The state equation between ν_e and ν_ξ in matter is, from Eq. (4.131),

$$\frac{d}{dt}\begin{pmatrix} \tilde{C}_e \\ \tilde{C}_\xi \end{pmatrix} = -i\tilde{\omega}_\odot \begin{pmatrix} -\cos 2\tilde{\theta}_\odot & \sin 2\tilde{\theta}_\odot \\ \sin 2\tilde{\theta}_\odot & \cos 2\tilde{\theta}_\odot \end{pmatrix} \begin{pmatrix} \tilde{C}_e \\ \tilde{C}_\xi \end{pmatrix}, \tag{6.36}$$

where, $\tilde{\omega}_\odot = \kappa_\odot \omega_0$, $\omega_0 = \Delta m^2_\pm / 4E (\geq 0)$ and

$$\kappa_\odot = \sqrt{(\cos 2\theta_\nu - \upsilon_\odot)^2 + \sin^2 2\theta_\nu}, \quad \tan 2\tilde{\theta}_\odot = \frac{\sin 2\theta_\nu}{\cos 2\theta_\nu - \upsilon_\odot}. \tag{6.37}$$

From Table 4.1, the relation between the mixing angles of θ_{12} and θ_ν are,

$$\theta_\nu = \theta_0 = \theta_{12} \text{ for NH and } \theta_\nu = \theta_0 + \frac{\pi}{2} = \theta_{12} + \frac{\pi}{2} \text{ for IH.} \tag{6.38}$$

This means

$$\cos 2\theta_\nu = \eta^{21}_{\mathrm{M}} \cos 2\theta_{12}, \quad \sin 2\theta_\nu = \eta^{21}_{\mathrm{M}} \sin 2\theta_{12}, \tag{6.39}$$

where $\eta^{21}_{\mathrm{M}} = +1$ for the normal hierarchy and $\eta^{21}_{\mathrm{M}} = -1$ for the inverted hierarchy.

The neutrinos produced in the sun experience varying density before exiting from the surface. If a neutrino is generated near the center of the sun, the time dependence of the potential parameter is, from Eqs. (4.130) and (6.28),

$$\upsilon_\odot(t) \sim \upsilon_\odot(0) \exp\left(-10 \frac{ct}{R_\odot}\right), \tag{6.40}$$

where the relation $r = ct$ is used. The potential parameters at the center of the sun is

$$|\upsilon_\odot(0)| \sim 0.25E[/\mathrm{MeV}], \tag{6.41}$$

which depends on the neutrino energy.

The state equation is the same as Eq. (6.36) except for that $\upsilon_\odot$ and therefore, $\tilde{\theta}_\odot$ and $\kappa_\odot$ are functions of the time.

$$\frac{d}{dt}\begin{pmatrix} \tilde{C}_e \\ \tilde{C}_\xi \end{pmatrix} = -i\tilde{\omega}_\odot(t) \begin{pmatrix} -\cos 2\tilde{\theta}_\odot(t) & \sin 2\tilde{\theta}_\odot(t) \\ \sin 2\tilde{\theta}_\odot(t) & \cos 2\tilde{\theta}_\odot(t) \end{pmatrix} \begin{pmatrix} \tilde{C}_e \\ \tilde{C}_\xi \end{pmatrix}, \tag{6.42}$$

where

$$\begin{aligned} \tilde{\omega}_\odot(t) &= \kappa_\odot(t)\omega_0, \\ \kappa_\odot(t) &= \sqrt{(\cos 2\theta_{12} - \eta^{21}_{\mathrm{M}}\upsilon_\odot(t))^2 + \sin^2 2\theta_{12}}, \\ \text{and} \quad \tan 2\tilde{\theta}_\odot(t) &= \frac{\sin 2\theta_{12}}{\cos 2\theta_{12} - \eta^{21}_{\mathrm{M}}\upsilon_\odot(t)}. \end{aligned} \tag{6.43}$$

The general neutrino wave function in the sun can be expressed by superpositions of the flavor eigenstates or the energy eigenstates as give by,

$$|\tilde{\psi}_\nu(t)\rangle = \tilde{C}_e(t)\,|\nu_e\rangle + \tilde{C}_\xi(t)\,|\nu_\xi\rangle = \tilde{C}_-(t)\,|\tilde{\nu}_-(t)\rangle + \tilde{C}_+(t)\,|\tilde{\nu}_+(t)\rangle\,. \tag{6.44}$$

Since the mass eigenstate depends on the matter density, the mass eigenstates $|\tilde{\nu}_\pm\rangle$ are functions of time.

The neutrino oscillation length in the sun is,

$$\tilde{\lambda}_\odot = \frac{\pi}{\kappa_\odot \omega_0} = \frac{\lambda_0}{\kappa_\odot}, \tag{6.45}$$

where λ_0 is the oscillation length in the vacuum.

$$\lambda_0 = \frac{\pi}{\omega_0} = \frac{4\pi E}{\Delta m^2_\pm} \sim 33 \times (E[/\mathrm{MeV}])[\mathrm{km}]. \tag{6.46}$$

Since the energy of the solar neutrinos is less than 20 MeV, the neutrino oscillation length in the sun is, $\tilde{\lambda}_\odot < 660\,\mathrm{km}$. Therefore, the neutrinos produced deep inside the sun oscillates many times before they reach the surface. The change of the potential parameter during each oscillation period is small as shown

$$\left| \frac{1}{\upsilon_\odot} \frac{d\upsilon_\odot}{dt} \frac{\tilde{\lambda}_\odot}{c} \right| = 10 \frac{\tilde{\lambda}_\odot}{R_\odot} < 0.01. \tag{6.47}$$

The angular velocity of the oscillation in the sun is

$$\tilde{\omega}_\odot > \sin 2\theta_{12}\omega_0 \sim \frac{\pi \sin 2\theta_{12}}{33 E_\nu[/\mathrm{MeV}]}[\mathrm{km}] > 1.4 \times 10^3 [1/\mathrm{s}]. \tag{6.48}$$

On the other hand, using (6.43),

$$|\dot{\tilde{\theta}}_\odot| = \frac{\sin 2\theta_{12} |\dot{\upsilon}_\odot|}{2\kappa^2_\odot} \sim \frac{5}{R_\odot} \frac{\sin 2\theta_{12} |\upsilon_\odot|}{\kappa^2_\odot} < 2[1/\mathrm{s}]. \tag{6.49}$$

Therefore, we can regard as $\tilde{\omega}_\odot \gg \dot{\tilde{\theta}}_\odot$.

It is generally difficult to analytically solve Eq. (6.42). However, an approximated solution can be obtained under the adiabatic condition, $\tilde{\omega}_\odot \gg \dot{\tilde{\theta}}_\odot$. The calculation to solve Eq. (6.42) is described in Sect. 8.6 and we use the following result.

$$\tilde{C}_\pm(t) = \tilde{C}_\pm(0) \exp\left[\mp i \frac{\Delta m_\pm}{2} \int_0^t \kappa_\odot(t) dt \right] \equiv \tilde{C}_\pm(0) \exp\left[\mp i \Omega(t) \right], \tag{6.50}$$

where $\Omega(t)$ corresponds to the time-integrated phase rotation. Equation (6.50) indicates the mass eigenstates stay the original mass eigenstates. The wave function at time t is

$$|\tilde{\psi}_\nu(t)\rangle = \tilde{C}_-(0) e^{i\Omega(t)} |\tilde{\nu}_-(t)\rangle + \tilde{C}_+(0) e^{-i\Omega(t)} |\tilde{\nu}_+(t)\rangle . \tag{6.51}$$

At $t = 0$, the neutrino is produced as pure ν_e. Thus, the initial condition is given by,

$$|\tilde{\psi}_\nu(0)\rangle = |\nu_e\rangle = \cos\tilde{\theta}_\odot(0)\,|\tilde{\nu}_-(0)\rangle - \sin\tilde{\theta}_\odot(0)\,|\tilde{\nu}_+(0)\rangle\,. \tag{6.52}$$

This relation leads $\tilde{C}_-(0) = \cos\tilde{\theta}_\odot(0)$ and $C_+(0) = \sin\tilde{\theta}_\odot(0)$. At $t = T_R$ the neutrino reaches to the surface of the sun. The neutrino wave function $\tilde{\psi}_\nu(T_R)$ can be written as

$$|\tilde{\psi}_\nu(T_R)\rangle = \cos\tilde{\theta}_\odot(0)\,|\tilde{\nu}_-(T_R)\rangle\,e^{i\Omega(T_R)} - \sin\tilde{\theta}_\odot(0)\,|\tilde{\nu}_+(T_R)\rangle\,e^{-i\Omega(T_R)}. \tag{6.53}$$

The neutrino state at the surface is equivalent to that in the vacuum.

$$|\tilde{\nu}_\pm(T_R)\rangle = |\nu_\pm\rangle\,. \tag{6.54}$$

After that the neutrino travels to the earth taking $T_A \sim 500\,\mathrm{s}$. The wave function at the earth is.

$$|\tilde{\psi}_\nu(T_R+T_A)\rangle = \cos\tilde{\theta}_\odot(0)\,|\nu_-\rangle\,e^{i(\Omega(T_R)-\frac{m_-}{\gamma}T_A)} - \sin\tilde{\theta}_\odot(0)\,|\nu_+\rangle\,e^{-i(\Omega(T_R)+\frac{m_+}{\gamma}T_A)}. \tag{6.55}$$

The probability that ν_e remains as ν_e at the earth is, using (4.62),

$$\begin{aligned} P_{\nu_e\to\nu_e} &= |\,\langle\nu_e|\tilde{\psi}_\nu(T_R+T_A)\rangle\,|^2 \\ &= \left|\cos\tilde{\theta}_\odot(0)\cos\theta_\nu e^{i(\Omega(T_R)-(\frac{m_-}{\gamma})T_A)} + \sin\tilde{\theta}_\odot(0)\sin\theta_\nu e^{-i(\Omega(T_R)+(\frac{m_+}{\gamma})T_A)}\right|^2 \\ &= \frac{1}{2}\left(1+\cos 2\tilde{\theta}_\odot(0)\cos 2\theta_\nu + \sin 2\tilde{\theta}_\odot(0)\sin 2\theta_\nu\cos(2\Omega(T_R)+\frac{\Delta m}{\gamma}T_A)\right). \end{aligned} \tag{6.56}$$

The neutrinos are produced at various places and with random directions in the sun. Therefore, neutrinos have different T_R with the difference much larger than the oscillation period. The averaging the phase $\Omega(T_R)$ results in,

$$\langle\cos(2\Omega(T_R) + \frac{\Delta m}{\gamma}T_A)\rangle \to 0, \tag{6.57}$$

and the 3rd term of Eq. (6.56) vanishes. Finally the survival probability of $\overline{\nu}_e$ is

$$P_{\nu_e\to\nu_e} \sim \frac{1}{2}\left(1+\cos 2\theta_\nu\cos 2\tilde{\theta}_\odot(0)\right). \tag{6.58}$$

This means that the oscillation probability depends only on the mixings at the neutrino generation in the sun, $\tilde{\theta}_\odot(0)$ and in the vacuum, θ_ν.

From Fig. 4.10a,

$$\cos 2\tilde{\theta}_\odot(0) = \frac{\cos 2\theta_\nu - \upsilon_\odot(0)}{\kappa_\odot(0)} = \frac{\eta^{21}_{\mathrm{M}} \cos 2\theta_{12} - \upsilon_\odot(0)}{\kappa_\odot(0)} \tag{6.59}$$

and the survival probability of the solar neutrino is, numerically

$$\begin{aligned} P_{\nu_e \to \nu_e} &= \frac{1}{2}\left(1 + \frac{\cos 2\theta_{12}(\cos 2\theta_{12} - \eta^{21}_{\mathrm{M}}\upsilon_\odot(0))}{\kappa_\odot(0)}\right) \\ &\sim \frac{1}{2}\left(1 + \frac{0.38(1.5 - \eta^{21}_{\mathrm{M}} E_\nu[/\mathrm{MeV}])}{\sqrt{(1.5 - \eta^{21}_{\mathrm{M}} E_\nu[/\mathrm{MeV}])^2 + 13.8}}\right). \end{aligned} \tag{6.60}$$

Figure 6.1 shows the energy dependence of the solar neutrino survival probabilities for normal hierarchy, inverted hierarchy and the case there is no matter effect. Comparison with the experimental results in Fig. 6.1 shows,

$$\eta^{21}_{\mathrm{M}} > 0, \tag{6.61}$$

thus Δm^2_{21} mass hierarchy is determined to be the normal.

Knowing that the Δm^2_{21} mass hierarchy is normal, the oscillation amplitude and the heavy neutrino component of ν_e at a radius r in the sun are

$$\sin^2 2\tilde{\theta}_\odot(r) = \frac{\sin^2 2\theta_{12}}{\kappa^2_\odot(r)}, \quad \sin^2 \tilde{\theta}_\odot(r) = \frac{1}{2}\left(1 - \frac{\cos 2\theta_{12} - \upsilon_\odot(0)e^{(-10r/R_\odot)}}{\kappa_\odot(r)}\right), \tag{6.62}$$

where

$$\kappa_\odot(r) = \sqrt{\left(\cos 2\theta_{12} - \upsilon_\odot(0)e^{(-10r/R_\odot)}\right)^2 + \sin^2 2\theta_{12}}. \tag{6.63}$$

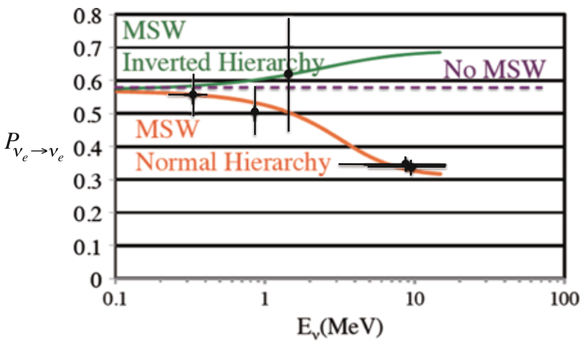

Fig. 6.1 Energy dependence of survival probability of the solar neutrinos for the normal hierarchy, inverted hierarchy and no MSW effect cases. The calculation was made based on the approximation of $\theta_{13} = 0$. The data points are the results of the experiments. See also Fig. 5.29

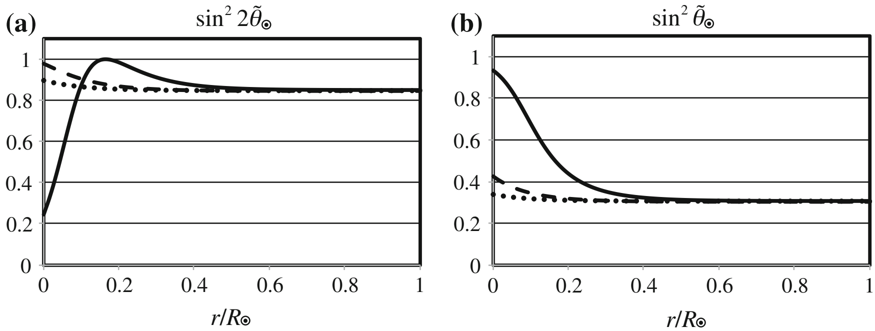

Fig. 6.2 **a** Oscillation amplitude. **b** Heavy neutrino component of ν_e. The horizontal axis is the relative radius of the neutrino position. The *solid*, *dashed* and *dotted lines* are for 8, 1 and 0.3 MeV solar neutrinos, respectively. The parameter $\tilde{\theta}_\odot$ is the mixing angle in the sun. The matter density in the sun is assumed as Eq. (6.28) and θ_{13} is assumed to be 0

The heavy neutrino component of electron neutrino and oscillation amplitude at various radius are shown in Fig. 6.2.

The 8 MeV neutrinos pass through the resonance region at $r \sim 0.2\ R_\odot$. Although the heavy neutrino component is 30 % in the vacuum, it is dominant part of electron neutrinos with energy $E = 8$ MeV at the center of the sun. The matter effect is small for low energy neutrinos. These dependence on the energy of the matter effect produce the energy dependence of the solar neutrino deficit.

6.3 Present Knowledge of the Neutrino Oscillation Parameters

6.3.1 Global Analysis for the Oscillation Parameters

So far, the discussion were made based on the approximations to the two flavor analysis making use of the properties that two Δm^2's are pretty different and that $\sin^2\theta_{13}$ is small. However, to obtain the oscillation parameters more precisely, it is necessary to perform a global three flavor oscillation analysis. Table 6.1 summarizes such analysis results taken from Ref. [2].

Using these values, the mixing matrix elements can be numerically calculated as

$$\begin{aligned} U_{\mathrm{NH}} &= \begin{pmatrix} 0.82 & 0.55 & -0.052+0.14i \\ -0.39+0.079i & 0.64+0.053i & 0.65 \\ 0.40+0.090i & -0.53+0.060i & 0.74 \end{pmatrix}, \\ U_{\mathrm{IH}} &= \begin{pmatrix} 0.82 & 0.55 & -0.087+0.13i \\ -0.36+0.072i & 0.65+0.048i & 0.67 \\ 0.43+0.079i & -0.53+0.052i & 0.73 \end{pmatrix}. \end{aligned} \tag{6.64}$$

Table 6.1 Best fit oscillation parameters

Parameter	Mass hierarchy case	Best fit	1σ range
Δm^2_{21}		7.54×10^{-5} eV^2	$(7.32–7.80) \times 10^{-5}$ eV^2
$\sin^2\theta_{12}$		0.308	(0.291–0.325)
Δm^2_{31}	NH	2.47×10^{-3} eV^2	$(2.41–2.53) \times 10^{-3}$ eV^2
	IH	2.42×10^{-3} eV^2	$(2.36–2.48) \times 10^{-3}$ eV^2
$\sin^2\theta_{13}$	NH	0.0234	(0.0215–0.0254)
	IH	0.0240	(0.0218–0.0259)
$\sin^2\theta_{23}$	NH	0.437	(0.414–0.470)
	IH	0.455	(0.424–0.594)
δ	NH	$1.39\,\pi$	$(1.12–1.77)\,\pi$
	IH	$1.31\,\pi$	$(0.98–1.60)\,\pi$

The errors of δ are still large and the values may significantly change in the future. From [2]

They show that the mixture between the flavor and mass eigenstates are larger than the CKM matrix for the quark mixing.

The probabilities of finding mass-eigenstate ν_k in flavor-eigenstate ν_α is given by taking the absolute square of each element of (6.64), $P_{\alpha k} = |U_{\alpha k}|^2$. For both hierarchies,

$$P_{\alpha k} \sim \begin{pmatrix} 0.68 & 0.30 & 0.023 \\ 0.16 & 0.42 & 0.43 \\ 0.17 & 0.28 & 0.55 \end{pmatrix}. \tag{6.65}$$

6.3.2 Determination of the Transition Matrix Elements

The mixing matrix measured by the experiments are shown in Eq. (6.64). The corresponding transition amplitudes can be calculated from the relation given in Eq. (3.59),

$$\mathscr{T} = UMU^\dagger, \tag{6.66}$$

where the absolute values of m_i are required for the calculation.

If the absolute electron neutrino mass is measured and the Δm^2_{31} mass hierarchy is determined, all the neutrino mass can be determined as follows. In general direct ν_e mass experiments measure $m^2_{\nu_e}$ instead of m_{ν_e},[1]

$$\langle m^2_{\nu_e} \rangle = |U_{e1}|^2 m_1^2 + |U_{e2}|^2 m_2^2 + |U_{e3}|^2 m_3^2. \tag{6.67}$$

[1] See Sect. 7.3.1.

Using the observable parameters, m_i^2 can be determined as follows:

$$\begin{cases} m_1^2 = \langle m_{\nu_e}^2 \rangle - |U_{e2}|^2 \Delta m_{21}^2 - \eta_M^{31} |U_{e3}|^2 |\Delta m_{31}^2| \\ m_2^2 = \langle m_{\nu_e}^2 \rangle + (1 - |U_{e2}|^2) \Delta m_{21}^2 - \eta_M^{31} |U_{e3}|^2 |\Delta m_{31}^2| \\ m_3^2 = \langle m_{\nu_e}^2 \rangle + \eta_M^{31} (1 - |U_{e3}|^2) |\Delta m_{31}^2| \end{cases} , \tag{6.68}$$

where $\eta_M^{31} = +1$ for Δm_{31}^2 normal hierarchy (NH) ($m_3 > m_1$) and $\eta_M^{31} = -1$ for inverted hierarchy (IH) ($m_3 < m_1$). For NH,

$$\text{NH} : \begin{cases} m_1^2 \sim \langle m_{\nu_e}^2 \rangle - 8.1 \times 10^{-5} [\text{eV}^2] \\ m_2^2 \sim \langle m_{\nu_e}^2 \rangle - 5.1 \times 10^{-6} [\text{eV}^2] \\ m_3^2 \sim \langle m_{\nu_e}^2 \rangle + 2.4 \times 10^{-3} [\text{eV}^2]. \end{cases} \tag{6.69}$$

For IH,

$$\text{IH} : \begin{cases} m_1^2 \sim \langle m_{\nu_e}^2 \rangle + 3.5 \times 10^{-5} [\text{eV}^2] \\ m_2^2 \sim \langle m_{\nu_e}^2 \rangle + 1.1 \times 10^{-4} [\text{eV}^2] \\ m_3^2 \sim \langle m_{\nu_e}^2 \rangle - 2.4 \times 10^{-3} [\text{eV}^2]. \end{cases} \tag{6.70}$$

Since we do not know $\langle m_{\nu_e}^2 \rangle$ yet, we assume the lightest neutrino mass is 0 to give a reference situation.

For NH, $m_3 > m_2 > m_1 = 0$ and $\sqrt{\langle m_{\nu_e}^2 \rangle} \sim 10\,\text{meV}$. The neutrino mass matrix becomes,

$$M_{\text{NH}}(m_1 = 0) \sim \begin{pmatrix} 0 & 0 & 0 \\ 0 & 8.7 & 0 \\ 0 & 0 & 50 \end{pmatrix} \text{meV}. \tag{6.71}$$

In this case the transition matrix can be calculated using Eq. (6.64) as

$$\mathscr{T}_{\text{NH}}(m_1 = 0) \sim \begin{pmatrix} 3.8 & 1.4 + 4.5i & -4.4 + 5.1i \\ 1.4 - 4.5i & 25 & 21 \\ -4.4 - 5.1i & 21 & 30 \end{pmatrix} \text{meV}. \tag{6.72}$$

For IH, $m_2 > m_1 > m_3 = 0$ and $\sqrt{\langle m_{\nu_e}^2 \rangle} \sim 49\,\text{meV}$. The mass matrix in this case is

$$M_{\text{IH}}(m_3 = 0) \sim \begin{pmatrix} 49 & 0 & 0 \\ 0 & 50 & 0 \\ 0 & 0 & 0 \end{pmatrix} \text{meV}. \tag{6.73}$$

The transition matrix is

$$\mathscr{T}_{\text{IH}}(m_3 = 0) \sim \begin{pmatrix} 48 & 3.1 - 4.2i & 2.9 - 4.6i \\ 3.1 + 4.2i & 28 & -24 \\ 2.9 + 4.6i & -24 & 23 \end{pmatrix} \text{meV}. \tag{6.74}$$

If the effective ν_e mass is much larger than the scale of the mass differences, $\langle m_{\nu_e}^2\rangle \gg |\Delta m_{31}^2|$, all the neutrino masses become similar, $m_1 \sim m_2 \sim m_3 \sim m_{\nu_e}$. This situation is called the degenerate mass hierarchy. For the degenerate mass hierarchy, the neutrino mass matrix can be approximated as

$$M\left(\langle m_{\nu_e}^2\rangle \gg |\Delta m_{31}^2|\right) \sim \sqrt{\langle m_{\nu_e}^2\rangle} + \frac{1}{\sqrt{\langle m_{\nu_e}^2\rangle}} M_\Delta, \tag{6.75}$$

where

$$M_\Delta = \frac{1}{2}\left(-|U_{e3}|^2 \Delta m_{31}^2 I + \begin{pmatrix} -|U_{e2}|^2\Delta m_{21}^2 & 0 & 0 \\ 0 & (1-|U_{e2}|^2)\Delta m_{21}^2 & 0 \\ 0 & 0 & \Delta m_{31}^2 \end{pmatrix}\right). \tag{6.76}$$

The transition matrix is,

$$\mathscr{T}\left(\langle m_{\nu_e}^2\rangle \gg |\Delta m_{31}^2|\right) = \sqrt{\langle m_{\nu_e}^2\rangle} I + \frac{1}{\sqrt{\langle m_{\nu_e}^2\rangle}}[U M_\Delta U^\dagger]. \tag{6.77}$$

Using the numerical values in Eqs. (6.64), (6.69) and (6.70), the transition amplitudes are

$$\begin{aligned} &\mathscr{T}_{\mathrm{NH}}\left(\langle m_{\nu_e}^2\rangle \gg |\Delta m_{31}^2|\right) \\ &\sim \sqrt{\langle m_{\nu_e}^2\rangle} I + \frac{1}{\sqrt{\langle m_{\nu_e}^2\rangle}} \begin{pmatrix} 0 & -0.29+1.2i & -0.58+1.3i \\ -0.29-1.2i & 5.0 & 5.9 \\ -0.58-1.3i & 5.9 & 6.5 \end{pmatrix} \times 10^{-4} \end{aligned} \tag{6.78}$$

and

$$\begin{aligned} &\mathscr{T}_{\mathrm{IH}}\left(\langle m_{\nu_e}^2\rangle \gg |\Delta m_{31}^2|\right) \\ &\sim \sqrt{\langle m_{\nu_e}^2\rangle} I + \frac{1}{\sqrt{\langle m_{\nu_e}^2\rangle}} \begin{pmatrix} 0 & 0.83-1.0i & 0.66-1.1i \\ 0.83+1.0i & -5.0 & -6.0 \\ 0.66+1.1i & -6.0 & -6.1 \end{pmatrix} \times 10^{-4}, \end{aligned} \tag{6.79}$$

where the unit is in [eV^2].

What causes these transitions is an important question. The standard model does not include these transitions and new physics is supposed to exist in them. It is instructive to compare with the quark transition matrix,

$$\mathscr{T}_{\text{quark}} = V_{\text{CKM}} \begin{pmatrix} m_d & 0 & 0 \\ 0 & m_s & 0 \\ 0 & 0 & m_b \end{pmatrix} V_{\text{CKM}}^{\dagger} \sim \begin{pmatrix} 10 & 20 & 8-14i \\ 20 & 90 & 170 \\ 8+14i & 170 & 4200 \end{pmatrix} \text{MeV}. \tag{6.80}$$

For the quark case, these transitions are generated by the Yukawa coupling to the Higgs field in the standard model and the transition amplitudes correspond to the product of the coupling constants and the Higgs vacuum expectation value. For neutrinos, because the transition amplitudes are extremely smaller than quark's, it is believed to be unnatural to think that the origin of the transitions are the same as quarks. What is the origin of the neutrino transitions is an important open question.

6.4 $\nu_\mu - \nu_\tau$ Symmetry and Tri-bimaximal Mixing

Before the θ_{13} was measured to be finite, it was thought that it could be zero due to some kind of symmetry. $\nu_\mu - \nu_\tau$ symmetry is one of such possibilities which predicts $\sin^2 2\theta_{13} = 0$ and $\sin^2 2\theta_{23} = 1$. Although $\sin^2 2\theta_{13}$ turned out to be finite, it is small and the $\nu_\mu - \nu_\tau$ symmetry seems to approximately hold. It is instructive to see how such the symmetry determines the mixing angles and masses.

The θ_{12} is measured to be large but not maximal. The observed mixing angles can be approximated by the so-called tri-bimaximal mixing. In this section, we will play with a toy model of the $\nu_\mu - \nu_\tau$ symmetry and study the relation between the tri-bimaximal mixing and transition amplitudes.

6.4.1 A Toy Model for $\nu_\mu - \nu_\tau$ Symmetry

We assume neutrino transition amplitudes do not change by swapping ν_μ and ν_τ. In this case, a possible neutrino state equation is,

$$\frac{d}{dt}\begin{pmatrix} C_e \\ C_\mu \\ C_\tau \end{pmatrix} = -\frac{i}{\gamma}\begin{pmatrix} \mu_e & \tau_{e\ell} & \tau_{e\ell} \\ \tau_{e\ell} & \mu_\ell & \tau_{\mu\tau} \\ \tau_{e\ell} & \tau_{\mu\tau} & \mu_\ell \end{pmatrix}\begin{pmatrix} C_e \\ C_\mu \\ C_\tau \end{pmatrix}, \tag{6.81}$$

where the imaginary phase is omitted to make discussions simple. This is justified by the fact that $s_{13} = 0$ is derived from the $\nu_\mu - \nu_\tau$ symmetry and the imaginary phase does not appear in the probabilities. In addition, $\tau_{e\ell} \geq 0$ and $\mu_\ell + \tau_{\mu\tau} > \mu_e$ are assumed to reduce the complexity from the unnecessary degrees of freedom. We obtain the following mixing matrix from Eq. (6.81).[2]

[2] It is difficult to derive Eqs. (6.82)–(6.86) by hand calculation (the author used Mathematica).

$$\begin{pmatrix} C_e \\ C_\mu \\ C_\tau \end{pmatrix} = \frac{1}{\sqrt{2}} \begin{pmatrix} \sqrt{2}\cos\phi & \sqrt{2}\sin\phi & 0 \\ -\sin\phi & \cos\phi & 1 \\ \sin\phi & -\cos\phi & 1 \end{pmatrix} \begin{pmatrix} C_1 \\ C_2 \\ C_3 \end{pmatrix}, \tag{6.82}$$

where

$$\tan 2\phi = \frac{2\sqrt{2}\tau_{e\ell}}{\mu_\ell - \mu_e + \tau_{\mu\tau}}. \tag{6.83}$$

Overall sign of the wave functions is chosen for ease to the later discussion. One of the elements of the mixing matrix turns out to be 0 and we assign it to the element U_{e3}.

On the other hand, the mixing matrix expressed by the standard parameters (4.106) with $\theta_{13} = 0$ is written as

$$\begin{pmatrix} C_e \\ C_\mu \\ C_\tau \end{pmatrix} = \begin{pmatrix} c_{12} & s_{12} & 0 \\ -s_{12}c_{23} & c_{12}c_{23} & s_{23} \\ s_{12}s_{23} & -c_{12}s_{23} & c_{23} \end{pmatrix} \begin{pmatrix} C_1 \\ C_2 \\ C_3 \end{pmatrix}. \tag{6.84}$$

From the comparison with (6.82), the mixing angles are determined as follows:

$$\theta_{13} = 0, \quad \theta_{23} = \frac{\pi}{4}, \quad \theta_{12} = \phi. \tag{6.85}$$

Therefore, the $\nu_\mu - \nu_\tau$ symmetry can explain both the small $\sin^2 2\theta_{13}$ and large $\sin^2 2\theta_{23}$ at once.

The observed relation $m_2 > m_1$ determines the correspondence between the flavor eigenstates and mass eigenstates. The masses are,

$$\begin{aligned} m_1 &= \frac{1}{2}\left(\mu_e + \mu_\ell + \tau_{\mu\tau} - \sqrt{8\tau_{e\ell}^2 + (\mu_\ell - \mu_e + \tau_{\mu\tau})^2}\right), \\ m_2 &= \frac{1}{2}\left(\mu_e + \mu_\ell + \tau_{\mu\tau} + \sqrt{8\tau_{e\ell}^2 + (\mu_\ell - \mu_e + \tau_{\mu\tau})^2}\right), \\ m_3 &= \mu_\ell - \tau_{\mu\tau}. \end{aligned} \tag{6.86}$$

Note that $m_1 + m_2 + m_3 = \mu_e + 2\mu_\ell$ and $m_2 > m_1$ are satisfied.

6.4.2 Tri-bimaximal Mixing

The measured $\sin^2\theta_{12}$ is close to 1/3 as shown in Table 6.1. Therefore, $\sin\theta_{12}$ can be approximated to be $\sin\theta_{12} = 1/\sqrt{3}$. $\sin\theta_{23} = 1/\sqrt{2}$ and $\sin\theta_{13} = 0$ are predicted from the assumption of the $\nu_\mu - \nu_\tau$ symmetry. In this case, the mixing matrix become

$$U_{\mathrm{TBM}} = \begin{pmatrix} \sqrt{2/3} & 1/\sqrt{3} & 0 \\ -1/\sqrt{6} & 1/\sqrt{3} & 1/\sqrt{2} \\ 1/\sqrt{6} & -1/\sqrt{3} & 1/\sqrt{2} \end{pmatrix} \sim \begin{pmatrix} 0.82 & 0.58 & 0 \\ -0.41 & 0.58 & 0.71 \\ 0.41 & -0.58 & 0.71 \end{pmatrix}. \tag{6.87}$$

This approximation roughly agrees with the measurement (6.64). This is called the *tri-bimaximal mixing* (TBM). In our toy model, the TBM mixing of θ_{12} can be related to the transition parameters as follows:

$$\tan 2\theta_{12} = 2\sqrt{2} = \tan 2\phi = \frac{2\sqrt{2}\tau_{e\ell}}{\mu_\ell - \mu_e + \tau_{\mu\tau}}, \tag{6.88}$$

which can be satisfied if there is following relation,

$$\mu_\ell + \tau_{\mu\tau} = \mu_e + \tau_{e\ell}. \tag{6.89}$$

In this case, the relation between the mass and transition amplitudes is, from Eq. (6.86),

$$\begin{pmatrix} m_1 \\ m_2 \\ m_3 \end{pmatrix} = \begin{pmatrix} 1 & 0 & -1 \\ 1 & 0 & 2 \\ -1 & 2 & -1 \end{pmatrix} \begin{pmatrix} \mu_e \\ \mu_\ell \\ \tau_{e\ell} \end{pmatrix}, \tag{6.90}$$

and the transition matrix is,

$$\mathscr{T} = \frac{m_1 + m_2 + m_3}{3} + \frac{1}{6} \begin{pmatrix} -2\Delta m_{31} & 2\Delta m_{21} & 2\Delta m_{21} \\ 2\Delta m_{21} & \Delta m_{31} & -\Delta m_{31} - \Delta m_{32} \\ 2\Delta m_{21} & -\Delta m_{31} - \Delta m_{32} & \Delta m_{31} \end{pmatrix}. \tag{6.91}$$

References

1. H. Nunokawa, S. Parke, R. Zukanovich Funchal, PRD **72**, 013009 (2005)
2. F. Capozzi, G.L. Fogli, E. Lisi, A. Marrone, D. Montanino, A. Palazzo, PRD **89**, 093018 (2014)

Chapter 7
Future Possibilities of Neutrino Oscillation Experiments

Abstract In this chapter, possibility for the future neutrino experiments are discussed. The remaining issues of neutrino oscillation studies are, to measure the CP violation parameter δ, to determine Δm^2_{31} mass hierarchy and the θ_{23} octant degeneracy. Approximated neutrino oscillation formulas with matter effects are introduced first and then possibilities of future experiments to address the remaining issues are discussed based on them. There are anomalies in various neutrino oscillation experiments which can be explained if there is fourth neutrino that is called sterile neutrino. The search for the sterile neutrino is another important subject in the future neutrino oscillation experiments and is discussed here. In order to determine the transition amplitudes, the absolute neutrino mass is necessary in addition to the neutrino oscillation parameters. The relation between the measured neutrino oscillation parameters and possible absolute mass measurements are discussed. Finally the neutrino-less double beta decay experiment, that can determine the absolute neutrino mass and whether the neutrino is Majorana particle or Dirac particle, is explained.

Keywords CP violation · Mass hierarchy · θ_{23} degeneracy · Sterile neutrino · Majorana particle · Double beta decay

7.1 Measurement of Remaining Oscillation Parameters

The remaining issues for the neutrino oscillation experiments are,

(1) Measurement of CP violation δ,
(2) Δm^2_{31} mass hierarchy determination,
(3) Solution for θ_{23} octant degeneracy,
(4) Solving sterile neutrino anomalies.

In addition to the oscillation measurements,

(5) Absolute neutrino mass measurement is necessary to determine the transition amplitudes.

All of these issues require high precision measurements to solve.

F. Suekane, *Neutrino Oscillations*, Lecture Notes in Physics 898,
DOI 10.1007/978-4-431-55462-2_7

7.1.1 Approximated Oscillation Formulas with Known Parameters

As we have seen, the leading components of the neutrino oscillation parameters have been measured. The future experiments are to measure the sub-leading terms and more precise oscillation formulas are necessary to evaluate the possibilities.

In the studies of neutrino oscillation, the experimental conditions are often arranged so as to detect the neutrinos near an oscillation maximum. Therefore, it is useful to approximate the oscillation probability formulas around the oscillation maximums by making use of the smallness of $|\Delta m^2_{21}/\Delta m^2_{31}|$ and s^2_{13}.

The ratio of the observed two squared mass differences is,

$$\varepsilon_m \equiv \frac{\Delta m^2_{21}}{\Delta m^2_{31}} = \frac{\Phi_{21}}{\Phi_{31}} \sim \pm 0.03. \tag{7.1}$$

Since it is known that $\Delta m^2_{21} > 0$, the "+" sign corresponds to the normal Δm^2_{31} mass hierarchy ($m_3 > m_1$) and the "−" sign corresponds to the inverted hierarchy ($m_3 < m_1$). Note that always $\varepsilon_m \Phi_{31} = \Phi_{21} > 0$.

The size of the small mixing angle θ_{13} is

$$s^2_{13} \sim 0.026. \tag{7.2}$$

Therefore, ε_m and s^2_{13} have the similar smallness and it is appropriate to approximate the oscillation formulas by powers of them. The following approximations can be used up to the relative order $O(s^2_{13})$,

$$c_{13} \sim c^2_{13} \sim 1, \quad \sin 2\theta_{13} \sim 2s_{13}. \tag{7.3}$$

For three flavor neutrino oscillations, there are three oscillation maximums, corresponding to $\Phi_{21} = \pi/2$, $|\Phi_{31}| = \pi/2$ and $|\Phi_{32}| = \pi/2$. However, we have identified only two oscillation maximums by the experiments which can be explained by the fact that the $\Delta\hat{m}^2_{32}$ and $\Delta\hat{m}^2_{31}$ maximums differs only 3 % or less.

For neutrino oscillations at $\Phi_{31} \sim \pi/2$, Φ_{21} is small and the following approximations can be made.

$$\begin{aligned} \sin 2\Phi_{21} &= \sin 2\varepsilon_m \Phi_{31} = 2\varepsilon_m \Phi_{31} + O(\varepsilon_m^3), \\ \sin^2 \Phi_{21} &= \sin^2 \varepsilon_m \Phi_{31} = 0 + O(\varepsilon_m^2). \end{aligned} \tag{7.4}$$

Using the relation

$$\Phi_{32} = \Phi_{31} - \Phi_{21} = (1 - \varepsilon_m)\Phi_{31}, \tag{7.5}$$

$\sin 2\Phi_{32}$ and $\sin^2 \Phi_{32}$ can be approximately related to Φ_{31} as follows:

$$\begin{aligned}\sin 2\Phi_{32} &= \sin 2\Phi_{31} - 2\varepsilon_m \Phi_{31} \cos 2\Phi_{31} + O(\varepsilon_m^2),\\ \sin^2 \Phi_{32} &= \sin^2 \Phi_{31} - \varepsilon_m \Phi_{31} \sin 2\Phi_{31} + O(\varepsilon_m^2).\end{aligned} \tag{7.6}$$

Calculations for the approximation of the oscillation probabilities are described in Sect. 8.5.

The oscillation probability $@\Phi_{31}$ is given by Eq. (8.111),

$$\begin{aligned}P_{\nu_\alpha \to \nu_\beta}(@\Phi_{31}) = \delta_{\alpha\beta} &- 4|U_{\alpha 3}|^2(\delta_{\alpha\beta} - |U_{\beta 3}|^2) \sin^2 \Phi_{31}\\ &+ 8\varepsilon_m \Phi_{31} \sin \Phi_{31} \Re[\Lambda_{32}^{\alpha\beta} e^{i\Phi_{31}}] + O(\varepsilon_m^2).\end{aligned} \tag{7.7}$$

The reactor $\overline{\nu}_e$ neutrino experiments $@\Phi_{31}$ measure the oscillation probability,

$$\begin{aligned}P_{\overline{\nu}_e \to \overline{\nu}_e}(@\Phi_{31}) &= 1 - \sin^2 2\theta_{13} \sin^2 \Phi_{31} + O(\varepsilon_m^2)\\ &\sim 1 - 0.1 \sin^2 \Phi_{31} + O(10^{-3}).\end{aligned} \tag{7.8}$$

The atmospheric and accelerator neutrino experiments which observe the ν_μ disappearance measure the oscillation probability,

$$\begin{aligned}P_{\nu_\mu \to \nu_\mu}(@\Phi_{31}) &= 1 - (\sin^2 2\theta_{23} - s_{23}^2 \sin^2 2\theta_{13} \cos 2\theta_{23}) \sin^2 \Phi_{31}\\ &\quad + \varepsilon_m \Phi_{31} \sin 2\Phi_{31} (c_{12}^2 \sin^2 2\theta_{23} - s_{23}^2 J_{123} \cos \delta) + O(\varepsilon_m^2)\\ &\sim 1 - \sin^2 \Phi_{31} + 0.021\Phi_{31} \sin 2\Phi_{31} + O(10^{-3}),\end{aligned} \tag{7.9}$$

where a parameter,

$$J_{123} \equiv \sin 2\theta_{12} \sin 2\theta_{23} \sin 2\theta_{13} \sim 0.29 \tag{7.10}$$

is used.

For $\nu_\mu \to \nu_e$ and $\nu_\mu \to \nu_\tau$ appearance measurements, the probabilities are given by,

$$\begin{aligned}P_{\nu_\mu \to \nu_e}(@\Phi_{31}) &= s_{23}^2 \sin^2 2\theta_{13} \sin^2 \Phi_{31} + \varepsilon_m \Phi_{31} \sin \Phi_{31} J_{123} \cos(\Phi_{31} + \delta) + O(\varepsilon_m^2)\\ &\sim 0.05(\sin^2 \Phi_{31} + 0.18\Phi_{31} \sin \Phi_{31} \cos(\Phi_{31} + \delta)) + O(10^{-3}),\end{aligned} \tag{7.11}$$

and

$$\begin{aligned}P_{\nu_\mu \to \nu_\tau}(@\Phi_{31}) &= \cos 2\theta_{13} \sin^2 2\theta_{23} \sin^2 \Phi_{31}\\ &\quad - \varepsilon_m \Phi_{31} \sin \Phi_{31} \begin{pmatrix} 2c_{12}^2 \sin^2 2\theta_{23} \cos \Phi_{31} \\ - J_{123}(\sin \Phi_{31} \sin \delta - \cos 2\theta_{23} \cos \Phi_{31} \cos \delta) \end{pmatrix} + O(\varepsilon_m^2)\\ &\sim (0.949 - 0.01\Phi_{31} \sin \delta) \sin^2 \Phi_{31} - 0.021\Phi_{31} \sin 2\Phi_{31} + O(10^{-3}).\end{aligned} \tag{7.12}$$

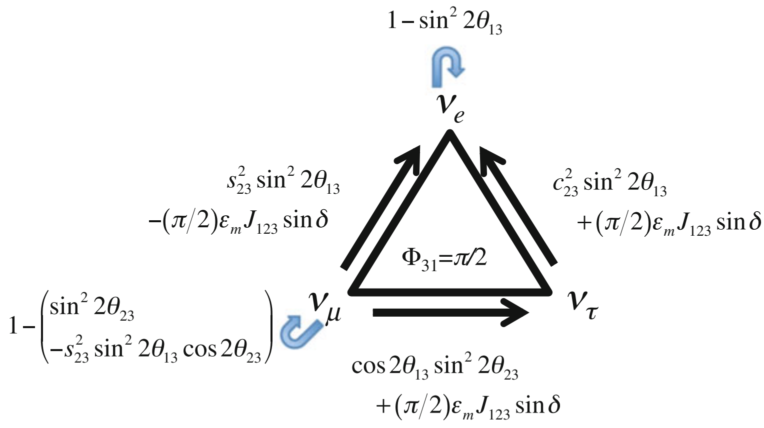

Fig. 7.1 Oscillation probabilities @Φ_{31}

Those oscillation probabilities at the Φ_{31} oscillation maximum are graphically summarized in Fig. 7.1. The oscillation probabilities for anti-neutrinos and for the oscillation of the reverse direction can be obtained by changing the sign of δ, such as $\delta \to -\delta$. For example, both $P_{\bar{\nu}_\mu \to \bar{\nu}_e}$ and $P_{\nu_e \to \nu_\mu}$ can be expressed from the same equation,

$$P_{\bar{\nu}_\mu \to \bar{\nu}_e} = P_{\nu_e \to \nu_\mu} = P^*_{\nu_\mu \to \nu_e}, \tag{7.13}$$

where P^*_X is the probability obtained by changing the sign of δ in the formula of P_X. The disappearance probability can be calculated by summing the two appearance probabilities from the same source. For example,

$$1 - P_{\nu_e \to \nu_e} = P_{\nu_e \to \nu_\mu} + P_{\nu_e \to \nu_\tau}. \tag{7.14}$$

Note that the appearance probabilities depend on $\sin\delta$. However, if the two appearance probabilities from the same source are summed to obtain the disappearance probability, the $\sin\delta$ terms completely cancel out. This means that CP violation has to be searched for by using the appearance experiments.

For oscillations @Φ_{21}, only ν_e and $\bar{\nu}_e$ disappearances have been measured. Near the L/E relation @Φ_{21}, the oscillation phases of Φ_{31} and Φ_{32} are,

$$\Phi_{31} \sim \Phi_{32} = \frac{\Phi_{21}}{\varepsilon_m} \sim O(30). \tag{7.15}$$

This means the oscillation phase changes by 100 % for 3 % of the energy difference. If the energy uncertainty of the experiment is larger than 3 %, the oscillation patterns due to Φ_{31} and Φ_{32} oscillations are washed out and only averaged effect is observed. The averaging of the Φ_{31} oscillation can be approximated as,

$$\begin{aligned} \sin^2\Phi_{31} \sim \sin^2\Phi_{32} &= \sin^2(\Phi_{21}/\varepsilon_m) \to \tfrac{1}{2}, \\ \sin 2\Phi_{31} \sim \sin 2\Phi_{32} &= \sin 2(\Phi_{21}/\varepsilon_m) \to 0. \end{aligned} \tag{7.16}$$

In this case, the general oscillation probability formula is, from Eq. (8.119), given by

$$P_{\nu_\alpha\to\nu_\beta}(@\Phi_{21}) = \delta_{\alpha\beta}(1-2|U_{\alpha 3}|^2) + 2|U_{\alpha 3}|^2|U_{\beta 3}|^2 - 4\sin\Phi_{21}\Im\left[\Lambda_{21}^{\alpha\beta}e^{i\Phi_{21}}\right]. \tag{7.17}$$

For the survival probability of electron type neutrino is,

$$\begin{aligned} P_{\nu_e\to\nu_e}(@\Phi_{21}) = P_{\overline{\nu}_e\to\overline{\nu}_e}(@\Phi_{21}) &= \cos 2\theta_{13}(1-\sin^2 2\theta_{12}\sin^2\Phi_{21}) + O(s_{13}^4) \\ &\sim 0.95(1-0.85\sin^2\Phi_{21}) + O(10^{-3}). \end{aligned} \tag{7.18}$$

This means that the solar and reactor experiments $@\Phi_{21}$ have a slight dependence on θ_{13} through $\cos 2\theta_{13}$. This disappearance probability is the sum of the following two appearance probabilities,

$$\begin{aligned} P_{\nu_e\to\nu_\mu}(@\Phi_{21}) = \tfrac{1}{2}s_{23}^2\sin^2 2\theta_{13} + c_{13}^2\sin 2\theta_{12}\sin\Phi_{21}\times \\ \begin{pmatrix} ((c_{23}^2 - s_{23}^2 s_{13}^2)\sin 2\theta_{12} + s_{13}\sin 2\theta_{23}\cos 2\theta_{12}c_\delta)\sin\Phi_{21} \\ -\, s_{13}\sin 2\theta_{23}s_\delta\cos\Phi_{21} \end{pmatrix} \end{aligned} \tag{7.19}$$

and

$$\begin{aligned} P_{\nu_e\to\nu_\tau}(@\Phi_{21}) = \tfrac{1}{2}c_{23}^2\sin^2 2\theta_{13} + c_{13}^2\sin 2\theta_{12}\sin\Phi_{21}\times \\ \begin{pmatrix} ((s_{23}^2 - c_{23}^2 s_{13}^2)\sin 2\theta_{12} - s_{13}\sin 2\theta_{23}\cos 2\theta_{12}c_\delta)\sin\Phi_{21} \\ +\, s_{13}\sin 2\theta_{23}s_\delta\cos\Phi_{21} \end{pmatrix}. \end{aligned} \tag{7.20}$$

Note that if probabilities (7.19) and (7.20) are summed, several terms are canceled out and $\sin^2\theta_{23}$ and $\cos^2\theta_{23}$ terms are added to unity. As a result, δ terms vanish and the disappearance probability becomes very simple as shown in (7.18). Figure 7.2 summarizes the oscillation formulas at $@\Phi_{21}$.

7.1.2 CP Violation δ

It is important to measure the CP violation in lepton interactions to study the origin of the flavor mixing and to understand its effect to our world. At the beginning of our universe, matter and antimatter are supposed to be produced the same amount. However, the current universe consists mainly of the matter. This means a CP violating process should have taken place in the history of the universe. A CP violation effect is introduced in the standard neutrino oscillation formula as an imaginary component

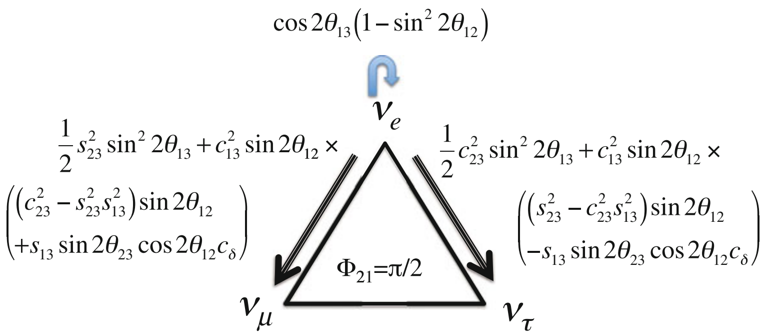

Fig. 7.2 Oscillation probabilities at $\Phi_{21} = \pi/2$. Oscillation between ν_μ and ν_τ @ Φ_{21} has not been observed yet

of the fermion mixing matrix. The probability of the CP violation is proportional to the Jarlskog invariant [1] defined by

$$J_r = s_{12}c_{12}s_{23}c_{23}s_{13}c_{13}^2 \sin\delta. \tag{7.21}$$

This means the CP violation effect depends on all the mixing matrix parameters.

CP violation has already been measured in quark interactions. However, for the quark case, all the mixing angles are small and the Jarlskog invariant is only $J_q \sim 3\times 10^{-5}$. It is thought that the CP violation observed in the quark interactions is too small to explain the current matter dominance of the universe. For lepton case, θ_{12} and θ_{23} are large and recently θ_{13} turned out to be finite and the Jarlskog invariant for neutrino mixing is $J_\nu \sim 4\times 10^{-2}\sin\delta_\nu$, which can be 1,000 times larger than J_q and the J_ν may be able to explain the current matter dominant universe.

The neutrino CP violation effect can be measured from the asymmetry between $P_{\nu_\mu\to\nu_e}$ and $P_{\overline{\nu}_\mu\to\overline{\nu}_e}$ at around the oscillation maximum of $\Phi_{31} = 0(1)$,

$$\begin{aligned} A_{\text{CP}} &= \frac{P_{\nu_\mu\to\nu_e}(@\Phi_{31}) - P_{\overline{\nu}_\mu\to\overline{\nu}_e}(@\Phi_{31})}{P_{\nu_\mu\to\nu_e}(@\Phi_{31}) + P_{\overline{\nu}_\mu\to\overline{\nu}_e}(@\Phi_{31})} \\ &\sim \frac{-\varepsilon_m\Phi_{31}\sin\Phi_{31}J_{123}\sin\delta}{s_{23}^2\sin^2 2\theta_{13}\sin\Phi_{31} + \varepsilon_m\Phi_{31}\cos\Phi_{31}J_{123}\cos\delta}. \end{aligned} \tag{7.22}$$

The CP asymmetry at the oscillation maximum $\Phi_{31} = \pi/2$ is calculated to be,

$$A_{\text{CP}} \sim -\frac{\pi\sin 2\theta_{12}}{\tan\theta_{23}\sin 2\theta_{13}}\varepsilon_m\sin\delta \sim -0.27\sin\delta. \tag{7.23}$$

At first sight, it seems that smaller θ_{13} is better to detect the CP violation because the A_{CP} is proportional to $1/\sin 2\theta_{13}$ in Eq. (7.23) and becomes larger. However, in actual experiments, the number of $\nu_\mu \to \nu_e$ and $\overline{\nu}_\mu \to \overline{\nu}_e$ events are proportional to $\sin^2 2\theta_{13}$ and the statistic uncertainty, ($\sigma_{\text{stat.}}$), is also proportional to $1/\sin 2\theta_{13}$.

Table 7.1 Long baseline accelerator experiments [2]

Project	Baseline (km)	Accelerator→Detector	Status (2014)
K2K	250	KEK→Kamioka	Completed
T2K	295	JPARC→Kamioka	On going
Hyper Kamiokande	295	JPARC→Kamioka	Proposed
OPERA	730	CERN→Gran Sasso	On going
ICARUS	730	CERN→Gran Sasso	On going
MINOS	735	Fermi→Soudan	Completed
NOVA	810	Fermi→Ash River	Under construction
LBNE	1,300	Fermi→Sanford Lab	Proposed
LENA	2,290	CERN→Finland	Proposed
GLACIER	–	–	Proposed

Therefore, the significance of detecting CP asymmetry, $A_{\mathrm{CP}}/\sigma_{\mathrm{stat.}}$, is rather insensitive to the θ_{13} value when the statistic error dominates. A number of long baseline accelerator experiments are proposed as listed in Table 7.1.

There is a difficulty to measure the CP violation using this asymmetry. In order to measure the oscillation probabilities, ν_μ or $\overline{\nu}_\mu$ beam with energy of order of GeV are sent to a detector at several hundred kilometers away. Since the earth is spherical, the neutrino beam goes through the underground of the earth. From Eq. (4.142), the matter effect of the earth on the oscillation can be significantly large. The matter effect comes from the weak potential and its sign is opposite for the neutrinos and the antineutrinos. This indicates that the neutrino oscillation probability in matter is different for neutrinos and antineutrinos and a spurious CP asymmetry is generated. The effect of this spurious CP asymmetry is discussed in the next subsection.

7.1.3 Earth Matter Effect for High Energy Neutrinos

In order to evaluate the earth matter effect, it is necessary to solve the three-flavor state equation (6.29). However in general, the derivation is very complicated. We will simplify the discussion by using the following approximations. We can not ignore the θ_{13} terms this time because the leading term of the $\nu_\mu \to \nu_e$ probability (7.11) starts with $\sin^2 2\theta_{13}$. At a baseline of $\sin^2 \Phi_{13} \sim O(1)$, $\sin^2 \Phi_{12} \sim 0$ and we can regard effectively $m_2 \sim m_1$ in the calculation. Therefore, the mass matrix can be approximated as

$$M = \begin{pmatrix} m_1 & 0 & 0 \\ 0 & m_1 & 0 \\ 0 & 0 & m_3 \end{pmatrix}. \tag{7.24}$$

The transition matrix in this case is,

$$\mathscr{T} = U_\nu M U_\nu^\dagger = m_1 + \Delta m_{31} \begin{pmatrix} s_{13}^2 & s_{13}c_{13}s_{23}e^{-i\delta} & s_{13}c_{13}c_{23}e^{-i\delta} \\ s_{13}c_{13}s_{23}e^{i\delta} & c_{13}^2 s_{23}^2 & c_{13}^2 s_{23}c_{23} \\ s_{13}c_{13}c_{23}e^{i\delta} & c_{13}^2 s_{23}c_{23} & c_{13}^2 c_{23}^2 \end{pmatrix}, \tag{7.25}$$

where $\Delta m_{31} = m_3 - m_1$. Note that θ_{12} has disappeared and the state equation can be written simply as

$$\frac{d}{dt}\begin{pmatrix} C_e \\ C_\zeta \\ C_\xi \end{pmatrix} = -\frac{i}{\gamma}\left[m_1 + \Delta m_{31} \begin{pmatrix} s_{13}^2 & s_{13}c_{13}e^{-i\delta} & 0 \\ s_{13}c_{13}e^{i\delta} & c_{13}^2 & 0 \\ 0 & 0 & 0 \end{pmatrix}\right] \begin{pmatrix} C_e \\ C_\zeta \\ C_\xi \end{pmatrix}, \tag{7.26}$$

where

$$\begin{pmatrix} C_\xi \\ C_\zeta \end{pmatrix} = \begin{pmatrix} c_{23} & -s_{23} \\ s_{23} & c_{23} \end{pmatrix} \begin{pmatrix} C_\mu \\ C_\tau \end{pmatrix}. \tag{7.27}$$

C_ξ is decoupled from C_e and the state equation between C_e and C_ζ is

$$\frac{d}{dt}\begin{pmatrix} C_e \\ C_\zeta \end{pmatrix} = -\frac{i}{\gamma}\left[\overline{m}_{31} + \frac{\Delta m_{31}}{2} \begin{pmatrix} -\cos 2\theta_{13} & \sin 2\theta_{13}e^{-i\delta} \\ \sin 2\theta_{13}e^{i\delta} & \cos 2\theta_{13} \end{pmatrix}\right] \begin{pmatrix} C_e \\ C_\zeta \end{pmatrix}, \tag{7.28}$$

where $\overline{m}_{31} = (m_1 + m_3)/2$. The matter effect is obtained by adding the weak potentials to the transition matrix,

$$\frac{d}{dt}\begin{pmatrix} C_e \\ C_\zeta \end{pmatrix} = -i\left[m_0 + \frac{\Delta m_{31}^2}{4E} \begin{pmatrix} -\cos 2\theta_{13} + \upsilon_\oplus & \sin 2\theta_{13}e^{-i\delta} \\ \sin 2\theta_{13}e^{i\delta} & \cos 2\theta_{13} - \upsilon_\oplus \end{pmatrix}\right] \begin{pmatrix} C_e \\ C_\zeta \end{pmatrix}, \tag{7.29}$$

where $m_0 = \overline{m}_{31}^2/E + V_Z + V_W/2$ and $\upsilon_\oplus$ is the potential parameter of the earth. Equation (7.29) has a similar form as Eq. (4.129). The probability of the oscillation $\nu_e \to \nu_\zeta$ in matter can be obtained by substituting $(\theta_\nu,\ \omega_0,\ \upsilon_W)$ in Eqs. (4.136), (4.132) by $(\theta_{13},\ \Delta m_{31}^2/4E,\ \upsilon_\oplus)$, respectively,

$$P_{\nu_e \to \nu_\zeta}(@\Phi_{31}) = \frac{\sin^2 2\theta_{13}}{\kappa_\oplus^2} \sin^2 \kappa_\oplus \Phi_{31}, \tag{7.30}$$

where

$$\kappa_\oplus = \sqrt{(\cos 2\theta_{13} - \upsilon_\oplus)^2 + \sin^2 2\theta_{13}} \sim 1 - \upsilon_\oplus. \tag{7.31}$$

On the other hand,

$$P_{\nu_e \to \nu_\xi}(@\Phi_{31}) = 0, \tag{7.32}$$

and therefore, the survival probability of ν_e is

$$P_{\nu_e \to \nu_e}(@\Phi_{31}) = 1 - \frac{\sin^2 2\theta_{13}}{\kappa_\oplus^2} \sin^2 \kappa_\oplus \Phi_{31}, \tag{7.33}$$

Since the ν_μ component of ν_ζ is s_{23}, the $\nu_e \to \nu_\mu$ oscillation probability is,

$$P_{\nu_e \to \nu_\mu}(@\Phi_{31}) = s_{23}^2 \frac{\sin^2 2\theta_{13}}{\kappa_\oplus^2} \sin^2 \kappa_\oplus \Phi_{31}. \tag{7.34}$$

Similarly,

$$P_{\nu_e \to \nu_\tau}(@\Phi_{31}) = \frac{c_{23}^2 \sin^2 2\theta_{13}}{\kappa_\oplus^2} \sin^2 \kappa_\oplus \Phi_{31}. \tag{7.35}$$

From the CPT invariance,

$$P_{\nu_\mu \to \nu_e} = P^*_{\nu_e \to \nu_\mu} = \frac{s_{23}^2 \sin^2 2\theta_{13}}{\kappa_\oplus^2} \sin^2 \kappa_\oplus \Phi_{31}. \tag{7.36}$$

As for the calculations of the matter effect for higher order terms, we borrow the results from Refs. [3, 4],

$$\begin{aligned} P_{\nu_\mu \to \nu_e}(@\Phi_{31}) \sim & s_{23}^2 \sin^2 2\theta_{13} \frac{\sin^2(\kappa_\oplus \Phi_{31})}{\kappa_\oplus^2} \\ & + \varepsilon_m J_{123} \frac{\sin(\kappa_\oplus \Phi_{31})}{\kappa_\oplus} \frac{\sin(\upsilon_\oplus \Phi_{31})}{\upsilon_\oplus} \cos(\Phi_{31} + \delta). \end{aligned} \tag{7.37}$$

The signs of $\upsilon_\oplus$, Φ_{31} and ε_m depend on the mass hierarchy and the signs of $\upsilon_\oplus$ and δ change for antineutrinos as shown in Table 7.2. We can write the signs of those parameters explicitly as follows:

$$\upsilon_\oplus \to \eta_C \eta_M^{31} |\upsilon_\oplus|, \;\; \Phi_{31} \to \eta_M^{31} |\Phi_{31}|, \;\; \varepsilon_m \to \eta_M^{31} |\varepsilon_m| \;\text{ and }\; \delta \to \eta_C \delta, \tag{7.38}$$

where $\eta_M^{31} = \pm 1$ for normal and inverted hierarchy and $\eta_C = \pm 1$ for neutrino and antineutrino oscillations, respectively.

Using the sign parameters, a oscillation formula which includes the antineutrino and inverted mass hierarchy is written as,

Table 7.2 Sign of the parameters for ν, $\bar{\nu}$ and Δm^2_{31} mass hierarchy

	$\lvert\upsilon_\oplus\rvert$	$\lvert\Phi_{31}\rvert$	$\lvert\varepsilon_m\rvert$	δ	η_C	η^{31}_{M}
ν, NH	$+$	$+$	$+$	$+$	$+$	$+$
ν, IH	$-$	$-$	$-$	$+$	$+$	$-$
$\bar{\nu}$, NH	$-$	$+$	$+$	$-$	$-$	$+$
$\bar{\nu}$, IH	$+$	$-$	$-$	$-$	$-$	$-$

$$
\begin{aligned}
P_{\nu_\mu\to\nu_e}(@\Phi_{31}) &\sim s^2_{23}\sin^2 2\theta_{13}\frac{\sin^2\left((1-\eta^{31}_{\mathrm{M}}\eta_{\mathrm{C}}|\upsilon_\oplus|)|\Phi_{31}|\right)}{(1-\eta^{31}_{\mathrm{M}}\eta_{\mathrm{C}}|\upsilon_\oplus|)^2} \\
&+\eta^{31}_{\mathrm{M}}|\varepsilon_m|J_{123}\frac{\sin\left((1-\eta^{31}_{\mathrm{M}}\eta_{\mathrm{C}}|\upsilon_\oplus|)|\Phi_{31}|\right)}{(1-\eta^{31}_{\mathrm{M}}\eta_{\mathrm{C}}|\upsilon_\oplus|)}\frac{\sin(|\upsilon_\oplus||\Phi_{31}|)}{|\upsilon_\oplus|} \\
&\times\cos(\eta^{31}_{\mathrm{M}}|\Phi_{31}|+\eta_{\mathrm{C}}\delta).
\end{aligned}
\tag{7.39}
$$

It is useful to express $\upsilon_\oplus$ as a function of the baseline L and the oscillation phase Φ to evaluate the matter effects of various experiments. From (4.130),

$$
\upsilon=\frac{2\sqrt{2}E_\nu G_F n_e}{\Delta m^2}=\frac{G_F n_e}{\sqrt{2}\Phi}L=\frac{1}{\Phi}\frac{L}{L_M},
\tag{7.40}
$$

where $L_M\equiv\sqrt{2}/G_F n_e$ is a typical length of the matter effect. For the earth matter effect, it is

$$
L_M\to L_\oplus\sim 1.4\times10^{-12}\,\mathrm{cm^3MeV^2}\sim 3{,}500\,\mathrm{km}\quad\text{from}\quad\rho_\oplus=3\,\mathrm{g/cm^3}.
\tag{7.41}
$$

Usually oscillation experiments are performed at $\Phi\sim\pi/2$ where $|\upsilon_\oplus|=L/5{,}800\,\mathrm{km}$. For T2K or HyperKamiokande experiments, $L\sim300\,\mathrm{km}$ and $|\upsilon_\oplus|\sim0.05$ and for NOVA experiment, $L\sim800\,\mathrm{km}$ and $|\upsilon_\oplus|\sim0.15$ and the oscillation probability at the oscillation maximum can be further approximated from Eq. (7.39) as

$$
P_{\nu_\mu\to\nu_e}(@\Phi_{31}=\pi/2)\sim\frac{s^2_{23}\sin^2 2\theta_{13}}{(1-\eta^{31}_{\mathrm{M}}\eta_{\mathrm{C}}|\upsilon_\oplus|)^2}-\eta_{\mathrm{C}}\frac{\pi}{2}\frac{|\varepsilon_m|J_{123}\sin\delta}{(1-\eta^{31}_{\mathrm{M}}\eta_{\mathrm{C}}|\upsilon_\oplus|)}+O(\upsilon^2_\oplus).
\tag{7.42}
$$

Figure 7.3 shows the baseline dependence of the $\nu_\mu\to\nu_e$ appearance probability assuming $\sin\delta=-1$ and $\sin^2 2\theta_{23}>0.97$. By combining two oscillation measurements at different baselines, the intercept to the $L=0$ axis in Fig. 7.3, where there is no matter effect, can be determined. The oscillation probability at the intercept is

$$
P_{\nu_\mu\to\mu_e}(@|\Phi_{31}|=\pi/2,L=0)=s^2_{23}\sin^2 2\theta_{13}-\eta_{\mathrm{C}}\frac{\pi}{2}|\varepsilon_m|J_{123}\sin\delta.
\tag{7.43}
$$

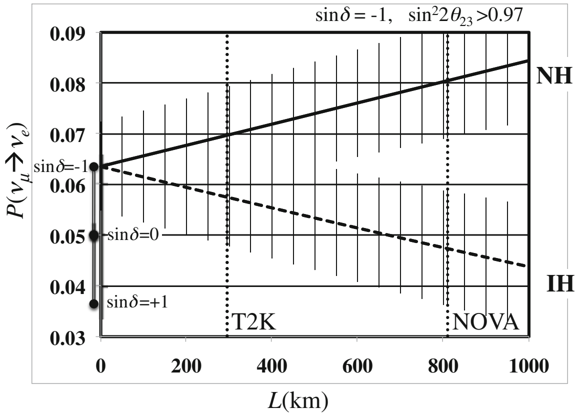

Fig. 7.3 Baseline dependence of $\nu_\mu \to \nu_e$ appearance probability at the Φ_{31} oscillation maximum. The *horizontal axis* is the baseline. The *vertical axis* is $P_{\nu_\mu \to \nu_e}$. The *thin vertical lines* show the ambiguity from the θ_{23} octet degeneracy. The positions of the intercept at $L = 0$ for $\sin\delta = 0, \pm 1$ are shown. The baselines of the T2K and NOVA are shown

Since θ_{23}, θ_{13}, J_{123} and ε_m can be measured elsewhere, it may be possible to determine $\sin\delta$ from the measurement.[1]

Currently T2K is in operation and NOVA is about to start. It is expected that the probability (7.43) will be measured in the near future.

7.1.4 θ_{23} *Octant Degeneracy*

The largest uncertainty in Eq. 7.43, except for $\sin\delta$ comes from θ_{23}. θ_{23} has been measured from the ν_μ disappearance near Δm^2_{31} maximum to be $\sin^2 2\theta_{23} \sim 1$. However, there are two possible values of s^2_{23} for a given $\sin^2 2\theta_{23}$ as follows,

$$s^2_{23} = \frac{1 \pm \sqrt{1 - \sin^2 2\theta_{23}}}{2}. \tag{7.44}$$

Since the difference between the two solutions is $\sqrt{1 - \sin^2 2\theta_{23}}$, it can be large even if $(1 - \sin^2 2\theta_{23})$ is small. For example, if $\sin^2 2\theta_{23}$ is measured to be $\sin^2 2\theta_{23} > 0.97$, the range of the possible s^2_{23} is $0.41 < s^2_{23} < 0.59$, which corresponds to as much as $\pm 20\,\%$ of uncertainty. This is called the octant θ_{23} degeneracy problem. As can be seen in Fig. 7.3, the non-0 $\sin\delta$ can not be confirmed better than 2σ significance even if $|\sin\delta| = 1$ due to this uncertainty for $\sin^2 2\theta_{23} > 0.97$. In order to solve this problem, it is necessary to show $\sin^2 2\theta_{23}$ is very close to unity or determine which solution is correct by combining other oscillation measurements.

[1] Strictly speaking, this is not a measurement of the CP *asymmetry*. The measured $\sin\delta$ can be associated with the CP asymmetry effect when the standard three flavor neutrino scheme is correct.

7.1.5 CP Asymmetry and the Matter Effect

As shown in Sect. 7.1.2, the CP violation phase δ can be measured from the difference of the probabilities of the $\nu_\mu \to \nu_e$ and $\overline{\nu}_\mu \to \overline{\nu}_e$ oscillations. The CP asymmetry to be observed under existence of the earth matter effect is given by,

$$A_{\mathrm{CP}}(\Phi_{31} = \pi/2) = \frac{P_{\nu_\mu \to \mu_e} - P_{\overline{\nu}_\mu \to \overline{\nu}_e}}{P_{\nu_\mu \to \mu_e} + P_{\overline{\nu}_\mu \to \overline{\nu}_e}} \sim -\frac{\pi|\varepsilon_m| \sin 2\theta_{12}}{\tan\theta_{23} \sin 2\theta_{13}} \sin\delta + 2\eta_{\mathrm{M}}^{31} |\upsilon_\oplus|$$
$$\sim -0.27 \sin\delta \pm \frac{L}{2{,}800\ (\mathrm{km})}. \tag{7.45}$$

This relation shows that the matter effect (the second term) gives an spurious asymmetry as large as the true CP violation asymmetry (the first term) if the baseline is several hundreds kilometers or more. Figure 7.4 shows the baseline dependence of A_{CP} with matter effect. To measure the $\sin\delta$, it is necessary to remove the effect of the spurious asymmetry caused by the matter effect unless the baseline is very short. By combining two measurements at different baselines, it is possible to know the mass hierarchy and to obtain the genuine CP asymmetry. A difficulty of the measurement is that the probability of $\nu_\mu \to \nu_e$ oscillation is only $\sim$5 % and the CP asymmetry is a fraction of it. Moreover, the $\overline{\nu}_e$-nucleus reaction cross sections are 1/3 of the ν_e+ nucleus cross sections and three time more $\overline{\nu}_\mu$ flux is necessary to obtain equivalent

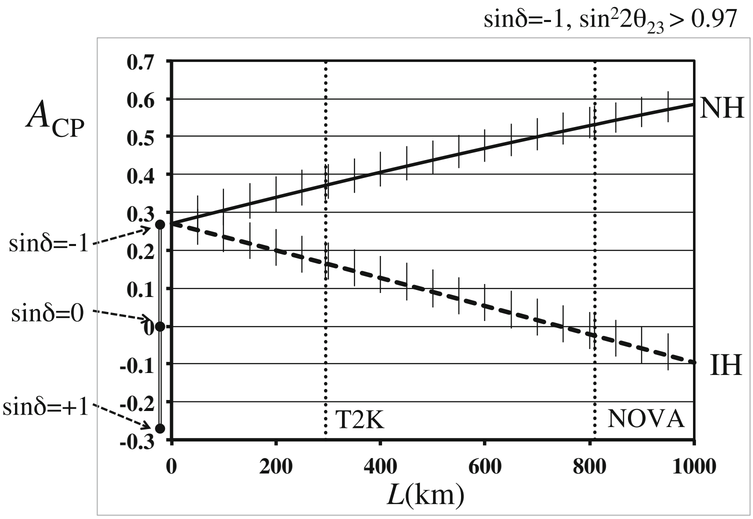

Fig. 7.4 Baseline dependence of A_{CP}. The *horizontal axis* is the baseline. The *vertical axis* is the asymmetry, A_{CP}. The *thin vertical lines* show the ambiguity from the θ_{23} octant degeneracy. The positions of the intercept at $L = 0$ for $\sin\delta = 0, \pm 1$ are shown. The baselines of the T2K and NOVA are shown

statistic uncertainties to the ν_e detection. Therefore, a very high neutrino flux and large detector mass are necessary to measure the CP violation.

7.1.6 Determination of the Δm^2_{31} Mass Hierarchy

Determining the Δm^2_{31} mass hierarchy is an important next experimental target, not only for the CP asymmetry measurement but because it is related to the lower limit of the absolute neutrino masses. As we will see in Sect. 7.3, if the Δm^2_{31} mass hierarchy is IH, the ν_e mass can be predicted to be 50 meV or more. Also there is the minimum double beta decay mass of ∼15 meV which will become a next good target sensitivity for neutrino-less double beta decay experiments. Either neutrino is Majorana or Dirac particle can be definitely determined with this sensitivity.

The matter effect changes the sign of the weak potential depending on the mass hierarchy and if the sign of the matter effect can be measured, the mass hierarchy can be determined. The Δm^2_{21} mass hierarchy η^{21}_{M} was measured by matter effect of the solar neutrino oscillation. Similarly η^{31}_{M} can in principle be measured by the matter effect for Φ_{31} oscillations. One possibility is the already-described baseline dependence of $P_{\nu_\mu \to \mu_e}$ or A_{CP}, shown in Figs. 7.3 and 7.4. Although there is ambiguity due to θ_{23} degeneracy, it is independent of the baseline. Therefore, the slopes of the baseline dependence of these parameters are not sensitive to the θ_{23} ambiguity.

7.1.6.1 Direct $\Delta\hat{m}^2$ Comparison

In principle, the Δm^2_{31} mass hierarchy can be determined by comparing $|\Delta m^2_{31}|$ and $|\Delta m^2_{32}|$. Since $\Delta m^2_{12} + \Delta m^2_{23} + \Delta m^2_{31} = 0$ and $\Delta m^2_{21} > 0$, $|\Delta m^2_{31}| > |\Delta m^2_{32}|$ means the normal hierarchy and $|\Delta m^2_{31}| < |\Delta m^2_{32}|$ means the inverted hierarchy.

One straightforward way is to compare the effective mass squared differences, $\Delta\hat{m}^2_{31}$ and $\Delta\hat{m}^2_{32}$ which are shown in Eqs. (6.23) and (6.25).

The difference between $\Delta\hat{m}^2_{31}$ and $\Delta\hat{m}^2_{32}$ is expressed from (6.26) as,

$$\begin{aligned}\frac{2(\Delta\hat{m}^2_{31} - \Delta\hat{m}^2_{32})}{\Delta\hat{m}^2_{31} + \Delta\hat{m}^2_{32}} &\sim \pm\,(1 - s_{12}t_{23}\tan 2\theta_{12}\cos\delta)\frac{2\cos 2\theta_{12}|\Delta m^2_{21}|}{|\Delta m^2_{31}| + |\Delta m^2_{32}|} \\ &\sim \pm\,0.012 \times (1 \pm 0.3),\end{aligned} \tag{7.46}$$

where the overall sign depends on mass hierarchy and the ambiguity of ±0.3 comes from the unknown δ. If $\Delta\hat{m}^2_{31} > \Delta\hat{m}^2_{32}$, it is normal hierarchy and vice versa. In order to determine the mass hierarchy, it is necessary to distinguish the difference of 1.7 ∼ 3.1% depending on δ. $\Delta\hat{m}^2_{32}$ has been measure with a precision of a few % by the MINOS and T2K experiments and $\Delta\hat{m}^2_{31}$ has been measured with precision of ∼10 % by the Daya Bay experiment. A difficult point of this method is that $\Delta\hat{m}^2_{32}$ and $\Delta\hat{m}^2_{31}$ are measured using neutrinos with very different energy scales and energy spectra, with different neutrino detection scheme. Therefore, it is not easy to reduce the relative systematic errors between the measurements to such accuracy.

7.1.6.2 Reactor Experiment at the First Φ_{12} Oscillation Maximum

There is another idea to determine the mass hierarchy by reactor based experiments [5]. The complete formula for the reactor neutrino disappearance is, from Eq. (4.95),

$$\begin{aligned} P_{\overline{\nu}_e \to \overline{\nu}_e} &= 1 - 4 \sum_{i>j} |U_{ei}|^2 |U_{ej}|^2 \sin^2 \Phi_{ij} \\ &= 1 - c_{13}^4 \sin^2 2\theta_{12} \sin^2 \Phi_{21} - \sin^2 2\theta_{13} (c_{12}^2 \sin^2 \Phi_{31} + s_{12}^2 \sin^2 \Phi_{32}). \end{aligned} \tag{7.47}$$

The spectrum is a overlay of constant term plus terms of three oscillation frequencies. At the first oscillation maximum of Φ_{12}, which corresponds to a baseline of $L \sim$ 50 km, the constant term and the Φ_{21} term in Eq. (7.47) are suppressed and the contributions of the Φ_{32} and the Φ_{31} terms are relatively enhanced. If the energy spectrum is analyzed by the Fourier analysis with a parameter $1/E_\nu$, three peaks at

$$\omega = |\Delta m_{31}^2|, \quad |\Delta m_{32}^2| \quad \text{and} \quad |\Delta m_{21}^2| \tag{7.48}$$

shall be observed in the frequency space. The Δm_{21}^2 peak locates much lower than the Δm_{31}^2 and Δm_{32}^2 peaks in the frequency and can be distinguished easily. Δm_{31}^2 and Δm_{32}^2 peaks are expected to separate by 3 % apart. Because $s_{12}^2 \sim 0.3$, $s_{12}^2 < c_{12}^2$ and the amplitude of $\sin^2 \Phi_{31}$ term in Eq. (7.47) is larger than that of $\sin^2 \Phi_{32}$. Therefore, the power of the Δm_{31}^2 peak in the Fourier analysis is larger than that of the Δm_{32}^2 peak. This means the larger peak corresponds to $|\Delta m_{31}^2|$ and the smaller peak corresponds to $|\Delta m_{32}^2|$. As shown in Fig. 7.5, if the power of the higher frequency peak is larger

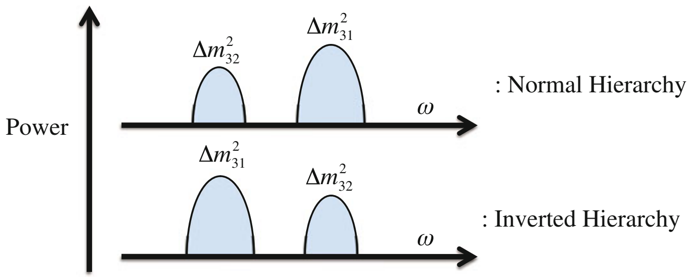

Fig. 7.5 Expected power spectrum of the Fourier analysis of the energy spectrum for reactor neutrinos at a baseline 50 km. The *horizontal axis* ω corresponds to the oscillation frequency and the *vertical axis* is the power of the Fourier analysis. The *larger peak* is the $|\Delta m_{31}^2|$ peak and the *smaller peak* is the $|\Delta m_{32}^2|$ peak. If the $|\Delta m_{31}^2|$ peak locates higher ω than the $|\Delta m_{32}^2|$ peak, it is normal Hierarchy and vice versa

than that of the lower frequency peak, it means $|\Delta m_{31}^2| > |\Delta m_{32}^2|$, which corresponds to the normal hierarchy, and if the power of the higher frequency peak is smaller than that of the lower frequency peak, it means $|\Delta m_{31}^2| < |\Delta m_{32}^2|$, which corresponds to the inverted hierarchy. In this measurement, there is a merit that it is not necessary to know the absolute location of the peaks and the measurement is relatively insensitive to the energy scale error. Although the separation of the peaks of 3 % is larger than the $\Delta\hat{m}^2$ separation of ~1 %, a very good energy resolution is still necessary for the neutrino detector. Currently JUNO [6] is proposed in China and RENO50 [7] is proposed in Korea.

7.2 Sterile Neutrino Anomalies

There have been a number of anomalies and spurious results in the history of the neutrino experiments. Some of them have disappeared but a few of them have led great discoveries. The continuous energy spectrum of the β rays led the idea of neutrinos. Anomaly of deficits of solar and atmospheric neutrinos resulted in the discoveries of the neutrino oscillations. Therefore, anomalies may be clues to new physics and we have to be sincere about experimental facts.

Currently some neutrino oscillation experiments indicate anomalies which could be explained if fourth neutrino that is called sterile neutrino would exist and the standard neutrinos would oscillate to them.

7.2.1 The LSND, KARMEN, MiniBooNE and ICARUS Experiments

In mid 1990s, LSND (Liquid Scintillator Neutrino Detector) group searched for $\overline{\nu}_\mu \to \overline{\nu}_e$ oscillation [8]. $\overline{\nu}_\mu$ is produced in the decay chain from π^+ as shown in Eq. (7.49). The pions are produced by a 800 MeV LAMPF high intensity proton accelerator. Since the energy of the pions are not so high, π^+ and μ^+ stop in the target materials.

$$\begin{aligned} &\pi^+(\text{stop}) \to \mu^+ + \nu_\mu \\ &\qquad\qquad\quad \hookrightarrow \mu^+(\text{stop}) \to e^+ + \overline{\nu}_\mu + \nu_e \end{aligned} \tag{7.49}$$

In this beam energy, the π^- production rate is much smaller than the π^+ one. In addition, π^- and its decay product μ^- are absorbed in the beam stop materials before they decay. Therefore, the background $\overline{\nu}_e$ flux from π^- decay chain is highly suppressed. Figure 7.6 shows the LSND beam line and the neutrino detector. The detector was located at 30 m downstream of the beam stop. The neutrino target is

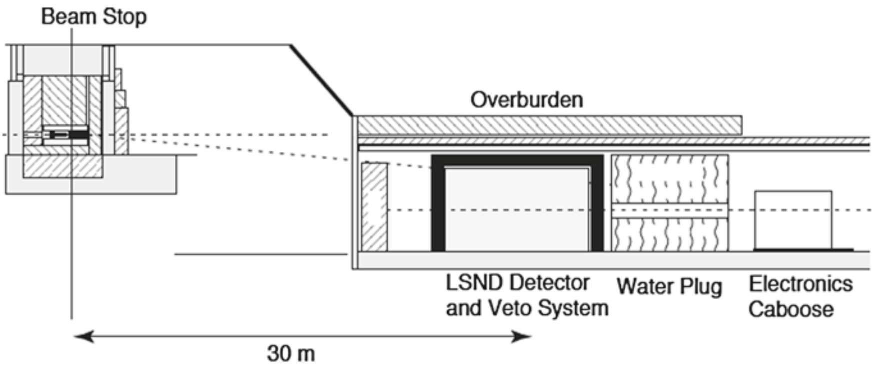

Fig. 7.6 A schematic view of the LSND experiment [9]

low-light yield liquid scintillator of 176 tons, which can detects both the scintillation and Čerenkov lights. The scintillator was contained in a stainless steel cylindrical tank whose inner wall is covered by 1220 photomultipliers with the cathode diameter 8 inch. $\overline{\nu}_e$ is detected using the inverse β decay reaction with a proton and identified by a delayed coincidence signal;

$$\begin{aligned} &\overline{\nu}_e + p \rightarrow e^+(<53\,\mathrm{MeV}) + n \\ &\qquad\qquad\qquad\qquad\qquad \hookrightarrow n + p \rightarrow d + \gamma(2.2\,\mathrm{MeV}). \end{aligned} \tag{7.50}$$

Figure 7.7 shows the energy and L/E distributions of $\overline{\nu}_e$ events for the LSND experiment. They observed an excess of $87.9 \pm 22.4 \pm 6.0$ $\overline{\nu}_e$ events over the backgrounds, for which the allowed oscillation parameters are $\sin^2 2\theta > 10^{-3}$ and

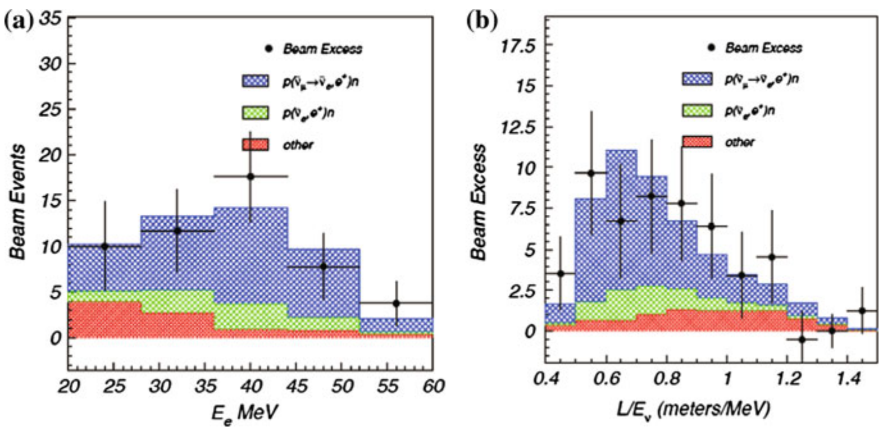

Fig. 7.7 LSND data. **a** Energy distribution of $\overline{\nu}_e$ candidate events. The *shaded region* shows expected distribution from a combination of neutrino backgrounds and neutrino oscillations at low Δm^2. **b** L_ν/E_ν distribution, where L_ν is the baseline, and E_ν is the neutrino energy. The data agree well with an expectation based on neutrino oscillation. From Ref. [9]

$\Delta m^2 > 3 \times 10^{-2}\,\mathrm{eV}^2$. The LSND group also reported positive $\nu_\mu \to \nu_e$ oscillation [10] at the similar oscillation parameters.

However, if we admit $\Delta m^2_{21} \sim 7.5 \times 10^{-5}\,\mathrm{eV}^2$ and $\Delta m^2_{31} \sim 2.5 \times 10^{-3}\,\mathrm{eV}^2$ which have been confirmed by various experiments, there is no combinations of the neutrino masses which gives the LSND result. Therefore, the LSND observation contradicts the standard three flavor neutrino scheme. This is called the *LSND anomaly*.

To investigate the LSND anomaly, the KARMEN experiment searched for $\overline{\nu}_\mu \to \overline{\nu}_e$ oscillation using the ISIS rapid-cycling proton synchrotron whose energy is 800 MeV [11]. The baseline was shorter (17.7 m) than LSND. KARMEN did not observe the excess of $\overline{\nu}_e$ and set the upper limit of $\sin^2 2\theta$ and Δm^2.

MiniBooNE experiment at FNAL searched for both $\nu_\mu \to \nu_e$ and $\overline{\nu}_\mu \to \overline{\nu}_e$ appearance oscillations using higher energy neutrinos which were produced from the pion decay in flight using the 8 GeV proton beam at the FNAL Booster [12]. They observed excesses of both the ν_e and $\overline{\nu}_e$ signals. The relation between the typical neutrino energies and the baselines of these experiments are shown in Fig. 5.1.

ICARUS is a liquid argon TPC based neutrino detector locates at the Gran Sasso lab. in Italy [13]. They looked for $\nu_\mu \to \nu_e$ signals using CNGS neutrinos from CERN whose average energy is 20 GeV and baseline of 730 km. As of year 2013, ICARUS has not observed positive ν_e appearance signal and set the upper limit of $\sin^2 2\theta < 1 \times 10^{-2}$ at $\Delta m^2 > 10^{-2}\,\mathrm{eV}^2$.

Figure 7.8a shows the oscillation parameter regions of the positive results from LSND, MiniBooNE and the negative results from KARMEN, ICARUS. There are allowed regions at $\Delta m^2 > 0.2\,\mathrm{eV}^2$ and $\sin^2 2\theta < 0.01$.

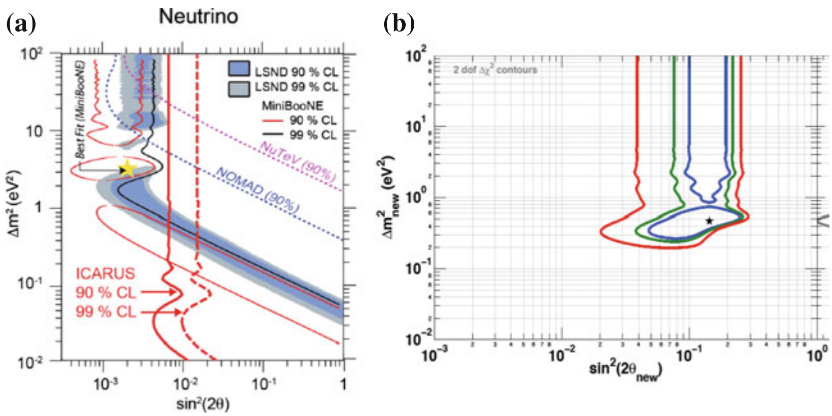

Fig. 7.8 **a** Combined regions of the positive LSND, MiniBooNE results and the negative KARMEN, ICARUS results [13] for $\nu_\mu \to \nu_e$ and $\overline{\nu}_\mu \to \overline{\nu}_e$ signals. **b** Allowed regions from the combination of short baseline reactor neutrino experiments, the GALLEX and SAGE calibration source experiments for $\overline{\nu}_e \to \overline{\nu}_e$ and $\nu_e \to \nu_e$ deficits [14]

7.2.2 Gallium and Reactor Neutrino Anomalies

The GALLEX and SAGE groups calibrated their solar neutrino detector using intense ν_e's from the strong ^{51}Cr and ^{37}Ar sources.

Those sources emit monochromatic ν_e's from the electron capture reactions of

$$
\begin{aligned}
e^- + {}^{51}\mathrm{Cr} &\to {}^{51}\mathrm{V} + \nu_e, \\
e^- + {}^{37}\mathrm{Ar} &\to {}^{37}\mathrm{Cl} + \nu_e.
\end{aligned}
\tag{7.51}
$$

The ν_e energies of the main branching are 0.82 and 0.90 MeV for ^{51}Cr and ^{37}Ar, respectively. These sources were put in their Ga detectors and the reaction rate of

$$\nu_e + {}^{71}\mathrm{Ga} \to {}^{71}\mathrm{Ge} + e^-, \tag{7.52}$$

was measured and it was found that the event rates are smaller than expectations.

An average of the ratio between the observed and the expected rates is

$$R = 0.86 \pm 0.05, \tag{7.53}$$

which indicates that the significance of the deficit of the neutrino is 2.8 σ. A possible explanation of the deficit is that neutrino oscillation with very short oscillation length changed ν_e to other neutrino flavor in the detector.

Another anomaly has been pointed out for the reactor neutrinos. Recent re-evaluation of the reactor $\overline{\nu}_e$ flux [15–17] shows that observed neutrino fluxes by various short-baseline reactor neutrino experiments are ~6 % smaller than the new prediction. This is called the "Reactor Neutrino Anomaly". Again this anomaly can be explained by assuming the existence of neutrino oscillation at very short baselines. Figure 7.8b shows the allowed parameter region of the possible oscillation based on the Gallium, and reactor neutrino anomalies.

7.2.3 Sterile Neutrino

Anomalies observed by the LSND, MiniBooNE, the ν_e sources and the reactor neutrino experiments can be explained if four or more neutrinos exist and they oscillate with the standard neutrinos with oscillation parameters of $\sin^2 2\theta = 0.001 \sim 0.1$ and $\Delta m^2 > 0.1\,\mathrm{eV}^2$. However, the fourth neutrino is ruled out from the neutrino counting experiments using the probability of $e^+e^- \to Z^0 \to \nu\overline{\nu}$ reactions. If the fourth neutrino exists, it must not couple to weak bosons. Since the fourth neutrino does not couple to strong nor electroweak interactions, we can not observe the fourth neutrino directly. Therefore, the fourth neutrino is called the *sterile neutrino* which we label as ν_s.

The oscillation formula can be extended to include the sterile neutrinos by expanding the flavor index α to $(\nu_e, \nu_\mu, \nu_\tau, \nu_s, \ldots)$ and the mass index j to $(1, 2, 3, 4, \ldots)$, in the equation of the neutrino mixing (4.85). The expanded mixing matrix would be expressed by

$$\begin{pmatrix} |\nu_e\rangle \\ |\nu_\mu\rangle \\ |\nu_\tau\rangle \\ |\nu_s\rangle \\ \vdots \end{pmatrix} = \begin{pmatrix} U^*_{e1} & U^*_{e2} & U^*_{e3} & U^*_{e4} & \cdots \\ U^*_{\mu 1} & U^*_{\mu 2} & U^*_{\mu 3} & U^*_{\mu 4} & \cdots \\ U^*_{\tau 1} & U^*_{\tau 2} & U^*_{\tau 3} & U^*_{\tau 4} & \cdots \\ U^*_{s1} & U^*_{s2} & U^*_{s3} & U^*_{s4} & \cdots \\ \vdots & \vdots & \vdots & \vdots & \ddots \end{pmatrix} \begin{pmatrix} |\nu_1\rangle \\ |\nu_2\rangle \\ |\nu_3\rangle \\ |\nu_4\rangle \\ \vdots \end{pmatrix}. \tag{7.54}$$

Assuming a simple case that there is only one sterile neutrino with mass $m_4 \sim 1\,\mathrm{eV}^2$ and $|U_{s4}|^2 \gg |U_{\alpha 4}|^2$, the oscillation probabilities at $(E/L \sim 1\,\mathrm{eV}^2)$ are calculated to be

$$\begin{aligned} P_{\nu_e \to \nu_s} &\sim 4|U_{s4}|^2|U_{e4}|^2 \sin^2\left(\frac{m_4^2 L}{4E_\nu}\right) \quad \text{and} \\ P_{\nu_\mu \to \nu_e} &\sim 4|U_{e4}|^2|U_{\mu 4}|^2 \sin^2\left(\frac{m_4^2 L}{4E_\nu}\right). \end{aligned} \tag{7.55}$$

Therefore, if $|U_{s4}|^2 \sim 0.5$, $|U_{e4}|^2 \sim 0.1$ and $|U_{\mu 4}|^2 \sim 0.01$, all the experimental results shown in Fig. 7.8 could be consistently explained. There are a number of experimental projects which search for the sterile neutrinos.

In Chap. 2, we classified the fermions based on the interactions they make and pointed out the classification has the nesting structure as shown in Fig. 2.1. Since the sterile neutrino, if it exists, does not couple with any known interactions, it is outside of the Matryoshka doll as shown in Fig. 7.9 and the anomalies suggest some kind of transitions, which connect the sterile neutrino to standard neutrinos, exists.

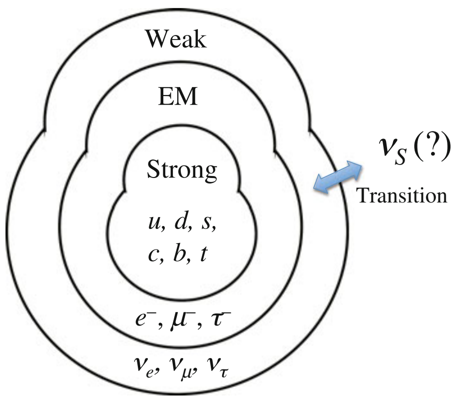

Fig. 7.9 Sterile neutrino (ν_S) might locate outside of the standard model Matryoshka doll (See also Fig. 2.1). There might be a transition between the standard neutrinos

7.3 Absolute Neutrino Masses

The absolute neutrino masses and the neutrino oscillation parameters are complementary to determine the transition amplitudes. All the neutrino mixing angles have been measured and the measurement of the absolute neutrino mass has become all the more important. Generally, experiments measure a weighted average of the squared masses of the mass eigenstates. The mixing matrix elements measured by the neutrino oscillation experiments give the "weight" and the Δm^2's give the relative difference between the masses. The measured neutrino oscillation parameters put limitations to the possible neutrino mass ranges and therefore, give strong motivations to the absolute neutrino mass experiments.

7.3.1 *Effective Mass of ν_e*

Experimentally, most strict upper limit of neutrino mass is obtained from the measurement of the tritium β decay,

$$^3\mathrm{H} \to {}^3\mathrm{He} + e^- + \overline{\nu}_e. \tag{7.56}$$

The small Q-value of the decay (18 keV) is suitable to search for small neutrino masses. Since the tritium atom has simple structure and is usable as gaseous source, the corrections of atomic effects for the energy spectrum of the β ray are very small. Therefore, the tritium is one of the best β sources to search for the $\overline{\nu}_e$ mass.

The energy spectrum of the e^- in this decay in the case neutrinos have mass m_ν is,

$$N(p_e)dp_e \propto p_e^2 (E_0 - E_e)^2 \sqrt{1 - \frac{m_{\nu^2}}{(E_0 - E_e)^2}} dp_e. \tag{7.57}$$

Therefore, the neutrino mass can be measured from the shift and the distortion of the end point of the e^- energy spectrum. The neutrino mass is measured as m_{ν^2} instead of m_ν in the experiments. Mainz [18] and Troitsk [19] experiments have measured the upper limit $\sqrt{m^2_{\nu_e}} < 2\,\mathrm{eV}$. KATRIN [20] experiment whose expected sensitivity is 0.2 eV is under construction now.

The $\overline{\nu}_e$ state is a superposition of the mass eigenstates $\overline{\nu}_i$ as given in Eq. (8.19),

$$|\overline{\nu}_e\rangle = U_{e1}\,|\overline{\nu}_1\rangle + U_{e2}\,|\overline{\nu}_2\rangle + U_{e3}\,|\overline{\nu}_3\rangle\,, \tag{7.58}$$

where U_{ei} are the elements of the mixing matrix for neutrinos. If the energy resolution of the β-decay experiment were good enough, we would see three peaks at m_i^2 with heights $|U_{ei}|^2$ in the mass-squared spectrum as shown in Fig. 7.10. However, the actual resolution of the mass measurement is much worse than the separations between the m_i^2 peaks and we will observe a broad peak in the histogram whose

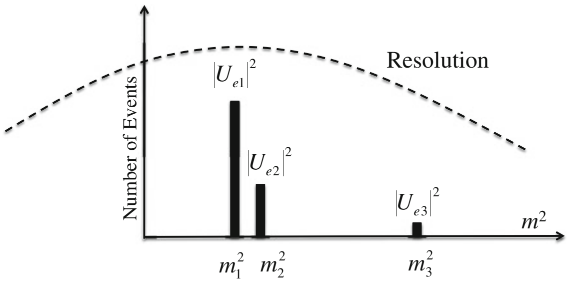

Fig. 7.10 Histogram for m^2 distribution for $m_{\nu_e}^2$ measurement. Expected number of events is proportional to $|U_{ei}|^2$. The *dashed line* indicates the resolution of the experiment. The center value of the peak is the weighted average of m_i^2 as defined by Eq. (7.59)

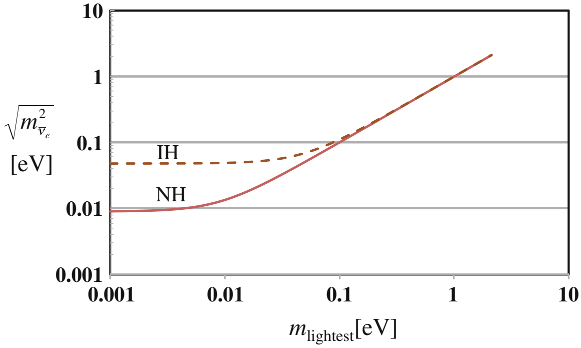

Fig. 7.11 The ν_e mass dependence on the lightest neutrino mass (m_{lightest}). The *vertical axis* is $\langle\sqrt{m_{\nu_e}^2}\rangle$. The *solid line* is the normal hierarchy and the *dashed line* is the inverted hierarchy

center value is the weighted average of the m_i^2 as indicated by the dashed line in Fig. 7.10. The experiments recognize the weighted average as the electron neutrino mass squared $m_{\nu_e}^2$,[2]

$$\begin{aligned} \langle m_{\nu_e}^2\rangle &= |U_{e1}|^2 m_1^2 + |U_{e2}|^2 m_2^2 + |U_{e3}|^2 m_3^2 \\ &= c_{13}^2(c_{12}^2 m_1^2 + s_{12}^2 m_2^2) + s_{13}^2 m_3^2. \end{aligned} \tag{7.59}$$

Two out of the three mass squared in Eq. (7.59) can be replaced by the observed Δm_{21}^2 and $|\Delta m_{31}^2|$. The lightest neutrino mass is m_1 for NH and m_3 for IH. Therefore, the effective ν_e mass can be expressed using the lightest neutrino mass as follow,

$$\langle m_{\nu_e}^2\rangle = \begin{cases} m_1^2 + s_{13}^2|\Delta m_{31}^2| + c_{13}^2 s_{12}^2 \Delta m_{21}^2 \sim m_1^2 + (10\ \mathrm{meV})^2 & \text{for NH} \\ m_3^2 + c_{13}^2|\Delta m_{31}^2| + c_{13}^2 s_{12}^2 \Delta m_{21}^2 \sim m_3^2 + (50\ \mathrm{meV})^2 & \text{for IH.} \end{cases} \tag{7.60}$$

Figure 7.11 shows the relation between $\sqrt{\langle m_{\nu_e}^2\rangle}$ and the lightest neutrino mass. For IH, the ν_e mass will be definitely observed above 50 meV.

Once $\langle m_{\nu_e}^2\rangle$ is measured and the mass hierarchy is determined, all the neutrino masses can be determined from the relation (6.68).

[2] We assume CPT symmetry and $m_{\bar{\nu}} = m_\nu$ throughout the text.

7.3.2 *Effective Masses of* ν_μ *and* ν_τ

From the same discussions for the $\overline{\nu}_e$ mass, which derived Eq. (7.59), the $\langle m^2_{\nu_\mu}\rangle$ and $\langle m^2_{\nu_\tau}\rangle$ can be expressed by,

$$\langle m^2_{\nu_\alpha}\rangle = |U_{\alpha 1}|^2 m_1^2 + |U_{\alpha 2}|^2 m_2^2 + |U_{\alpha 3}|^2 m_3^2, \tag{7.61}$$

where α stands for μ or τ. Using Eq. (7.59), the $\langle m^2_{\nu_\mu}\rangle$ and $\langle m^2_{\nu_\tau}\rangle$ can be expressed by the $\langle m^2_{\nu_e}\rangle$ as follows:

$$\begin{aligned}\langle m^2_{\nu_{\mu/\tau}}\rangle &= \langle m^2_{\nu_e}\rangle + \Delta m^2_{21}(|U_{\mu/\tau 2}|^2 - |U_{e2}|^2) + \eta_{\mathrm{M}}^{31}|\Delta m^2_{31}|(|U_{\mu/\tau 3}|^2 - |U_{e3}|^2)\\ &\sim \langle m^2_{\nu_e}\rangle + \eta_{\mathrm{M}}^{31}|U_{\mu/\tau 3}|^2|\Delta m^2_{31}|.\end{aligned} \tag{7.62}$$

Therefore, $\langle m^2_{\nu_\mu}\rangle$ and $\langle m^2_{\nu_\tau}\rangle$ can be determined from $\langle m^2_{\nu_e}\rangle$ measurement as given by

$$\begin{cases}\langle m^2_{\nu_\mu}\rangle \sim \langle m^2_{\nu_e}\rangle + \eta_{\mathrm{M}}^{31}(30\ \mathrm{meV})^2\\ \langle m^2_{\nu_\tau}\rangle \sim \langle m^2_{\nu_e}\rangle + \eta_{\mathrm{M}}^{31}(36\ \mathrm{meV})^2.\end{cases} \tag{7.63}$$

Since the ν_e mass has been measured to be smaller than 2 eV, the ν_μ and ν_τ masses are also 2 eV or less. On the other hand, the current experimental upper limits of $\nu_{\mu/\tau}$ masses are $m_{\nu_\mu} < 0.19$ MeV, from the pion decay and $m_{\nu_\tau} < 18$ MeV, from the τ decay. It seems to be practically impossible to measure ν_μ and ν_τ masses directly using currently available technologies.

7.3.3 *Double Beta Decay Mass* $m_{\beta\beta}$

In the standard model, the masses of the quarks and the charged leptons are generated by the Yukawa coupling to the Higgs field. If neutrino mass is also generated the same way as shown in Fig. 7.12a, the mass is called the *Dirac mass*.

The neutrino masses are much smaller than those of the charged fermions and it is believed to be unnatural to consider that the neutrino masses are generated by the same mechanism as the charged fermions. Another possibility to generate neutrino mass is a transition between ν_L and $\overline{\nu}_R$ as shown in Fig. 7.12b. The diagram 7.12a requires unknown ν_R but the diagram 7.12b requires only known neutrino states, ν_L and $\overline{\nu}_R$. In this case, a neutrino mass eigenstate is

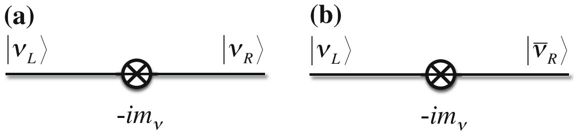

Fig. 7.12 Possible schemes to generate neutrino mass. **a** Dirac neutrino mass. **b** Majorana neutrino mass

$$|\nu_M\rangle = \frac{1}{\sqrt{2}}(|\nu_L\rangle + |\overline{\nu}_R\rangle). \tag{7.64}$$

This type of neutrino is called the *Majorana neutrino* and its mass is called the *Majorana mass*. A peculiar property of this state is that the neutrino and antineutrino state (CP state) are identical.

$$|\overline{\nu}_M\rangle = \frac{1}{\sqrt{2}}(|\overline{\nu}_R\rangle + |\nu_L\rangle) = |\nu_M\rangle\,. \tag{7.65}$$

The diagram 7.12b also shows that if a neutrino is generated as $\overline{\nu}_R$ by β decay at time $t = 0$, it turns into ν_L after infinitesimal time δt, like (3.21), as,

$$|\overline{\nu}_R\rangle \to |\overline{\nu}_R\rangle - im_\nu\,|\nu_L\rangle\,\delta t. \tag{7.66}$$

In principle the absolute mass of the neutrino can be measured by making use of this process as described in the next section.

7.3.3.1 Neutrinoless Double Beta Decays

Currently, the only practical way to test if the neutrino is Majorana type or not is to observe neutrinoless double beta ($0\nu2\beta$) decays,

$${}^{Z}A \to {}^{Z+2}A + e^- + e^-. \tag{7.67}$$

The Feynman diagram of the $0\nu2\beta$ decay is shown in Fig. 7.13. If neutrino is a massive Majorana particle, the following process can take place. (1) A neutron in the nucleus initiates β-decay producing e^- and $\overline{\nu}_\mathrm{R}$. (2) $\overline{\nu}_\mathrm{R}$ changes to ν_L due to the transition amplitude shown in Fig. 7.12b. (3) Another neutron emits virtual W^-. (4) The ν_L interacts with the virtual W^- and turns to e^-. As a result, two electrons and no neutrino are emitted from the nucleus. Since there are no neutrinos in the final state and the recoil energy of the nucleus is very small, the total energy of the two electrons is monochromatic which makes it possible to distinguish the $0\nu2\beta$ decay signals from $2\nu2\beta$ decay background.

Since there are 3 flavor neutrinos and the flavor changes by the neutrino oscillation, the neutrino mixing for the three neutrino flavors has to be taken into account when evaluating the $0\nu2\beta$ decay rates.

$$\begin{pmatrix} |\overline{\nu}_e\rangle \\ |\overline{\nu}_\mu\rangle \\ |\overline{\nu}_\tau\rangle \end{pmatrix} = \begin{pmatrix} U_{e1} & U_{e2} & U_{e3} \\ U_{\mu1} & U_{\mu2} & U_{\mu3} \\ U_{\tau1} & U_{\tau2} & U_{\tau3} \end{pmatrix} \begin{pmatrix} |\overline{\nu}_1\rangle \\ |\overline{\nu}_2\rangle \\ |\overline{\nu}_3\rangle \end{pmatrix}. \tag{7.68}$$

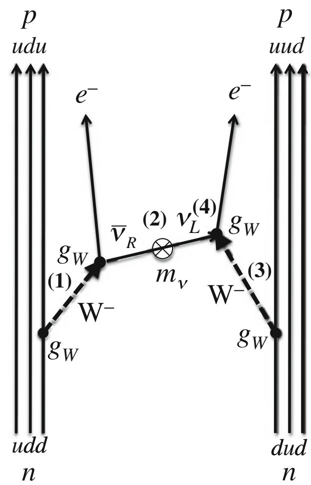

Fig. 7.13 The Feynman diagram of $0\nu 2\beta$ decay. The *numbers* in parentheses correspond to the processes described in the text

The wave function of the neutrinos produced at $t = 0$ in the β decay of the process (1) is

$$|\psi_\nu(0)\rangle = |\overline{\nu}_{eR}\rangle = U_{e1}\,|\overline{\nu}_{1R}\rangle + U_{e2}\,|\overline{\nu}_{2R}\rangle + U_{e3}\,|\overline{\nu}_{3R}\rangle\,. \tag{7.69}$$

The neutrino changes its helicity and particle-antiparticle properties due to the diagram of Fig. 7.13b. Equation (7.66) shows that each mass eigenstate in (7.69) changes to

$$|\overline{\nu}_{iR}\rangle \to |\overline{\nu}_{iR}\rangle - im_i\,|\nu_{iL}\rangle\,\delta t, \tag{7.70}$$

and the neutrino wave function becomes

$$|\psi(\delta t)\rangle = |\overline{\nu}_{eR}\rangle - i\,(m_1U_{e1}\,|\nu_{1L}\rangle + m_2U_{e2}\,|\nu_{2L}\rangle + m_3U_{e3}\,|\nu_{3L}\rangle)\,\delta t, \tag{7.71}$$

after infinitesimal time δt. $|\nu_{eL}\rangle$ state interacts with W boson in the process (4). Since

$$|\nu_{eL}\rangle = U_{e1}^*\,|\nu_{1L}\rangle + U_{e2}^*\,|\nu_{2L}\rangle + U_{e3}^*\,|\nu_{3L}\rangle\,, \tag{7.72}$$

the $|\nu_{eL}\rangle$ component of the wave function (7.71) is

$$\langle\nu_{eL}|\psi(\delta t)\rangle = -i\left(m_1U_{e1}^2 + m_2U_{e2}^2 + m_3U_{e3}^2\right)\delta t. \tag{7.73}$$

When the decay probability is calculated, δt is integrated with a weight of the nuclear matrix element and the decay width is obtained as

$$\Gamma = \frac{1}{\tau} = G|\mathscr{M}_A|^2|\langle m_{\beta\beta}\rangle|^2, \tag{7.74}$$

where G corresponds to effective coupling constant which is proportional to G_F^4, and $\mathscr{M}_A$ is the matrix element of the nuclear transition. $\langle m_{\beta\beta}\rangle$ is called the "effective Majorana mass",

$$\langle m_{\beta\beta}\rangle \equiv |m_1 U_{e1}^2 + m_2 U_{e2}^2 + m_3 U_{e3}^2|. \tag{7.75}$$

The mixing matrix elements in the probability (7.74) have the form of $U_{ei}^2 U_{ej}^2$. This is different from the neutrino oscillation probability, $|U_{ei}|^2|U_{ej}|^2$ and the discussions in Sect. 4.2.3 on the possible free parameters of the mixing matrix does not apply here. In this case, the minimum number of the imaginary phase in $U_{\alpha i}$ is not restricted to just one.

If the standard parametrization of the mixing matrix with the additional phases is used, the effective Majorana mass is expressed as

$$\langle m_{\beta\beta}\rangle = \left| c_{13}^2(c_{12}^2 m_1 + s_{12}^2 m_2 e^{i\alpha}) + s_{13}^2 m_3 e^{i\beta} \right|. \tag{7.76}$$

As we discussed for the ν_e mass measurement in Sect. 7.3.1, we can express the effective Majorana mass with the lightest neutrino masses using observed neutrino oscillation parameters. For normal mass hierarchy (NH), the lightest neutrino mass is m_1 and

$$m_2 = \sqrt{m_1^2 + \Delta m_{21}^2},\ m_3 = \sqrt{m_1^2 + |\Delta m_{31}^2|}. \tag{7.77}$$

For inverted mass hierarchy (IH), the lightest neutrino mass is m_3 and

$$m_1 = \sqrt{m_3^2 + |\Delta m_{31}^2|},\ m_2 = \sqrt{m_3^2 + |\Delta m_{31}^2| + \Delta m_{21}^2}. \tag{7.78}$$

By putting these parameters, together with the mixing matrix elements into Eq. (7.76), $\langle m_{\beta\beta}\rangle$ is calculated as shown in Fig. 7.14. For IH, $\langle m_{\beta\beta}\rangle$ is greater than $\sim$15 meV.

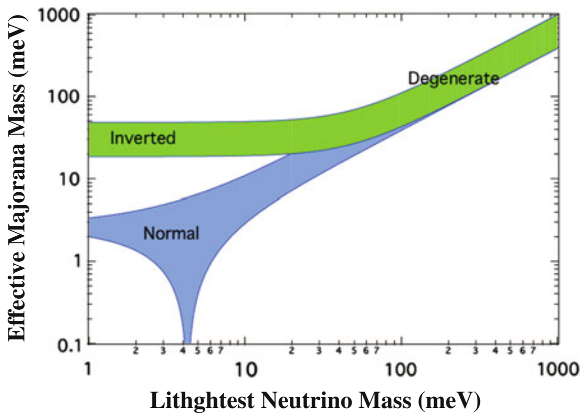

Fig. 7.14 The effective Majorana mass as a function of the lightest neutrino mass. From Ref. [21]

This means if the mass hierarchy is determined to be IH by other experiments, double beta decay experiments which has sensitivity of 15 meV or better can definitely determine whether the neutrino is Majorana or Dirac. For instance, if $0\nu 2\beta$ events are observed, the neutrino is Majorana, however if $0\nu 2\beta$ events can not be observed at $\langle m_{\beta\beta} \rangle > 15$ meV, it is Dirac particle. For NH, the effective Majorana mass does not have minimum value. The effective Majorana mass can be zero for a specific combination of the parameters. There have been a number of experiments to measure $0\nu 2\beta$ decays but there have been no firm evidence of positive signals so far [1, Chap. 1].

References

1. C. Jarlskog, PRLbf **55**, 1039 (1985)
2. M. Goodman, Neutrino OscillationIndustry, (http://www.hep.anl.gov/ndk/hypertext/)
3. E.K. Akhmedov, R. Johansson, M. Lindner, T. Ohlsson, T. Schwetz, JHEP **04**, 078 (2004)
4. T. Schwetz, arXiv:hep-ph/0703279v1 (2007)
5. J.G. Learned, S.T. Dye, S. Pakvasa, R.C. Svoboda, PRD 78:071302 (2008)
6. Y.-F. Li, arXiv:1402.6143v1 (2014)
7. http://astrophysics.skku.edu/docs/2013/S5_Kim
8. LSND Collaboration, PRL **77**, 3082 (1996)
9. LSND Collaboration, PRC **64**, 065501 (2001)
10. LSND Collaboration, PRL **81**, 1774 (1998)
11. KARMEN Collaboration, PRC **57**, 3414 (1998)
12. MiniBooNE Collaboration, PRL **105**, 181801 (2010)
13. M. Antonello et al., arXiv:1307.4699v3 [hep-ex], 6 April 2003
14. K.N. Abazajian et al., arXiv:1204.5379 [hep-ph], 18 April 2012
15. T.A. Mueller et al., PRC **83**, 054615 (2011)
16. G. Mention et al., PRC **83**, 054615 (2011)
17. P. Huber, arXiv:1106.0687 (2012)
18. Mainz Collaboration, Eur. Phys. J. C **33**, S805–S807 (2004)
19. Troitsk Collaboration, PRD **84**, 112003 (2011)
20. Katrin Collaboration, arXiv:hep-ex/0109033, NIM **A623**, 442–444 (2010)
21. S.R. Elliott, arXiv:1110.6159v1 (2011)

Chapter 8
Appendix

8.1 Notations Used in This Book

The definition of some parameters and notations used in this text may be different from the ones used in other books. In this appendix, the definition of the parameters used in this text is summarized.

8.1.1 A Summary of Symbols and Abbreviations

i, j: Index of mass, α, β: Index of flavor.
l: Leptons. Sometimes specifically shows charged leptons.
q: Quarks. Momentum transfer.
f: Fermions. Sometimes specifically shows mass eigenstate.
f': Flavor eigenstate fermion.
$x_W = \sin^2\theta_W$: Weak mixing angle.
U_ν: MNSP mixing matrix.
θ_{ij}: Mixing angle.
$s_{ij} = \sin\theta_{ij},\ c_{ij} = \cos\theta_{ij},\ t_{ij} = \tan\theta_{ij}\ s_\delta = \sin\delta,\ c_\delta = \cos\delta, \Delta m^2_{ij} = m_i^2 - m_j^2$.
$\Phi_{ij} = \Delta m^2_{ij} L/4E_\nu$: Oscillation phase.
$@\Phi_{ij} =$ "at $\Phi_{ij} \sim \pi/2$".
$\eta^{ij}_{\mathrm{M}} = +1$ for normal mass hierarchy of masses m_i, m_j and -1 for inverted mass hierarchy.
$\eta_{\mathrm{C}} = +1$ for neutrino and -1 for antineutrino.
$\eta = \frac{\mathbf{p}}{E+m} = \frac{\beta\gamma}{1+\gamma}$.
$J_r = s_{12}c_{12}s_{23}c_{23}s_{13}c^2_{13}\sin\delta$: Jarlskog invariant.
$J_{123} = \sin 2\theta_{12}\sin 2\theta_{23}\sin 2\theta_{13}$.
$\varepsilon_m = \Delta m^2_{21}/\Delta m^2_{31}$.
$\upsilon = 2\sqrt{2}EG_F n_e/\Delta m^2$: weak potential parameter.

F. Suekane, *Neutrino Oscillations*, Lecture Notes in Physics 898,
DOI 10.1007/978-4-431-55462-2_8

$\Lambda_{ij}^{\alpha\beta} = U_{\alpha i} U_{\alpha j}^* U_{\beta_j} U_{\beta_i}^*$.
$P_X^* = P_X(\delta \to -\delta)$.
$\odot$: Sun, $\oplus$: Earth.

8.1.2 Parameter Values

$c = 2.997\,924\,58 \times 10^8\,\mathrm{ms}^{-1}$.
$\hbar = 6.582\,119\,3 \times 10^{-22}\,\mathrm{MeVs}$.
$\hbar c = 197.327\,\mathrm{MeVfm}$.
$\alpha = \frac{e^2}{4\pi} = \frac{1}{137.035\,999\,0}$.
$M_Z = 91.188\,\mathrm{GeV/c^2}, \quad M_W = 80.39\,\mathrm{GeV/c^2}$.
$x_W = \sin^2\theta_W = 0.2312$.
$G_F = 1.166\,378 \times 10^{-5}\,\mathrm{GeV}^{-2}$.

8.1.3 Pauli Matrices and Identity Matrix

$$\sigma_i \sigma_j = i\sigma_k; \quad (i,\ j,\ k) \text{ are cyclic.} \tag{8.1}$$

$$\sigma_i \sigma_j + \sigma_j \sigma_i = 2\delta_{ij}. \tag{8.2}$$

$$\sigma_i^\dagger = \sigma_i. \tag{8.3}$$

$$I = \begin{pmatrix} 1 & 0 \\ 0 & 1 \end{pmatrix}, \quad \sigma_x = \sigma_1 = \begin{pmatrix} 0 & 1 \\ 1 & 0 \end{pmatrix}, \quad \sigma_y = \sigma_2 = \begin{pmatrix} 0 & -i \\ i & 0 \end{pmatrix}, \quad \sigma_z = \sigma_3 = \begin{pmatrix} 1 & 0 \\ 0 & -1 \end{pmatrix}. \tag{8.4}$$

$$\sigma_+ = \sigma_x + i\sigma_y = 2\begin{pmatrix} 0 & 1 \\ 0 & 0 \end{pmatrix}, \quad \sigma_- = \sigma_x - i\sigma_y = 2\begin{pmatrix} 0 & 0 \\ 1 & 0 \end{pmatrix}. \tag{8.5}$$

8.1.4 Dirac Matrices

$$\gamma^\mu\gamma^\nu + \gamma^\nu\gamma^\mu = 2g^{\mu\nu}, \quad g^{\mu\nu} = \begin{pmatrix} 1 & 0 & 0 & 0 \\ 0 & -1 & 0 & 0 \\ 0 & 0 & -1 & 0 \\ 0 & 0 & 0 & -1 \end{pmatrix}. \tag{8.6}$$

$$\gamma^{\mu\dagger} = \gamma^0\gamma^\mu\gamma^0. \tag{8.7}$$

$$\gamma^0 = \begin{pmatrix} I & 0 \\ 0 & -I \end{pmatrix}, \quad \gamma^1 = \begin{pmatrix} 0 & \sigma_x \\ -\sigma_x & 0 \end{pmatrix}, \quad \gamma^2 = \begin{pmatrix} 0 & \sigma_y \\ -\sigma_y & 0 \end{pmatrix}, \quad \gamma^3 = \begin{pmatrix} 0 & \sigma_z \\ -\sigma_z & 0 \end{pmatrix}. \tag{8.8}$$

$$\gamma^5 = i\gamma^0\gamma^1\gamma^2\gamma^3 = \begin{pmatrix} 0 & I \\ I & 0 \end{pmatrix}. \tag{8.9}$$

$$\gamma_R = \frac{1+\gamma^5}{2} = \frac{1}{2}\begin{pmatrix} I & I \\ I & I \end{pmatrix}, \quad \gamma_L = \frac{1-\gamma^5}{2} = \frac{1}{2}\begin{pmatrix} I & -I \\ -I & I \end{pmatrix}. \tag{8.10}$$

$$\psi_L = \gamma_L\psi, \quad \psi_R = \gamma_R\psi. \tag{8.11}$$

8.1.5 Spin

$$\hat{s}(\theta,\phi) = \begin{pmatrix} e^{-i(\phi/2)}\cos(\theta/2) \\ e^{i(\phi/2)}\sin(\theta/2) \end{pmatrix}. \tag{8.12}$$

$$\chi_1 = \begin{pmatrix} 1 \\ 0 \end{pmatrix}, \quad \chi_2 = \begin{pmatrix} 0 \\ 1 \end{pmatrix}. \tag{8.13}$$

$$\begin{aligned} \psi_P &= \frac{1+\hat{\mathbf{p}}\sigma}{2}\psi: \quad \text{spin is parallel to the momentum.} \\ \psi_A &= \frac{1-\hat{\mathbf{p}}\sigma}{2}\psi: \quad \text{spin is antiparallel to the momentum.} \end{aligned} \tag{8.14}$$

8.1.6 Fierz Transformation

From Fierz identity [1];

$$\begin{aligned} [\bar{\chi}\gamma^\mu\psi][\bar{\psi}\gamma_\mu\chi] = {} & [\bar{\chi}\chi][\bar{\psi}\psi] - \frac{1}{2}[\bar{\chi}\gamma^\mu\chi][\bar{\psi}\gamma_\mu\psi] \\ & - \frac{1}{2}[\bar{\chi}\gamma^\mu\gamma_5\chi][\bar{\psi}\gamma_\mu\gamma_5\psi] - [\bar{\chi}\gamma_5\chi][\bar{\psi}\gamma_5\psi], \end{aligned} \tag{8.15}$$

and

$$\begin{aligned} [\bar{\chi}\gamma^\mu\gamma_5\psi][\bar{\psi}\gamma_\mu\gamma_5\chi] = {} & -[\bar{\chi}\chi][\bar{\psi}\psi] - \frac{1}{2}[\bar{\chi}\gamma^\mu\chi][\bar{\psi}\gamma_\mu\psi] \\ & - \frac{1}{2}[\bar{\chi}\gamma^\mu\gamma_5\chi][\bar{\psi}\gamma_\mu\gamma_5\psi] + [\bar{\chi}\gamma_5\chi][\bar{\psi}\gamma_5\psi]. \end{aligned} \tag{8.16}$$

Then

$$[\overline{\chi}\gamma^{\mu}\psi][\overline{\psi}\gamma_{\mu}\chi] + [\overline{\chi}\gamma^{\mu}\gamma_5\psi][\overline{\psi}\gamma_{\mu}\gamma_5\chi] = -[\overline{\chi}\gamma^{\mu}\chi][\overline{\psi}\gamma_{\mu}\psi] - [\overline{\chi}\gamma^{\mu}\gamma_5\chi][\overline{\psi}\gamma_{\mu}\gamma_5\psi]. \tag{8.17}$$

8.1.7 Neutrino Oscillation Related Formula

8.1.7.1 Mixing Matrices for Neutrinos and Antineutrinos

$$\begin{aligned}
\psi_{\nu}(t) &= C_{\nu_e}(t)\,|\nu_e\rangle + C_{\nu_\mu}(t)\,|\nu_\mu\rangle + C_{\nu_\tau}(t)\,|\nu_\tau\rangle \\
&= D_1 e^{-im_1 t}\,|\nu_1\rangle + D_2 e^{-im_2 t}\,|\nu_2\rangle + D_3 e^{-im_3 t}\,|\nu_3\rangle\,. \\
\psi_{\overline{\nu}}(t) &= \overline{C}_{\nu_e}(t)\,|\overline{\nu}_e\rangle + \overline{C}_{\nu_\mu}(t)\,|\overline{\nu}_\mu\rangle + \overline{C}_{\nu_\tau}(t)\,|\overline{\nu}_\tau\rangle \\
&= \overline{D}_1 e^{im_1 t}\,|\overline{\nu}_1\rangle + \overline{D}_2 e^{im_2 t}\,|\overline{\nu}_2\rangle + \overline{D}_3 e^{im_3 t}\,|\overline{\nu}_3\rangle\,.
\end{aligned} \tag{8.18}$$

$$\begin{aligned}
&\begin{pmatrix} C_{\nu_e} \\ C_{\nu_\mu} \\ C_{\nu_\tau} \end{pmatrix} = \begin{pmatrix} U_{e1}, & U_{e2}, & U_{e3} \\ U_{\mu 1}, & U_{\mu 2}, & U_{\mu 3} \\ U_{\tau 1}, & U_{\tau 2}, & U_{\tau 3} \end{pmatrix} \begin{pmatrix} C_1 \\ C_2 \\ C_3 \end{pmatrix}, \quad \begin{pmatrix} |\nu_e\rangle \\ |\nu_\mu\rangle \\ |\nu_\tau\rangle \end{pmatrix} = \begin{pmatrix} U^*_{e1}, & U^*_{e2}, & U^*_{e3} \\ U^*_{\mu 1}, & U^*_{\mu 2}, & U^*_{\mu 3} \\ U^*_{\tau 1}, & U^*_{\tau 2}, & U^*_{\tau 3} \end{pmatrix} \begin{pmatrix} |\nu_1\rangle \\ |\nu_2\rangle \\ |\nu_3\rangle \end{pmatrix}, \\
&\begin{pmatrix} \overline{C}_{\nu_e} \\ \overline{C}_{\nu_\mu} \\ \overline{C}_{\nu_\tau} \end{pmatrix} = \begin{pmatrix} U^*_{e1}, & U^*_{e2}, & U^*_{e3} \\ U^*_{\mu 1}, & U^*_{\mu 2}, & U^*_{\mu 3} \\ U^*_{\tau 1}, & U^*_{\tau 2}, & U^*_{\tau 3} \end{pmatrix} \begin{pmatrix} \overline{C}_1 \\ \overline{C}_2 \\ \overline{C}_3 \end{pmatrix}, \quad \begin{pmatrix} |\overline{\nu}_e\rangle \\ |\overline{\nu}_\mu\rangle \\ |\overline{\nu}_\tau\rangle \end{pmatrix} = \begin{pmatrix} U_{e1}, & U_{e2}, & U_{e3} \\ U_{\mu 1}, & U_{\mu 2}, & U_{\mu 3} \\ U_{\tau 1}, & U_{\tau 2}, & U_{\tau 3} \end{pmatrix} \begin{pmatrix} |\overline{\nu}_1\rangle \\ |\overline{\nu}_2\rangle \\ |\overline{\nu}_3\rangle \end{pmatrix}.
\end{aligned} \tag{8.19}$$

8.1.7.2 Parametrization of the Mixing Matrix

$$\begin{aligned}
U_\nu &= \begin{pmatrix} 1 & 0 & 0 \\ 0 & c_{23} & s_{23} \\ 0 & -s_{23} & c_{23} \end{pmatrix} \begin{pmatrix} c_{13} & 0 & s_{13}e^{-i\delta} \\ 0 & 1 & 0 \\ -s_{13}e^{i\delta} & 0 & c_{13} \end{pmatrix} \begin{pmatrix} c_{12} & s_{12} & 0 \\ -s_{12} & c_{12} & 0 \\ 0 & 0 & 1 \end{pmatrix} \\
&= \begin{pmatrix} c_{12}c_{13} & s_{12}c_{13} & s_{13}e^{-i\delta} \\ -s_{12}c_{23} - c_{12}s_{23}s_{13}e^{i\delta} & c_{12}c_{23} - s_{12}s_{23}s_{13}e^{i\delta} & s_{23}c_{13} \\ s_{12}s_{23} - c_{12}c_{23}s_{13}e^{i\delta} & -s_{23}c_{12} - s_{12}c_{23}s_{13}e^{i\delta} & c_{23}c_{13} \end{pmatrix}.
\end{aligned} \tag{8.20}$$

8.2 A Working Lagrangian with Neutrino Flavor Transition

In the standard model, neutrino is assumed to be massless and there is no ν_R state. However, neutrino oscillation revealed that the neutrinos actually have finite masses and mixings. In this appendix, the standard model Lagrangian is slightly expanded to implement the neutrino mass and mixing. Although the origin of the neutrino oscillation is not understood yet, we assume that there are neutrino flavor transitions just like the quarks here. The standard model Lagrangian can be obtained by setting the neutrino mixing matrix as the identical matrix.

8.2.1 Electroweak Part of the Working Lagrangian

We express the electroweak part of the working Lagrangian with neutrino mixing as,

$$\begin{aligned}\mathscr{L}_{\mathrm{EW}} = \sum_f &(i[\overline{f}\gamma^\mu\partial_\mu f] - m_f[\overline{f}f] + eQ_f[\overline{f}\gamma^\mu f]A_\mu \\ &- g_W([\overline{f'_{UL}}\gamma^\mu f'_{DL}]W^-_\mu + \mathrm{H.C.}) - g_Z(C^f_{\mathrm{L}}[\overline{f_{\mathrm{L}}}\gamma^\mu f_{\mathrm{L}}] + C^f_{\mathrm{R}}[\overline{f_{\mathrm{R}}}\gamma^\mu f_{\mathrm{R}}])Z_\mu) \\ &- \frac{1}{2}M_W^2 W^-_\mu W^{+\mu} - \frac{1}{2}M_Z^2 Z_\mu Z^\mu + \mathscr{L}_{\mathrm{GK}}. \end{aligned} \tag{8.21}$$

where $\mathscr{L}_{\mathrm{GK}}$ is the kinetic term of the gauge bosons.[1] The symbol f represents the mass eigenstate fermions and f' represents flavor eigenstate,

$$\begin{aligned} f &= u,\ c,\ t,\ d,\ s,\ b,\ e,\ \mu,\ \tau,\ \nu_1,\ \nu_2,\ \nu_3; \\ f' &= u,\ c,\ t,\ d',\ s',\ b',\ e,\ \mu,\ \tau,\ \nu_e,\ \nu_\mu,\ \nu_\tau. \end{aligned} \tag{8.22}$$

For, u, c, t, e, μ, τ, the flavor eigenstate and mass eigenstate are defined to be identical. f'_U represents the up-type weak eigenstate fermions and f'_D represents the down-type weak eigenstate fermions,

$$f'_U = u,\ c,\ t,\ \nu_e,\ \nu_\mu,\ \nu_\tau, \quad f'_D = d',\ s',\ b',\ e,\ \mu,\ \tau. \tag{8.23}$$

f_L and f_R represent left-handed and right-handed fermions, respectively.

$$f_L = \gamma_L f, \quad f_R = \gamma_R f. \tag{8.24}$$

The weak eigenstates and mass eigenstate are connected by the Cabbibo-Kobayashi-Maskawa (CKM) matrix, V_{CKM} for quarks and Maki-Nakagawa-Sakata-Pontecorvo (MNSP) matrix, U_ν for neutrinos.

$$\begin{pmatrix} d' \\ s' \\ b' \end{pmatrix} = \begin{pmatrix} V_{ud} & V_{us} & V_{ub} \\ V_{cd} & V_{cs} & V_{cb} \\ V_{td} & V_{ts} & V_{tb} \end{pmatrix} \begin{pmatrix} d \\ s \\ b \end{pmatrix}, \qquad \begin{pmatrix} \nu_e \\ \nu_\mu \\ \nu_\tau \end{pmatrix} = \begin{pmatrix} U_{e1} & U_{e2} & U_{e3} \\ U_{\mu 1} & U_{\mu 2} & U_{\mu 3} \\ U_{\tau 1} & U_{\tau 2} & U_{\tau 3} \end{pmatrix} \begin{pmatrix} \nu_1 \\ \nu_2 \\ \nu_3 \end{pmatrix}. \tag{8.25}$$

[1] See [2] for explicit formula.

The coupling coefficients of the fermion-Z^0 are

$$(C_{\mathrm{L}}^f,\ \ C_{\mathrm{R}}^f) = \begin{cases} (1 - 2Q_f \sin^2\theta_W, & -2Q_f \sin^2\theta_W) \ \text{ for } \ f_U, \\ (-1 - 2Q_f \sin^2\theta_W, & -2Q_f \sin^2\theta_W) \ \text{ for } \ f_D, \end{cases} \tag{8.26}$$

where $\sin^2\theta_W$ is the weak mixing angle ($\sim$0.23).

There are the relations,[2]

$$e = \sqrt{2} g_W \sin\theta_W = g_Z \sin 2\theta_W, \quad M_W = M_Z \cos\theta_W. \tag{8.27}$$

8.2.2 Dirac Equation of Neutrinos with Cross Transitions

The unitarity of the mixing matrices (8.25) indicates that there are following relations,

$$\begin{gathered} \overline{d}d + \overline{s}s + \overline{b}b = \overline{d'}d' + \overline{s'}s' + \overline{b'}b', \\ \overline{\nu}_1\nu_1 + \overline{\nu}_2\nu_2 + \overline{\nu}_3\nu_3 = \overline{\nu}_e\nu_e + \overline{\nu}_\mu\nu_\mu + \overline{\nu}_\tau\nu_\tau. \end{gathered} \tag{8.28}$$

The corresponding terms in the Lagrangian (8.21), such as $\sum_f \overline{f}\gamma^\mu\partial_\mu f$ and $\sum_f Q_f [\overline{f}\gamma^\mu f]$,[3] can be expressed the same way by using either the weak eigenstate and mass eigenstate. However, since the fermion masses are different for different flavors, the fermion mass term, $\sum_f m_f[\overline{f}f]$ is not identical to $\sum_f m_f[\overline{f'}f']$. If the mass term is expressed by the weak eigenstate, the neutrino term can be written as

$$m_i[\overline{\nu_i}\nu_i] = \sum_{\alpha\beta}(m_i U_{\beta i} U_{\alpha i}^*)[\overline{\nu_\beta}\nu_\alpha]. \tag{8.29}$$

The Lagrangian for the free neutrino is,

$$\mathscr{L}_{\nu 0} = \sum_\alpha i[\overline{\nu_\alpha}\gamma^\mu\partial_\mu\nu_\alpha] - \sum_{\alpha\beta}\mu_{\beta\alpha}[\overline{\nu_\beta}\nu_\alpha], \tag{8.30}$$

where $\mu_{\beta\alpha} = \sum_i m_i U_{\beta i} U_{\alpha i}^*$. The Euler-Lagrange equation, in terms of ν_α leads

$$0 = \partial_\mu\left(\frac{\partial\mathscr{L}_{\nu 0}}{\partial(\partial_\mu\nu_\alpha)}\right) - \frac{\partial\mathscr{L}_{\nu 0}}{\partial\nu_\alpha} = i\partial_\mu(\overline{\nu_\alpha})\gamma^\mu + \sum_\beta \mu_{\beta\alpha}\overline{\nu_\beta}. \tag{8.31}$$

[2] The relation to the standard expression of the weak coupling is $g_W = g/\sqrt{2}$, $g_Z = g/2\cos\theta_W$, where g is the SU(2) gauge coupling constant.

[3] Q_f is the same for d, s, b.

By taking the complex conjugate, we obtain

$$i\gamma^{\mu}\partial_{\mu}\nu_{\alpha} - \sum_{\beta}\mu_{\alpha\beta}\nu_{\beta} = 0, \tag{8.32}$$

where the relation $\mu^*_{\beta\alpha} = \mu_{\alpha\beta}$ is used. This is the Dirac equation of neutrinos with the same type of flavor transition amplitudes as quarks.

8.3 General Solution for Two Flavor State Equation

The state equation to solve is,

$$i\frac{d}{dt}\begin{pmatrix}\alpha(t)\\ \beta(t)\end{pmatrix} = \begin{pmatrix}-\mu & \tau^*\\ \tau & \mu\end{pmatrix}\begin{pmatrix}\alpha(t)\\ \beta(t)\end{pmatrix}, \tag{8.33}$$

where there is a normalization relation,

$$|\alpha|^2 + |\beta|^2 = 1. \tag{8.34}$$

Equation (8.33) can be rewritten as

$$i\frac{d}{dt}\begin{pmatrix}\alpha\\ \beta\end{pmatrix} = \omega\begin{pmatrix}-\cos 2\theta & e^{-i\phi}\sin 2\theta\\ e^{i\phi}\sin 2\theta & \cos 2\theta\end{pmatrix}\begin{pmatrix}\alpha\\ \beta\end{pmatrix} \equiv \omega\hat{\mathscr{T}}\begin{pmatrix}\alpha\\ \beta\end{pmatrix}, \tag{8.35}$$

where

$$\tau = |\tau|e^{i\phi}, \quad \omega = \sqrt{\mu^2 + |\tau|^2} \text{ and } \tan 2\theta = \frac{|\tau|}{\mu}. \tag{8.36}$$

$\hat{\mathscr{T}}$ is the normalized transition matrix. In order to obtain the eigenvalues and eigenvectors, we require that

$$i\frac{d}{dt}\begin{pmatrix}\alpha\\ \beta\end{pmatrix} = \omega\hat{\mathscr{T}}\begin{pmatrix}\alpha\\ \beta\end{pmatrix} = \lambda\begin{pmatrix}\alpha\\ \beta\end{pmatrix}, \tag{8.37}$$

where λ corresponds to the eigen value to be determined from this relation. The second relation in Eq. (8.37) is

$$\begin{pmatrix}-\omega\cos 2\theta - \lambda & \omega e^{-i\phi}\sin 2\theta\\ \omega e^{i\phi}\sin 2\theta & \omega\cos 2\theta - \lambda\end{pmatrix}\begin{pmatrix}\alpha\\ \beta\end{pmatrix} = 0. \tag{8.38}$$

Since the matrix in Eq. (8.38) can not have the inverse for non-0 α and β solution, the eigenvalues are,

$$\lambda_{\pm} = \pm\omega. \tag{8.39}$$

The relation between α and β for each case is,

$$e^{-i\phi}\sin 2\theta\beta_{\pm}, = (\cos 2\theta \pm 1)\alpha_{\pm}. \tag{8.40}$$

Together with the normalization condition (8.34), the eigenvectors are

$$\begin{pmatrix}\alpha_-\\ \beta_-\end{pmatrix} = \begin{pmatrix}\cos\theta\\ -e^{i\phi}\sin\theta\end{pmatrix}, \quad \begin{pmatrix}\alpha_+\\ \beta_+\end{pmatrix} = \begin{pmatrix}\sin\theta\\ e^{i\phi}\cos\theta\end{pmatrix}. \tag{8.41}$$

Therefore, the unitary matrix

$$U = \begin{pmatrix}\cos\theta & \sin\theta\\ -e^{i\phi}\sin\theta & e^{i\phi}\cos\theta\end{pmatrix} \tag{8.42}$$

diagonalizes $\hat{\mathscr{T}}$,

$$U^{\dagger}\hat{\mathscr{T}}U = \begin{pmatrix}-1 & 0\\ 0 & 1\end{pmatrix}. \tag{8.43}$$

The state equation (8.35) becomes,

$$\frac{d}{dt}\begin{pmatrix}\alpha'\\ \beta'\end{pmatrix} = -i\omega\begin{pmatrix}-1 & 0\\ 0 & 1\end{pmatrix}\begin{pmatrix}\alpha'\\ \beta'\end{pmatrix}, \tag{8.44}$$

where

$$\begin{pmatrix}\alpha'\\ \beta'\end{pmatrix} = U^{\dagger}\begin{pmatrix}\alpha\\ \beta\end{pmatrix}. \tag{8.45}$$

The solution of Eq. (8.44) is

$$\begin{pmatrix}\alpha'(t)\\ \beta'(t)\end{pmatrix} = \begin{pmatrix}e^{i\omega t} & 0\\ 0 & e^{-i\omega t}\end{pmatrix}\begin{pmatrix}\alpha'(0)\\ \beta'(0)\end{pmatrix}. \tag{8.46}$$

Therefore, the general solution of (8.35) is,

$$\begin{aligned}\begin{pmatrix}\alpha(t)\\ \beta(t)\end{pmatrix} &= U\begin{pmatrix}e^{i\omega t} & 0\\ 0 & e^{-i\omega t}\end{pmatrix}U^{\dagger}\begin{pmatrix}\alpha(0)\\ \beta(0)\end{pmatrix}\\ &= \begin{pmatrix}\sin^2\theta e^{-i\omega t}+\cos^2\theta e^{i\omega t} & e^{-i\phi}\sin\theta\cos\theta(e^{i\omega t}-e^{-i\omega t})\\ e^{i\phi}\sin\theta\cos\theta(e^{i\omega t}-e^{-i\omega t}) & \sin^2\theta e^{i\omega t}+\cos^2\theta e^{-i\omega t}\end{pmatrix}\begin{pmatrix}\alpha(0)\\ \beta(0)\end{pmatrix}.\end{aligned} \tag{8.47}$$

8.4 Dirac Equation and Wave Packet

8.4.1 Dirac Equation

The Dirac equation is,

$$\left[i\gamma_\mu \partial^\mu - m\right] \psi(x) = 0, \tag{8.48}$$

where the γ_μ is four component matrices which satisfy the following condition,

$$\gamma_\mu \gamma_\nu + \gamma_\nu \gamma_\mu = 2g_{\mu\nu}. \tag{8.49}$$

We use the γ matrices of the following notation;

$$\gamma_0 = \begin{pmatrix} I & 0 \\ 0 & -I \end{pmatrix}, \quad \gamma = \begin{pmatrix} 0 & \sigma \\ -\sigma & 0 \end{pmatrix}. \tag{8.50}$$

The identity and Pauli matrices are,

$$I = \begin{pmatrix} 1 & 0 \\ 0 & 1 \end{pmatrix}, \ \sigma_x = \begin{pmatrix} 0 & 1 \\ 1 & 0 \end{pmatrix}, \ \sigma_y = \begin{pmatrix} 0 & -i \\ i & 0 \end{pmatrix}, \ \sigma_z = \begin{pmatrix} 1 & 0 \\ 0 & -1 \end{pmatrix}. \tag{8.51}$$

By using the matrix forms (8.50), the Dirac equation can be expressed by a matrix form as follows:

$$\begin{pmatrix} i\partial_t - m & i(\sigma \cdot \boldsymbol{\partial}) \\ -i(\sigma \cdot \boldsymbol{\partial}) & -i\partial_t - m \end{pmatrix} \psi(x) = 0. \tag{8.52}$$

8.4.2 Plane Wave Solution

Plane wave is a wave which extends infinitely in the space and time at a fixed energy and momentum;

$$\psi(x) = we^{-ikx}, \tag{8.53}$$

where $x = (t, \mathbf{x})$ and $k = (\omega, \mathbf{k})$ and w is a four component spinor,

$$w = \begin{pmatrix} u \\ v \end{pmatrix}, \tag{8.54}$$

where, u and v are two component spinors. By putting the plane wave (8.53) in the Dirac equation (8.52), we obtain

$$\begin{pmatrix} \omega - m & -\mathbf{k} \cdot \sigma \\ \mathbf{k} \cdot \sigma & -\omega - m \end{pmatrix} \begin{pmatrix} u \\ v \end{pmatrix} e^{-ikx} = 0. \tag{8.55}$$

In the case that the fermion is at rest ($\mathbf{k} = \mathbf{0}$), the equations reduce to

$$\begin{cases} (\omega - m)u = 0 \\ (\omega + m)v = 0. \end{cases} \tag{8.56}$$

There are three sets of solutions, ($\omega = any, u = 0, v = 0$), ($\omega = m, u = any, v = 0$) and ($\omega = -m$, $u = 0$, $v = any$). The first solution means that the fermion does not exist in the system. The second and third solutions correspond to the positive energy and negative energy solutions, respectively. The general wave function of a fermion at rest is a sum of the these solutions.

$$\psi(x) = \begin{pmatrix} u \\ 0 \end{pmatrix} e^{-imt} + \begin{pmatrix} 0 \\ v \end{pmatrix} e^{imt}. \tag{8.57}$$

For a finite momentum ($\mathbf{k} \neq \mathbf{0}$), the Dirac equation (8.55) becomes the following simultaneous equations,

$$\begin{cases} (\omega - m)u - \mathbf{k} \cdot \sigma v = 0 \\ \mathbf{k} \cdot \sigma u - (\omega + m)v = 0. \end{cases} \tag{8.58}$$

If $\omega = m$ or $-m$, we obtain the non-existing solution, $u = 0$ and $v = 0$. For $\omega \neq \pm m$, there are the relations,

$$v = \frac{\mathbf{k} \cdot \sigma}{\omega + m} u, \quad u = \frac{\mathbf{k} \cdot \sigma}{\omega - m} v. \tag{8.59}$$

By substituting v in the second relation in (8.59) by the first relation, we obtain a requirement,

$$(\omega^2 - m^2 - \mathbf{k}^2)u = 0. \tag{8.60}$$

For non-0 u,

$$\omega^2 - m^2 - \mathbf{k}^2 = 0. \tag{8.61}$$

This can be satisfied for

$$\mathbf{k} = \pm\mathbf{p} \ \text{ and } \ \omega = \pm\sqrt{(\pm\mathbf{p})^2 + m^2} \equiv \pm E. \tag{8.62}$$

We choose (ω, $\mathbf{k}$) = (E, $\mathbf{p}$) and ($-E$, $-\mathbf{p}$) because they can be obtained using the proper Lorentz transformation of (ω, $\mathbf{k}$) = ($\pm m$, $\mathbf{0}$) and the wave functions of the positive and negative energy states are, using (8.59),[4]

[4] It is possible to derive the same formula by Lorentz boost of the wave function at rest. See for example [3].

$$\begin{aligned}\psi_+(x) &= \begin{pmatrix} u \\ \frac{\mathbf{k}\cdot\sigma}{\omega+m}u \end{pmatrix} e^{-i(\omega t-\mathbf{kx})} = \begin{pmatrix} u \\ \frac{\mathbf{p}\cdot\sigma}{E+m}u \end{pmatrix} e^{-i(Et-\mathbf{px})}, \\ \psi_-(x) &= \begin{pmatrix} \frac{\mathbf{k}\cdot\sigma}{\omega-m}v \\ v \end{pmatrix} e^{-i(\omega t-\mathbf{kx})} = \begin{pmatrix} \frac{\mathbf{p}\cdot\sigma}{E+m}v \\ v \end{pmatrix} e^{i(Et-\mathbf{px})}.\end{aligned} \tag{8.63}$$

Physically the negative energy state which propagates backward in time is recognized as an antiparticle. On the other hand, the positive energy state which propagates forward in time is recognized as regular particle. The general wave function is a sum of them,

$$\psi(x) = \begin{pmatrix} u \\ (\eta\cdot\sigma)u \end{pmatrix} e^{-ipx} + \begin{pmatrix} (\eta\cdot\sigma)v \\ v \end{pmatrix} e^{ipx}, \tag{8.64}$$

where we defined

$$p \equiv (E, \mathbf{p}), \quad \eta \equiv \frac{\mathbf{p}}{E+m} = \frac{\gamma\beta}{\gamma+1}. \tag{8.65}$$

Usually we normalize the wave equation as follows,

$$|\psi_\pm|^2 = 2E. \tag{8.66}$$

For example,

$$|\psi_+|^2 = \frac{2E}{E+m}|u|^2 = 2E \tag{8.67}$$

and

$$|u|^2 = E+m. \tag{8.68}$$

Therefore, we can rewrite

$$u = \sqrt{E+m}\,\hat{u}, \tag{8.69}$$

where $|\hat{u}|^2 = 1$.

Using the normalization, the general wave function which satisfies the Dirac equation (8.48) can be expressed as

$$\psi(x) = \sqrt{E+m}\left[\begin{pmatrix} \hat{u} \\ (\eta\cdot\sigma)\hat{u} \end{pmatrix} e^{-ipx} + \begin{pmatrix} (\eta\cdot\sigma)\hat{v} \\ \hat{v} \end{pmatrix} e^{ipx}\right], \tag{8.70}$$

where in this case,

$$|\hat{u}|^2 + |\hat{v}|^2 = 1. \tag{8.71}$$

8.4.3 Wave Packet

The plane wave extends infinitely in the space and time. However, the actual particle exits within a limited region in space. These state can be expressed by a superposition of plane waves which have a narrow momentum spread. For one dimensional case,

$$\Psi(t,z) = \int_{-\infty}^{+\infty} a(p) e^{i(pz-E(p)t)} dp, \tag{8.72}$$

where $a(p)$ represent a momentum distribution. We assume it is a Gaussian shape with the mean and standard deviation of the momentum, $\overline{p}$ and σ_p, respectively,

$$a(p) = N \exp\left[-\frac{(p-\overline{p})^2}{4\sigma_p^2}\right]. \tag{8.73}$$

$N = (2\pi)^{-3/4}\sigma_p^{-1/2}$ is the normalization coefficient. Note that the coefficient of the σ_p^2 is "4" because the probability is square of wave function. By defining a parameter $q \equiv p_z - \overline{p}$, the integration (8.72) becomes,

$$\Psi(t,z) = N \int_{-\infty}^{+\infty} \exp\left[-\frac{q^2}{4\sigma_p^2}\right] \exp\left[i\left((q+\overline{p})z - \sqrt{(q+\overline{p})^2 + m^2 t}\right)\right] dq. \tag{8.74}$$

We assume the width of the momentum spread is much smaller than the mean momentum, $\sigma_p \ll \overline{p}$. In this case, only $|q| \sim \sigma_p$ region contributes to the integration and the following approximation is possible.

$$\sqrt{(q+\overline{p})^2 + m^2} \sim \sqrt{\overline{p}^2 + m^2 + 2\overline{p}q} \sim \overline{E} + \frac{\overline{p}}{\overline{E}} q = \overline{E} + \overline{\beta} q, \tag{8.75}$$

where $\overline{E} \equiv \sqrt{\overline{p}^2 + m^2}$ and $\overline{\beta} \equiv \overline{p}/\overline{E}$. Then,

$$\Psi(t,z) \sim N e^{i(\overline{p}z - \overline{E}t)} \int_{-\infty}^{+\infty} \exp\left[-\frac{q^2}{4\sigma_p^2}\right] \exp\left[i\Delta z q\right] dq, \tag{8.76}$$

where $\Delta z \equiv z - \overline{\beta} t$ represents deviation from $z = \overline{\beta} t$. Since q-odd component of the integrand is cancelled off, the integration becomes

$$\begin{aligned} \Psi(t,z) &= N e^{i(\overline{p}z - \overline{E}t)} \int_{-\infty}^{+\infty} \exp\left[-\frac{q^2}{4\sigma_p^2}\right] \cos(\Delta z q) dq \\ &= (2/\pi)^{1/4} \sqrt{\sigma_p} e^{-\sigma_p^2 (\Delta z)^2} e^{i(\overline{p}z - \overline{E}t)}, \end{aligned} \tag{8.77}$$

where the general integral relation,

$$\int_{-\infty}^{+\infty} e^{-a^2x^2} \cos bx dx = \frac{\sqrt{\pi}}{a} \exp\left[-\frac{b^2}{4a^2}\right]; \quad (a > 0) \tag{8.78}$$

is used. The probability density of the existence of the particle at (t, z) is,

$$|\Psi(t, z)|^2 = \frac{1}{\sqrt{2\pi}\sigma_z} \exp\left[-\frac{(z - \overline{\beta}t)^2}{2\sigma_z^2}\right]; \quad \sigma_z = \frac{1}{2\sigma_p}. \tag{8.79}$$

This formula indicates that the particle exists only at around $z \sim \overline{\beta}t$ with spacial spread σ_z. This means that the particle is moving with the velocity $\overline{\beta}$. This is called the wave packet. At the beginning of this discussion, we assumed that the state has momentum spread σ_p and in the end we obtained a wave packet with spacial spread σ_z. The relation between the momentum and spacial spreads is

$$\sigma_p \sigma_z = 1/2. \tag{8.80}$$

Therefore, if the momentum spread is wide, the spatial spread is narrow, and vice versa. This corresponds to the uncertainty principle.

8.4.3.1 Derivation of Wave Packet Oscillation

Equation (4.34) shows the probability that ν_μ is produced at the space-time $x = 0$ and it changes to ν_e at the space-time x. The integrand of Eq. (4.35) can explicitly be written as

$$I = \frac{1}{\sqrt{2\pi}\sigma_z} \int_{-\infty}^{\infty} \left[\begin{aligned} & e^{-(z-\beta_2 t)^2/2\sigma_z^2} + e^{-(z-\beta_1 t)^2/2\sigma_z^2} \\ & \quad - 2e^{-((z-\beta_2 t)^2 + (z-\beta_1 t)^2)/4\sigma_z^2} \cos(\Delta k z - \Delta E t) \end{aligned} \right] dt. \tag{8.81}$$

The first two integrands can be integrated using the relation,

$$\frac{1}{\sqrt{2\pi}\sigma_z} \int_{-\infty}^{\infty} e^{-(z-\beta_i t)^2/2\sigma_z^2} dt = \frac{1}{\beta_i} \sim 1. \tag{8.82}$$

The power of the exponential function in the third integrand can be expressed as the quadratic function of the time t,

$$(z - \beta_2 t)^2 + (z - \beta_1 t)^2 = 2\overline{\beta^2}\left(t - \frac{\overline{\beta}}{\overline{\beta^2}} z\right)^2 + \frac{(\Delta\beta)^2}{2\overline{\beta^2}} z^2, \tag{8.83}$$

where $\overline{\beta} = \frac{\beta_1+\beta_1}{2}$, $\overline{\beta^2} = \frac{\beta_1^2+\beta_2^2}{2}$ and $\Delta\beta = \beta_1 - \beta_2$. The integration of the third integrant can be performed as

$$\begin{aligned}
&\int_{-\infty}^{+\infty} e^{-((\Delta z_2)^2+(\Delta z_1)^2)/4\sigma_z^2} \cos(\Delta kL - \Delta Et)dt \\
&= \exp\left(-\frac{(\Delta\beta)^2 z^2}{8\sigma_z^2\overline{\beta^2}}\right) \int_{-\infty}^{\infty} \exp\left(-\frac{\overline{\beta^2}}{2\sigma_z^2}\left(t - \frac{\overline{\beta}}{\overline{\beta^2}}z\right)^2\right) \cos(\Delta kz - \Delta Et)dt \\
&= \sigma_z\sqrt{\frac{2\pi}{\overline{\beta^2}}} \cos\left[\left(\Delta k - \frac{\overline{\beta}}{\overline{\beta^2}}\Delta E\right)z\right] \exp\left[-\frac{1}{8\overline{\beta^2}}\left[\left(\frac{\Delta E}{\sigma_k}\right)^2 + \left(\frac{\Delta\beta z}{\sigma_z}\right)^2\right]\right] \\
&\sim \sigma_z\sqrt{2\pi} \cos\left[(\Delta k - \Delta E)\,z\right] \exp\left[-\frac{1}{8}\left[\left(\frac{\Delta E}{\sigma_k}\right)^2 + \left(\frac{\Delta\beta z}{\sigma_z}\right)^2\right]\right], \qquad (8.84)
\end{aligned}$$

where $\overline{\beta} \sim 1$, $\overline{\beta^2} \sim 1$, $\overline{\beta}/\overline{\beta^2} \sim 1 - (\Delta\beta)^2/4 \sim 1$ are used. Finally, the integration (8.81) is

$$I \sim 2\left(1 - \cos\left[(\Delta k - \Delta E)\,z\right] \exp\left[-\frac{1}{8}\left[\left(\frac{\Delta E}{\sigma_k}\right)^2 + \left(\frac{\Delta\beta z}{\sigma_z}\right)^2\right]\right]\right). \qquad (8.85)$$

8.5 Three Flavor Neutrino Oscillation Probabilities

In this appendix, we will derive the probabilities of the three flavor neutrino oscillations. In Sect. 8.5.1, the general probabilities are expressed by the mixing matrix elements $U_{\alpha j}$. In Sect. 8.5.2, specific probabilities are expressed using the standard mixing parameters θ_{ij} and δ. In Sect. 8.5.3, the probabilities near the two oscillation maximums are approximated for the practical handling of the data and in Sect. 8.5.4, important oscillation formulas with the matter effect are summarized.

8.5.1 Derivation of Three Flavor Oscillation Formula

We start with the oscillation probability formula (4.88),

$$P_{\nu_\alpha\to\nu_\beta} = \sum_{j,k} \Lambda^{\alpha\beta}_{kj} e^{i2\Phi_{kj}}, \qquad (8.86)$$

where

$$\Lambda^{\alpha\beta}_{kj} = U_{\alpha k}U^*_{\beta k}U^*_{\alpha j}U_{\beta j}, \quad \text{and} \quad \Phi_{kj} = \frac{\Delta m^2_{kj}L}{4E}. \qquad (8.87)$$

Equation (8.86) can be separated into the CP-odd and CP-even terms by using the unitarity of the mixing matrix and the symmetry between $k > j$ and $k < j$, as follows:

$$P_{\nu_\alpha \to \nu_\beta} = (\sum_{j=k} + \sum_{k>j} + \sum_{k<j})\Lambda_{kj}^{\alpha\beta} e^{i2\Phi_{kj}} = \sum_j |U_{\alpha j}|^2 |U_{\beta j}|^2 + 2\sum_{k>j} \Re[\Lambda_{kj}^{\alpha\beta} e^{2i\Phi_{kj}}]. \tag{8.88}$$

From the relations below,

$$\sum_{kj} \Lambda_{kj}^{\alpha\beta} = \sum_k U_{\alpha k} U_{\beta k}^* \sum_j U_{\alpha j}^* U_{\beta j} = (\delta_{\alpha\beta})^2 = \delta_{\alpha\beta}$$

and (8.89)

$$\sum_{kj} \Lambda_{kj}^{\alpha\beta} = (\sum_{k=j} + \sum_{k>j} + \sum_{k<j})\Lambda_{kj}^{\alpha\beta} = \sum_j |U_{\alpha j}|^2 |U_{\beta j}|^2 + 2\sum_{k>j} \Re[\Lambda_{kj}^{\alpha\beta}],$$

the following equation can be obtained,

$$\sum_j |U_{\alpha j}|^2 |U_{\beta j}|^2 = \delta_{\alpha\beta} - 2\sum_{k>j} \Re[\Lambda_{kj}^{\alpha\beta}]. \tag{8.90}$$

Therefore, the oscillation probability (8.88) becomes,

$$P_{\nu_\alpha \to \nu_\beta} = \delta_{\alpha\beta} - 2\sum_{k>j} \Re[\Lambda_{kj}^{\alpha\beta}(1 - e^{2i\Phi_{kj}})] = \delta_{\alpha\beta} - 4\sum_{k>j} \sin\Phi_{kj} \Im[\Lambda_{kj}^{\alpha\beta} e^{i\Phi_{kj}}]. \tag{8.91}$$

Since,

$$\Lambda_{kj}^{\alpha\beta} e^{i\Phi_{kj}} = (\Re[\Lambda_{kj}^{\alpha\beta}] + i\Im[\Lambda_{kj}^{\alpha\beta}])(\cos\Phi_{kj} + i\sin\Phi_{kj}), \tag{8.92}$$

the probability (8.91) can be written as

$$P_{\nu_\alpha \to \nu_\beta} = \delta_{\alpha\beta} - 4\sum_{k>j} \Re[\Lambda_{kj}^{\alpha\beta}] \sin^2\Phi_{kj} - 2\sum_{k>j} \Im[\Lambda_{kj}^{\alpha\beta}] \sin 2\Phi_{kj}. \tag{8.93}$$

This expression is often used in text books.

Using the relation $\Lambda_{kj}^{\beta\alpha} = \left(\Lambda_{kj}^{\alpha\beta}\right)^*$, the probability of oscillation for the reversed direction is

$$\begin{aligned} P_{\nu_\beta \to \nu_\alpha} &= \delta_{\beta\alpha} - 4\sum_{k>j} \Re[\Lambda_{kj}^{\beta\alpha}] \sin^2\Phi_{kj} - 2\sum_{k>j} \Im[\Lambda_{kj}^{\beta\alpha}] \sin 2\Phi_{kj} \\ &= \delta_{\alpha\beta} - 4\sum_{k>j} \Re[\Lambda_{kj}^{\alpha\beta}] \sin^2\Phi_{kj} + 2\sum_{k>j} \Im[\Lambda_{kj}^{\alpha\beta}] \sin 2\Phi_{kj}. \end{aligned} \tag{8.94}$$

From CPT invariance, there is a relation $P_{\bar{\nu}_\alpha\to\bar{\nu}_\beta} = P_{\nu_\beta\to\nu_\alpha}$ and the oscillation formula of antineutrinos is

$$\begin{aligned} P_{\bar{\nu}_\alpha\to\bar{\nu}_\beta} &= P_{\nu_\beta\to\nu_\alpha} \\ &= \delta_{\alpha\beta} - 4\sum_{k>j}\Re[\Lambda_{kj}^{\alpha\beta}]\sin^2\Phi_{kj} + 2\sum_{k>j}\Im[\Lambda_{kj}^{\alpha\beta}]\sin 2\Phi_{kj}. \end{aligned} \tag{8.95}$$

This is equivalent to reverse the sign of imaginary number in the equation, $\delta \to -\delta$.

8.5.2 Complete Oscillation Formulas

The mixing matrix is parametrized by θ_{12}, θ_{23}, θ_{13} and δ as follows:

$$U = \begin{pmatrix} c_{12}c_{13} & s_{12}c_{13} & s_{13}e^{-i\delta} \\ -s_{12}c_{23} - c_{12}s_{23}s_{13}e^{i\delta} & c_{12}c_{23} - s_{12}s_{23}s_{13}e^{i\delta} & s_{23}c_{13} \\ s_{12}s_{23} - c_{12}c_{23}s_{13}e^{i\delta} & -s_{23}c_{12} - s_{12}c_{23}s_{13}e^{i\delta} & c_{23}c_{13} \end{pmatrix}. \tag{8.96}$$

The complete oscillation formulas expressed by the mixing angles are

$$P_{\nu_e\to\nu_e} = 1 - \sin^2 2\theta_{13}(c_{12}^2\sin^2\Phi_{31} + s_{12}^2\sin^2\Phi_{32}) - c_{13}^4\sin^2 2\theta_{12}\sin^2\Phi_{21}, \tag{8.97}$$

$$\begin{aligned} P_{\nu_\mu\to\nu_\mu} &= (c_{13}^2\sin^2 2\theta_{23} + s_{23}^4\sin^2 2\theta_{13})\sin^2\Phi_{32} \\ &+ (s_{12}^2c_{13}^2\sin^2 2\theta_{23} + c_{12}^2s_{23}^4\sin^2 2\theta_{13} + c_\delta s_{23}^2 c_{13}J_{123})(\sin^2\Phi_{31} - \sin^2\Phi_{32}) \\ &+ \begin{pmatrix} \sin^2 2\theta_{12}(c_{23}^2 - s_{23}^2s_{13}^2)^2 + s_{13}^2\sin^2 2\theta_{23}(1 - c_\delta^2\sin^2 2\theta_{12}) \\ + c_\delta s_{13}(c_{23}^2 - s_{23}^2s_{13}^2)\sin 4\theta_{12}\sin 2\theta_{23} \end{pmatrix}\sin^2\Phi_{21}, \end{aligned} \tag{8.98}$$

and

$$\begin{aligned} P_{\nu_\mu\to\nu_e} &= s_{23}^2\sin^2 2\theta_{13}(c_{12}^2\sin^2\Phi_{31} + s_{12}^2\sin^2\Phi_{32}) \\ &+ \frac{c_\delta c_{13}J_{123}}{2}(\sin^2\Phi_{31} - \sin^2\Phi_{32}) \\ &+ \frac{1}{4}(2s_{23}^2s_{13}^2\sin^2 2\theta_{12}\sin 2\theta_{13} - J_{123}(\sin 2\theta_{12} + 2c_\delta s_{13}\cos 2\theta_{12}))\sin^2\Phi_{21} \\ &+ \frac{1}{4}s_\delta J_{123}(c_{13}(\sin 2\Phi_{31} - \sin 2\Phi_{32}) + s_{13}\sin 2\Phi_{21}), \end{aligned} \tag{8.99}$$

where,

$$J_{123} = \sin 2\theta_{12}\sin 2\theta_{23}\sin 2\theta_{13}. \tag{8.100}$$

Probabilities of other oscillation modes can be obtained from the above three probabilities as

$$P_{\nu_\mu \to \nu_\tau} = 1 - P_{\nu_\mu \to \nu_\mu} - P_{\nu_\mu \to \nu_e}, \tag{8.101}$$

$$P_{\nu_e \to \nu_\tau} = 1 - P_{\nu_e \to \nu_e} - P^*_{\nu_\mu \to \nu_e}, \tag{8.102}$$

$$\begin{aligned} P_{\nu_\tau \to \nu_\tau} &= 1 - P_{\nu_\tau \to \nu_\mu} - P_{\nu_\tau \to \nu_e} \\ &= P_{\nu_\mu \to \nu_\mu} + P_{\nu_e \to \nu_e} + P_{\nu_\mu \to \nu_e} + P^*_{\nu_\mu \to \nu_e} - 1, \end{aligned} \tag{8.103}$$

where P_X^* is obtained by replacing $\delta \to -\delta$ in the formula of P_X.

8.5.3 Approximated Oscillation Formulas Near the Oscillation Maximums

The complete oscillation formulas derived in the previous sections are complicated and may not be useful for practical analysis of the experimental data. In this section, oscillation formulas near the oscillation maximums are simplified by ignoring higher orders of the small parameters, s_{13}^2 and $|\Delta m_{21}^2/\Delta m_{31}^2|$,

$$\varepsilon_m \equiv \frac{\Delta m_{21}^2}{\Delta m_{31}^2} = \frac{\Phi_{21}}{\Phi_{31}} \sim \pm 0.03, \quad s_{13}^2 \sim 0.026. \tag{8.104}$$

Since ε_m and s_{13}^2 have similar smallness, approximation can be performed with powers of ε_m and s_{13}^2. The following relation will be used,

$$c_{13} = 1 + O(s_{13}^2), \quad s_{13} = \frac{1}{2}\sin 2\theta_{13} + O(s_{13}^3). \tag{8.105}$$

8.5.3.1 Oscillations Around Φ_{31} Maximum

Since $\Phi_{21} = \varepsilon_m \Phi_{31}$, Φ_{21} is small at $|\Phi_{31}| \sim O(1)$ and the following approximations can be made.

$$\begin{aligned} \sin 2\Phi_{21} &= \sin 2\varepsilon_m \Phi_{31} = 2\varepsilon_m \Phi_{31} + O(\varepsilon_m^3), \\ \sin^2 \Phi_{21} &= \sin^2 \varepsilon_m \Phi_{31} = 0 + O(\varepsilon_m^2). \end{aligned} \tag{8.106}$$

Φ_{32} can be related to Φ_{31} using the relation $\Phi_{32} = \Phi_{31} - \Phi_{21} = (1 - \varepsilon_m)\Phi_{31}$ as follows:

$$\begin{aligned} \sin 2\Phi_{32} &= \sin 2\Phi_{31} - 2\varepsilon_m \Phi_{31} \cos 2\Phi_{31} + O(\varepsilon_m^2), \\ \sin^2 \Phi_{32} &= \sin^2 \Phi_{31} - \varepsilon_m \Phi_{31} \sin 2\Phi_{31} + O(\varepsilon_m^2). \end{aligned} \tag{8.107}$$

We apply the approximations to the oscillation probability form (8.93). The second term of the right hand side is,

$$
\begin{aligned}
\Re\left[\sum_{k>j}\Lambda_{kj}^{\alpha\beta}\sin^2\Phi_{kj}\right] &= \Re\left[\Lambda_{21}^{\alpha\beta}\sin^2\Phi_{21}+\Lambda_{31}^{\alpha\beta}\sin^2\Phi_{31}+\Lambda_{32}^{\alpha\beta}\sin^2\Phi_{32}\right]\\
&\sim \Re\left[\Lambda_{31}^{\alpha\beta}\sin^2\Phi_{31}+\Lambda_{32}^{\alpha\beta}(\sin^2\Phi_{31}-\varepsilon_m\sin 2\Phi_{31})\right]\\
&= \Re\left[(\Lambda_{31}^{\alpha\beta}+\Lambda_{32}^{\alpha\beta})\sin^2\Phi_{31}-\varepsilon_m\Phi_{31}\Lambda_{32}^{\alpha\beta}\sin 2\Phi_{31}\right]\\
&= |U_{\alpha 3}|^2(\delta_{\alpha\beta}-|U_{\beta 3}|^2)\sin^2\Phi_{31}-\varepsilon_m\Phi_{31}\Re[\Lambda_{32}^{\alpha\beta}]\sin 2\Phi_{31}+O(\varepsilon_m^2),
\end{aligned}
\tag{8.108}
$$

where the relation,

$$
\begin{aligned}
\Lambda_{31}^{\alpha\beta}+\Lambda_{32}^{\alpha\beta} &= U_{\alpha 3}U_{\beta 3}^*(U_{\alpha 1}^*U_{\beta 1}+U_{\alpha 2}^*U_{\beta 2}) = U_{\alpha 3}U_{\beta 3}^*(\delta_{\alpha\beta}-U_{\alpha 3}^*U_{\beta 3})\\
&= |U_{\alpha 3}|^2(\delta_{\alpha\beta}-|U_{\beta 3}|^2) \ \in \ \Re
\end{aligned}
\tag{8.109}
$$

is used. The third term of right hand side of Eq. (8.93) is

$$
\begin{aligned}
\Im\left[\sum_{k>j}\Lambda_{kj}^{\alpha\beta}\sin 2\Phi_{kj}\right] &= \Im\left[\Lambda_{21}^{\alpha\beta}\sin 2\Phi_{21}+\Lambda_{31}^{\alpha\beta}\sin 2\Phi_{31}+\Lambda_{32}^{\alpha\beta}\sin 2\Phi_{32}\right]\\
&\sim \Im\left[2\varepsilon_m\Phi_{31}\Lambda_{21}^{\alpha\beta}+\Lambda_{31}^{\alpha\beta}\sin 2\Phi_{31}+\Lambda_{32}^{\alpha\beta}(\sin 2\Phi_{31}-2\varepsilon_m\Phi_{31}\cos 2\Phi_{31})\right]\\
&= \Im\left[(\Lambda_{31}^{\alpha\beta}+\Lambda_{32}^{\alpha\beta})\sin 2\Phi_{31}+2\varepsilon_m\Phi_{31}(\Lambda_{21}^{\alpha\beta}-\Lambda_{32}^{\alpha\beta}\cos 2\Phi_{31})\right]\\
&= 2\varepsilon_m\Phi_{31}\Im\left[(\Lambda_{21}^{\alpha\beta}+\Lambda_{12}^{\alpha\beta})-\Lambda_{12}^{\alpha\beta}-\Lambda_{32}^{\alpha\beta}(1-2\sin^2\Phi_{31})\right]\\
&= 2\varepsilon_m\Phi_{31}\Im\left[-(\Lambda_{12}^{\alpha\beta}+\Lambda_{32}^{\alpha\beta})+2\Lambda_{32}^{\alpha\beta}\sin^2\Phi_{31}\right]\\
&= 4\varepsilon_m\Phi_{31}\sin^2\Phi_{31}\Im\left[\Lambda_{32}^{\alpha\beta}\right]+O(\varepsilon_m^2).
\end{aligned}
\tag{8.110}
$$

By putting Eqs. (8.108) and (8.110) into Eq. (8.93), the approximated oscillation probability is

$$
\begin{aligned}
P_{\nu_\alpha\to\nu_\beta}(@\Phi_{31}) = \delta_{\alpha\beta} &- 4|U_{\alpha 3}|^2(\delta_{\alpha\beta}-|U_{\beta 3}|^2)\sin^2\Phi_{31}\\
&+ 8\varepsilon_m\Phi_{31}\sin\Phi_{31}\Re[\Lambda_{32}^{\alpha\beta}e^{i\Phi_{31}}]+O(\varepsilon_m^2).
\end{aligned}
\tag{8.111}
$$

Note that if Φ_{32} is used instead of Φ_{31} as the reference parameter, the formula becomes slightly different,

$$
\begin{aligned}
P_{\nu_\alpha\to\nu_\beta}(@\Phi_{32}) = \delta_{\alpha\beta} &- 4|U_{\alpha 3}|^2(\delta_{\alpha\beta}-|U_{\beta 3}|^2)\sin^2\Phi_{32}\\
&- 8\varepsilon_m\Phi_{31}\sin\Phi_{32}\Re[\Lambda_{32}^{\alpha\beta}e^{i\Phi_{32}}]+O(\varepsilon_m^2),
\end{aligned}
\tag{8.112}
$$

Table 8.1 Summary of oscillations probabilities $@\Phi_{31}$. $J_{123} = \sin 2\theta_{12} \sin 2\theta_{23} \sin 2\theta_{13}$

Mode and probability $@\Phi_{31}$
M: $\nu_e \to \nu_e, \quad \bar{\nu}_e \to \bar{\nu}_e$ P: $1 - \sin^2 2\theta_{13} \sin^2 \Phi_{31} - \varepsilon_m^2 \Phi_{31}^2 \sin^2 2\theta_{12} + O(s_{13}^4)$
M: $\nu_\mu \to \nu_\mu, \quad \bar{\nu}_\mu \to \bar{\nu}_\mu$ P: $1 - (\sin^2 2\theta_{23} - s_{23}^2 \sin^2 2\theta_{13} \cos 2\theta_{23}) \sin^2 \Phi_{31}$ $+ \varepsilon_m \Phi_{31} \sin 2\Phi_{31} (c_{12}^2 \sin^2 2\theta_{23} - s_{23}^2 J_{123} \cos\delta)$
M: $\nu_\tau \to \nu_\tau, \quad \bar{\nu}_\tau \to \bar{\nu}_\tau$ P: $1 - (\sin^2 2\theta_{23} + c_{23}^2 \cos 2\theta_{23} \sin^2 2\theta_{13})$ $+ \varepsilon_m \Phi_{31} \sin 2\Phi_{31} (J_{123} c_{23}^2 \cos\delta + c_{12}^2 \sin^2 2\theta_{23})$
M: $\nu_\mu \to \nu_e, \quad \bar{\nu}_e \to \bar{\nu}_\mu$ P: $s_{23}^2 \sin^2 2\theta_{13} \sin^2 \Phi_{31} + \varepsilon_m \Phi_{31} \sin \Phi_{31} J_{123} \cos(\Phi_{31} + \delta)$
M: $\nu_e \to \nu_\tau, \quad \bar{\nu}_\tau \to \bar{\nu}_e$ P: $c_{23}^2 \sin^2 2\theta_{13} \sin^2 \Phi_{31} - \varepsilon_m \Phi_{31} \sin \Phi_{31} J_{123} \cos(\Phi_{31} - \delta)$
M: $\nu_\mu \to \nu_\tau, \quad \bar{\nu}_\tau \to \bar{\nu}_\mu$ P: $\cos 2\theta_{13} \sin^2 2\theta_{23} \sin^2 \Phi_{31} + \varepsilon_m \Phi_{31} \sin \Phi_{31} \times$ $\big(J_{123}(\sin \Phi_{31} \sin\delta - \cos 2\theta_{23} \cos \Phi_{31} \cos\delta) - 2c_{12}^2 \sin^2 2\theta_{23} \cos \Phi_{31}\big)$

where $\varepsilon_m = \Delta m_{21}^2 / \Delta m_{32}^2$ this time. It is necessary to clearly specify which reference parameter is used in the discussions.

The disappearance probability is,

$$P_{\nu_\alpha \to \nu_\alpha}(@\Phi_{31}) = 1 - 4\,|U_{\alpha 3}|^2\,((1 - |U_{\alpha 3}|^2) \sin^2 \Phi_{31} + 4\varepsilon_m \Phi_{31} |U_{\alpha 2}|^2 |U_{\alpha 3}|^2 \sin 2\Phi_{31}) + O(\varepsilon_m^2). \tag{8.113}$$

The appearance probability is

$$P_{\nu_\alpha \to \nu_\beta \neq \nu_\alpha}(@\Phi_{31}) = 4|U_{\alpha 3}|^2 |U_{\beta 3}|^2 \sin^2 \Phi_{31} + 8\varepsilon_m \Phi_{31} \sin \Phi_{31} \Re[\Lambda_{32}^{\alpha\beta} e^{i\Phi_{31}}] + O(\varepsilon_m^2). \tag{8.114}$$

From these formulas, the oscillation probabilities for various oscillation modes can be calculated as summarized in Table 8.1.

8.5.3.2 Oscillations Around Φ_{21} Maximum

Near the Φ_{21} oscillation maximum,

$$\Phi_{32} \sim \Phi_{31} = \Phi_{12}/\varepsilon_m \sim \pi/2\varepsilon_m \sim 30, \tag{8.115}$$

and the energy spectra caused by Φ_{32} and Φ_{31} terms rapidly oscillate. If the energy resolution is worse than $|\varepsilon_m| \sim 3\,\%$, the oscillation effect is averaged as

$$\begin{aligned}\sin^2\Phi_{32} \sim \sin^2\Phi_{31} = \sin^2(\Phi_{21}/\varepsilon_m) \to \tfrac{1}{2},\\ \sin 2\Phi_{32} \sim \sin 2\Phi_{31} = \sin 2(\Phi_{21}/\varepsilon_m) \to 0.\end{aligned} \tag{8.116}$$

The second term of the general oscillation probability formula (8.93) becomes,

$$\begin{aligned}4\Re\left[\sum_{k>j}\Lambda_{kj}^{\alpha\beta}\sin^2\Phi_{kj}\right] &= 2\Re\left[(\Lambda_{31}^{\alpha\beta}+\Lambda_{32}^{\alpha\beta}) + 2\Lambda_{21}^{\alpha\beta}\sin^2\Phi_{21}\right]\\ &= 2|U_{\alpha 3}|^2(\delta_{\alpha\beta}-|U_{\beta 3}|^2) + 4\sin^2\Phi_{21}\Re\left[\Lambda_{21}^{\alpha\beta}\right],\end{aligned} \tag{8.117}$$

and the third term becomes

$$2\Im\left[\sum_{k>j}\Lambda_{kj}^{\alpha\beta}\sin 2\Phi_{kj}\right] \sim 2\sin 2\Phi_{21}\Im[\Lambda_{32}^{\alpha\beta}]. \tag{8.118}$$

By putting (8.117) and (8.118) into Eq. (8.93), the oscillation probability formula $@\Phi_{21}$ is obtained as

$$P_{\nu_\alpha\to\nu_\beta}(@\Phi_{21}) \sim \delta_{\alpha\beta}(1-2|U_{\alpha 3}|^2) + 2|U_{\alpha 1}|^2|U_{\beta 3}|^2 - 4\sin\Phi_{21}\Im\left[\Lambda_{21}^{\alpha\beta}e^{i\Phi_{21}}\right]. \tag{8.119}$$

For the disappearance case, it is

$$P_{\nu_\alpha\to\nu_\alpha}(@\Phi_{21}) = 1 - 2|U_{\alpha 3}|^2(1-|U_{\alpha 3}|^2) - 4|U_{\alpha 1}|^2|U_{\alpha 2}|^2\sin^2\Phi_{21}, \tag{8.120}$$

Table 8.2 Oscillation probabilities at $@\Phi_{12}$. $c_\delta = \cos\delta$, $s_\delta = \sin\delta$ are used

Mode and probability $@\Phi_{21}$
M: $\nu_e \to \nu_e$, $\bar{\nu}_e \to \bar{\nu}_e$ P: $\cos 2\theta_{13}(1-\sin^2 2\theta_{12}\sin^2\Phi_{21}) + O(s_{13}^4)$
M: $\nu_e \to \nu_\mu$, $\bar{\nu}_\mu \to \bar{\nu}_e$ P: $\frac{1}{2}s_{23}^2\sin^2 2\theta_{13} + c_{13}^2\sin 2\theta_{12}\sin\Phi_{21}\times$ $\left(((c_{23}^2 - s_{23}^2 s_{13}^2)\sin 2\theta_{12} + s_{12}\sin 2\theta_{23}\cos 2\theta_{12}c_\delta\right)\sin\Phi_{21} + s_{13}\sin 2\theta_{23}s_\delta\cos\Phi_{21}\big)$
M: $\nu_e \to \nu_\tau$, $\bar{\nu}_\tau \to \bar{\nu}_e$ P: $\frac{1}{2}c_{23}^2\sin^2 2\theta_{13} + c_{13}^2\sin 2\theta_{12}\sin\Phi_{21}\times$ $\left(((s_{23}^2 - s_{23}^2 s_{13}^2)\sin 2\theta_{12} - s_{12}\sin 2\theta_{23}\cos 2\theta_{12}c_\delta\right)\sin\Phi_{21} - s_{13}\sin 2\theta_{23}s_\delta\cos\Phi_{21}\big)$

and for the appearance case, it is

$$P_{\nu_\alpha \to \nu_{\beta \neq \alpha}}(@\Phi_{21}) = 2|U_{\alpha 3}|^2 |U_{\beta 3}|^2 - 4 \sin \Phi_{21} \Im \left[\Lambda_{21}^{\alpha\beta} e^{i\Phi_{21}} \right]. \tag{8.121}$$

Using those equations, $P_{\nu_e \to \nu_e}(@\Phi_{21})$, $P_{\nu_e \to \nu_\mu}(@\Phi_{21})$ and $P_{\nu_e \to \nu_\tau}(@\Phi_{21})$ are calculated and the results are summarized in Table 8.2.

8.5.4 Oscillation Formula with Matter Effect

The oscillation formulas with the matter effect with precision better than described in Sect. 7.1 are complicate to derive and we borrow the results from the references shown in the tables.

Tables 8.3 and 8.4 summarize the important oscillation probabilities with the earth matter effect.

For solar neutrinos, ν_e is generated in the sun and the matter effect at its generation point and the density change along its path have to be taken into account. Table 8.5 show a simple case which is derived in Sect. 6.2.

Table 8.3 Oscillation probabilities with matter effect at $@\Phi_{31}$ [4]

Mode and probability $@\Phi_{31}$
M: $\nu_e \to \nu_e, \quad \overline{\nu}_e \to \overline{\nu}_e$ $\tilde{P}$: $1 - \sin^2 2\theta_{13} \frac{\sin^2((1-\eta_C \upsilon_\oplus)\Phi_{31})}{(1-\eta_C \upsilon_\oplus)^2} - \varepsilon_m^2 \sin^2 2\theta_{12} \frac{\sin^2(\upsilon_\oplus \Phi_{31})}{\upsilon_\oplus^2} + O(s_{13}^4)$
M: $\nu_\mu \to \nu_e, \quad \overline{\nu}_\mu \to \overline{\nu}_e$ $\tilde{P}$: $s_{23}^2 \sin^2 2\theta_{13} \frac{\sin^2((1-\eta_C \upsilon_\oplus)\Phi_{31})}{(1-\eta_C \upsilon_\oplus)^2} + \varepsilon_m J_{123} \cos(\Phi_{31} + \eta_C \delta) \frac{\sin(\upsilon_\oplus \Phi_{31})}{\upsilon_\oplus} \frac{\sin((1-\eta_C \upsilon_\oplus)\Phi_{31})}{1-\eta_C \upsilon_\oplus}$ $+ \varepsilon_m^2 c_{23}^2 \sin^2 2\theta_{12} \frac{\sin^2(\upsilon_\oplus \Phi_{31})}{\upsilon_\oplus^2} + O(\varepsilon_m s_{13}^2)$
M: $\nu_\mu \to \nu_\mu, \quad \overline{\nu}_\mu \to \overline{\nu}_\mu$ $\tilde{P}$: $1 - \sin^2 2\theta_{23} \sin^2 \Phi_{31} - s_{23}^2 \sin^2 2\theta_{13} \frac{\sin^2((1-\eta_C \upsilon_\oplus)\Phi_{31})}{(1-\eta_C \upsilon_\oplus)^2}$ $+ \frac{\sin^2 2\theta_{13} \sin^2 2\theta_{23}}{2(1-\eta_C \upsilon_\oplus)} \left(\sin \Phi_{31} \cos(\upsilon_\oplus \Phi_{31}) \frac{\sin((1-\eta_C \upsilon_\oplus)\Phi_{31})}{1-\eta_C \upsilon_\oplus} - \frac{\eta_C \upsilon_\oplus \Phi_{31}}{2} \sin 2\Phi_{31} \right)$ $+ \varepsilon_m c_{12}^2 \sin^2 2\theta_{23} \Phi_{31} \sin 2\Phi_{31} - \varepsilon_m J_{123} c_\delta \cos \Phi_{31} \frac{\sin(\upsilon_\oplus \Phi_{31})}{\upsilon_\oplus} \frac{\sin((1-\eta_C \upsilon_\oplus)\Phi_{31})}{1-\eta_C \upsilon_\oplus}$ $- \frac{\varepsilon_m J_{123}}{1-\eta_C \upsilon_\oplus} \cos 2\theta_{23} c_\delta \sin \Phi_{31} \left(\eta_C \upsilon_\oplus \sin \Phi_{31} - \frac{\sin(\upsilon_\oplus \Phi_{31})}{\upsilon_\oplus} \cos((1-\eta_C \upsilon_\oplus)\Phi_{31}) \right)$

Table 8.4 Oscillation probabilities with matter effect $@\Phi_{12}$ [5]

Mode and probability $@\Phi_{21}$
M: $\nu_e \to \nu_e, \quad \overline{\nu}_e \to \overline{\nu}_e$ $\tilde{P}$: $\cos 2\theta_{13} \left(1 - \frac{\sin^2 2\theta_{12}}{(1-\eta_C \upsilon_\oplus \cos 2\theta_{12})^2} \sin^2((1 - \eta_C \upsilon_\oplus \cos 2\theta_{12})\Phi_{21}) \right) + O(s_{13}^4)$

Table 8.5 Oscillation probabilities of solar neutrinos with matter effect

Mode and probability of solar neutrino oscillation	
M:	$\nu_e \to \nu_e$
$\tilde{P}$:	$\frac{1}{2}\left(1+\frac{\cos 2\theta_{12}(\cos 2\theta_{12}-\upsilon_{\odot}(0))}{\sqrt{(\cos 2\theta_{12}-\upsilon_{\odot}(0))^2+\cos^2 2\theta_{12}}}\right)$

$\upsilon_{\odot}(0)$ is the charge current weak potential at the neutrino generation point. From Eq. (6.60)

8.6 Oscillation with Slowly-Changing Mixing Amplitude

In Sect. 6.2, neutrino oscillation in a slowly changing matter density is discussed. In this appendix, we will solve the state equation (6.42), which has a form of

$$\frac{d}{dt}\begin{pmatrix} C_\alpha(t) \\ C_\beta(t) \end{pmatrix} = -i\omega(t)\begin{pmatrix} -\cos 2\theta(t) & \sin 2\theta(t) \\ \sin 2\theta(t) & \cos 2\theta(t) \end{pmatrix}\begin{pmatrix} C_\alpha(t) \\ C_\beta(t) \end{pmatrix} \equiv -i\Theta(t)\begin{pmatrix} C_\alpha \\ C_\beta \end{pmatrix}. \tag{8.122}$$

In Sect. 6.2, ω is the neutrino oscillation frequency of the order of 10^4 rad/s, while $\dot{\theta}$ is the rate of the change of the mixing angle caused by the change of the matter density, which is of the order of 10 rad/s or less. Therefore, $\dot{\theta}$ is much smaller than the oscillation frequency ω,

$$\dot{\theta} \ll \omega. \tag{8.123}$$

In order to solve the Eq. (8.122), we define new parameters $C_\pm$ as follows:

$$\begin{pmatrix} C_-(t) \\ C_+(t) \end{pmatrix} \equiv \begin{pmatrix} \cos\theta(t) & -\sin\theta(t) \\ \sin\theta(t) & \cos\theta(t) \end{pmatrix}\begin{pmatrix} C_\alpha(t) \\ C_\beta(t) \end{pmatrix} \equiv V(t)\begin{pmatrix} C_\alpha(t) \\ C_\beta(t) \end{pmatrix}. \tag{8.124}$$

The time differentiation of C_α and C_β can be expressed by using $C_\pm(t)$ and $V(t)$ as,

$$\frac{d}{dt}\begin{pmatrix} C_\alpha \\ C_\beta \end{pmatrix} = \frac{d}{dt}\left[V^\dagger\begin{pmatrix} C_- \\ C_+ \end{pmatrix}\right] = V^\dagger\begin{pmatrix} \dot{C}_- \\ \dot{C}_+ \end{pmatrix} + \dot{V}^\dagger\begin{pmatrix} C_- \\ C_+ \end{pmatrix}. \tag{8.125}$$

By putting Eqs. (8.124) and (8.125) into Eq. (8.122), the differential equations for $C_\pm$ are obtained as follows:

$$\begin{pmatrix} \dot{C}_- \\ \dot{C}_+ \end{pmatrix} = -\left[iV\Theta V^\dagger + V\dot{V}^\dagger\right]\begin{pmatrix} C_- \\ C_+ \end{pmatrix}. \tag{8.126}$$

Here,

$$iV\Theta V^{\dagger} = i\omega \begin{pmatrix} \cos\theta & -\sin\theta \\ \sin\theta & \cos\theta \end{pmatrix} \begin{pmatrix} -\cos 2\theta & \sin 2\theta \\ \sin 2\theta & \cos 2\theta \end{pmatrix} \begin{pmatrix} \cos\theta & \sin\theta \\ -\sin\theta & \cos\theta \end{pmatrix}$$
$$= i\omega \begin{pmatrix} -1 & 0 \\ 0 & 1 \end{pmatrix},$$

and

$$V\dot{V}^{\dagger} = \dot{\theta} \begin{pmatrix} \cos\theta & -\sin\theta \\ \sin\theta & \cos\theta \end{pmatrix} \begin{pmatrix} -\sin\theta & \cos\theta \\ -\cos\theta & -\sin\theta \end{pmatrix} = \dot{\theta} \begin{pmatrix} 0 & 1 \\ -1 & 0 \end{pmatrix}. \tag{8.127}$$

Therefore, Eq. (8.126) becomes

$$\begin{pmatrix} \dot{C}_- \\ \dot{C}_+ \end{pmatrix} = -i\omega \begin{pmatrix} -1 & -i\dot{\theta}/\omega \\ i\dot{\theta}/\omega & 1 \end{pmatrix} \begin{pmatrix} C_- \\ C_+ \end{pmatrix}. \tag{8.128}$$

So far, the equation is exact.

Since there is a condition (8.123), Eq. (8.128) can be approximated to

$$\begin{pmatrix} \dot{C}_- \\ \dot{C}_+ \end{pmatrix} = -i\omega(t) \begin{pmatrix} -1 & 0 \\ 0 & 1 \end{pmatrix} \begin{pmatrix} C_- \\ C_+ \end{pmatrix}. \tag{8.129}$$

Its solution is,

$$\begin{pmatrix} C_-(t) \\ C_+(t) \end{pmatrix} = \begin{pmatrix} e^{i\Omega(t)} & 0 \\ 0 & e^{-i\Omega(t)} \end{pmatrix} \begin{pmatrix} C_-(0) \\ C_+(0) \end{pmatrix}, \tag{8.130}$$

where $\Omega(t) = \int_0^t \omega(t)dt$. Finally, from the relation (8.124),

$$\begin{aligned} \begin{pmatrix} C_\alpha(t) \\ C_\beta(t) \end{pmatrix} &= \begin{pmatrix} \cos\theta & \sin\theta \\ -\sin\theta & \cos\theta \end{pmatrix} \begin{pmatrix} C_-(t) \\ C_+(t) \end{pmatrix} \\ &= \begin{pmatrix} \cos\theta & \sin\theta \\ -\sin\theta & \cos\theta \end{pmatrix} \begin{pmatrix} e^{i\Omega} & 0 \\ 0 & e^{-i\Omega} \end{pmatrix} \begin{pmatrix} \cos\theta & -\sin\theta \\ \sin\theta & \cos\theta \end{pmatrix} \begin{pmatrix} C_\alpha(0) \\ C_\beta(0) \end{pmatrix} \\ &= \left[\cos\Omega(t) - i\sin\Omega(t) \begin{pmatrix} -\cos 2\theta(t) & \sin 2\theta(t) \\ \sin 2\theta(t) & \cos 2\theta(t) \end{pmatrix}\right] \begin{pmatrix} C_\alpha(0) \\ C_\beta(0) \end{pmatrix}. \end{aligned} \tag{8.131}$$

References

1. L.B. Okun, *Leptons and Quarks* (North Holland) (1985)
2. W. Greiner, B. Müller, *Gauge Theory of Weak Interactions* (Springer) (1993)
3. J.D. Bjorken, S.D. Drell, *Relativistic Quantum Mechanics* (McGraw-Hill Book Company) (1965)
4. E.K. Akhmedov, R. Johansson, M. Lindner, T. Ohlsson, T. Schwetz, JHEP **04**, 078 (2004)
5. F. Capozzi, E. Lisi, A. Marrone, arxiv:1309.1638v1 [hep-ph] (2013)

Index

F. Suekane, *Neutrino Oscillations*, Lecture Notes in Physics 898,
DOI 10.1007/978-4-431-55462-2

P